UNIVERSITY OF LJUBLJANA
FACULTY OF MATHEMATICS AND PHYSICS
DEPARTMENT OF PHYSICS

Zala Lenarčič

NONEQUILIBRIUM PROPERTIES OF MOTT INSULATORS

Doctoral thesis

Advisor: prof. dr. Peter Prelovšek

Ljubljana, 2015

UNIVERZA V LJUBLJANI
FAKULTETA ZA MATEMATIKO IN FIZIKO
ODDELEK ZA FIZIKO

Zala Lenarčič

NERAVNOVESNE LASTNOSTI MOTTOVIH IZOLATORJEV

Doktorska disertacija

Mentor: prof. dr. Peter Prelovšek

Ljubljana, 2015

Izjava o avtorstvu in objavi elektronske oblike

Izjavljam:

— da sem doktorsko disertacijo z naslovom *NERAVNOVESNE LASTNOSTI MOTTOVIH IZOLATORJEV* izdelal/-a kot rezultat lastnega raziskovalnega dela pod mentorstvom prof. dr. Petra Prelovška,

— da je elektronska oblika dela identična s tiskano obliko in

— da Fakulteti za matematiko in fiziko Univerze v Ljubljani dovoljujem objavo elektronske oblike svojega dela na spletnih straneh Repozitorija Univerze v Ljubljani.

Ljubljana, dne Podpis:

Uokvirjanje zvedavosti.

Acknowledgements

It has been a process. Within it I was exposed to the great intuition and the passion for physics of my advisor, Peter Prelovšek. From him I learned (no matter the complexity) one should search for simple messages and clean formulations. Complementary, with Tomaž Prosen I realized science can be done in a calm, nearly contemplative manner, and I saw how beauty exposes itself though the exactness. Beyond solitary calculations, interactions formed nodes, they added new threads. I appreciate all junctions we formed with Janez Bonča, Martin Eckstein, Jure Kokalj, Jan Kogoj, Marcin Mierzejewski and Denis Golež. To whom I thank for all the marks he left on me and my physics. And all that time, the web of my people and my family was strong enough to protect me from falling.

Povzetek

Mottovi izolatorji so nekakšna baza: teoretično, ker so osnovno stanje Hubbardovega modela pri polovični zasedenosti orbital ter zadostni interakciji U in eksperimentalno, ker z dopiranjem postanejo superprevodni. Razvoj časovno-ločljivih eksperimentalnih tehnik, predvsem optične spektroskopije, je odprl nov vpogled v njihovo naravo. Pri t.i. "pump-probe" eksperimentih s femtosekundno časovno resolucijo lahko sledimo relaksaciji vzbuditev, ustvarjenih z začetnim "pump" pulzom. V okviru disertacije je posebna pozornost posvečena vzbuditvam Mottovega izolatorja preko Mottove energijske vrzeli. Iz časovnih skal relaksacije efektivno nabitih delcev, ki pri taki vzbuditvi nastanejo, dobimo uvid v moč sklopitve med njimi in drugimi prostostnimi stopnjami, npr. spinsko in fononsko. Teoretično razumevanje je pri tem ključno v prepoznavanju različnih izvorov in prispevkov.

V disertaciji je zaobjet celoten krog, od vzbuditve Mottovega izolatorja do relaksacije. Najprej postavimo Mottov izolator v konstantno električno polje in izračunamo polje, pri katerem nastajanje nabitih delcev postane izrazito. V spinsko skoraj polariziranem sistemu se polje da poiskati kot eksplicitno funkcijo Mottove energijske vrzeli. Večina ostalega dela je posvečena analizi in motivaciji "pump-probe" eksperimentov. Pri tem ločeno analiziramo kratkočasovno in dolgočasovno obnašanje, ki v realnih eksperimentih ustreza femtosekundni in pikosekundni skali. Nabite delce sklopimo s spinskimi in fononskimi prostostnimi stopnjami, zato, da bi razumeli kako moč sklopitve vpliva na hitrost relaksacije. Za ustrezno analizo je optična prevodnost modelov tesne vezi generalizirana na časovno odvisne sisteme. Znotraj dolgočasovnega dinamike je zanimiv predvsem proces rekombinacije efektivno pozitivnih in negativnih delcev, v katerem je velika energija para nabitih delcev predana manjšim, tipično bozonskim vzbuditvam. Ob predpostavki majhne gostote nabitih delcev je pokazano, da se v dvo-dimenzionalnih sistemih izmerjene pikosekundne rekombinacijske čase da razložiti z emisijo spinskih vzbuditev, medtem ko je v enodimenzionalnih sistemih tak mehanizem neučinkovit. Vsaj v (efektivno enodimenzionalnih) organskih soleh, z izrazito energijskimi fononi, se rekombinacijske čase da razložiti z emisijo fononov. Ne glede na točno obliko eksitacij, ki sprejmejo energijo para, je hitrost rekombinacije eksponentno zavrta s številom eksitacij, ki pri takem procesu nastanejo.

Preplet koherentnega in nekoherentnega vzbujanja je bil opazovan na primeru odprte interagirajoče spinske verige.

Ključne besede:
Mottov izolator, dielektični preboj, odprti kvantni sistemi, pump-probe eksperimenti, optična prevodnost, relaksacija in rekombinacija foto-induciranih nabojev.

PACS: 71.27.+a, 71.30.+h, 77.22.Jp, 78.47.-p, 74.20.Mn, 78.47.J-, 74.72.Cj, 75.10.Pq, 05.60.Gg, 03.65.Yz.

Abstract

Mott insulators are one of paradigmatic systems; theoretically because they are the ground state of the celebrated Hubbard model at half filling for sufficient U and experimentally because they are the parent compound that under chemical doping exhibits superconducting properties. A novel insight into their nature has been obtained with the development of the time-resolved experimental techniques, especially the optical spectroscopy. With the resolution down to few tens of femto-seconds, the dynamics following an excitation process can be tracked, as typically performed in so called pump-probe experiments. Within this thesis a special focus has been put on excitations over the Mott-Hubbard gap, when effectively charged particles are photoinduced. They are generated as objects out of equilibrium that are yet to go through several stages of relaxation. Measured timescales for latter processes can be a valuable information on the coupling between the charge and other, e.g. spin and phonon, degrees of freedom.

The theoretical understanding of mechanisms that govern the dynamics is essential to distinguish possible contributions. We explore different aspects, from the excitation to the relaxation. After applying a constant electric field to a one-dimensional Mott insulator we establish the rate at which charged particles are produced. Moreover, for spin-polarized systems we find the threshold field, at which the production becomes substantial, as a function of the Mott-Hubbard gap. The majority of other work focuses on pump-probe experiments, where we separately treat short- and long-time behavior of charges. By first exciting them well above the gap we show that via the coupling to spins, and possibly also phonons, charges can rapidly transmit their excess of energy to the most efficient bath through a procedure consisting of several stages and final equilibration between bosonic degrees of freedom. Different stages have separated timescales, however, all in the range of femto-seconds. For a proper analysis of the short-time dynamics we generalize the optical conductivity for tight-binding models to systems out of equilibrium. Within the long-time behavior the recombination of effectively positive and negative charges is a process of greatest interest and complexity due to the energy of size of the Mott-Hubbard gap that has to be redistributed to smaller fractions. By addressing the systems with a low density of excited charges, we show that in two-dimensional systems the emission of spin excitation is a viable recombination scenario, while in one-dimension, due to the charge-spin separation, the energy is more efficiently transmitted to phonons, especially if they have large frequencies and coupling to the charge as e.g. in organic salts. Regardless of the type of recipient bosons, the recombination rate turns out to be exponentially suppressed by the number of bosonic modes created.

By opening the system to the environment the interplay of the coherent and the incoherent driving is studied on a chain of interacting spinless fermions.

Keywords: Mott insulator, dielectric breakdown, driven dissipative interacting systems, pump-probe experiments, optical conductivity, photo-induced charge relaxation and recombination.

PACS: 71.27.+a, 71.30.+h, 77.22.Jp, 78.47.-p, 74.20.Mn, 78.47.J-, 74.72.Cj, 75.10.Pq, 05.60.Gg, 03.65.Yz.

Contents

Chapter 1

Introduction

If one was given a box, not knowing about its content and without being allowed to open it, a typical reaction would be to shake it. The essence of the nonequilibrium many-body physics is actually not far from that: by exciting the object of interest, one hopes to obtain more information about its constituents and especially the interactions between them, as typically explored in condensed matter systems. Even without any engineering, the equilibration of the excited interacting system is truly inherent to several physical processes, e.g., the dynamics of the early universe, the evolution of neutron stars, etc. Understanding particular features of the equilibration, but even more the generalities, is a challenging, but rewarding task. Raising the awareness of possible overlaps between different nonequilibrium realizations, unprecedented options of simulating, e.g. early universe behavior with table-top experiments exploiting cold atoms or condensed matter, might turn out enlightening.

A possible approach towards the nonequilibrium is from a known territory: the equilibrium. Especially in the theory, several concepts have to be revised before being attributed to the nonequilibrium dynamics, which in return give the information about their origin, formation, etc. (i) The statistical physics, being one of the fundamentals of the equilibrium description, was one of the first to be reconsidered. This initiated a series of studies dealing with the thermalization of excited systems; classifying different stages, recognizing role of ergodicity and searching for the generalization of the Gibbs ensemble, which would describe the situation long after the perturbation, especially in non-ergodic systems. (ii) Another quite general recycled concept is the quasi-particle picture. The novel contribution of the nonequilibrium approach is that the quasi-particle formation can be explicitly followed, while timescales of such a process contain the information about its nature, i.e. they vary depending on degrees of freedom involved. In reverse, clear experimental results discerning those differences could indisputably resolve the hierarchy of interactions. From this perspective the nonequilibrium approach in many cases disentangles the building blocks of otherwise complex objects. (iii) When driving an integrable system with e.g. Markovian dissipation at the boundary, it is interesting to check how much of the integrability structure of the bulk Hamiltonian has survived. (iv) Phase transitions can be extended to a new class of dynamical ones.

And of course these are just some of prominent examples. Even more important, precisely through the nonequilibrium one can access what would be inaccessible in equilibrium.

1.1 Mott insulators

Besides nonequilibrium, the other crucial ingredient of this thesis are Mott insulators. Interest for such insulators has been raised back in 1937, when it was observed [1] that some transition metal oxides, which should behave as conductors according to the band theory, turned out to be insulators.

Within the band theory, electron-electron interactions are neglected or treated within an effective single-electron model, while their motion is dominantly influenced by their interaction with ions, represented by a periodic potential. According to the Bloch theorem, states can be labeled by a momentum $\mathbf{k}$ and dwell within the band b with dispersion $\epsilon_b(\mathbf{k})$, which is independent of the band filling. Due to the periodic potential, bands can be separated from each other and if the chemical potential lies between two such band, then all bands are either completely filled or empty. Such system should behave as an insulator since states with $\mathbf{k}$ and $-\mathbf{k}$ are always both occupied, and when summed over cannot contribute to transport.

However, if some band is half filled, metallic response is expected, as was the case with previously mentioned transition metal oxides. First theoretical response to that observation was made by Mott and Peierls (1937) [2], who suggested that drastic modification of the theory, present at that time, should be needed. Pointing in the right direction, they also proposed it is quite possible that the electrostatic interaction between the electrons prevent them from moving at all, resulting in reduced conductivity. Mott later made a more profound attempt to build the electron theory of transition metals [3]. However, the first model based theory was proposed by Hubbard in 1963 [4].

As the simplest attempt to capture the correlated nature, model assumes the effective electron-electron interaction to be local, implicitly supposing that electrons dominantly sit on and not between lattice sites. For a system at half filling (having one electron per site), the energy to add another electron (which necessarily leads to a double occupancy of one site) is parametrized by U. Model relies on another assumption: the *tight-binding approximation* within which electrons hop between neighboring sites of lattice (determined with basis vectors $\mathbf{a}_m$), as parametrized by tunneling amplitude t, that (when interaction is being neglected) gives them a cosine dispersion

$$\epsilon(\mathbf{k}) = -2t \sum_m \cos(\mathbf{k} \cdot \mathbf{a}_m) \tag{1.1}$$

with at bipartite lattices a bandwidth $W = 2zt$, where z is the number on nearest neighbors. By combining both ingredients we obtain the renowned *Hubbard model*

$$H = -t \sum_{ij,s} c^\dagger_{i,s} c_{j,s} + U \sum_{i,s} n_{i,\uparrow} n_{i,\downarrow}, \tag{1.2}$$

where $c^\dagger_{i,s}$ is creation operator and $n_{i,s} = c^\dagger_{i,s} c_{i,s}$ operator giving local number of electrons with spin s. At half-filling and sufficient U its ground state has insulating nature, being separated from excited states with the Mott-Hubbard gap, which explains the introductory experimental observation. For more precise studies of concrete material also more elaborate multi-orbital models have been proposed and examined [5].

Within a discrete lattice perspective, excitations can be viewed as doubly occupied sites (called doublons) and non-occupied sites (called holons), having an effec-

tive negative and positive charge with respect to the background. In the ground state their existence is suppressed, while they are essentially present in the excited states. Being well mobile, they form the upper and the lower Hubbard band, respectively, however, these bands cannot be captured with simple single-electron states. Inherent correlation effects can be in a simplified picture visualized by the distortion of the spin background, caused by hopping of holon or doublon. As most transparently seen via the Schrieffer-Wolff transformation of the Hubbard model, leading to the effective t-J model [6], the electron-electron interaction is passed on as a Heisenberg-like interaction term H_J between the neighboring pair of spins $\langle i, j\rangle$,

$$H_{tJ} = H_{kin} + H_U + H_J, \quad H_J = J \sum_{\langle i,j\rangle} \mathbf{S}_i \cdot \mathbf{S}_j, \tag{1.3}$$

with $J = 4t^2/U$ obtained from the second order perturbation theory. Kinetic term H_{kin} has the same form as in Eq. (1.2), yet operators within it are projected so that they conserve the number of charges (holons or doublons), while H_U takes into account the energy of possibly existing doublons. From this effective model it is clear that electron correlations intertwine even excitations on different energy scales (e.g. U and J) and make considerations of such problems difficult and complex.

Till present times the Hubbard model remained basic framework for the description of correlation effects between the electrons. Although the simplest, it is still unsolved for any dimension $d > 1$. On the other hand, its solution for the one-dimensional systems [7] became one of the tools how to tackle the correlated systems in various aspects and situations. Besides, it motivated also the development of several numerical methods.

1.2 Experimental motivation

Since much of the inspiration for the theory developed within this thesis grew from existing experiments, we start with a review of experiments that are directly or just conceptually connected to the topics addressed in the main body. We briefly mention also some of the related theoretical studies, most of them being reported again in the theoretical Sec. 1.3.

A whole range of experimental techniques has gone through a notable progress, necessary to produce and analyze the dynamics of strongly interacting systems out of equilibrium. The field of ultra cold atoms [8, 9], actually initiated in parallel with the foundation of the field of the nonequlibrium many-body dynamics, has served in great deal to its challenges. However, also other more material-based techniques, with longer history in condensed matter physics, successfully adapted to treat dynamics of interacting systems. A quite general approach is the so called pump-probe scheme where an initial laser pump pulse excites the system, while subsequent probe pulses test the transient electronic structure at different time delays, as employed by the leading techniques in the field, time- and angle-resolved photo emission spectroscopy (tARPES) [10, 11] and time-resolved optical spectroscopy [12, 13, 14, 15]. Bridging the experiments with possible applications, besides the long-standing quest to understand and overcome the issues of the high-temperature superconductivity [15, 16, 17], optical spectroscopy technique recognized possible technological utilization of strongly correlated electron systems for ultrafast optoelectronics. In particular one-dimensional (1D) charge-transfer insulators can exhibit

strong nonlinear absorption $\chi^{(3)}$ as a consequence of the coherence between pump and probe pulse, but also fast (pico-second) relaxation of created charge-transfer excitations [18]. Besides the fact that in charge-transfer insulators $\chi^{(3)}$ is much bigger, it also has much shorter relaxation times than in band and Peierls insulators [19]. Rapid changes of reflectivity are observed also in the simple linear absorption with a pump pulse of energy larger than the gap, simply determined by the lifetime of excitations [13, 14, 20, 21]. Another promising peculiarity are also hidden states, which can be accessed only via nonequilibrium trajectory. Being stable at low temperature and unstable under another laser pulse, electrical current or thermal erase procedure, they could be used as a new type of fast memory [22].

1.2.1 Optical spectroscopy of Mott insulators

The majority of work presented in this thesis is actually stimulated by existing results, or could be observed in future experiments using the time-resolved optical spectroscopy on excited Mott insulators. In the following these experiments will be outlined more extensively. In general, compounds examined with optical spectroscopy differ from superconducting to insulating, according to the purpose of studies. Typically effectively low dimensional (one- or two-dimensional) materials vary from transition metal oxides [12, 13, 14], Ni-chains [19, 23, 24], to organic molecular compounds [20, 21, 25, 26]. Studies that were performed on Mott insulators share the following observations [13, 14, 20, 21]:

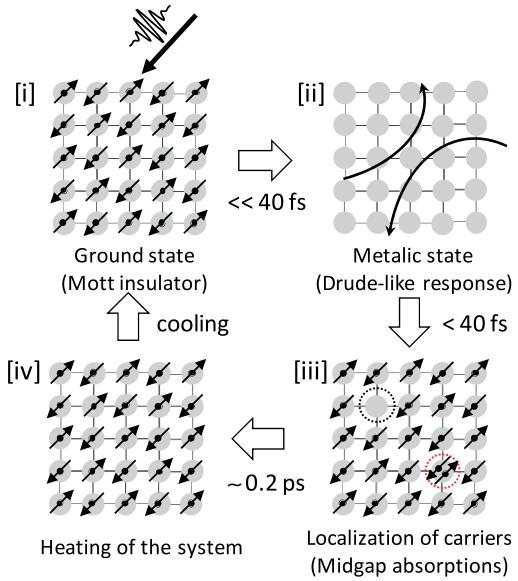

Figure 1.1: Pump-probe scheme for an excitation of a 2D Mott insulator, taken from [14].

(a) Initially a pump pulse with energy larger than the Mott-Hubbard (or the charge-transfer) gap creates effectively charged excitations that can be in Hubbard-like picture viewed as empty sites - holons, and doubly occupied sites - doublons. These can be related to holes and additional electrons in chemically doped material.

(b) At very short femto-second (fs) timescales these excitations yield a Drude-like low frequency response. The dissipationless Drude component, corresponding to the coherent motion of charges, indicates that an insulator to metal transition is photo-induced. However, this feature disappears faster then the other features (Fig. 1.2), probably due to the localization of charged carriers or their binding into excitons.

(c) The presence of charged excitations, even after the Drude responde is gone, is seen either indirectly in the non-zero deviation of reflectivity from the equilibrium one [20, 21], or directly through in-gap features of the absorption spectra [13, 14]. The connection to chemical doping can be drawn by comparing the position of in-gap (mid-infrared) peaks in photo- and chemical doping (see Fig. 1.2)), which suggests that one peak can be associated with holons and the other with doublons [14], due to the hole-electron asymmetry in charge-transfer insulators. The amplitude of in-gap peaks or of the reflectivity deviation then decreases in the pico-second (ps) timescale, which must be the timescale for the recombination of holon-doublon pairs.

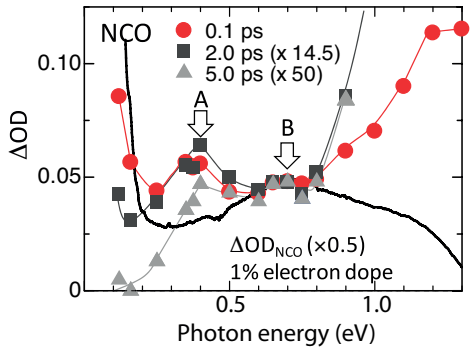

Figure 1.2: The difference in absorption spectra (relative to the equilibrium value) at different delays of the probe pulse obtained on Nd_2CuO_4. Peak A is attributed to holes and B to electrons. Fig. is taken from Ref. [14].

(d) In every holon-doublon recombination process a large amount of energy ($\sim$ Mott-Hubbard gap) is transferred to other degrees of freedom (spin, phonon, or other charged particles), causing heating of the system. Such a scenario is supported by the change of the spectral shape in the near-infrared region, similar to changes caused by an increase in temperature [14]. An eventual cooling, which should be related to the coupling to lattice vibrations, happens on much longer, approximately nano-second timescales.

Therefore phenomena can be split into three parts: (i) particle creation and short-time response in fs, (ii) charge recombination in ps, and (iii) the thermalization of the system.

On the short-time charge relaxation. The creation of charged particles and their distribution right after the pump pulse is an interesting theoretical problem, however it is not going to be treated within this thesis. To the best of our knowledge, there are no proper quantum calculations based on the coupling between correlated material and light, beside the semi-classical approaches where light is introduced through

the vector potential [27, 28, 29] via the Peierls substitution [30]. This should be especially important to adequately treat the coherent effect of the overlapping pump and probe pulse, when the energy of the pump pulse is smaller than the Mott-Hubbard gap [18]. However, when the pump energy is larger than the gap, it is sensible to assume that one photon creates one holon-doublon pair with corresponding energy. Especially if the energy of the pump pulse is considerably larger than the Mott-Hubbard (or the charge transfer) gap, then even the short-time dynamics can be non-trivial, since created particles have to reduce their energy via coupling to spin or phonon degrees of freedom [31]. The time resolution of existing experiment is just on the edge of being able to probe such dynamics [32].

On Mott-Hubbard excitons. The observation that shortly after the excitation the Drude component in optical response disappears is to our knowledge not thoroughly understood. It should be related to the charge localization, but possibly also to the formation of a holon-doublon bound state (exciton), directly and indirectly shown to exist in examined materials. Direct observation of excitons is non-trivial if they are optically non-active, which is actually the case for 2D cuprates [33, 34, 35] where the only way to detect them is via non-linear susceptibility. For relevant materials such measurement do support the exciton existence [36]. On the other hand, in 1D systems the lowest exciton state is optically active [37] and is nearly degenerate with another exciton of even parity, again detectable only by the third-order susceptibility [19]. The indirect confirmation of excitons is actually dynamical, via the time-dependence of the charge density n in pump-probe experiments. Since it turns out to be exponential [14, 21],

$$n(t) \propto e^{-t/\tau_r}, \tag{1.4}$$

with the recombination time τ_r independent of the initial charge density, the recombination process must be independent of the probability for holon and doublon to meet. This can only be satisfied if they are already in a bound state. In the opposite case, the rate equation

$$-\frac{dn}{dt} \propto n^\gamma, \quad \gamma = 2, 3, \tag{1.5}$$

which takes into account that the probability to meet the recombination partner is proportional to n^2 would not lead to an exponential decay. $\gamma = 2$, typically called as bimolecular process, would correspond to a holon and a doublon recombining in a process including a large number of final excitations. On the other hand, $\gamma = 3$ would be observed in a process with a single scattering with another holon or doublon. In this, so called *Auger process*, the energy of the holon-doublon pair is transmitted to the kinetic energy of the third charge and is possible only if the Mott-Hubbard gap is smaller that the Hubbard band width, as is typically the case for examined materials. Such reasoning has been confirmed also by the non-exponential decay in Ca_2CO_3 [38], effectively 1D Mott insulator known to have negligible excitonic effect [19], where the decay of the charge density followed the latter equation for $\gamma = 2$. Depending on the pump pulse and the origin of the binding, exciton state can also cease to exist. If pump pulse has high fluence and energy much larger that the gap, then already the short-time relaxation of charged particles will melt any ordering of the spin background, even in 2D. Especially in 2D systems, where spin ordering is sufficient for holon-doublon binding, its melting should drastically change the dynamics of the charge density, as seen in [39].

On the charge recombination. The timescale that limits the repetition rate of the pump-probe scheme as a possible switching device is actually the one on which charged excitations recombine, since this is the crucial step for the system to relax back to its ground state. It is a challenging theoretical problem since due to the large energy of charged excitations such process must have a great complexity. Precisely this complexity makes it slow, happening on *ps* timescale, orders of magnitude slower than the microscopic scale, set by the Hamiltonian hopping parameter $\hbar/t \sim 2fs$, which determines the scale for dynamics of the individual charge relaxation. The basic difference is that the initial charge relaxation (due to coupling with spin and phonon degrees of freedom) can be viewed as a consequential step-by-step process in which the energy is transmitted to bosonic baths, while in the recombination the emission of large energy is instantaneous. To treat the whole process one should assume a sensible initial state and then propose a mechanism that suggests where the energy is transmitted. The initial state, the dimensionality, and available bosons (possibly dependent on the system studied) play an important role in recognizing the minimal and dominant mechanism. A major part of this thesis is dedicated to the exploration of the recombination process, assuming that after the short-time relaxation holon and doublon bind in an exciton state. We propose that in 2D systems [13, 14] energy is transmitted to spin excitations [34, 35], while in 1D organic insulators [20, 21] to molecular vibrations with high frequency [40], particular to materials with a complex structure.

Very similar processes of the exciton recombination have been observed and theoretically addressed also in *carbon nanotubes* [41], where measured lifetimes turn out to be 10 to 100 ps [42, 43, 44].

1.2.2 Mott insulator to metal phase transition induced by electric field

A steady-state alternative to the above processes is the field induced insulator-to-metal transition. In one of early works [45] external voltage was applied to crystals of $SrCuO_2$ and Sr_2CuO_3 (effectively 1D Mott insulators) leading to the observation of a discontinuous drop in the resistivity above some threshold voltage value, which could not be attributed to the Joule heating and must be intrinsic to the highly nonequilibrium system with threshold voltage/field showing a strong temperature dependence, approximately following $E_{th}(T)/E_{th}(0) \approx \exp(-T/T_0)$.

Same observation and also $E_{th}(T)$ dependence was obtained also with $W_xV_{1-x}O_2$ nanowires [46], with an additional detail that for the reversed metal-to-insulator transition the threshold field temperature dependence was different, $E_{th} \propto \sqrt{T_c - T}$. Such a hysteresis might suggest in the reversed process (starting in the metallic phase) the pre-existing charge carriers can cause the Joule heating while participating in the initial high current.

Insulator-to-metal transition was observed also in $GaTa_4Se_{8-x}Te_x$ [47], following several other experiments on the family of chalcogenide Mott insulators [48, 49, 50, 51]. Supported by the threshold field dependence on the Mott-Hubbard gap ($E_{th} \propto \Delta^{5/2}$), which is observed in the avalanche breakdowns in narrow-gap semiconductors [52], the authors proposed that the mechanism for the breakdown must be the same, as review in the theoretical part 1.3.1.

A substantial nonlinear resistance effect was observed also in organic salts [53]

and attributed to the melting of insulating charge-order domains due to a steady flow. Surprisingly, the sample turns out to work as a DC-AC converter for a range of voltages as well. Phenomena was explained by the coexistence of two stable solutions, so that AC response actually comes from the oscillations between the two states.

Very recently [54] an ultrafast switching into a metastable metallic state, indicating on a non-thermal tunneling mechanism, has been displayed in a VO_2 thin film by non-resonant excitation with high-field multi-terahertz transients. The non-thermal switching that happens on a timescale below 100fs depends only on the amplitude of the applied field. The concentration of the metallic phase increases rapidly above about 8 MV/cm. Measured conductivity can be fitted with $\sigma(F) = \sigma_0 \exp(-\pi F_{th}/F)$, giving $F_{th} = 14.2$MV/cm. Since no excitonic self-trapping is observed this also indicates that spatially separated doublon-holon pairs are generated via field-induced tunneling.

1.2.3 Ultracold atoms

In addition to the real materials, certainly the cleanest realization of the closed-system dynamics can be obtained with ultracold atoms, confined with magnetic or optical fields and cooled down to few pico-kelvins by laser and evaporative cooling [8]. Such set-ups can realize several theoretical models for bosonic and fermionic particles, with high control over the confining potentials and ability to tune the interactions over a wide range using Feshbach resonances [55]. Being isolated from the environment, quantum states with coherence longer than the typical timescales of the dynamics can be prepared. Due to the low density of the atom gas in these systems, the dynamics has longer timescales then in condensed-matter, therefore it can be followed without ultrafast probes. System can be brought out of equilibrium by quenching the depth of the lattice potential [56] or by tilting it [57]. Dynamics of ultracold gases can be imaged either in the confining trapping potential (via direct access to the density distribution $n(x)$ in position space) or after they are released, in the time-of-flight expansion (measuring the momentum distribution $n(k)$). Only by splitting the gas into two halves and superimposing them in the time-of-flight expansion (by using the matterwave interference) the complex phase of the quantum field can be accessed [58]. Internal degrees of freedom, such as hyperfine manifold of total angular momentum of atoms can be used to assign them the spin, opening the field to study spin dynamics as well [59, 60]. In order to relate to several (older and recent) studies of the paradigmatic Hubbard model, preparation of a Mott insulator of fermionic atoms in an optical lattice [61] was an essential step that enabled cold atom community to tackle problems common to condensed-matter ones.

Due to the high control over different parameters, cold-atoms are probably the most flexible experimental setting ever used. For example, the motion of atoms can be restricted to lower dimensions simply by enhancing the confining potentials, and especially with 1D Bose gas with repulsive contact interactions one can prepare an approximately integrable quantum system, which displays all the peculiarities of integrable models, such as the ballistic transport of initially localized ultracold bosons [62], the prethermalization (mentioned in the theoretical Sec. 1.3) [63], etc. Especially important to embed this thesis into a broader context, quite remarkably, there exist similarities also to the dynamics observed in pump-probe experiments:

On doublon relaxation. Doublon relaxation observed in fermionic cold atom set-ups [64, 65] is directly related to the holon-doublon recombination in materials excited with a pump pulse. A sample of repulsively interacting ultracold fermions is loaded onto a 3D optical lattice of cubic symmetry. Depending on parameters U, t system can be in metallic or insulating regime, but always with the double occupancy smaller than 15%. Additional excitations are then created by a sinusoidal modulation of the lattice depth with a frequency close to U, which lifts the double occupancy to the final value of 15% to 35%, and therefore creates a highly excited nonequilibrium state. After a free evolution at the initial lattice depth, the remaining double occupancy is probed by a sudden increase of the lattice depth, which prevents further tunneling. Then the amount of atoms residing on singly/doubly occupied sites is measured. Within the observation time, the double occupancy decays exponentially with a decay time only weakly dependent on the initial doublon density. As already mentioned, due to the low density of the ultracold gas the absolute timescale for the doublon decay is much longer (in regime of seconds), compared to the condensed-matter one (in pico-seconds). However, dimensionless dependences on ratios, e.g. U/t, can be the same. The lifetime of doublons has serious implications for the use of cold atom systems to simulate the equilibrium properties of the Hubbard model, since it constrains the maximum sweep rate of Hamiltonian parameters: by increasing U/t density of doublons should decrease, however, the doublon lifetime provides the dominant equilibration timescale for this. Sharing fundamental similarities on the level of the problem, conditions in cold atom systems are still quite different from typical pump-probe ones, since in the former much larger amount of doublons and corresponding holons is created, so that the background is already compressible. Consequently, the dominant mechanism for the decay of doublon relies on multiple low-energy scattering processes in which the kinetic energy of involved background fermions is enlarged, or by highly exciting only a few fermions that then relax further. Such mechanism has been confirmed also with DMFT studies [66] and with a diagrammatic approach to the Bose-Hubbard system [67], both of them sharing similar conditions to the previously mentioned studies due to $T > 0$. Situation with a high density of charged excitations could be created in pump-probe experiments by a pump pulse with very high fluence. However, since in realistic materials the gap is typically smaller than the bandwidth of the upper Hubbard band, the decay of doublon could be also of an Auger-type, where only a single remaining charge is excited. This should be revealed in a power-law decay of the charge density, as determined by the rate equation $-\dot{n} \propto n^3$.

On spread of thermal correlations. Another overlapping example is the observation that initially local thermal correlations (in a prethermalized state) spread into the system in a light-cone like evolution due to the phononic excitations [68, 69, 70]. This is determined from the evolution of the two-point correlation function extracted from the interference pattern of two identical halves of gas, as mentioned earlier. Similar observation is made also in our study of the relaxation for an excited holon, injected into an ordered spin background. The holon would first locally perturb the spin background, creating a hot vicinity around it, while in the second stage this local perturbation would cool down by being spread into the whole system via magnon waves with well defined maximal velocity [71].

On additional external field. The application of an external bias to materials can be in principle related to the tilting of the lattice potential in cold atom set-up. Due

to essential lack of the dissipation and with coherence well controlled, nearly perfect Bloch oscillations (which actually prevent the system to conduct) were observed for the latter [57]. However, it was demonstrated that adding a harmonic modulation to an already tilted lattice potential causes a force $F(t) = F_0 + \Delta F \sin(2\pi\nu t + \phi)$ that can lead to center-of-mass motion, i.e., transport. If driving was slightly off-resonant to the Bloch frequency ν_B, $\nu = \nu_B + \delta\nu$, matter-wave (super-Bloch) oscillations extending over hundreds of lattice sites were observed. By appropriately switching the detuning, an efficient transport can be engineered.

1.3 Theoretical framework

The field of interacting systems driven out of equilibrium has spread into several directions; it raised fundamental questions that turned out to be supporting branches of the whole field and it lead to the generalization of several numerical techniques. A major progress on numerical techniques has been made by extending dynamical mean-field theory (DMFT) [72] and density matrix renormalization group (DMRG) [73] to the nonequilibrium dynamics, while numerical results within this thesis were obtained with the (time-dependent generalization of) exact diagonalization within the Lanczos basis and the diagonalization within the limited functional space. Since both of them are extensively explained in [74] they shall not be revised again.

In the following we review some of the theoretical studies related to ours and to some of the already mentioned experiments. With an aim to put our work in a broader context we give a glimpse of topics that turned to drive the field forward as well.

1.3.1 Dielectric breakdown of Mott insulators

As argued in the experimental overview, Sec. 1.2.2, the richness of possible interpretations and scenarios, based on experimental results, make it really tough for the theorist to extract and present some general mechanism. Of course, the central question for the theory is the threshold field F_{th} strength at which the resistance of an insulating sample drops abruptly and can be approached on several levels.

The results on 1D periodic systems at zero temperature, treated within Hubbard model, point towards the description with a generalized Landau-Zener tunneling [27, 75, 76, 77, 78, 79]. The standard Landau-Zener theory [80, 81] gives the probability for the tunneling between two single-particle states with difference of energies ϵ_1, ϵ_2 having a hyperbolic shape, $\lim_{F\to\pm\infty} |\epsilon_1 - \epsilon_2| = \alpha_0 F$, as a function of an external parameter $F.$, e.g. field.

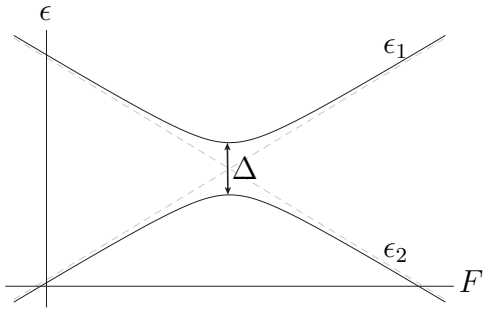

If initially (at $F \to -\infty$) in one of the states, the probability to transit into the other state, as a consequence of a steady change of parameter F, $\dot{F} = F_0$, is given by $P = \exp(-\pi\Delta^2/2\hbar\alpha)$, where Δ is the minimal energy difference and $\alpha = \alpha_0 F_0$ the rate at which the energy difference between the adiabatic states is changed, $\lim_{F\to\pm\infty} |\epsilon_1 - \epsilon_2| = \alpha t$. We should stress that the standard Landau-Zener expression (now applied to many-body states), according to which the threshold field F_{th} should scale as $F_{th} \propto \Delta^2$ with the Mott-Hubbard gap Δ, is observed in the spin non-polarized system only at sufficiently small interaction U and has to be generalized otherwise [27]. In addition, also by reducing the spin polarization a different dependence is observed, and it goes towards $F_{th} \propto \Delta^{3/2}$, obtained in the nearly spin-polarized system [79]. Still, same type of behavior has been confirmed within DMFT [82] and by studies that included leads as well [83, 84].

A general problem of zero temperature results seemed to be that based on extrapolations one has to compare them with experimental results [45] (obtained at $T > 0$) showing obvious strong temperature dependence. Still, using sensible extrapolation, seemingly high theoretical fields $10^6 - 10^7$ Vcm^{-1} (in comparison to typically measurements at $T > 0$ with $E_{th} \sim 10^3 - 10^4$ Vcm^{-1}) could be reproduced [85]. However, the most recent experiment applying THz field on VO_2 films [54] is probably the first to really demonstrate the appropriateness of the tunneling process described within the above theoretical considerations, as confirmed by similarly high threshold field $10^6 - 10^7$ Vcm^{-1}.

Another DMFT study that included the on-site coupling to the thermostat [86] proposed that the dissipation can be crucial for the breakdown mechanism, because it causes Hubbard band edges to leak into the gap. These states can then assist the transition from lower to upper Hubbard band, which supposedly leads to a different dependence of the threshold field on the Mott-Hubbard gap, $F_{th} \sim \Delta$. However, one should note that a similar dependence on the gap was obtained also in the already mentioned DMFT study [82] without the thermostat, from a quasi-stationary current and actually agrees with the generalized Landau-Zener expression, which at large U actually shows approximately $F_{th} \sim \Delta$ dependence as well. Further DMFT studies, which focus on the effect of the Joule heating, showed that much smaller fields, $F \sim 10^{-3}U$, can cause metal-to-insulator transition or coexistence of both phases. Such fields are actually closer to the measured ones, yet their effects seem to be opposite to what is expected, since higher field can lead to transition into insulating phase, which might be a DMFT related result. Still, a possible coexistence of phases might be an important signature for some experimental realizations, as explained in the following.

Already in experiments on cuprate chains [45], the switching into a low-resistive state appeared with a delay time of $10 - 1000$ ms, suggesting that it may be due to the formation of conductive domains that expand in a percolation process. Importance of the latter process was stressed in the theory that accompanied experiments on $GaTa_4Se_{8-x}Te_x$ [47] where the breakdown process was modeled with a resistive network of cells, being either in the insulating or the metallic state with corresponding resistance and energy. Since the voltage drop on insulating cells depends on the fraction of metallic ones, even a thermal activation of some cell can cause an avalanche and a consequent overall metallic response. Reproducing the experimental results for $GaTa_4Se_{8-x}Te_x$ scenario seems plausible, however, one should probably carefully study the effect of the temperature and the Mott-Hubbard gap on the ini-

tial activation. Since addressed materials have narrow gaps such mechanism might be appropriate for them, but not for other Mott insulators with larger gaps, where thermal activation could be highly suppressed, possibly allowing the 'Landau-Zener' tunneling process. Also from this aspect the experimental results on VO_2 [54] are different, since transition happens much faster, within the resolution time of $100fs$, ruling out the resistive switching.

1.3.2 Charge recombination

As mentioned already in the experimental Sec. 1.2, there exist some theoretical studies that examined the charge recombination in different set-ups.

The problem of doublon decay has been addressed in the Bose-Hubbard [67] and the Fermi-Hubbard model [64, 65] in connection with ultracold gases in optical lattices using the diagrammatic approach, revealing an exponential dependence of the decay rate on the onsite repulsion U. Since in the latter case charge densities are quite high, the dominant mechanism relies on energy transfer to the kinetic energy of other particles. The decay of double occupancy was considered also within the excited half filled Hubbard model via the time-dependent single-site DMFT [28, 66], confirming similar dependence on U that suggests the same recombination mechanism. One should note that besides being at rather high effective temperatures T, by construction the single-site DMFT method does not incorporate non-local spin fluctuations. Recombination of a holon-doublon pair into spin excitations at low and high temperatures was addressed within the nth order perturbation theory [87], however, possible correlations between holon and doublon were neglected, since the prime interest was actually the decay of unpaired fermions in attractive Hubbard model.

The exciton recombination has been theoretically addressed also for the case of carbon nanotubes [41]. Proposed mechanisms and importance of initial conditions resemble several points discussed for Mott insulators. Authors examined the decay of free-excitons, trapped (localized) excitons, and excitons in doped nanotubes, concluding that the multi-phonon emission is inefficient in the case of free excitons, however, can reproduce measured decay times assuming localized excitons. The enhancement of the decay rate for localized excitons is due to a larger exciton-phonon matrix element and a stronger effective exciton-phonon coupling. For doped nanotubes the multi-phonon decay is subdominant in comparison to the purely electronic (Auger-type) one, where the decay of the exciton is accompanied by the creation of an electron-hole pair in the valence band.

1.3.3 Broader view

Thermalization

Besides the actual time-dependent phenomena, it is worthwhile to focus on the state of the system in the long-time limit per se [88]. When addressing the so called *thermalization* one essentially asks whether system is able to erase the memory of its initial state, if excited well enough that it has non-zero energy density relative to the ground state. Since this is typically examined with unitary evolution in closed systems, thermalization is actually associated with spreading of the quantum entanglement, which at long times makes the information of the initial state inaccessible.

Quite remarkably but also naturally, this process, in which build up of fluctuations characteristic for equilibrium is of essential importance, can be described by classical hydrodynamics [89]. Putting the procedure in a more formal language; if we split the system in the subsystem A with few degrees of freedom and the remaining part B, B can be behave as a reservoir for A. If the system thermalizes, the reduced density matrix for A, $\rho_A(t) = Tr_B\{\rho(t)\}$, when averaged over long times should be equal to the thermal $\rho_A^{(eq)}(T)$, characterized by the temperature T (if energy is the only conserved quantity). Tempting due to its generality, the *eigenstate thermalization hypothesis* (ETH) says that if for an arbitrary initial state the subsystem A thermalizes to $\rho_A^{(eq)}(T)$ at some chosen temperature T, then all many body eigenstates are thermal [90, 91]. A lot of theoretical effort has been dedicated to test this hypothesis, searching for the conditions at which it fails, in some cases raising doubts in its generality. Two classes of systems where the (Boltzmann-type of) thermalization and also the ETH fail are non-ergodic systems, e.g. due to the integrability or the disorder. Integrable systems are exceptional due to infinitely many extensive conserved quantities that are sum of local and possibly even quasi-local operators [92]. The long-time average of the density matrix is subsequently not characterized only by the temperature, but with a set of conserved quantities, captured within the so called *generalized Gibbs ensemble* (GGE) [93]. The generality of such a description was vastly tested by performing *quantum quenches* [94], typically supporting the original formulation of GGE, yet sometimes with deviations that showed on its necessary extension [92, 95, 96]. However, integrable models are in a way special and not robust to the perturbation on the Hamiltonian [97, 98].

The other class of systems that does not show thermalization and therefore violated the ETH, so called *many-body localized systems* [99, 100], seems to be in this sense much more robust. Basically, the reasoning is that at a sufficient disorder any highly-excited strongly interacting state cannot mix with other states due to (with localization) exponentially suppressed overlap among them. The quantum phase transition between the localized and the delocalized phase cannot be studied with usual statistical mechanical ensembles since they average over many eigenstate, however, it has been tackled by a real space renormalization group method, illuminating the nature of the critical point and of (de)localized states near the transition [101, 102]. Relating back to the characterization of the thermalization in the previous paragraph, the entanglement at the transition and in the localized phase was shown to grow slower (as $\sim \log t$) than in delocalized systems.

Many systems show an additional stage, named *prethermalization* [103], before the actual thermalization. The origin of this stage is still under discussion. Vaguely and generally speaking, it should be related with the timescale needed for the system to become its own bath, with the initial coherence scrambled. Examples where it typically appears are nearly-integrable systems [98, 104, 105], systems with different energy scales where only part of the system thermalizes [106], systems near the many-body localization transition [107], and even in higher-dimensional systems [108, 109, 110]. It is particularly interesting to pin down different regimes in terms of thermal critical points and nonthermal fixed points [110], possibly looking for the fingerprints of the dynamic phase transition on the excitations generated in the quench [111]. Remarkably, the role of nonequilibrium instabilities for the process of the thermalization was treated also in the relation with the early universe cosmology [112], pointing out that scaling solutions in the vicinity of the nonthermal fixed

point govern the nonequilibrium dynamics only if classical-statistical fluctuations dominate. Since nonthermal fixed points are unstable with respect to quantum corrections, these eventually lead to thermalization.

Open driven systems

Far from equilibrium dynamics can be initiated also by applying external chemical or thermal bias [113, 114]. Following an initial transient, the nonequilibrium steady state (NESS) and its (transport) properties are typically of central interest. A possible framework is a hybrid approach of an open system formalism [115, 116], where bulk of the interacting quantum systems is treated fully coherently, being evolved with a unitary Hamiltonian, while the environment acts incoherently as Markovian quantum noise at system's boundaries. Such set-up has triggered reexamination of the integrability of models that are known to be integrable in closed systems and has lead to several analytical solutions [117, 118, 119, 120]. Especially important is the quest to relate the form of the NESS density matrix with integrability structures inherent to the Yang-Baxter equation [121, 122], relating the integrability in open systems in a cleanest way to the one in closed [123]. Within this thesis the interplay between coherent and incoherent dynamics, in addition to strong interactions in the bulk, will be examined and shown to lead to interesting current rectification phenomena [124]. Besides those fundamental question, the role and the impact of the environment onto nonequilibrium experiments is yet to be explored and addressed. Especially in the experiments with cold atoms, where coupling to the environment can be actually controlled by tuning the off-resonant lasers, the effect of atom losses can be considered for systems prepared in many-body localized state [125]. Or just the opposite, one could address the build up of the coherent bulk dynamics by incoherent insertion of external atoms [126]. The steady-state phenomena due to constant external drive can be treated also in closed system, if it possesses degrees of freedom that can act as a bath, e.g. spin or phonon excitations [127, 128, 129, 130], or explicit on-site coupling to a thermostat composed of non-interacting independent electron reservoirs at given temperature and chemical potential [131].

The generality (appreciated)

Even without a focused intention, some of above issues appeared in our studies as well. E.g., within the relaxation of charges prethermalization, rather than full thermalization was observed; the effect of the many-body localization could be observed also in open chain, etc. One of the purposes of this introduction is to show how intertwined the area is, with similar observations, mechanisms, and dependences appearing in different contexts. Therefore it is natural to expect that after the initial expansion of research interests, the time has come when general conclusions from various studies should be recognized and stressed.

Chapter 2

Mott insulator in strong constant external field

When a constant field is applied to a Mott insulator several questions can be posed. Depending on the structure and boundary conditions of the system, one has access to different stages. In a closed system, with no dissipation channel to the environment, a constant field would in principle heat it up due to a constant energy increase, therefore one cannot discuss the true steady state. However, the process of exciting the system from its insulating ground state can still be studied. Even more, it has been shown [82] that charge excitations are actually (Stark) localized by strong fields, so that the only effective contribution to the charge current comes from the charge creation (due to the field). Therefore it is of a great importance to establish the rate at which charged excitations are produces, as a function of e.g. the field and the Mott-Hubbard gap. As long as the presence of already created charges does not influence production process, it should be validly described also by $T = 0$ calculation. On the other hand, to calculate proper steady-state quantities one has to open the system and couple it to the environment that can act as a source and a drain, as typically realized with some leads [83, 84, 132], or we have to introduce some internal dissipation that models coupling of the bulk of the system to some thermostat where energy can be dissipated [86, 128, 131].

In Section 2.1 we calculate the $T = 0$ rate at which ground state (g.s.) of Mott insulator decays due to the presence of a constant electric field, which causes transitions into excited non-insulating states. Problem is accessed from the most controlled limit of the nearly spin polarized system, where all but one spin are turned e.g. up. Despite the simplicity such systems still possesses the crucial Mott-Hubbard ingredient: the insulating g.s. which is due to an on-site Coulomb interaction separated from the excited states with a Mott-Hubbard gap. The absence complicated spin background reduces the problem to a two-particle description; one particle representing the empty site - *holon*, and the other representing the doubly occupied site - *doublon*, corresponding to the effectively charged excitations created by the electric field. Having understanding of this simplest case, spin magnetization is reduced while we track the simple picture of the nearly polarized case for as long as possible. Based on the calculation of the g.s. decay rate for three-dimensional nearly spin-polarized system, it is conjectured that the threshold field has same dependence on Mott-Hubbard gap in any dimension.

In Section 2.2 system is opened at the boundaries and coupled to the environment

via Markovian processes. In addition to a real force due to an external field applied to the bulk, the system is driven also via a pseudo-force due to the bias in Markovian processes at the boundaries. Effect of both drivings is characterized by the steady-state current, extracted from the nonequilibrium steady state density matrix of the corresponding Liouville master equation in the Lindblad form. In this case the bulk of the one-dimensional (1D) system is described with (possibly inhomogeneous) XXZ spin model in transverse magnetic field gradient, which can be via the Wigner-Jordan transformation mapped to a spinless fermion chain in electric field. We develop a systematic asymptotic expansion of the spin/particle current in the limits of large field and/or large interaction. For the latter case the bulk of the system can be actually thought of as a Mott insulator, where the insulating state is represented by spinless fermions occupying every second side. In this language holon (doublon) would be identified with two successive empty (occupied) sites. Besides the highly nonequilibrium conditions, this is another reason why considered problem is related to the rest of the thesis. However, the Hamiltonian for spinless model cannot restrict the number of doublon and holons, therefore analysis cannot be directly related to the holon-doublon production addressed in Sec. 2.1.

Content of this Chapter is reported in Refs. [79, 124].

2.1 Dielectric breakdown of Mott insulators

First we investigate finite 1D systems with L sites and periodic boundary conditions (p.b.c.) at half-filling $N_u+N_d = L$, where $N_{u/d}$ is number of up/down spins. We separately examine sectors with different magnetization $m = S^z/L$, $S^z = (N_u - N_d)/2$. The description developed in 1D is then generalized also to higher dimensional systems and tested explicitly with calculations for three-dimensional bipartite lattice with L sites. Further on we use units $\hbar = e_0 = a_0 = 1$.

2.1.1 One-dimensional nearly spin-polarized system

Let us first consider the problem of a single overturned spin, i.e. $\Delta S^z = L/2 - S^z = 1$. We study the prototype 1D Hubbard model,

$$H = -t\sum_{i,\sigma}(e^{i\phi}c^\dagger_{i+1,\sigma}c_{i\sigma} + \text{H.c}) + U\sum_i n_{i\uparrow}n_{i\downarrow}, \tag{2.1}$$

where $c^\dagger_{i\sigma}, c_{i\sigma}$ are creation (annihilation) operators for electrons with spin $\sigma =\uparrow,\downarrow$ at site i. Further on we put $t = 1$, defining the unit of energy.

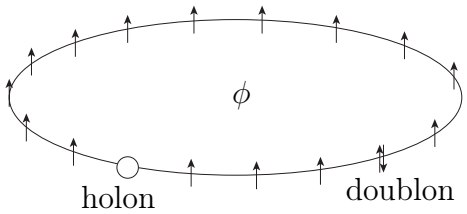

The action of an external electric field F is induced via the Peierls phase ϕ, which is derived from a transformation of creation/annihilation operators, manifested only in the kinetic terms and therefore effectively attributed to the hopping parameter

[30]. The phase ϕ is related to the integral of vector potential between sites i and $i+1$, so that in the case of a homogeneous vector potential its time derivative is set by the electric field, i.e. $\dot{\phi}(\tau) = F(\tau)$. In simple words, electric field is determined by a time-dependent magnetic flux, piercing the ring that represents the system.

In the single overturned spin sector wave functions are naturally expressed in terms of $|\varphi_{jm}\rangle$,

$$|\varphi_{j,m}\rangle = (-1)^j c^\dagger_{m,\downarrow} c_{j,\uparrow} |\tilde{0}\rangle, \quad |\tilde{0}\rangle = \prod_j c^\dagger_{j,\uparrow}|0\rangle, \quad j \in [0, L-1], \tag{2.2}$$

correspond to an empty site (holon) at site j and a doubly occupied site (doublon) at site m. Taking into account the translational symmetry of the model (2.1) with p.b.c. (even with time-dependent $\phi(\tau)$) at given (total) momentum $q = 2\pi m_q/L, m_q \in [0, L-1]$ the relevant basis is

$$|\Psi^l_q\rangle = \frac{1}{\sqrt{L}} \sum_j e^{iqj} |\varphi_{j,j+l}\rangle, \; l \in [0, L-1]. \tag{2.3}$$

At fixed ϕ adiabatic eigenfunctions can be then searched in the form $|n\rangle = \sum_j d^n_j |\Psi^j_q\rangle$, leading to the eigenvalue equation (obtained using the Fourier transform of coefficients, $d^n_j = (1/\sqrt{L}) \sum_k e^{ikj} d^n_k$),

$$-\frac{1}{U} = \frac{1}{L} \sum_{q'} \frac{1}{E_n - U + 2(\cos(q'-\phi) + \cos(q'-\phi-q))}. \tag{2.4}$$

In the limit $L \to \infty$ the g.s. energy E_0 representing the holon-doublon (HD) bound state can be expressed explicitly,

$$E_0 = U - \sqrt{U^2 + 16\cos^2\left(\frac{q}{2}\right)}, \tag{2.5}$$

as derived in App. A.1. We note that (in spite of its q-dependence) the g.s. is non-conducting, since its charge stiffness $\mathcal{D}_0 \propto \partial^2 E_0/\partial\phi^2 \to 0$ for $L \to \infty$. On the other hand, excited states form a continuum with the lower edge (in $L \to \infty$ limit) at $E_1 = U - 4\cos(q/2)$.

Since $\phi(\tau)$ conserves the total q, we further on consider only solutions within the $q = 0$ subspace, representing the absolute g.s. wave function $|0\rangle$ with d^0_j. Here the charge gap $\Delta = E_1 - E_0$ and the related g.s. localization parameter κ are (as derived in App. A.1) given by

$$\begin{aligned} &\Delta = -4 + \sqrt{U^2+16} = 4(\cosh\kappa - 1), \\ &d^0_j = A e^{-\kappa|j|} e^{i\phi j}, \; A = \sqrt{\tanh\kappa}. \end{aligned} \tag{2.6}$$

When we consider the time-dependent $\phi(\tau)$, the full spectra of adiabatic states $E_n(\phi)$, shown in Fig. 2.1 for a finite L, is needed. In the early works on dielectric breakdown of the unpolarized ($m = 0$) Mott insulator [75, 76] it has been suggested that electric field causes transitions from the g.s. to the first excited state, which can be captured within the usual Landau-Zener (LZ) tunneling, giving the transition rate between two states with hyperbolic energy difference. In our case, at finite $L \gg 1/\kappa$ g.s. energy E_0 is essentially ϕ-independent but the same holds as well

for lowest excited states $E_n, n \gtrsim 1$, which makes an usual two-level LZ approach not straightforward to apply. If we suppose that field induced transition probability between successive excited states is high (neglecting finite size gaps between them) excited states are well represented by 'free' holon-doublon (HD) pair states $|k\rangle = \sum_j d_j^k |\Psi_q^j\rangle$ with

$$d_j^k = \frac{e^{ikj}}{\sqrt{L}}, \quad \epsilon_k(\phi) = U - 4\cos(\phi - k), \quad k = \frac{2\pi m_k}{L}. \tag{2.7}$$

In Fig. 2.1 exemplar dispersion for a single k is marked with a solid black line. The actual transition rate between neighboring states can be estimated using LZ formula, suggesting that the approximation with free HD pairs is sensible for small to moderate U. In the large U limit it becomes questionable, since then also dispersions of excited levels get softer. As shown further on, relevant transitions due to time-dependent $\phi(\tau)$ initially happen to effective states $|k\rangle$ with $|m_k| \gg 1$ since the g.s. $|0\rangle$ is well localized, as understood from the simple Heisenberg uncertainty principle.

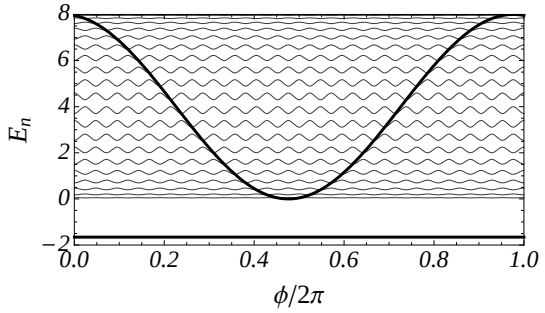

Figure 2.1: Energy levels E_n vs. phase ϕ in the system with $L = 21$ sites and $U = 4$. Thick line represents the g.s. and the effective HD pair state dispersion.

Let us consider the decay of the g.s. $|0\rangle$ after switching on a constant field $F(\tau > 0) = F, \phi = F\tau$. This quantity should be relevant for the initial stage of experiments and might not fully capture the long-time steady state. Let us expand the time-dependent wave function in term of eigenstates, $|\psi(\tau)\rangle = \sum_n a_n(\tau)|n(\phi)\rangle \times \exp(-\int_0^\tau E_n(\tau')d\tau')$. We present an analysis for the initial decay when most of the weight is still within the g.s., i.e., we may assume $|a_0(\tau)| \approx 1 \gg |a_{n\neq 0}(\tau)|$. In such case the excited state amplitude time-dependence $a_n(\tau)$ is given by

$$a_n(\tau) = -F \int_0^\tau d\tau' \Phi_n(\tau') \exp\left(i \int_0^{\tau'} \omega_n(\tau'')d\tau''\right), \tag{2.8}$$

where $\Phi_n = \langle n|\partial/\partial\phi|0\rangle$ and $\omega_n(\tau) = E_n(\phi) - E_0$, as obtained from the Schrödinger equation.

Analytically progress can be made by using effective HD states $|k\rangle$ as approximate excited states with

$$\omega_k(\xi) = \epsilon_k(\xi + k) - E_0 = 4(\cosh\kappa - \cos\xi), \quad \xi = F\tau - k. \tag{2.9}$$

By using the relation

$$\langle k|0\rangle\omega_k = \langle k|H_0 + U - H|0\rangle = U\langle k|n_{0\downarrow}|0\rangle = \frac{UA}{\sqrt{L}}, \tag{2.10}$$

where H_0 denotes only kinetic term in Eq. (2.1), one can express Φ_k in Eq. (2.8) as

$$\Phi_k = \langle k|\frac{\partial}{\partial\phi}|0\rangle = \frac{\partial}{\partial\phi}\langle k|0\rangle = \frac{UA}{\sqrt{L}}\frac{\partial\omega_k^{-1}}{\partial\phi}. \tag{2.11}$$

From this it is clear that the matrix elements Φ_k in Eq. (2.8) do not favor transitions to lowest lying excited state but rather to $|k-\phi| \sim \kappa/\sqrt{3}$, therefore the reduction to a two-level problem of the g.s. and the first excited state, and the simple usage of the LZ formula are not appropriate.

The rate of $a_k(\tau)$ following from Eqs. (2.8), (2.11) is not steady. Since we are interested in low F we average it over the Bloch period $\tau_B = 2\pi/F$ to get $\bar{a} = a_k(\tau_B)$, which is approximately the same for the majority of k (fixing here $k = \pi$),

$$\bar{a} = -\frac{AU}{\sqrt{L}}\int_{-\pi}^{\pi} d\xi \left(\frac{1}{\omega_\pi(\xi)}\right)' \exp\left(\frac{i}{F}\int_{-\pi}^{\xi} d\xi'\omega_\pi(\xi')\right) \tag{2.12}$$

$$\sim \frac{iAU}{F\sqrt{L}}\int_{-\pi}^{\pi} d\xi \exp\left(\frac{i}{F}\int_{-\pi}^{\xi} d\xi'\omega_\pi(\xi')\right), \tag{2.13}$$

after per partes integration of Eq. (2.12) and neglecting the first fast oscillating part, smaller also due to an additional prefactor F. Final simplification for small F can be made by replacing

$$\cosh\kappa - \cos\xi \sim \xi^2/2 + \Delta/4 \tag{2.14}$$

and extending integration in Eq. (2.13) to $\xi = \pm\infty$. Latter replacement and extension of the integration interval are justified with observation that the majority of the transition still happens into the lower part of excited states spectra. This leads to an analytical expression for the decay rate Γ, defined by $|a_0|^2 \sim \exp(-\Gamma\tau)$, where $\Gamma = L|\bar{a}|^2/\tau_B$,

$$\Gamma = \frac{\Delta^{3/2}B(\Delta)}{3\pi F}K^2_{\frac{1}{3}}\left(\frac{\sqrt{2}\Delta^{3/2}}{3F}\right) \sim \frac{B(\Delta)}{\sqrt{8}}\exp\left(-\frac{(2\Delta)^{3/2}}{3F}\right) \tag{2.15}$$

where $K_{1/3}(x)$ is the modified Bessel function and $B(\Delta) = \Delta(\Delta+8)^{3/2}/(\Delta+4)$. The last exponential approximation is valid for small enough Γ and can be obtained also from the saddle point approximation of the integral Eq. (2.12), as derived in App. A.2. The main conclusion of the analysis is that Γ in Eq. (2.15) depends on $\Delta^{3/2}/F$, unlike the usual LZ theory predictions [75, 76] yielding Δ^2/F. Because the threshold field is usually defined with the expression $\Gamma \propto \exp(-\pi F_{th}/F)$, Eq. (2.15) directly leads to $F_{th} = (2\Delta)^{3/2}/(3\pi)$.

It is straightforward to verify the validity of approximations for $N_d = 1$ via a direct numerical solution of the time-dependent Schrödinger equation (TDSE) with $\phi = F\tau$ within the full basis at $q = 0$ and finite but large $L > 100$. Time dependence of the g.s. weight $|a_0(\tau)|^2$ is presented in Fig. 2.2 for typical case $U = 4$ and different fields $F = 0.2 - 0.5$. Results for the case of an instantaneous switching $F(\tau > 0) = F$ (shown for $F = 0.5$) reveal some oscillations (with the frequency proportional to the gap Δ) but otherwise clear exponential decay with well defined Γ. In order to minimize the fast-switching effect we use in Fig. 2.2 and further on mostly smooth transient [82], i.e., field increases as $F(\tau < 0) = F\exp(3\tau/\tau_B)$ to its final value $F(\tau > 0) = F$.

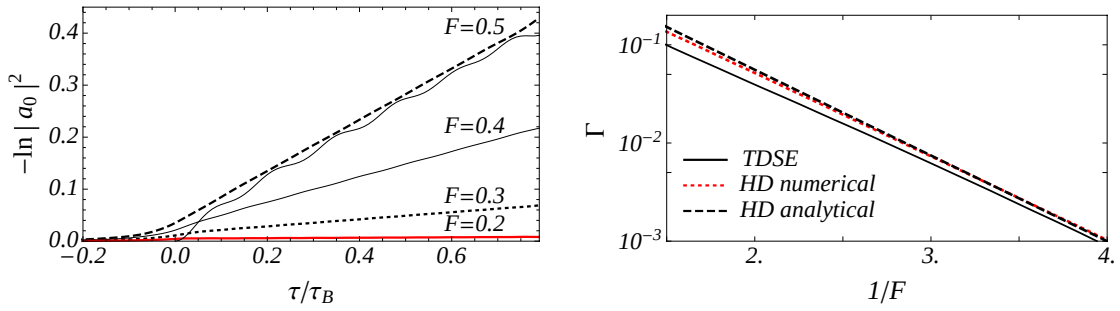

Figure 2.2: Left: Ground state weight $\ln|a_0|^2$ vs. time τ/τ_B for $U = 4$ and different fields $F = 0.2 - 0.5$. For $F = 0.5$ comparison of results for smoothly and instantaneously switched $F(\tau)$ is presented while for $F < 0.5$ only smooth switching is used. Right: Ground state decay rate Γ (log scale) vs. $1/F$ for $U = 4$ as evaluated by direct numerical solution of TDSE (full line), decay into free HD states, numerically integrating Eq. (2.12) (dotted), and analytical expression, Eq. (2.15) (dashed).

In Fig. 2.2 we compare results for Γ as obtained via three different methods: (a) direct numerical solution of TDSE, (b) analytical approximation with an average decay rate into free HD states, numerically integrating Eq. (2.12), and (c) the explicit expression (2.15), where an additional simplification with the parabolic dispersion of excited states is used. The agreement between different methods is satisfactory within the whole regime of small Γ, while deviations between analytical and numerical results become visible only for large $\Gamma \sim 0.1$. Moreover, results confirm the expected variation $\ln\Gamma \propto 1/F$ essentially in the whole investigated range of F.

2.1.2 One-dimensional system with lower spin-polarization

Now we lower the spin magnetization. If different HD pairs in the initial insulating g.s. wave function do not interact much, it seems natural to expect that a similar mechanism of the dielectric breakdown via decay into free HD pairs remains valid at finite $N_d > 1$. In order to test this scenario we perform the numerical solution of TDSE for the model, Eq. (2.1), with a finite field $F(\tau)$. Calculations for all S^z sectors, covering the whole regime $0 \leq m < 1/2$, are performed on finite Hubbard chains with up to $L = 16$ sites. The Lanczos procedure is used for the determination of the initial g.s. wave function $|0\rangle$, as well as for the time integration of the TDSE [133]. The field $F(\tau)$ is turned on in a smooth manner again. The expectation that different exponentially localized HD pairs tend to be maximally separated is supported by the most weighted contributions in the g.s. wave function. Since the decay rate of the g.s. weight $|a_0|^2$ is therefore expected to scale with the number of overturned spins N_d, the relevant quantity to follow and compare is $(1/N_d)\ln|a_0|^2(\tau)$.

In Fig. 2.3 we present numerical results for the time dependence of normalized g.s. weight $\ln|a_0|^2/N_d$ as obtained via a direct solution of the TDSE for $L = 16$ within the whole range of magnetizations $1/2 > m \geq 0$ (relevant $1 \leq N_d \leq L/2$) for two cases of $U = 4, 10$, respectively, and the span of appropriate fields F. Examples are chosen such to represent the charge gap (for a single HD pair) being small $\Delta \sim 1.3 < W$ and large $\Delta \sim 6.5 > W$, respectively, relative to the noninteracting

bandwidth $W = 4$. The main conclusion following from Fig. 2.3 is that the g.s.

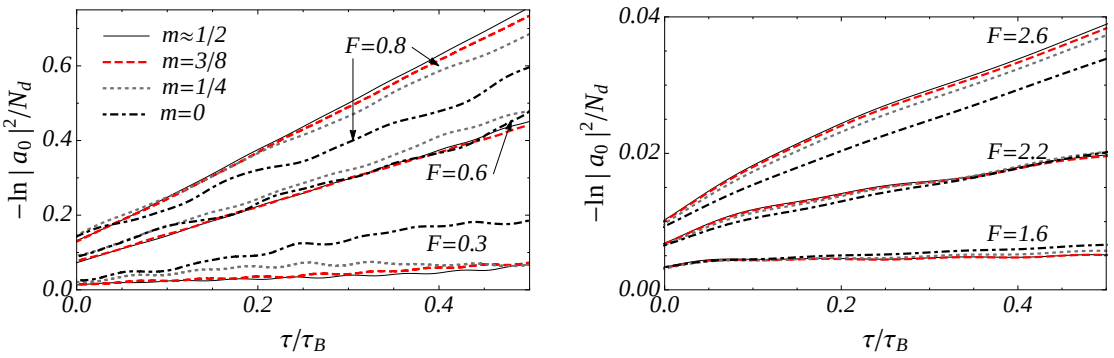

Figure 2.3: Normalized g.s. weight $(1/N_d)\ln|a_0|^2$ vs. time τ/τ_B for left: $U = 4$ and fields $F = 0.3, 0.6, 0.8$, right: $U = 10$ and $F = 1.6, 2.2, 2.6$, for various spin states $1 \leq N_d \leq L/2$.

weight $|a_0|^2$ indeed decays proportional to N_d, confirming the basic mechanism of the field-induced creation of (nearly independent) HD pairs. The decay rate Γ, defined as $|a_0|^2 \propto \exp(-\Gamma N_d\ \tau)$ is essentially independent of N_d in well polarized systems with $m \geq 1/4$. At least for the latter magnetization range the single overturned spin result is well applicable. For larger $U = 10$, which corresponds to stronger localization of HD pairs within the g.s. (as characterized by κ), the invariance of Γ extends even to lower polarizations. There are some visible deviations at $m \leq 1/4$ for smaller $U = 4$, indicating on larger Γ and correspondingly faster decay of unpolarized g.s. with $m = 0$ relative to nearly saturated $m \sim 1/2$. Part of the deviation in Γ can be attributed to the dependence of the charge gap on the magnetization $\Delta(m)$. The thermodynamic ($L \to \infty$) value $\Delta_0 = \Delta(m = 0)$ is known via the Bethe Ansatz solution

$$\Delta_0 = \frac{16}{U}\int_1^\infty \frac{dx\ \sqrt{x^2-1}}{\sinh(2\pi x/U)} \tag{2.16}$$

[7, 134], while values for $\Delta(m \sim 1/2)$, given by Eq. (2.6), are somewhat larger than Δ_0 with the relative difference becoming more pronounced for $U < 4$.

Finally let us consider the threshold field for the decay F_{th}, defined by $\Gamma \propto \exp(-\pi F_{th}/F)$. In Fig. 2.4 we present results for F_{th} as function of the gap Δ. To extract it we use numerical data for $\Gamma(F)$, obtained from numerical $|a_0|^2(\tau)$. As the reference charge gap, $\Delta(m \sim 1/2)$ is used for $m \sim 1/2$ and $m = 1/4$, while $\Delta(m = 0) = \Delta_0$. Some deviation between $m \sim 1/2$ and $m = 1/4$ results can be attributed to actually slightly smaller gap for the latter magnetization. For comparison we plot also the analytical result emerging from Eq. (2.15), $F_{th} \propto \Delta^{3/2}$, as well as the dependence following from the LZ approach [75, 76] with $F_{th} = \Delta^2/8$. We notice that by increasing Δ (or equivalently U) threshold field for $m = 1/4$ approaches $m \approx 1/2$ result. This agrees with the picture where by increasing U the g.s. HD pairs become more localized and consequently decay independently of neighboring pairs. On the other hand, in this limit of the nearly polarized system the approximation of excited states with free HD pairs, Eq. (2.7), becomes less appropriate, as seen in deviation of HD curve from the $m \approx 1/2$ points. A general observation would be correlations due to finite concentration of N_d/L enhance the

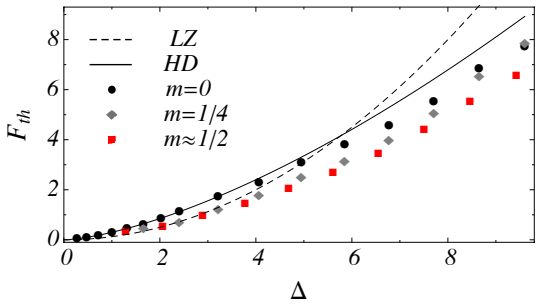

Figure 2.4: Threshold field F_{th} vs. charge gap Δ for different magnetizations $m \sim 1/2$ (given by $N_d = 1$) and $m = 1/4, 0$ as obtained numerically for $L = 16$. Full curve (HD) represent the analytical approximation, Eq. (2.15), while the dashed curve is the LZ approach result from Ref. [76].

decay. It is important to note, that standard Landau-Zener dependence agrees with the numerically establish F_{th} at $m = 0$ only up to some Δ. A more general dependence based on Bethe ansatz which resolved this problems has been obtained in Refs. [27, 78].

An important simple message, conveyed by Oka [27], is that the threshold field should be approximately $F_{th} \approx \Delta/2\xi$, where ξ is the HD correlation length for the g.s.. Relation is based on argumentation that to create a free holon-doublon pair (with an energy Δ above the g.s.), the field has to cause tunneling of electron over the distance ξ on which holon and doublon are bound. The nearly-polarized limit is again the simplest to check this scenario, where $\xi \approx \kappa^{-1}$. Approximately relating κ and Δ through Eq. (2.6) as $\kappa \approx \sqrt{\Delta/2}$, the same scaling of the threshold field $F_{th} \sim \Delta^{3/2}$ is obtained again.

2.1.3 More dimensional nearly spin-polarized system

In the following we show that even higher-dimensional nearly spin-polarized systems follow the same breakdown mechanism and exhibit similar decay rate of the corresponding g.s. as the one-dimensional case. Seemingly artificial, the result could serve as a non-trivial test for higher-dimensional numerical methods, e.g. tDMFT. When increasing the dimension of the bipartite lattice, one should be aware that for $d \geq 3$ there exist a critical interaction U_c below which there is no HD bound state. One way to see it is that when written in terms of the energy and the density of states, integral in Eq. (2.4) diverges only for $d = 1, 2$ so that consequently any U yields solutions that define the gap.

For a general dimension the Peierls phase that introduces electric field $\mathbf{F}(\tau) = -\partial_\tau \mathbf{A}(\tau)$ has to be written more carefully, however, Hamiltonian is still of the same form

$$H = -\sum_{i,j,\sigma} t_{ji}(\tau)\, c^\dagger_{j\sigma} c_{i\sigma} + U \sum_i n_{i\uparrow} n_{i\downarrow}, \quad t_{ji}(\tau) = t \exp\left(-i(\mathbf{R}_j - \mathbf{R}_i)\cdot \mathbf{A}(\tau)\right), \quad (2.17)$$

where i, j, are nearest neighbor (n.n.) sites and $\mathbf{R}_j$ coordinate of the electron labeled by j. For a system with p.b.c. the total momentum $\mathbf{q}$ remains a good quantum

number, defining the basis $|\Psi_{\mathbf{q}}^{\mathbf{R}_l}\rangle$,

$$|\Psi_{\mathbf{q}}^{\mathbf{R}_l}\rangle = \frac{1}{L^{1/2}} \sum_j e^{i\mathbf{q}\cdot\mathbf{R}_j} |\tilde{\varphi}_{j,j+l}\rangle, \quad |\tilde{\varphi}_{j,m}\rangle = c^\dagger_{m,\downarrow} c_{j,\uparrow} |\tilde{0}\rangle, \quad |\tilde{0}\rangle = \prod_j c^\dagger_{j,\uparrow} |0\rangle, \tag{2.18}$$

where L is the number of all sites. To avoid any ambiguity on the hopping sign we redefine the wave functions $|\tilde{\varphi}_{j,m}\rangle$ as well. Application of Hamiltonian on such basis leads to the eigenvalue equation

$$-\frac{1}{U} = \frac{1}{L} \sum_{\mathbf{q}'} \frac{1}{E_n - U + 2\sum_m [\cos(\mathbf{e}_m \cdot (\mathbf{A} + \mathbf{q}')) - \cos(\mathbf{e}_m \cdot (\mathbf{A} - \mathbf{q} + \mathbf{q}'))]}, \tag{2.19}$$

where $\mathbf{e}_m$ is the basis vector in the m direction. For such choice the lowest excited state and the g.s. have minimal energy at total momentum $\mathbf{q} = \{\pi, \pi, \dots\}$.

The g.s. wave function can be for a general dimension d approximated by

$$d^0_{\mathbf{R}_j} = \begin{cases} B \frac{e^{-\kappa|\mathbf{R}_j| - i\mathbf{A}\cdot\mathbf{R}_j}}{|\mathbf{R}_j|^{(d-1)/2}} & \text{for } j \neq 0, \\ A & \text{for } j = 0, \end{cases}$$

where $2\kappa^2 \approx \Delta$ for $U \gtrsim U_c$, see App. A.3.

Excited states are as in $d = 1$ approximated by the free HD pair, characterized with the relative momentum $\mathbf{k}$, with time-dependent energy and wave function coefficients

$$\epsilon_{\mathbf{k}} = U - 4 \sum_m \cos(\mathbf{e}_m \cdot (\mathbf{A}(t) + \mathbf{k})), \quad d^{\mathbf{k}}_{\mathbf{R}_j} = e^{i\mathbf{k}\cdot\mathbf{R}_j}/L^{1/2}. \tag{2.20}$$

Unlike in $d = 1$ case, all effective levels for $d > 1$ do not have the same minimal energy difference with respect to the g.s., $\min(\epsilon_{\mathbf{k}} - E_0) = \Delta_{\mathbf{k}}$. To estimate the full transition rate we sum over all possible $\mathbf{k}$, using the results from $d = 1$ for the transition rate at a particular $\mathbf{k}$,

$$|a_{\mathbf{k}}|^2(\tau_B) \approx \frac{A^2 U^2}{L} \frac{\tau_B}{\sqrt{8\Delta_{\mathbf{k}}}} \exp\left(-\frac{2\sqrt{2}\Delta_{\mathbf{k}}^{3/2}}{3F}\right) \tag{2.21}$$

Since most of the transition from the g.s. is into the lower part of the excited states band, it can be approximated as

$$\Delta_{\mathbf{k}} = \Delta + 4 \sum_m{}' \cos(\mathbf{k} \cdot \tilde{\mathbf{e}}_m) \approx \Delta + 2 \sum_m{}' (\mathbf{k} \cdot \tilde{\mathbf{e}}_m)^2 = \Delta + 2k_\perp^2, \tag{2.22}$$

where $\sum'$ indicates that we sum only over directions $\tilde{\mathbf{e}}_m$ perpendicular to $\mathbf{A}$. For $d = 3$ calculation of Γ can be done analytically. If we introduce an integral cutoff

k^*, then

$$\Gamma = \sum_{\mathbf{k}} \frac{|a_{\mathbf{k}}|^2}{\tau_B} \approx \frac{A^2U^2}{\sqrt{8}} \int_0^{k^*} \frac{2\pi k_\perp dk_\perp}{(2\pi)^2} \frac{\exp(-2\sqrt{2}(\Delta + 2k_\perp^2)^{3/2}/3F)}{\sqrt{\Delta + 2k_\perp^2}} \tag{2.23}$$

$$= \frac{A^2U^2F^{1/3}}{16\pi 3^{2/3}} \left[\Gamma_{1/3}\left(\frac{2\sqrt{2}\Delta^{3/2}}{3F}\right) - \Gamma_{1/3}\left(\frac{2\sqrt{2}(2k^{*2}+\Delta)^{3/2}}{3F}\right)\right] \tag{2.24}$$

$$\approx \frac{A^2U^2F^{1/3}}{16\pi 3^{2/3}} \Gamma_{1/3}\left(\frac{2\sqrt{2}\Delta^{3/2}}{3F}\right) \tag{2.25}$$

$$\approx \frac{A^2U^2F}{32\pi\Delta} \exp\left(-\frac{2\sqrt{2}\Delta^{3/2}}{3F}\right) \tag{2.26}$$

where $\Gamma_{1/3}(x)$ is the incomplete gamma function. The second term from the integration can be neglected. Notably, practically the same dependence of the decay rate Γ on the Mott-Hubbard gap Δ is obtained for $d = 1$ and $d = 3$, which suggest it could be universal for any d.

Fig. 2.5 compares the decay rate Γ as a function of the field strength F obtained numerically (lines) and from Eq. (2.25) (points) for $d = 3$ at different interactions $U = 10, 12, 14$. At least the threshold field at which decay rate becomes substantial is well captures.

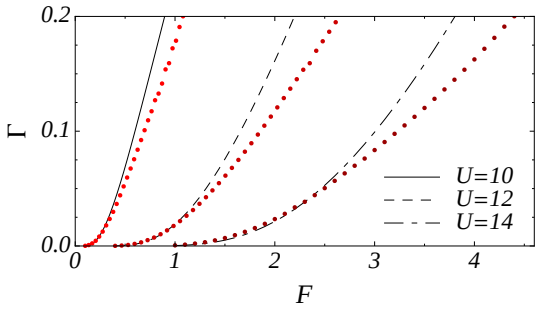

Figure 2.5: Comparison of the decay rate Γ as a function of the field strength F obtained numerically (lines) and from Eq. (2.25) (points) for three-dimensional systems at different interactions $U = 10, 12, 14$.

2.1.4 Insight into equilibrium insulator to metal transition

We should briefly note that the exact single holon-doublon pair result for the Mott-Hubbard gap Δ, obtained in the nearly-polarized limit, yields a novel insight also into the nature of the equilibrium metal-to-insulator (MIT) transition [135]. In Fig. 2.6 we plot the Mott-Hubbard (charge) gap for the nearly polarized and the non-polarized 1D, but also 2D triangular lattice (chosen due to their frustrated nature that suppresses the spin ordering). For 1D both results are known exactly, Eqs. (2.6,2.16), while for 2D triangular lattice they are obtained from an appropriate eigenvalue equation (2.19) in the nearly-polarized system and from the diagonalization of finite systems with up to $L = 16$ sites within the Lanczos basis for the non-polarized one [135].

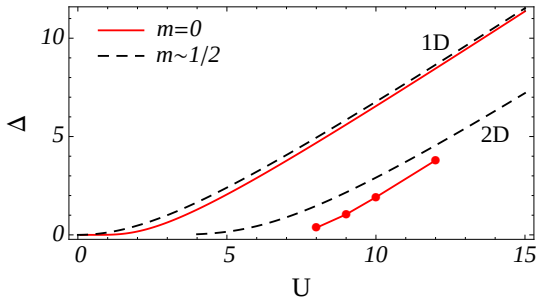

Figure 2.6: Δ vs. U for 1D chain and 2D triangular lattice, calculated for nearly polarized and non-polarized system.

Our main point is that the MIT transition can be motivated through the holon-doublon binding, most transparently studied in the nearly-polarized system. If the on-site interaction U is strong enough, it binds a holon and a doublon into a state, exponentially localized on an area determined by the interaction strength. At weak interactions, when binding is not sufficient, a collective behavior of holons and doublons can win over it, resulting in a metallic phase. In $d = 1, 2$ dimensions the binding of a single HD pair is always non-zero, showing only a pretty sharp crossover in Δ vs. U behavior, while a critical U_c strictly speaking exist only for $d \geq 3$. Numerical results on 2D triangular lattice on the other hand suggest discontinuous transition with a critical U_c. However, qualitative similarity of the charge gap Δ in different magnetization sectors supports our proposal that the physics of a single holon-doublon pair contains the essence of the behavior at any magnetization.

2.2 Boundary driven dissipative quantum chains in large external fields

In the following we address the dynamics of a system effectively coupled to the environment through incoherent Markovian quantum dissipation. Within the theory of open quantum systems [116] the evolution of system's density operator $\rho(t)$ is governed by the Lindblad-Gorini-Kossakowski-Sudarchain master equation [136, 137]

$$\frac{d}{dt}\rho(t) = \hat{\mathcal{L}}\rho(t) := -i[H, \rho(t)] + \sum_k \left(2L_k\rho(t)L_k^\dagger - \{L_k^\dagger L_k, \rho(t)\}\right), \tag{2.27}$$

where H determines the unitary part of the evolution, while dissipation is included through so called Lindblad operators L_k. Eq. (2.27) defines a general family of Markovian dynamical semigroups $\hat{\mathcal{U}}(t) = \exp(t\hat{\mathcal{L}})$, $\hat{\mathcal{U}}(t)\hat{\mathcal{U}}(t') = \hat{\mathcal{U}}(t+t'), t, t' \in \mathbb{R}^+$, which at all times preserve hermiticity, positivity and trace of the density matrix $\rho(t)$.

The general form (2.27) can be derived from the Hamiltonian dynamics of the total system, however, a physically clearer interpretation and structure of H and L_k are obtained under the following approximations [116]:

(i) *The weak-coupling (Born) approximation* assumes that influence of the system on the environment is small, so that the environment's density operator ρ_B is negligibly affected by the interaction, meaning we can factorize the density operator of the total system ρ_T as $\rho_T(t) = \rho(t) \otimes \rho_B$.

(ii) *Markov approximation* assumes that environmental excitations and correlations decay fast, over times τ_B which are not resolved. If τ_R is the scale over which system varies appreciably, then $\tau_R \gg \tau_B$ has to be obeyed. This approximation makes otherwise complicated integro-differential master equation local in time. One should note that a fast decay of correlations is physically possible only if the environment has a continuum of frequencies.

(iii) *Rotating wave (or secular) approximation* states that if the timescale of the intrinsic evolution of the system $\tau_S \sim |\omega - \omega'|^{-1}$ (set by the typical energy difference in the spectra of system's Hamiltonian) is much larger compare to the relaxation time τ_R of open system, $\tau_S \gg \tau_R$, then the fast oscillating terms in master equation that are proportional to $e^{i(\omega-\omega')t}$ can be neglected for $\omega \neq \omega'$, so that master equation finally obtains the Lindblad form (2.27).

Strictly speaking, H is not only the system's Hamiltonian since in principle it should be shifted by the so called Lamb shift Hamiltonian which causes renomalization of the unperturbed energy levels, induced by the system-reservoir coupling [116], however, we shall neglect this effect.

Besides, in our consideration the incoherent quantum processes described by L_k will have ultra-local nature, i.e., acting nontrivially either on the left or the right boundary of the chain. Microscopically are such terms justified in cases with on-site part of the Hamiltonian much larger than the one that yields interaction between sites, since then e.g. the local spin disturbance does not propagate into the system before being dissipated. An alternative phenomenological description of ultra-local

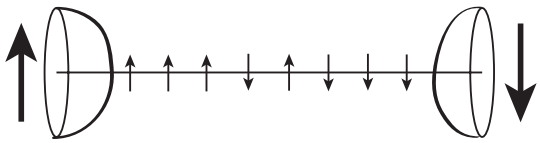

Figure 2.7: Illustration of open spin chain with a dissipative boundary driving.

dissipators can be obtained also in the frame of the repeated interactions protocol [138], which assumes that for a short time δt the end spin/particle is in contact with auxiliary spins/particles prepared in a thermal state. In the next step δt the auxiliary spins are replaced by fresh ones, as if prepared in a thermal state that does not remember the effect of the interaction in the previous step. In the limit $\delta t \to 0$ the original form (2.27) is recovered.

2.2.1 Quantum transport in boundary and field driven spin chain

We consider an open inhomogeneous XXZ spin 1/2 chain exposed to an additional magnetic field, so that the bulk of the system is governed by the Hamiltonian $H = H_{xxz} + V$,

$$H_{xxz} = H_{xx} + H_z, \quad H_{xx} = \sum_{j=1}^{n-1} 2\alpha_j(\sigma_j^+\sigma_{j+1}^- + \sigma_j^-\sigma_{j+1}^+), \quad H_z = \sum_{j=1}^{n-1} \Delta_j \sigma_j^z \sigma_{j+1}^z,$$

$$V = \sum_{j=1}^{n} f_j \sigma_j^z. \tag{2.28}$$

where parameters α_j, Δ_j may be site dependent. For the homogeneous case $\alpha_j = 1, \Delta_j = \Delta$ will be used. Note that in this section Δ is exceptionally used for the anisotropy parameter and not for the Mott-Hubbard gap. f_j determine the profile of the magnetic field. Using Wigner-Jordan transformation the problem can be mapped to spinless fermion chain where α_j map to free hopping amplitudes, Δ_j to interactions and f_j to electric potential. Density matrix of the system ρ may be described using the Liouville master equation in the Lindblad form, Eq. (2.27),

$$\frac{d\rho(t)}{dt} = \hat{\mathcal{L}}\rho := -i[H, \rho(t)] + \hat{\mathcal{D}}\rho, \tag{2.29}$$

where $\hat{\mathcal{D}}\rho = \sum_k 2L_k\rho(t)L_k^\dagger - \{L_k^\dagger L_k, \rho(t)\}$ now describes coupling to the bath at the edges. Here, only the extreme case of pure source/sink on the left/right end,

$$L_1 = \sqrt{\varepsilon}\sigma_1^+, \; L_2 = \sqrt{\varepsilon}\sigma_n^- \tag{2.30}$$

will be considered. We are not interested in the whole relaxation dynamics, but rather in the nonequilibrium steady state (NESS) $\rho_\infty = \lim_{t\to\infty}\rho(t)$, found as the fixed point

$$\hat{\mathcal{L}}\rho_\infty = 0. \tag{2.31}$$

The effect of the driving will be characterized by the spin current from site j to $j+1$

$$J_j = 2i\alpha_j(\sigma_j^+\sigma_{j+1}^- - \sigma_j^-\sigma_{j+1}^+), \tag{2.32}$$

which has to be for the inhomogeneous hopping parameters α_j defined site dependently, so that is in the limit $t \to \infty$, i.e. for NESS, its expectation is site independent, $J = \mathrm{tr}(J_j\rho_\infty)/\,\mathrm{tr}\rho_\infty$.

With the focus on large field or/and large interaction we split the Liouvillian into *diagonal* and *off-diagonal* parts $\hat{\mathcal{L}} = f\hat{\mathcal{L}}_0 + \hat{\mathcal{L}}_1$,

$$\hat{\mathcal{L}}_0\rho = -i[\tilde{V} + \tilde{H}_z, \rho], \quad \hat{\mathcal{L}}_1\rho = -i[H_{xx}, \rho] + \hat{\mathcal{D}}\rho, \tag{2.33}$$

where $\tilde{H}_z = \sum_{j=1}^{n-1} \tilde{\Delta}_j \sigma_j^z \sigma_{j+1}^z$, $\tilde{V} = \sum_{j=1}^{n} \tilde{f}_j \sigma_j^z$ with $\tilde{\Delta}_j \equiv \Delta_j/f$, $\tilde{f}_j \equiv f_j/f$. We consider $1/f$ as a formal small parameter, assuming $f \gg \alpha_j, \varepsilon$. Note that both diagonal generators, V or H_z, need not be large. We may either fix $\tilde{f}_n - \tilde{f}_1 = 1$, in which case f represents the total field/potential drop across the system while $\Delta_j = \mathcal{O}(1)$, or consider the large anisotropy (interaction) asymptotics $\tilde{\Delta}_j = \mathcal{O}(1)$ while $\tilde{f}_j = \mathcal{O}(f^{-1})$. Expanding NESS in powers of f^{-1}, $\rho_\infty = \sum_{p=0}^{\infty} f^{-p}\rho^{(p)}$, different orders are connected with the recurrence relation:

$$\hat{\mathcal{L}}_0\rho^{(p+1)} + \hat{\mathcal{L}}_1\rho^{(p)} = 0, \quad \hat{\mathcal{L}}_0\rho^{(0)} = 0. \tag{2.34}$$

Each order of ρ_∞ can be expanded in terms of a complete Pauli basis $\rho^{(p)} = \sum_{\{s_1,\ldots,s_n\}} M^{(p)}_{s_1,\ldots,s_n} \prod_j \sigma_j^{s_j}$, where $s_j \in \{0, z, +, -\}$, and $\sigma^0 = \mathbb{1}$. Condition for $\rho^{(0)}$ in Eq. (2.34) is satisfied for exponentially many products $\prod_j \sigma_j^{s_j}$ for which the sum $\sum_{j=1}^{n} f_j\xi_{s_j} + \sum_{j=1}^{n-1} \Delta_j \left((\xi_{s_j} + \xi_{s_{j+1}}) \pmod 2\right)$ vanishes, where $\xi_{s_j} = \pm 1$ for $s_j = \pm$ and $\xi_{s_j} = 0$ otherwise. However, exact numerical diagonalization of $\hat{\mathcal{L}}$ on small systems of even size $n \leq 8$ shows that for the strong field or the anisotropy $\rho^{(0)}$ is a diagonal projector

$$\rho^{(0)} = a_0 \prod_{j=1}^{\frac{n}{2}} \frac{1}{2}(\mathbb{1}_j + \sigma_j^z) \prod_{j=\frac{n}{2}+1}^{n} \frac{1}{2}(\mathbb{1}_j - \sigma_j^z) \tag{2.35}$$

with step-like magnetization profile. In the case of the large anisotropy this has already been observed [139] and given physical motivation suitable for our limit as well. Authors argued that the suppression of the current can be explained with the one-magnon spectra of Hamiltonian, i.e. its eigenstates within the sector with all but one spin turned e.g. up. In the case of large $\Delta > 1$ there exist two eigenstates having localized spin excitations on the left or the right boundary. Because these states (most strongly coupled to the bath) have exponentially suppressed tails, also the effect and the communication between source and sink is exponentially suppressed. Therefore only the closer bath is felt by spins in the chain (except in the center of the system), which orient according to it. In the case of large fields the situation is even more extreme, since all eigenstates within this sector consist of (Stark-like) localized one-magnon excitations. Thus, we conjecture that $\rho^{(0)}$ has the form of Eq. (2.35) for a system of arbitrary even length n. If n is odd $\rho^{(0)}$ contains two terms of the form (2.35) with a jump in magnetization between sites $(\frac{n-1}{2}, \frac{n+1}{2})$ or $(\frac{n+1}{2}, \frac{n+3}{2})$. Further on we assume even n, generalizing the solution to arbitrary n at the end of the derivation.

We introduce the following notation for local operators

$$\begin{aligned} &\frac{1}{2}(\mathbb{1} + \sigma^z) \equiv \left(\begin{smallmatrix}\uparrow\\ \uparrow\end{smallmatrix}\right), \quad \sigma^- \equiv \left(\begin{smallmatrix}\downarrow\\ \uparrow\end{smallmatrix}\right), \\ &\frac{1}{2}(\mathbb{1} - \sigma^z) \equiv \left(\begin{smallmatrix}\downarrow\\ \downarrow\end{smallmatrix}\right), \quad \sigma^+ \equiv \left(\begin{smallmatrix}\uparrow\\ \downarrow\end{smallmatrix}\right), \end{aligned} \tag{2.36}$$

i.e., $\binom{\nu}{\mu} \equiv |\nu\rangle\langle\mu|$, $\nu, \mu \in \{\uparrow, \downarrow\}$. E.g., $\rho^{(0)}$ is represented as a single component

$$\rho^{(0)} = a_0 \left(\begin{smallmatrix} \uparrow & \dots & \uparrow \\ \uparrow & \dots & \uparrow \end{smallmatrix} \middle| \begin{smallmatrix} \downarrow & \dots & \downarrow \\ \downarrow & \dots & \downarrow \end{smallmatrix} \right). \tag{2.37}$$

Vertical bar marks the center of the system. It is instructive to think of the effect that different parts of $\hat{\mathcal{L}}$ have on a chosen term $M^{(p)}_{s_1,\dots,s_n} \prod_j \sigma_j^{s_j}$ in such notation. The action of $\hat{\mathcal{L}}_0$ is diagonal, i.e. it does not change the operator product to which it is applied, while unitary part of $\hat{\mathcal{L}}_1$ causes exchange of neighboring pairs if different, $(\uparrow_j\downarrow_{j+1})$ or $(\downarrow_j\uparrow_{j+1})$. Dissipator $\hat{\mathcal{D}}$ is the only process to relate imaginary and real part of coefficients involved in the recurrence relation and is trivial if both μ, ν are aligned with the boundary driving.

Using the recurrence relation (2.34) higher order $\rho^{(p)}$ can be generated from $\rho^{(0)}$. E.g. the first order $\rho^{(1)}$ then consists of

$$\rho^{(1)} = a_1 \left[\left(\begin{smallmatrix} \uparrow & \dots & \uparrow & \downarrow \\ \uparrow & \dots & \uparrow & \uparrow \end{smallmatrix} \middle| \begin{smallmatrix} \uparrow & \downarrow & \dots & \downarrow \\ \downarrow & \downarrow & \dots & \downarrow \end{smallmatrix} \right) + \left(\begin{smallmatrix} \uparrow & \dots & \uparrow & \uparrow \\ \uparrow & \dots & \uparrow & \downarrow \end{smallmatrix} \middle| \begin{smallmatrix} \downarrow & \downarrow & \dots & \downarrow \\ \uparrow & \downarrow & \dots & \downarrow \end{smallmatrix} \right) \right]. \tag{2.38}$$

However, we will not strive to build the whole NESS density matrix, instead we will relate perturbatively only its component relevant for the NESS spin current.

2.2.2 Steady state spin current

We would like to identify the leading order terms in the current $J = \operatorname{tr}(J_j\rho_\infty)/\operatorname{tr}\rho_\infty$. In our diagrammatic notation tr is a sum of coefficients at configurations with the same upper and lower index at each site. Therefore $\operatorname{tr}\rho_\infty = a_0 + \mathcal{O}(f^{-2})$. Similarly, $\operatorname{tr}J_j\rho_\infty$ is a sum over configurations in ρ_∞ with $\sigma_j^{\pm}\sigma_{j+1}^{\mp}$ and $\mathbb{1}_l \pm \sigma_l^z$ elsewhere. Suppose we calculate current from the operator $J_{n/2}$. We will show that then the leading contribution comes from the components with $\mathbb{1}_l + \sigma_l^z$ for $l < n/2$ and $\mathbb{1}_l - \sigma_l^z$ for $l > n/2 + 1$.

We claim that in order to obtain the current from $\operatorname{tr}J_{n/2}\rho_\infty$ up to $\mathcal{O}(f^{-(n+2)})$ only the terms $\tilde{\rho} = \rho^{(0)} + \rho_{1,R} + \rho_{1,L} + \rho_{2,R} + \rho_{2,L}$ in the density matrix are relevant. Expression

$$\begin{aligned}
\rho_{1,R} = {} & \frac{a_1}{2f} \left(\begin{smallmatrix} \uparrow & \dots & \uparrow & \downarrow \\ \uparrow & \dots & \uparrow & \uparrow \end{smallmatrix} \middle| \begin{smallmatrix} \uparrow & \downarrow & \downarrow & \dots & \downarrow \\ \downarrow & \downarrow & \downarrow & \dots & \downarrow \end{smallmatrix} \right) + \frac{ia_n}{f^n} \left(\begin{smallmatrix} \uparrow & \dots & \uparrow & \downarrow \\ \uparrow & \dots & \uparrow & \uparrow \end{smallmatrix} \middle| \begin{smallmatrix} \uparrow & \downarrow & \downarrow & \dots & \downarrow \\ \downarrow & \downarrow & \downarrow & \dots & \downarrow \end{smallmatrix} \right) \\
& 2: \Downarrow \qquad\qquad n: \Uparrow \\
& + \frac{a_2}{f^2} \left(\begin{smallmatrix} \uparrow & \dots & \uparrow & \downarrow \\ \uparrow & \dots & \uparrow & \uparrow \end{smallmatrix} \middle| \begin{smallmatrix} \downarrow & \uparrow & \downarrow & \dots & \downarrow \\ \downarrow & \downarrow & \downarrow & \dots & \downarrow \end{smallmatrix} \right) + \frac{ia_{n-1}}{f^{n-1}} \left(\begin{smallmatrix} \uparrow & \dots & \uparrow & \downarrow \\ \uparrow & \dots & \uparrow & \uparrow \end{smallmatrix} \middle| \begin{smallmatrix} \downarrow & \uparrow & \downarrow & \dots & \downarrow \\ \downarrow & \downarrow & \downarrow & \dots & \downarrow \end{smallmatrix} \right) \\
& 3: \Downarrow \qquad\qquad n-1: \Uparrow \\
& \vdots \qquad\qquad \vdots \\
& \frac{n}{2}: \Downarrow \qquad\qquad \frac{n}{2}+2: \Uparrow \\
& + \frac{a_{\frac{n}{2}}}{f^{\frac{n}{2}}} \left(\begin{smallmatrix} \uparrow & \dots & \uparrow & \downarrow \\ \uparrow & \dots & \uparrow & \uparrow \end{smallmatrix} \middle| \begin{smallmatrix} \downarrow & \downarrow & \dots & \downarrow & \uparrow \\ \downarrow & \downarrow & \dots & \downarrow & \downarrow \end{smallmatrix} \right) + \frac{ia_{\frac{n}{2}+1}}{f^{\frac{n}{2}+1}} \left(\begin{smallmatrix} \uparrow & \dots & \uparrow & \downarrow \\ \uparrow & \dots & \uparrow & \uparrow \end{smallmatrix} \middle| \begin{smallmatrix} \downarrow & \downarrow & \dots & \downarrow & \uparrow \\ \downarrow & \downarrow & \dots & \downarrow & \downarrow \end{smallmatrix} \right) \\
& \hat{\mathcal{D}}: \Rightarrow
\end{aligned}$$

with $a_p \in \mathbb{R}$ introduces a sequence of terms connected by the recurrence relation (2.34), which takes *upper* $\uparrow_{n/2+1}$ in $\rho^{(1)}$ (in *red* color) to the right boundary and back to its initial position. After each step the coefficient involved is for a f^{-1} higher in

expansion, being *real* until the action of $\hat{\mathcal{D}}$ and *imaginary* after. $\rho_{1,L}$ is constructed symmetrically, taking *upper* $\downarrow_{n/2}$ to the left boundary and will be expanded in terms of coefficients b_p with $b_1 = a_1$. Other $\rho_{2,R(L)}$ originate from the second term of $\rho^{(1)}$ in Eq. (2.38) and correspond to shifting *lower* $\uparrow_{n/2+1}$ ($\downarrow_{n/2}$) to the right (left) boundary.

From this construction it is clear that the leading contribution to the current is of order f^{-n}, namely

$$J = -\frac{4\alpha_{\frac{n}{2}}(a_n + b_n)}{f^n\ a_0} + \mathcal{O}(f^{-(n+2)}) \tag{2.39}$$

since real coefficients a_1, b_1 get subtracted, while nth order coefficient in $\rho_{1,R}$ and $\rho_{2,R}$ (equivalently for $\rho_{1,L}$ and $\rho_{2,L}$) are complex conjugated and sum up yielding an additional factor 2 in Eq. (2.39). Any other operator product term having $\sigma^{\pm}_{n/2}\sigma^{\mp}_{n/2+1}$ and projectors $\mathbb{1}_i + \sigma^z_i$ for some $i > n/2+1$ is of higher order in f^{-1} due to obvious additional steps needed to create it from $\rho^{(0)}$. To calculate the spin current we have to express a_n, b_n with a_0. In the procedure each step yields an equation that relates coefficients from the consecutive orders via recurrence (2.34). Explicit relations obtained from $\rho_{1,R}$ are:

Step 1:

$$\begin{aligned} -2i\alpha_{\frac{n}{2}}a_0 + 2i\left(\tilde{\Delta}_{\frac{n}{2}-1} + \tilde{\Delta}_{\frac{n}{2}+1} + \tilde{f}_{\frac{n}{2}} - \tilde{f}_{\frac{n}{2}+1}\right)a_1 = 0 \\ a_1 = \frac{a_0\ \alpha_{\frac{n}{2}}}{\tilde{\Delta}_{\frac{n}{2}-1} + \tilde{\Delta}_{\frac{n}{2}+1} - \tilde{f}_{\frac{n}{2}+1} + \tilde{f}_{\frac{n}{2}}} \end{aligned} \tag{2.40}$$

Step $k,\ 1 < k < n/2$:

$$a_k = \frac{a_{k-1}\ \alpha_{\frac{n}{2}+k-1}}{\tilde{\Delta}_{\frac{n}{2}+k-1} + \tilde{\Delta}_{\frac{n}{2}+k} + \tilde{\Delta}_{\frac{n}{2}-1} - \tilde{\Delta}_{\frac{n}{2}} - \tilde{f}_{\frac{n}{2}+k} + \tilde{f}_{\frac{n}{2}}} \tag{2.41}$$

Step $n/2$:

$$a_{\frac{n}{2}} = \frac{a_{\frac{n}{2}-1}\ \alpha_{n-1}}{\tilde{\Delta}_{n-1} + \tilde{\Delta}_{\frac{n}{2}-1} - \tilde{\Delta}_{\frac{n}{2}} - \tilde{f}_n + \tilde{f}_{\frac{n}{2}}} \tag{2.42}$$

Step $n/2+1$ (action of dissipator $\hat{\mathcal{D}}$):

$$a_{\frac{n}{2}+1} = -\frac{a_{\frac{n}{2}}\ \varepsilon}{2\left[\tilde{\Delta}_{n-1} + \tilde{\Delta}_{\frac{n}{2}-1} - \tilde{\Delta}_{\frac{n}{2}} - \tilde{f}_n + \tilde{f}_{\frac{n}{2}}\right]} \tag{2.43}$$

Step $n/2+1+k, 1 \le k < n/2$:

$$a_{\frac{n}{2}+1+k} = \frac{a_{\frac{n}{2}+k}\ \alpha_{n-k}}{\tilde{\Delta}_{n-k-1} + \tilde{\Delta}_{n-k} + \tilde{\Delta}_{\frac{n}{2}-1} - \tilde{\Delta}_{\frac{n}{2}} - \tilde{f}_{n-k} + \tilde{f}_{\frac{n}{2}}} \tag{2.44}$$

Combining Eqs. (2.40 - 2.44) we finally obtain a_n as a function of a_0 and parameters of the Hamiltonian. b_n is expressed analogously,

$$\frac{a_n}{a_0} = -\frac{\varepsilon\alpha_{n-1}}{2\left(\tilde{\Delta}_{n-1}+\tilde{\Delta}_{\frac{n}{2}-1}-\tilde{\Delta}_{\frac{n}{2}}-\tilde{f}_n+\tilde{f}_{\frac{n}{2}}\right)^2}\prod_{k=1}^{\frac{n}{2}-1}\frac{\alpha_{\frac{n}{2}+k-1}\ \alpha_{\frac{n}{2}+k}}{\left(\tilde{\Delta}_{\frac{n}{2}+k}+\tilde{\Delta}_{\frac{n}{2}+k-1}+\tilde{\Delta}_{\frac{n}{2}-1}-\tilde{\Delta}_{\frac{n}{2}}-\tilde{f}_{\frac{n}{2}+k}+\tilde{f}_{\frac{n}{2}}\right)^2}, \tag{2.45}$$

$$\frac{b_n}{a_0} = -\frac{\varepsilon\alpha_1}{2\left(\tilde{\Delta}_1+\tilde{\Delta}_{\frac{n}{2}+1}-\tilde{\Delta}_{\frac{n}{2}}-\tilde{f}_{\frac{n}{2}+1}+\tilde{f}_1\right)^2}\prod_{k=1}^{\frac{n}{2}-1}\frac{\alpha_{\frac{n}{2}-k+1}\ \alpha_{\frac{n}{2}-k}}{\left(\tilde{\Delta}_{\frac{n}{2}-k}+\tilde{\Delta}_{\frac{n}{2}-k+1}+\tilde{\Delta}_{\frac{n}{2}+1}-\tilde{\Delta}_{\frac{n}{2}}-\tilde{f}_{\frac{n}{2}+1}+\tilde{f}_{\frac{n}{2}-k+1}\right)^2}. \tag{2.46}$$

For a homogeneous chain and field which is odd with respect to the center $f_j = -f_{n+1-j}$ expression for the current simplifies

$$J = \frac{4\varepsilon}{f^n}\ \left(\tilde{\Delta} - \tilde{f}_n + \tilde{f}_{\frac{n}{2}}\right)^{-2} \prod_{k=1}^{\frac{n}{2}-1} \left(2\tilde{\Delta} - \tilde{f}_{\frac{n}{2}+k} + \tilde{f}_{\frac{n}{2}}\right)^{-2}. \tag{2.47}$$

One should note that a shift of $\tilde{f}_j$ for a constant does not change the result. Obtained expression for the current is appropriate for a general inhomogeneous magnetic field, however, in the case of linear field profile $f_j - f_{j-1} \equiv g$ it has especially simple form in terms of a gradient g

$$J = \frac{16\varepsilon}{g^n}\ \left(\frac{2\Delta}{g} - n\right)^{-2} \prod_{k=1}^{\frac{n}{2}-1} \left(\frac{2\Delta}{g} - k\right)^{-2}. \tag{2.48}$$

For systems of odd size n one should consider $J_{(n-1)/2}$ (or $J_{(n+1)/2}$). The leading order contributions originate from the part of $\rho^{(0)}$ with jump in magnetization between sites $(\frac{n-1}{2}, \frac{n+1}{2})$ (or $(\frac{n+1}{2}, \frac{n+3}{2})$). The imaginary coefficient relevant for the current is then obtained as in system of even size $n-1$, having contribution only from the boundary that is closer to the magnetization jump. The current for odd n, homogeneous XXZ chain and field of odd symmetry w.r.t. the center of the system is then simply $J(n) = J(n-1)/4$. For an inhomogeneous chain or non-symmetric monotonic field the two components in $\rho^{(0)}$ have different weights, causing an additional prefactor in the latter equation.

In Fig. 2.8 we compare numerical and analytical results for the spin current J at linear field profile and homogeneous Hamiltonian with $\Delta = 5$ in systems of size $n = 4, 6, 8$. At $n = 4$ we show also an example with inhomogeneous Hamiltonian with parameters $\{\alpha_1, \alpha_2, \alpha_3\} = \{0.1, 0.3, 0.5\}, \{\Delta_1, \Delta_2, \Delta_3\} = \{-2.5, -5, -1\}$. Negative Δ_j are chosen for clarity since $J(-\Delta_j, -f_j) = J(\Delta_j, f_j)$. Evidently, expression (2.48) perfectly captures the dependence $J(g)$ at large enough gradients g and indicates the position of some of the resonances in the numerical result. From the construction of the perturbative solution it is clear that poles in Eqs. (2.45,2.46) appear when at some level of the perturbative hierarchy the action of the diagonal $\hat{\mathcal{L}}_0$ on considered operator product is trivial. Consequently, the hierarchy is disconnected and our expression not valid any more. Additional resonances observed in numerical results originate from other operator products which are annulled by $\hat{\mathcal{L}}_0$ that are not contained in $\tilde{\rho}$. In the resonances the hierarchy within ρ_∞ can be altered in a way that yields a contribution to the current in lower order of f^{-1}. Reordering within ρ_∞ can be motivated by degeneracy of eigenstates of the Hamiltonian H. It turns out that a resonance in the current appears whenever $|0\rangle = |\uparrow_1 \cdots \uparrow_{\frac{n}{2}} \downarrow_{\frac{n}{2}+1} \cdots \downarrow_n\rangle$, which is nearly an eigenstate for large anisotropy or large field, is degenerate with another eigenstate $|i\rangle$ (with less of insulating nature) with boundary spins at least partially compatible with the boundary driving. Such a degeneracy reduces the insulating effect of $|0\rangle\langle 0|$ and promotes $|0\rangle\langle i|, |i\rangle\langle 0|, |i\rangle\langle i|$ in ρ_∞. The range of validity of asymptotic expression (2.48), which is $g \in (-\infty, 0) \cup (g_c, \infty)$ for $\Delta > 0$, is set by the furthest resonance, yielding a critical gradient $g_c = 2\Delta$.

Our analysis can be used also to reveal the large anisotropy asymptotics at vanishing external fields by setting $\Delta_j = f\tilde{\Delta}_j, f_j = 0$ in Eqs. (2.45,2.46), yielding for the homogeneous XXZ chain $J = \varepsilon\ 2^{-\gamma}\Delta^{-n},\ \gamma = n^2/4 - n/2 - 2$ for even n

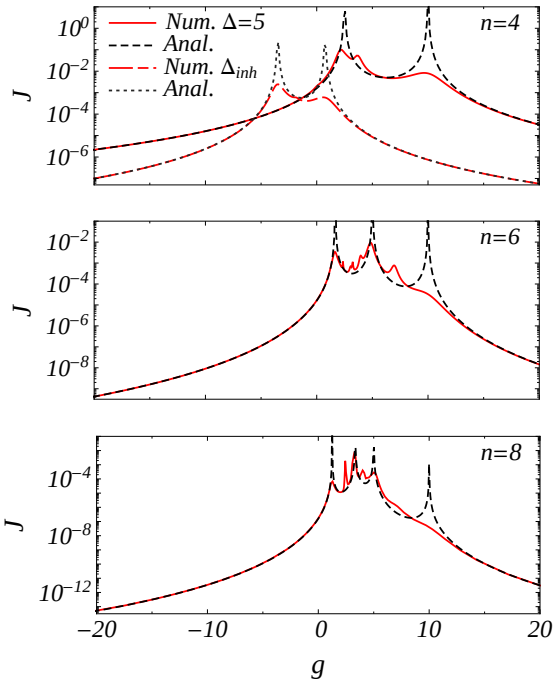

Figure 2.8: Spin current J as a function of gradient g for linear field profile and anisotropy $\Delta = 5$ and $\varepsilon = 1$ in systems of size $n = 4, 6, 8$ obtained numerically (num) and from Eq. (2.48) (ana). Curve at $n = 4$ labeled by Δ_{inh} shows same comparison for an inhomogeneous chain with parameters given in the text.

and $J = \varepsilon\ 2^{-\delta}\Delta^{-(n-1)}$, $\delta = (n-1)^2/4 - (n-1)/2$ for odd n, as noted numerically in [139].

2.2.3 Flux rectification

Asymmetry of the driving is revealed by changing the direction of the driving force, $f \to -f$, resulting in $J(f) \neq J(-f)$. Rectifying behavior is conveniently quantified by the rectification coefficient [140]

$$R = \frac{J(f) - J(-f)}{J(f) + J(-f)}, \tag{2.49}$$

which is zero in case of no rectification and reaches extreme values ± 1 when the system for fields in one direction behaves as a perfect insulator.

For gradients above the critical value the rectification coefficient R can be calculated for any system size n using the current asymptotics (2.45-2.48). In Fig. 2.9 we plot the dependence of R on the system size n (even only) for a homogeneous chain and linear field profile at three different gradients, $g = 3\Delta, 5\Delta, 10\Delta$. Circles correspond to exact results for small systems. Our results clearly show that in the thermodynamic limit R reaches the extreme value $\lim_{n\to\infty} R = \mathrm{sgn}(\Delta)$, corresponding to insulating behavior for gradients of opposite sign than anisotropy Δ.

Therefore we can point out two mechanisms for enhancing current rectification: (i) rectification coefficient $R \to 1$ in thermodynamic limit $n \to \infty$, at fixed large

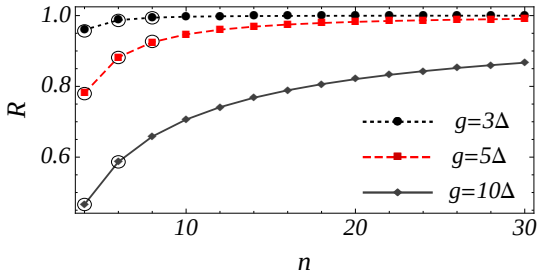

Figure 2.9: Dependence of the flux rectification R on system size n for $\Delta > 0, \varepsilon = 1$ and gradients $g = 3\Delta, 5\Delta, 10\Delta$ obtained from Eqs. (2.49,2.48). Circles correspond to exact numerics for small systems.

gradient $f/(n-1)$, for any nonzero anisotropy/interaction $\Delta \neq 0$, as a result of our asymptotic current formula; (ii) for resonant field (gradient) values where our asymptotic analysis fails, the current is of higher order in $1/f$ for one direction of the field f than in the other. This clearly yields rectification coefficient $R \to 1$ even at fixed finite size n. Note that there is no rectification effect in noninteracting chains $\Delta = 0$, in agreement with [140].

From this we can conclude that applying an inhomogeneous magnetic field is a convenient way to introduce asymmetry into the spin chain, since the spin current is obviously sensitive to the sign of the gradient of the magnetic field, $J(-g) \neq J(g)$. Let us try to illuminate the observed asymmetry. Assuming $\Delta_j < 0$, when the interaction prefers aligned spins, the magnetic field with $g > 0$ dictates the same orientation of spins as the Lindblad driving, resulting in an enhanced insulating behavior of NESS. If $g < 0$ their effects are contrary, manifested in the enlarged spin current. Returning back to the eigenstates of H in the bulk of the system; if the field and the boundary driving try to align spins in the same manner, for $\Delta_j < 0$ the insulating state with step-like magnetization (compatible with source/sink) will not be degenerate with any other eigenstate of H at arbitrary field strength. By reversing the field or the boundary driving, degeneracies become possible. Relation $J(-\Delta_j, -f_j) = J(\Delta_j, f_j)$ generalizes the argumentation to $\Delta_j > 0$, meaning that the same effect at $\Delta > 0$ is obtained with the field of opposite sign.

Putting the result into a broader context, one should recognize that it shows the importance of the Stark localization caused by the strong fields due to which the bulk of the system behaves as a Stark insulator. Even in the presence of extreme, but local boundary driving, the spin current through the system is still exponentially suppressed. Latter observation is very general since it holds for different types of bulk insulators: Stark - due to field, Mott - due to anisotropy, and MBL - due to disorder. We checked that in the case of disorder, e.g. for random $\tilde{f}_j$, large f asymptotics is the same, however, resonances in the current appear at values dependent on the random choice.

Chapter 3

Nonequilibrium optical linear response

A prototype procedure to study the nonequilibrium dynamics of correlated materials is to perform the pump-probe scheme and measure the optical absorption, as reviewed in the introduction, Sec. 1.2.1. The initial pump pulse causes strong excitation of the system, while the weaker probe pulse examines the evolution of the initial excitation by measuring the transmission and/or the reflection. Via Kramers-Kronig relations the dielectric function $\epsilon(\omega)$ can be extracted from the latter measurement, where its imaginary part $\epsilon''(\omega)$ is of central interest. It quantifies the possible absorption in the system and is related to the real part of the optical conductivity $\sigma(\omega)$ via $\epsilon_0\omega\epsilon''(\omega) = \sigma'(\omega)$, where ϵ_0 is the dielectric constant.

Being of smaller magnitude, the effect of the probe pulse can be theoretically treated using the linear response. In contrast to the equilibrium situation, the evolving system lacks the time-translational invariance, which is implicitly used in the standard derivation of the linear response to an external weak perturbation [141]. The aim of this Chapter is to generalize the linear response theory for a nonequilibrated system and to introduce the differential optical conductivity $\sigma(\omega, t)$ representing the causal linear response of the lattice current to an arbitrary electric-field pulse $\mathbf{E}(t' > t)$ (e.g. probe pulse) that acts on a general nonequilibrium many-body wave function $|\psi(t'')\rangle$ (created by e.g. pump pulse).

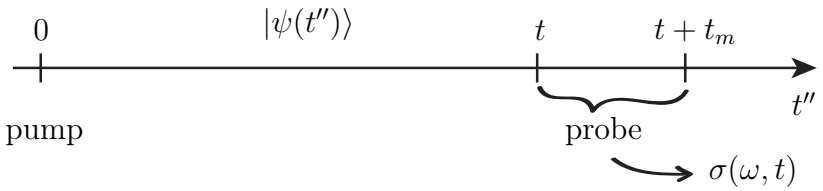

The derivation is performed within a tight-binding model of correlated electrons. Such a formulation allows definitions of the optical sum rule, as well as of the Drude weight $D(t)$ (the dissipationless response), which reveal their time dependence. Both expressions have inherent relations to their equilibrium or thermal analogs.

There are few variations on this theme, recently introduced by other authors. Such a formalism has been proposed also for continuous correlated systems [142], while adapted for the application of the dynamical mean-field theory (DMFT) and with a different choice of Fourier transform, $\sigma(\omega, t + t_m)$, [143] it has been used

for the analysis of the Hubbard model [82, 132, 143]. Another DMFT study developed similar formalism with an emphasis on the description of the time-dependent photoemission spectroscopy [144]. Whilst to characterize the stationary state after a quantum quench the most symmetric choice $\sigma(\omega, (t+t_m)/2)$ has been used and studied explicitly for a hard-core boson model [145]. There are also studies in which the effect of the probe field after the intensive pulse excitation is directly followed by the introduction of a (classical) driving time-dependent electric field, representing the probe pulse [146].

Further on we use units $\hbar = a_0 = 1$, where a_0 is the inter-site distance.

Content of this Chapter is reported in Ref. [147].

3.1 Time-dependent linear response

Let the dynamics of the system be governed by the time-dependent Hamiltonian $H(t) = H_0(t) + f(t)F$, where $f(t)F$ is a weak perturbation of strength $f(t)$ [1]. Evolution can be described by the density matrix $\rho(t)$, which is time evolved according to the von Neumann equation

$$i\frac{\partial}{\partial t}\rho(t) = [H(t), \rho(t)]. \tag{3.1}$$

Our goal is to calculate the deviations in the expectation value of some observable B in the presence of an external perturbation $f(t)F$.

Having interest only in lowest corrections we expand the density matrix $\rho(t)$ as $\rho(t) = \sum_{n=0}^{\infty} \rho_n(t)$, where $\rho_n(t)$ is proportional the nth order of $f(t)$. Lowest orders have to obey

$$i\frac{\partial}{\partial t}\rho_0(t) = [H_0(t), \rho_0(t)], \quad i\frac{\partial}{\partial t}\rho_1(t) = [H_0(t), \rho_1(t)] + f(t)[F, \rho_0(t)]. \tag{3.2}$$

Let the initial time (e.g. application of the pump pulse) be set to $t_0 = 0$, while the perturbation (e.g. the probe pulse) is turned on at time t. Then at some $t' > t$,

$$\rho_1(t') = i\int_t^{t'} dt'' f(t'') U(t', t'')\ [\rho_0(t''), F]\ U^\dagger(t', t''), \tag{3.3}$$

$$\rho_0(t'') = U(t'', 0)\rho_0(0)U^\dagger(t'', 0), \quad U(t', t) = \hat{T}[\exp(-i\int_t^{t'} H_0(t'')dt'')] \tag{3.4}$$

satisfy upper equations, as shown in App. B.1. Here $\hat{T}$ is the time ordering. If we define the interaction representation as $B^I(t') = U^\dagger(t', t)BU(t', t)$, then an approximate deviation in the expectation value of the observable B due to the perturbation F is

$$\delta\langle B\rangle_{t'} = Tr[\rho_1(t')B] = -i\int_t^{t'} dt'' f(t'')\ Tr\big[\rho_0(t)\ [B^I(t'), F^I(t'')]\big], \tag{3.5}$$

as shown in App. B.1.

[1] In this and the following Chapter t is exceptionally used for time since τ stands for the stress tensor, Eq. (3.7).

3.2 Nonequilibrium optical conductivity in tight-binding model

In this section the generalized linear response developed above is used to calculate the response of the electrical current to an electric field within a tight-binding model. In a general single-band tight-binding model of correlated electrons with periodic boundary conditions the effect of the electromagnetic field can be introduced via the vector potential $\mathbf{A}(t)$ through the usual gauge (Peierls) construction [30] (as mentioned in Sec. 2.1). The latter neglects the inter-band tunneling in multi-orbital models, and the field-induced distortions of the orbitals, but remains appropriate for the single-orbital case and weak fields. We consider the tight-binding Hamiltonian up to $\mathcal{O}(\mathbf{A}^3)$,

$$\begin{aligned} H(\mathbf{A}(t)) &= -\sum_{i,j,s} t_{ij} \exp(ie\mathbf{A}(t)\cdot\mathbf{R}_{ij}) c^\dagger_{js} c_{is} + H_{int} \\ &\approx H_0 - e\mathbf{A}(t)\cdot\mathbf{j} + \frac{e^2}{2}\mathbf{A}(t)\cdot\tau\mathbf{A}(t), \end{aligned} \tag{3.6}$$

written with the particle current $\mathbf{j}$ and the stress tensor τ operators,

$$\mathbf{j} = i\sum_{i,j,s} t_{ij}\mathbf{R}_{ij} c^\dagger_{js} c_{is}, \quad \tau = \sum_{i,j,s} t_{ij}\mathbf{R}_{ij}\otimes\mathbf{R}_{ij} c^\dagger_{js} c_{is}, \tag{3.7}$$

where $\mathbf{R}_{ij} = \mathbf{R}_j - \mathbf{R}_i$ and e the charge of electrons. The electrical current

$$\mathbf{j}_e(t) = -\partial H/\partial\mathbf{A}(t) = e\mathbf{j} - e^2\tau\mathbf{A}(t) \tag{3.8}$$

is a sum of the particle current and the diamagnetic contribution. We treat the case in which the unperturbed system is described by a pure (nonequilibrium) many-body wave function $|\psi(t)\rangle$, with the time evolution operator $U(t',t) = \exp[-iH_0(t'-t)]$, where $t' > t$, corresponding to the time-independent H_0. We use the above developed formalism to evaluate the linear response of $\mathbf{j}$ (now $B = \mathbf{j}$) to a general $\mathbf{A}(t'')$ applied at t (now $f(t)F = -e\mathbf{A}(t)\cdot\mathbf{j}$), whereas the diamagnetic part is already linear in $\mathbf{A}(t')$. Introducing the notation for expectation values $\langle O\rangle_t = \langle\psi(t)|O|\psi(t)\rangle$,

$$\begin{aligned} &\langle\mathbf{j}_e\rangle_{t'} = e\langle\mathbf{j}\rangle_{t'} - e^2\mathbf{A}(t')\langle\tau\rangle_{t'} + e^2\int_t^{t'} dt''\chi(t',t'')\mathbf{A}(t''), \\ &\chi(t',t'') = i\theta(t'-t")\langle[\mathbf{j}^I(t'),\mathbf{j}^I(t'')]\rangle_t, \quad \mathbf{j}^I(t') = U^\dagger(t',t)\mathbf{j}U(t',t). \end{aligned} \tag{3.9}$$

Differential conductivity $\sigma(t',t)$ is defined through the response to electric field $\mathbf{E}(\tilde{t})$,

$$\delta\langle\mathbf{j}_e\rangle_{t'} = V\int_t^{t'} d\tilde{t}\ \sigma(t',\tilde{t})\mathbf{E}(\tilde{t}), \tag{3.10}$$

V being the volume of the system. Taking into account $\mathbf{A}(t'') = -\int_t^{t''}\mathbf{E}(\tilde{t})d\tilde{t}$, the paramagnetic part can be written as

$$\begin{aligned} \delta\langle\mathbf{j}_e{}^p\rangle_{t'} =& e^2\int_t^{t'} dt''\chi(t',t'')\mathbf{A}(t'') = e^2\int_t^{t'} dt''\chi(t',t'')\Big(-\int_t^{t''}\mathbf{E}(\tilde{t})d\tilde{t}\Big) \\ =& \int_t^{t'} d\tilde{t}\mathbf{E}(\tilde{t})\Big(-e^2\int_{\tilde{t}}^{t'} dt''\chi(t',t'')\Big), \end{aligned} \tag{3.11}$$

where from the first to the second line we have reversed the order of the integration $\int_t^{t'} dt'' \int_t^{t''} d\tilde{t} \to \int_t^{t'} d\tilde{t} \int_{\tilde{t}}^{t'} dt''$. Similarly, the diamagnetic part is

$$\delta\langle \mathbf{j}_e^{\,d}\rangle_{t'} = -e^2\langle\tau\rangle_{t'}\mathbf{A}(t') = e^2\langle\tau\rangle_{t'}\int_t^{t'} d\tilde{t}\mathbf{E}(\tilde{t}) = \int_t^{t'} d\tilde{t}\mathbf{E}(\tilde{t})\; e^2\langle\tau\rangle_{t'}, \tag{3.12}$$

which yield the expression for the differential conductivity

$$\sigma(t',t) = \frac{e^2}{V}[\langle\tau\rangle_{t'} - \int_t^{t'} dt''\chi(t',t'')]. \tag{3.13}$$

For a nonequilibrium dynamics with no time-translational symmetry both t and t' have an equally important role, while $\sigma(t',t)$ is certainly the cleanest object that characterizes the response to an electric field. However, it is difficult to extract physical observation out of it. In particular, to relate it with the experimentally relevant $\epsilon(\omega,t)$ it should be Fourier-transformed.

For a nonstationary state there is no unique definition of the frequency-dependent $\sigma(\omega,t)$ [132, 142, 145]. We choose a plausible relation reflecting the causality and switching-on of the field (e.g. probe pulse) at time t, i.e., $\mathbf{E}(\tilde{t}<t)=0$,

$$\sigma(\omega,t) = \int_0^{t_m} ds\; \sigma(t+s,t)e^{i\omega s}, \tag{3.14}$$

where t_m is the width of the window in which we do the Fourier transformation. Formally $t_m\to\infty$ but in practice it is the maximum time of the probe duration. With such a definition, Eq. (3.14), we avoid the ambiguity of including times prior to the pump pulse. The sum rule for so defined $\sigma'(\omega,t) = \mathrm{Re}\;\sigma(\omega,t)$ then follows directly from Eq. (3.14),

$$\int_{-\infty}^{\infty} d\omega\; \sigma'(\omega,t) = \pi\sigma(t,t) = \frac{\pi e^2}{V}\langle\tau\rangle_t. \tag{3.15}$$

It is evident that the sum rule, Eq. (3.15), is a time-dependent quantity, i.e., $\langle\tau\rangle_t$ evaluated at the time t when the probe field is applied. Moreover, independent of the precise form of the Fourier transform it remains proportional to the $\langle\tau\rangle$ at the time held fixed in the transformation.

One can define also the Drude weight $D(t)$ as the dissipationless component,

$$\begin{aligned}\sigma'(\omega,t) &= 2\pi e^2 D(t)\delta(\omega) + \sigma'_{reg}(\omega,t)\\ D(t) &= \frac{1}{2Vt_m}\int_0^{t_m} ds[\langle\tau\rangle_{t+s} - \int_0^s ds'\chi(t+s,t+s')],\end{aligned} \tag{3.16}$$

again for $t_m\to\infty$. Equation (3.16) turns out to be a generalization of the equilibrium expression, $D = (1/2V)(\langle\tau\rangle - \chi'(\omega=0))$ [148]. In contrast to the sum rule, $D(t)$ following from Eq. (3.16) is expected to be dominated by $t', t'' \gg t$ in Eq. (3.13). Its dependence on t is revealed if written in the basis of eigenstates $|\phi_m\rangle$ of H_0. In the standard notation for matrix elements $\langle\phi_m|O|\phi_n\rangle = O_{mn}$ and amplitudes $\langle\phi_m|\psi(0)\rangle = a_m$ ($t=0$ chosen arbitrarily, e.g., when the nonequilibrium

state is prepared), we can express $D(t)$ in the eigenbasis, assuming that there are no degeneracies,

$$D(t) = \frac{1}{V}\sum_m |a_m|^2 \Big[\frac{\tau_{mm}}{2} - \sum_{n\neq m} \frac{|j_{mn}|^2}{(\epsilon_n - \epsilon_m)}\Big] + \frac{1}{2V}\sum_{m,n\neq m} a_m^* a_n \frac{j_{mn}(j_{mm}-j_{nn})}{(\epsilon_m - \epsilon_n)}\, e^{i(\epsilon_m-\epsilon_n)t}. \tag{3.17}$$

For the derivation see App. B.2. As relevant for the isotropic cases, $D(t) = D_{\alpha\alpha}(t)$ is the diagonal term with $j = \mathbf{j}_\alpha$. Obviously, the last term in Eq. (3.17) provides dependence on t if nonzero. However, unless we are dealing with some peculiar spectra ϵ_n, it is expected to vanish if averaged over t [145], yielding stationary $D(t) = D_0$, which is dependent only on the (initial) nonequilibrium state $|\psi(0)\rangle$ through a_m. This result stresses the influence of the initial state (e.g. right after the pump excitation) on the Drude component at much longer times. Moreover, the first two terms in Eq. (3.17) resemble the equilibrium expression [149], with thermal weights substituted by projection weights $|a_m|^2$. However, the latter derivation is feasible only for the time-independent H_0. Since pump and probe fields in realistic experiments usually overlap at short times (when the measured Drude component shows time dependence), it should be applied to the real experiment with some caution. One can express limiting D_0 also for the case with degeneracies, where it is of a more general form,

$$D_0 = \frac{1}{V}\sum_{\epsilon_m=\epsilon_n} a_m^* a_n \Big[\frac{\tau_{mn}}{2} - \sum_{\epsilon_l\neq\epsilon_m} \frac{j_{ml}j_{ln}}{(\epsilon_l - \epsilon_m)}\Big], \tag{3.18}$$

still being independent of the choice of the basis within the degenerate sector.

We have so far considered the response of a pure state $|\psi(t)\rangle$ and a t-independent unperturbed H_0. The formalism can be extended also to the more general density matrix, as well as to a time-dependent $H_0(t)$, e.g., representing the presence of the pump, where the time-evolution operator is $U(t',t) = \hat{T}[\exp(-i\int_t^{t'} H_0(t'')dt'')]$. In such a formulation the linear response of the particle current to the field applied at t is

$$\delta\langle\mathbf{j}\rangle_{t'} = -i\int_t^{t'} dt''(-e\mathbf{A}(t''))Tr\Big[\rho_0(t)[\mathbf{j}^I(t'),\mathbf{j}^I(t'')]\Big]. \tag{3.19}$$

where density matrix ρ_0 is possibly generalized to an ensemble of pure states. Optical conductivity is then

$$\sigma(t',t) = \frac{e^2}{V}\left(\langle\tau\rangle_{t'} - i\int_t^{t'} dt'' Tr\Big[\rho_0(t)[\mathbf{j}^I(t'),\mathbf{j}^I(t'')]\Big]\right), \tag{3.20}$$

where now $\langle\tau\rangle_t = Tr[\rho_0(t)\tau]$.

3.3 Numerical implementation

Let us discuss here the numerical implementation for $\sigma(\omega, t)$ only for the isotropic system in the case of a pure wave function $|\psi(t)\rangle$ and the time-independent H_0. The apparent disadvantage of the definition with Eq. (3.13) is that for a fixed t the evaluation of its paramagnetic part $\sigma^p(t, t')$ via Eq. (3.9),

$$\sigma^p(t,t') = -\frac{e^2}{V}\int_t^{t'} dt''\chi(t',t'') = \frac{e^2}{V}\int_t^{t'} dt''2Im[\langle\psi(t')|jU(t',t'')j|\psi(t'')], \qquad (3.21)$$

requires the propagation $U(t', t'')$ for each t''. Of course, numerically this is performed in a discrete manner. Top Fig. 3.1 sketches this procedure, where one line corresponds to the propagation from t'' to t' in time steps Δt (depicted by a single arrow). Application of j operator is depicted by a full circle. To numerically calculate the expression (3.21) all together $(n_m + 1)(n_m + 2)/2 \sim \mathcal{O}(t_m^2/\Delta t^2)$ operations are needed, where $n_m = (t' - t)/\Delta t - 1$.

Instead it is more efficient to calculate the integral inside the matrix element, Eq.(3.21), with propagation performed in discrete steps,

$$\int_t^{t'} dt''U(t',t'')j|\psi(t'')\rangle \approx \Delta t\sum_{n=0}^{n_m} U_\Delta^{n_m-n+1}\ j|\psi(t+n\Delta t)\rangle, \qquad (3.22)$$

where $U_\Delta = U(t'' + \Delta t, t'')$ is a propagation for Δt. The sum Eq. (3.22) can be then evaluated recursively,

$$|S_0\rangle = j|\psi(t)\rangle,\ |S_n\rangle = j|\psi(t+n\Delta t)\rangle + U_\Delta|S_{n-1}\rangle \text{ for } n > 0, \qquad (3.23)$$

so that finally

$$\sigma(t',t) = \frac{e^2}{V}\Big(\langle\tau\rangle_{t'} + 2\Delta t\ \mathrm{Im}\langle\psi(t')|j\ U_\Delta|S_{n_m}\rangle\Big). \qquad (3.24)$$

Such a procedure reduces the number of operations to $\mathcal{O}(t_m/\Delta t)$ and is sketched in the bottom Fig. 3.1. As visualized by the choice of gray scale, one step involves the propagation of a block ($U_\Delta|S_{n-1}\rangle$) and application of the current operator ($j|\psi(t + n\Delta t)\rangle$), marker by a dot to the right of the block. We note that quite analogous procedure can be applied for other transient correlation functions or for the time-dependent $H_0(t)$.

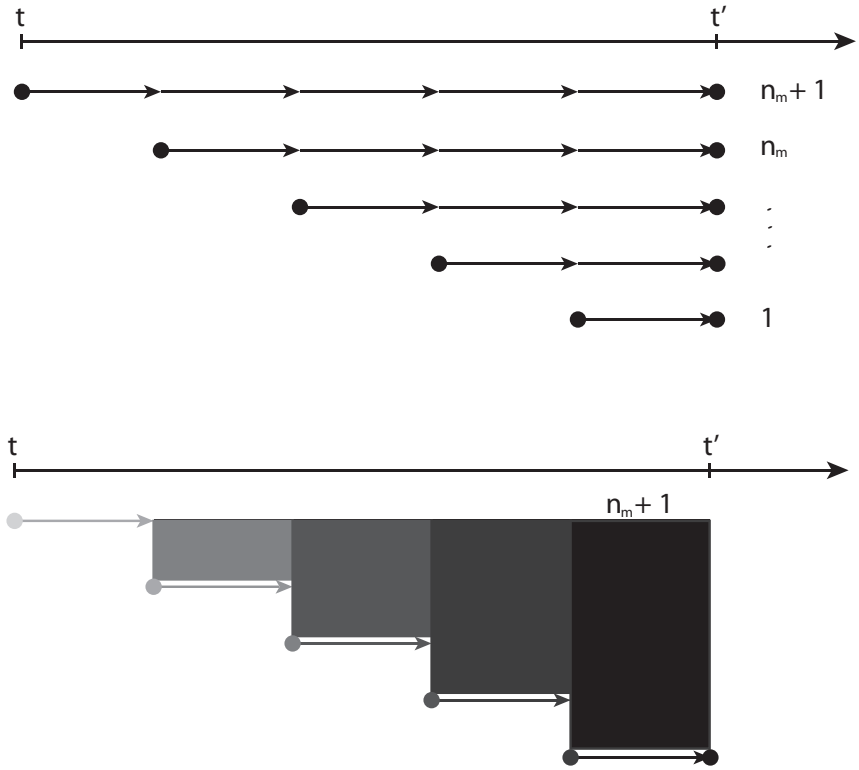

Figure 3.1: Top: A scheme of the basic evaluation of Eq. (3.21). Bottom: a scheme of the recursive evaluation of Eq. (3.21). Propagation for a time step Δt is depicted by a single arrow, while the application of j operator is visualized by a full circle.

Chapter 4

Initial charge relaxation in photo-doped Mott insulators

In this and the following Chapter we address the dynamics of Mott insulators, if excited above the Mott-Hubbard (MH) gap, with an intention to explain or motivate pump-probe experiments reviewed in the Introduction. Taking a chronological approach, the present Chapter considers the short-time dynamics of charges right after they are created with a pump pulse of energy larger than the MH gap, while the next Chapter focuses on the long-time dynamics with eventual recombination of charged excitations. In actual experiments on correlated materials, the short-time dynamics corresponds to the femto-second range, while the long-time dynamics corresponds to pico-seconds. While experimentally it is easier to measure slower processes, where a lower resolution of the time-resolved spectroscopy suffices; theoretically the situation is just the opposite, since explicit time evolution is more accurate for shorter times. For that reason theory is somewhat ahead of time-resolved spectroscopy experiments, when considering the very fast dynamics, and might turn out enlightening, as is the case for some very recent [32, 150, 151], but also future experiments.

In our study the process of charge excitation will be treated only approximately and in a quantized manner. It will be assumed that each photon (coming from the pump pulse) with energy larger than the gap excites a pair of effectively charged particles, which are in the single-band Hubbard model represented by a doubly occupied site (doublon) and a non-occupied site (holon). Furthermore, we assume that at the earliest stage of their existence both particles behave as independent, so that their relaxation can be treated separately, e.g. by studying a holon solely. To test this assumption one would have to know their actual distribution after the pulse excitation, which is beyond the scope of this study.

In a simplified scenario relevant for 2D cuprates, e.g. Nd_2CuO_4 and La_2CuO_4 [13, 14], we model the initial state (after the charge creation) by inserting a holon into an ordered 2D spin background. Within our model, inserting a doublon would yield equivalent results. In such a way we assume that excitation creation itself does not disturb the spin ordering. However, in such a state holon is well above its ground state (g.s.), therefore we can follow its relaxation towards it. The whole procedure and especially timescales involved, as well as the final stationary state are of our interest. Because relaxation of a holon is calculated on finite-size systems with periodic boundary conditions (p.b.c.), one can discuss also the aspect of the thermalization, even though we create just a local excitation, since due to the p.b.c.

results should actually mimic the finite density of charges.

The holon relaxation will be observed through different quantities. In Sec. 4.1 we will employ the formalism of the *non-equilibrium optical conductivity*, developed in the previous Chapter and treat the holon within the t-J model that couples charge to spin degrees of freedom. We will demonstrate how experimentally relevant quantities (like the Drude response, the mid-infrared peak, and the optical sum rule) develop in time. Knowing how much energy has been inserted in the finite system, we compare the stationary response at long times with the thermally expected one and discuss the thermalization of charged particle, introducing the concept of *time-dependent local temperature*. It turns out that particle fails to thermalize completely and stays in a pre-thermal state with the local temperature determined from the fluctuation-dissipation theorem. In Sec 4.2 we simulate 2D system by a 1D one with added staggered field that mimics the effect of the spin ordering in 2D and exerts an effective potential corresponding to the creation of string excitations in proper 2D calculations. In such a way we profit on clarity and manage to observe a *two-stage dynamics* of a holon coupled to spins. Especially the holon-spin correlations reveal Lieb-Robinson velocities [152] for each stage, which can be analytically explained, yielding a picture of the relaxation mechanism: initially the holon creates a local spin perturbation, which is then dispersed into the system via magnon waves. When

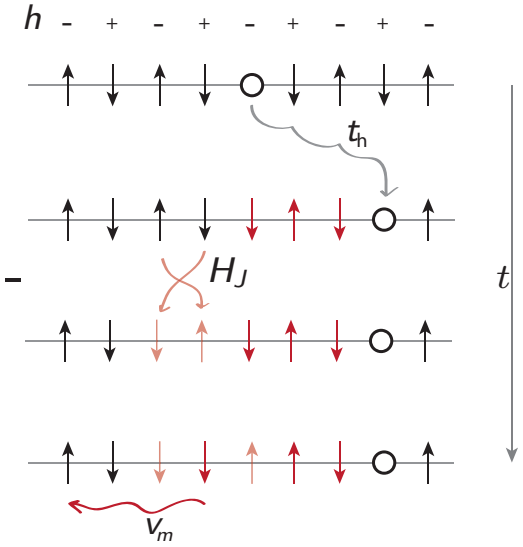

charge is coupled also to Holstein phonons main features of the dynamics remain the same with an additional interplay between both bosonic baths.

Our observations have overlaps with several other studies. In a similar set-up with holon being excited within the 2D t-J model, the short-time dynamics has been understood by considering the same process on the Bethe lattice with connectivity $z = 4$ [31]. There, with the effective Hamiltonian for the t-J_z model written in a string basis, a dimensionless time-dependent Schrödinger equation in the continuum limit revealed that time for the initial relaxation of the kinetic energy of a holon scales as $t \to tJ^{2/3}$ with super-exchange constant J. The importance of the charge-spin coupling for the relaxation of photo-induced charges in $d > 1$ systems has been recognized also in dynamical mean field (DMFT) studies. In [153] the relaxation time reflected the short-range spin correlation in the paramagnetic phase of the Hubbard model, being sensible to the temperature and showing an increase of the

relaxation time with temperature and excitation density. Furthermore, it has been shown that finite doping opens additional scattering channels and leads to a faster relaxation. While in [154] an efficient separation of photo-induced charges due to a gradient of the external (electric) field in a Mott heterostructure (setup with an array of coupled layers having different static potential energy) was observed only in the presence of antiferromagnetic correlations within each layer. Melting of Néel order in the Hubbard model has been studied within DMFT, addressing higher-dimensional systems [155], but also in 1D [156]. Especially the latter study arrived to very similar observation to ours, namely, starting from a perfect Néel state authors reported that double occupancy undergoes much faster dynamics than spin excitations. Importantly, in the increase of the von Neumann entropy two different slopes are observed; at short times slope is U independent and set by the hopping parameter, while at longer times it is similar to the exact spinon velocity, known from Bethe ansatz, which agrees with our two-stage scenario. Regarding the coupling to phonons, a separated insight into the nonequilibrium nature of the Holstein polaron has been obtained by exciting a charge within the Holstein model [157], surprisingly recognizing that at low charge-phonon coupling wave function can be a superposition of an excited polaron and nearly free charge.

Further on we set charge $e = 1$, while in figures the hopping parameter $t_h = 1$ is used as the unit of energy, as well as of time $t_0 = \hbar/t_h = 1$. Lattice spacing is set to $a_0 = 1$ so that the volume equals number of sites $V = N$. In this Chapter time is denoted by t, since τ is used for the stress tensor, Eq. (3.7).

Content of this Chapter is reported in Refs. [71, 147].

4.1 Optical response of excited holon

Fist we consider the optical response of a single excited charge carrier (holon) doped in an antiferromagnetic (AFM) Mott insulator. Its dynamics will be governed by the standard single-band t-J model,

$$H_0 = -t_h \sum_{\langle i,j\rangle,s} (\tilde{c}^\dagger_{i,s}\tilde{c}_{j,s} + \text{H.c.}) + J\sum_{\langle i,j\rangle}(\mathbf{S}_i \cdot \mathbf{S}_j - \frac{1}{4}n_i n_j), \tag{4.1}$$

where $\tilde{c}_{i,s} = c_{i,s}(1 - n_{i,-s})$ are fermion operators, projected onto the space with no double occupancy, and $\langle i, j\rangle$ are pairs of n.n. sites. Calculations are made on 2D square lattices, taking $J/t_h = 0.4$ as relevant for cuprates.

As mentioned in the introduction our goal is to obtain some understanding by calculating the time-dependent optical conductivity $\sigma(\omega, t)$, Eq. (3.14), for:
(a) the initial relaxation of charged particles that are photo-induced in the pump-probe experiments on cuprates [13, 14]. To simulate this process for the cases with low concentration of excited carriers we consider as the initial wave function a single holon localized on one site, $|\psi(0)\rangle$ being the eigenstate of the model, Eq. (4.1), where effective t_h is put to zero. Strictly speaking this is not equivalent to injecting a holon in AFM background, however, is not far from it either.
(b) We compare this result with another setting, which addresses pump-probe experiments on a weakly doped AFM insulator. The effect of a strong pump pulse applied to it can be simulated by the introduction of a phase shift in the hopping term of Eq. (4.1), changing $t_h \to t_h^{ij} = t_h \exp(i\theta_{ij})$, while the initial state can be

found as the g.s. of a single holon within the t-J model. We perform the maximum shift in the chosen direction x, i.e. $\theta_x = \pi$, since then both scenarios correspond to the same change in the total kinetic energy E_{kin}, calculated from the expectation value of the t_h term in Eq. (4.1). As obvious for the initially localized holon with $t_h(t = 0) = 0$, the excited state has $E_{kin}(t = 0) = 0$. For the choice $\theta_x = \pi$ the effect of the particular phase shift is to change the sign of hopping in the x direction. Due to the invariance under C_{4v} rotations this again yields zero total kinetic energy. Although we are primarily interested in the response of photo-induced charges, the comparison between (a) and (b) still yields a cross-check of how much observed features of $\sigma(\omega, t)$ actually depend on the type of the excitation and the initial wave function. Relating results from (b) to actual experiments on chemically doped cuprates, one should first examine what fraction of all chemically doped holes is really effected by the pump pulse, depending on the fluence of the pulse.

Results are obtained via two numerical methods. One is the exact diagonalization (ED) of small systems employing Lanczos method, where we study the 2D square lattices with $N \leq 26$ sites and p.b.c.. First we find the g.s. $|\psi(0)\rangle$. By solving the time-dependent Schrödinger equation, time evolution of $|\psi(t')\rangle$ and evaluation of recursive relations, Eq. (3.23), are obtained by employing the Lanczos basis [74, 158]. Since the available square lattices ($N = 18, 20, 26$) are in general not invariant under C_{4v} symmetry we perform the averaging of $\sigma' = (\sigma'_{xx} + \sigma'_{yy})/2$ for case (b) together with corresponding pulses $\theta_\alpha = \theta_x, \theta_y$. Another method to evaluate $\sigma(\omega, t)$ is the diagonalization within the limited functional space (EDLFS) [74, 159]. The EDLFS method systematically constructs states with distinct spin configurations in the proximity of the holon and can in principle deal with an infinite system, but is in practice still limited by the number of basis states taken into account. In the considered case spin excitations extend up to $L = 16$ lattice sites away from the holon.

Optical sum rule

First we analyze the time variation of $\langle \tau_{\alpha\alpha} \rangle$, representing the sum rule $\int_{-\infty}^{\infty} d\omega\, \sigma'(\omega, t)$, Eq. (3.15), which is for the tight-binding model (4.1) related to the kinetic energy,

$$\langle \tau_{\alpha\alpha} \rangle_t = -E_{kin,\alpha}(t), \tag{4.2}$$

where only hopping in the α direction is taken into account. In Fig. 4.1 we present ED and EDLFS results for $\langle \tau \rangle$ calculated directly from the kinetic energy for $|\psi(0)\rangle$, corresponding to the localized (loc) and the π-pulsed excitation ($\theta_x = \pi$), respectively. Averaging $\langle \tau \rangle = (\langle \tau_{xx} \rangle + \langle \tau_{yy} \rangle)/2$ is employed in ED calculations, whereas for EDLFS $\langle \tau \rangle = \langle \tau_{xx} \rangle$.

Although for both types of excitations $E_{kin}(t = 0) \sim 0$, the distinction in sum rules is apparent at earliest times, featuring the fact that the state of the initially localized holon has the rotational symmetry, whereas with the π pulse this symmetry is broken and $E_{kin,x}(t = 0) = -E_{kin,y}(t = 0)$.

From Fig. 4.1 it follows that for both types of initial states $\langle \tau \rangle$ rapidly relaxes toward a stationary value, which is only slightly above the g.s. value, denoted by $E^0_{kin,x}$. Here we only note that the fast relaxation with corresponding short time t_d can be related to the formation of the spin polaron, as explained in more details in Sec. 4.2. It has been observed and derived in earlier studies [160] that relaxation

time scales as $t_d \propto (J/t_h)^{-2/3}$, which can be explained with the generation of string states in the spin background. However, regardless of the precise understanding of the process a simple, but relevant message for the future experimental analysis is that when measuring ultra-fast response even the whole sum rule, not just particular peaks in the spectra, can be time-dependent.

Let us discuss the dynamics of the sum rule (kinetic energy) in more detail. In Fig. 4.1 we confirm that both methods, the ED and the EDLFS, give quite consistent result for $\langle\tau\rangle_t$ at short times $t < t_d \sim 1.5$ (for chosen $J = 0.4$). For intermediate times $t_d < t < t_i \sim 15$ the saturation of $-\langle\tau\rangle_t$ evaluated with ED is somewhat slower, which could indicate the influence of finite-size and p.b.c. effects. Namely, in small systems considered within the ED spin excitations populate the lattice and consequently influence further holon relaxation. The spread of the spin excitation is expected to saturate in $t_i \sim \sqrt{N}/J$, yielding an approximately stationary response afterwards. Within the EDLFS with in principle an infinite lattice, such effects are not present or appear only at later times due to the restricted basis. More than an artifact, ED results on small lattices should be relevant for optical sum rules of systems with a finite density of carriers, while those from EDLFS correspond to systems with vanishing density.

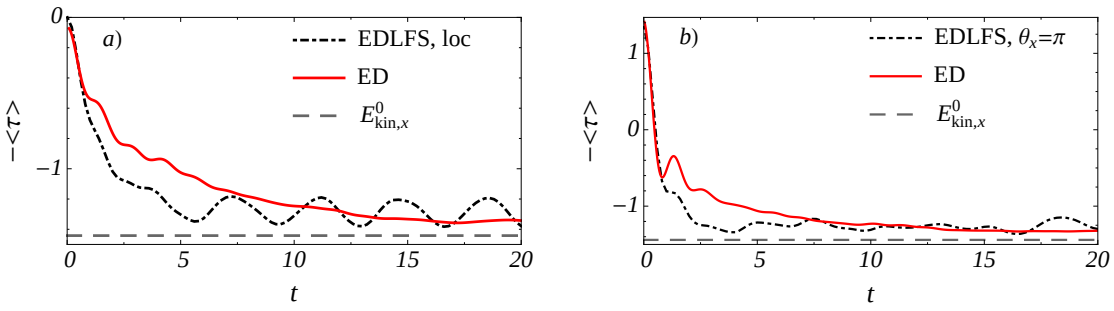

Figure 4.1: Sum rule $\langle\tau\rangle$ vs time t for $J = 0.4$ as obtained using the ED on $N = 26$ sites as well as the EDLFS. Results are presented for initial states of: (a) the localized holon and (b) the π-pulsed excited holon. The g.s. $E^0_{kin,x}$ value is also displayed.

It is evident that for long times $t > t_i$ kinetic energy (or equivalently the sum rule) approaches or oscillates around a quasi-stationary value, denoted by $E_{kin}(t \to \infty)$. Within the ED the latter value somewhat depends on the system size N in a sensible manner: in larger system it gets closer to the g.s. E^0_{kin}, as marked in Fig. 4.2. Since the ED is performed in a fixed-size system and the initial excited state is quite far from the g.s. one could expect that our non-integrable system thermalizes and is then described by an effective temperature $T_{eff} > 0$, so that different $E_{kin}(t \to \infty)$ are a consequence of different T_{eff}, depending on the type of quench and size of the system. In a finite system T_{eff} is set by the excitation energy so that the canonical expectation value of the energy equals the total initial energy,

$$\langle\psi(0)|H_0|\psi(0)\rangle = E_{tot}. \tag{4.3}$$

At $N = 26$ the effective temperature is approximately $T_{eff} = 0.35, 0.5$ for the initially localized holon and π-pulsed holon, respectively, and increases as N decreases. Our observation is that $E_{kin}(T_{eff})$ is still lower than $E_{kin}(t \to \infty)$ for all

finite systems considered, as seen in Fig. 4.2. This suggests that the system cannot completely thermalize, possibly due to the discreteness of spin excitations in finite systems. Discussion on this topic is continued under the subsection 'Time-dependent temperature'.

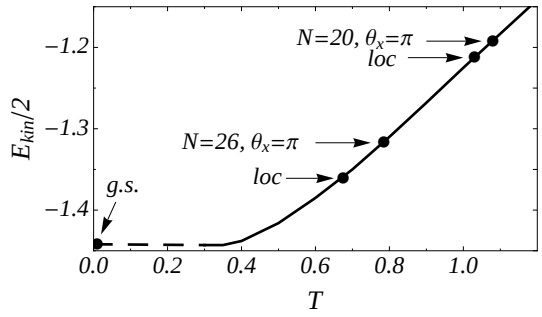

Figure 4.2: Equilibrium kinetic energy $E_{kin}/2$ vs temperature T for single holon on a system with $N = 26$ sites. Dots mark $E_{kin}(t \to \infty)/2$ for both types of excitations in $N = 20, 26$ systems and g.s..

Time-dependent optical conductivity $\sigma(\omega, t)$

In Fig. 4.3 we finally present results for the time-dependent optical spectra per holon $\tilde{\sigma}'(\omega, t) = N\sigma'(\omega, t)$ as obtained by ED and EDLFS, respectively. Cases of initially localized and π-pulse excited holons are compared. With respect to Fig. 4.1 chosen times represent different evolution stages: (a) $t \sim 0$ response of the initial excited state $|\psi(0)\rangle$, (b) response at approximately characteristic decay time $t = 1.5 \sim t_d$, and (c) $t = 10 \sim t_i$ already relaxed but not yet fully stationary response. To mimic the stationary response for finite systems an average $\tilde{\sigma}'(\omega, \bar{t})$ over responses in interval $t \in [20, 60] \gg t_d$ is presented in Fig. 4.4 and compared with the g.s. $\tilde{\sigma}'_0(\omega)$ and with the thermal-equilibrium $\tilde{\sigma}'_{th}(\omega)$ optical conductivity at appropriate effective $T_{eff} = 0.35, 0.5$, all obtained within the ED.

In the initial stage the response is very incoherent and for the π pulse case even predominantly negative $\tilde{\sigma}'(\omega, t) < 0$, which is compatible with the sum rule $\langle\tau\rangle_{t\sim 0} < 0$ in Fig. 4.1. The latter indicates on a highly nonequilibrium state $|\psi(0)\rangle$, corresponding to an inverse particle population [161], a natural consequence of the boost in momentum for e.g. $k_x = \pi$.

Before discussing the non-equilibrium response it is useful to know what specific features can be found already in the equilibrium, i.e. in the g.s. response. These features are in particular the (i) *mid-infrared* (MIR) peak and the (ii) *Drude weight* D. MIR peak at $\omega \sim 2.4\ J$ is a signature of string-like spin excited states, created by the charged particle within the 2D AFM background, therefore its characteristic position scales with exchange coupling J. The other, the Drude weight D, characterizes the dissipationless (coherent) part of the response at $\omega = 0$ and is a signature of the metallic-like behavior. From equilibrium studies of systems doped with holes [162] it is known that it accounts for $\sim 1/3$ of the weight in the sum rule at $T = 0$ and should acquire a finite width at $T > 0$ due to scattering processes.

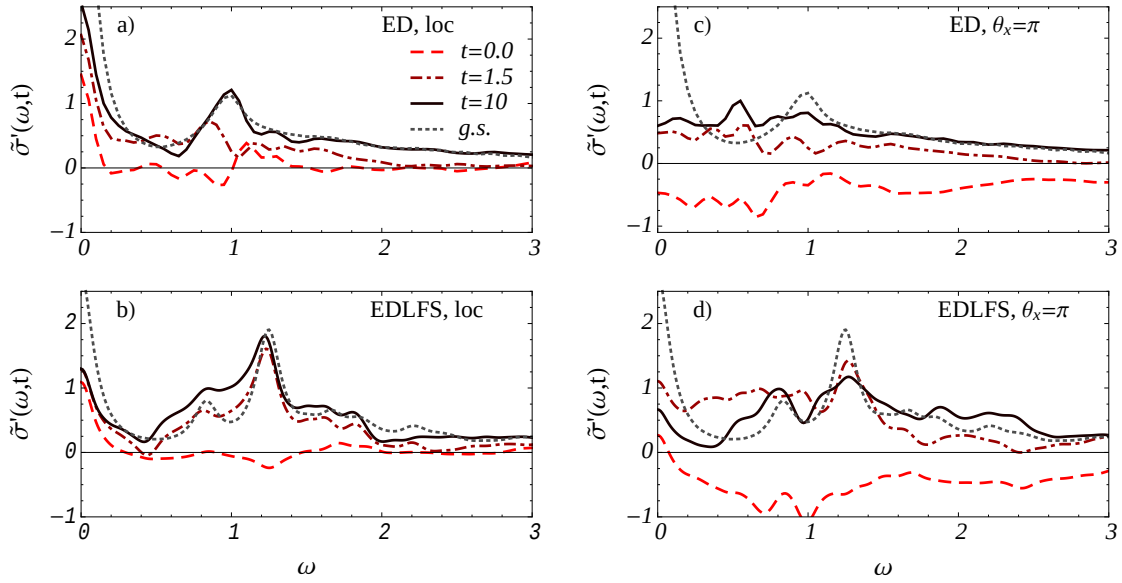

Figure 4.3: Time-dependent optical conductivity $\tilde{\sigma}'(\omega, t)$ (per holon) vs. ω as calculated at different times $t = 0, 1.5, 10$ for: (a) the initially localized holon with the ED on $N = 26$ sites, (b) localized holon with with the EDLFS, c) the π-pulse excited holon with the ED, and d) the π-pulse excited holon within EDLFS. For comparison the g.s. $\tilde{\sigma}_0(\omega)$ is shown. Broadening of the spectra $\delta\omega = 0.1$ is used.

Returning to the nonequilibrium spectra:
(i) We see in Figs. 4.3 a,b that the MIR-like peak appears also in $\tilde{\sigma}(\omega, t)$ and stabilizes very fast at $t \sim t_d$ for the localized holon, independent of the numerical method employed. On the other hand, after the π pulse (Figs. 4.3 c,d) the MIR peak is less pronounced. Especially within the ED, $\tilde{\sigma}'(\omega, t > t_d)$ is closer to the thermal $\tilde{\sigma}'_{th}(\omega)$ at appropriate $T_{eff} = 0.5$. In the equilibrium at such high $T > J$ the MIR peak (Figs. 4.4 a,b) is already smeared out due to the thermally disordered AFM spin background. Within the EDLFS results (Fig. 4.3 d) the MIR peak recovers better, which could be attributed to a lower density of spin excitations in effectively bigger systems.
(ii) We cannot strictly establish and determine the value of $D(t)$ as defined in Eqs. (3.16,3.17), since for that a full ED should be performed. Still, it is evident that with respect to the low-ω response different types of excitation lead to different behavior. Within the ED the π-pulse excited holon shows essentially no Drude peak, i.e., no corresponding low-ω remainder at $t > 0$. On the other hand, the initially localized holon displays a substantial low-ω peak and presumably $D(t) > 0$ at all $t > 0$, although the weight is smaller than in $\tilde{\sigma}_0(\omega)$. Note that we use broadening $\delta\omega = 0.1$. Using the EDLFS we notice a weak remainder of the low-ω contribution even for the π pulse, though much smaller than for the localized holon. These findings indirectly support Eq. (3.17) stating that the initial wave function determines the Drude weight value D_0. The existing experiments for photo-excited charged dynamics suggest eventual decay of the Drude component [14], opposite to what we obtain for the initially localized holon. For a more complete theoretical study it might be necessary to include other charged particles as well, since the disap-

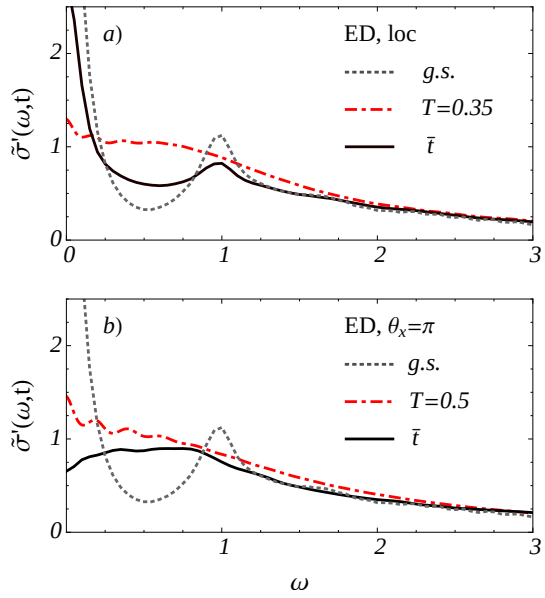

Figure 4.4: Long-time response $\tilde{\sigma}'(\omega, \bar{t})$ vs. ω as calculated with ED on $N = 26$, obtained by average over responses in interval $t \in [20, 60] \gg t_d$ for (a) initially localized holon, and (b) the π-pulse excited holon. Results are compared to the g.s. $\tilde{\sigma}_0(\omega)$ and the thermal $\tilde{\sigma}_{th}(\omega)$ at corresponding effective temperatures $T = 0.35, 0.5$. Spectra are broadened with $\delta\omega = 0.1$.

pearance of the Drude component could be related to the binding of a holon and a doublon into an exciton, as discussed (on a static level) in Sec. 5.2.3.

Peculiar response of the initially localized hole, being so different to what is thermally expected, motivates us to investigate it further. One possible extension, which still does not give a final answer, is presented in the following subsection. It would be desirable to understand whether the response of the localized holon is a consequence of the highly symmetrical initial condition that leads to some nontrivial conserved quantities, is it only a finite-size effect, or is there a more fundamental reason for inefficiency of the holon-magnon scattering, possibly originating in difference between their dispersions. Unfortunately this has not been settled within this thesis and might be pursued in the future.

Time-dependent temperature

Here we give an alternative insight into the pre-thermal nature of the spin polaron, formed after excitations discussed above.

One of possible probes of the thermalization after a (global) quench of the isolated many-body system is whether *fluctuation-dissipation theorem* (FDT), i.e. the relation between two-time correlation and linear response function, is obeyed [163]. In equilibrium one of the formulations of the FDT is the following; for a system that is governed by H and can be characterized by a density matrix ρ (which is in canonical equilibrium at temperature $T = \beta^{-1}$ the Gibbs density matrix $\rho(T) = \exp(-\beta H)/Z(\beta)$) we introduce the following functions for generic observ-

ables A and B (written in the Heisenberg representation):

$$\begin{aligned} C^{AB}(t',t) &= Tr[\rho A(t')B(t)] = \langle A(t')B(t)\rangle, \\ C^{AB}_{\pm}(t',t) &= \langle [A(t'),B(t)]_{\pm}\rangle, \\ R^{AB}(t',t) &= 2i\theta(t'-t)C^{AB}_{-}(t',t). \end{aligned} \tag{4.4}$$

In equilibrium system is time-translational invariant, therefore $C^{AB}_{\pm}(t',t) = C^{AB}_{\pm}(t'-t)$ so that it is convenient to deal with their Fourier transforms. FDT actually relates latter by the (so called) detailed balance relation [163]

$$ImR^{AB}(\omega) = \tanh\Big(\frac{\beta\omega}{2}\Big)C^{AB}_{+}(\omega). \tag{4.5}$$

For the case of auto-correlations, $A = B$, it can be written in an alternative way

$$\frac{C^{AA}(\omega) - C^{AA}(-\omega)}{C^{AA}(\omega) + C^{AA}(-\omega)} = \tanh\Big(\frac{\beta\omega}{2}\Big). \tag{4.6}$$

In nonequilibrium such a relation is not necessarily obeyed, although it might be extended by allowing $\beta(\omega)$. If for the system that has reached the stationary state $\beta(\omega) = \beta$, and equals the value set by the amount of the energy injected into the system, Eq. (4.3), then one can conclude that system has thermalized.

Even boulder, one could extend Eqs. (4.5, 4.6) also to the transient period of the time evolution, as has been done for the optical conductivity in Sec. 3.2. Since at that stage system is not in a stationary state yet, $C^{AA}(t',t)$ is Fourier transformed only over one, e.g. later time t', so that the generalized FDT for auto-correlations has the form

$$\frac{C^{AA}(\omega,t) - C^{AA}(-\omega,t)}{C^{AA}(\omega,t) + C^{AA}(-\omega,t)} = \tanh\Big(\frac{\beta(\omega,t)\omega}{2}\Big). \tag{4.7}$$

Through this relation we can investigate how thermal is the nature of our system at time t after the quench. By using different operators A (local or global) we have the option to probe the local or the global temperature of the system, which might not be the same, especially for our case with local initial excitation. Of course one can speak of any kind of temperature only after $\beta(\omega) \approx \beta$.

Let us return to the problem of holon relaxation and apply to it the upper consideration. One choice of the observable A is to use the current operator, $A = \mathbf{j}$. As a consequence, one should be aware that the temperature established from Eq. (4.7) should be interpreted as the temperature of the vicinity of the holon and not necessarily as the global temperature of the whole system. As such it turns out to be a local and time-dependent probe of the system. Due to the numerical implementation it is unfortunately impossible to probe e.g. spin background at some fixed point of space and compare it to the temperature established from $\mathbf{j}$, since distance can only be measured relative to the holon.

Observations are the following: (i) at short times $t < 6$ left side of Eq. (4.7) does not resemble the form of $\tanh(\dots)$, therefore one cannot assign any temperature to the locality of the holon. (ii) for $t \gtrsim 6$ there is some slight dependence $\beta(\omega)$, however one can fit $\tanh(\beta(t)\omega/2)$ to the left side of Eq. (4.7) with pretty high confidence and extract from it the time-dependent $\beta(t)$ parameter, yielding the temperature $T(t)$ presented in Fig. 4.5. Results are shown for system with $N = 20$ sites and both type of initial excitations. Subscripts only denote the direction of

the quench and/or current operator. It is revealed that for both types of relaxation a similar time-dependence with an exponential relaxation towards the stationary value is obtained, with a nontrivial observation that the temperature of the steady state, $t > 20$, is the same as if established from the kinetic energy of the steady state, Fig. 4.2. Namely, if we equal the steady state kinetic energy with the value obtained for a thermal ensemble, $E_{kin}(t \to \infty) = E_{kin}(\tilde{T}_{eff})$, then $\tilde{T}_{eff} \approx 1.02, 1.08$ at $N = 20$ and $\tilde{T}_{eff} = 0.68, 0.78$ at $N = 26$ sites, for the initially localized and the π-pulsed hole, respectively. These values match well with $T(t)$ at longer times in Fig. 4.5 (for $N = 26$ marked only with arrows).

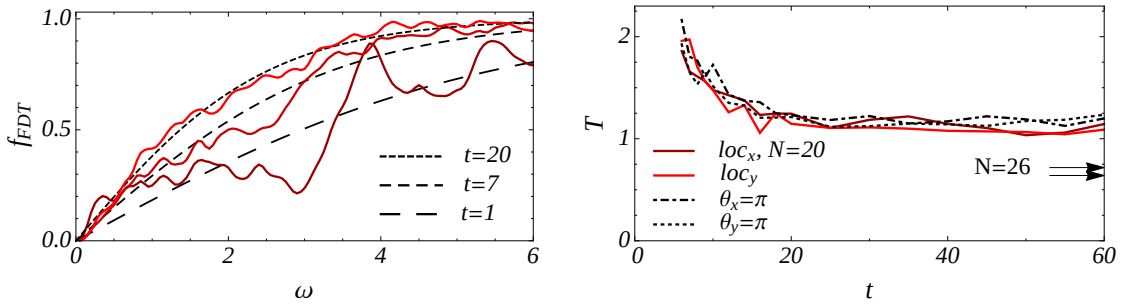

Figure 4.5: Left: $f_{FDT} = (C^{jj}(\omega,t) - C^{jj}(-\omega,t)/(C^{jj}(\omega,t) + C^{jj}(-\omega,t))$ for current operator in x direction and to it fitted $\tanh(\beta\omega/2)$ with β as the fitting parameter, obtained on system with $N = 20$ sites and $J = 0.4$ after initially localizing the hole. Right: the time dependence of the temperature T obtained from fitting for both types of the initial excitation of a holon. For $N = 26$ system only the steady-state values are marked.

From this analysis we can draw some physical interpretation. For a reason not completely understood (and possibly even of a numerical/finite-size nature) the vicinity of the holon fails to thermalize completely with the other part of the system. However, fluctuations necessary for the thermal nature of this region nonetheless build up, as revealed by applicability of the FDT. Through the time dependence of the local temperature one can literally observe cooling of the vicinity of the holon due to coupling to cooler more distant regions by emission of magnon-like excitations (see next Section). It remains to be resolved what is the reason for this pre-thermal-like polaron with surprisingly well defined local temperature.

4.2 Multi-stage dynamics of the spin-lattice polaron formation

In this Section we give a plausible picture for the initial relaxation of charges, photo-excited in Mott insulator. Hopefully justified at least at small charge densities, it is assumed that shortly after their creation, charges behave as independent, therefore we again treat only a single one, e.g. a holon. Simply speaking, the scenario that will be supported by concrete calculations is the following: supposing that holon is created at some site,

(i) in the first stage it perturbs the AFM background in its vicinity by simply hopping around,

(ii) in the second stage this local spin perturbation (as well as the excess local energy) is dispersed through magnons into the whole system.

To reduce the complexity we simulate 2D system with 1D spin chain in a staggered field h,

$$H = -t_h \sum_i (\tilde{c}^\dagger_{i,s} \tilde{c}_{i+1,s} + \text{H.c.}) + J \sum_i (\mathbf{S}_i \cdot \mathbf{S}_{i+1} - \frac{1}{4} n_i n_{i+1}) + h \sum_i (-1)^i S^z_i. \quad (4.8)$$

The staggered field mimics the spin order present in 2D (but absent in 1D) in which hopping of holon creates a string of excited spin exchange interactions. Similarly, hopping of holon in 1D causes shifts of spins into the preferentially oppositely oriented sublattice. Therefore a holon that has hopped for r sites feels potential

$$V(r) = h|r| + (1 - \delta_{r,0}) \frac{J}{2}, \quad (4.9)$$

which consequentially localizes it. To reproduce the magnetization profile on 2D lattice $h \approx 0.7J$ should be used, however, it will mainly be taken as a free parameter that helps to distinguish the two stages more clearly.

The two-stage scenario is neatly exposed through holon-spin correlations (as compared with their values in the ground state),

$$C_s(t, j) = \sum_i (-1)^{i+j} \Big[\langle \psi(t) | n^h_i S^z_{i+j} | \psi(t) \rangle - \langle \psi_G | n^h_i S^z_{i+j} | \psi_G \rangle \Big], \quad (4.10)$$

where $|\psi_G\rangle$ is the g.s. wave function (spin polaron) of the Hamiltonian with $t_h = 1$, while $|\psi(t)\rangle$ is the wave function obtained by time evolution with the quenched Hamiltonian in small time steps within the Lanczos basis on systems of $N = 26$ sites. Namely, the initial state with a localized holon is obtained as the g.s. of the Hamiltonian with $t_h = 0$ in Eq. (4.8) and is then propagated with $t_h = 1$. The two stages, (i) and (ii), are seen in $C_s(t, j)$ through two different (Lieb-Robinson) velocities in the propagation of correlations. In the first stage (i) it is actually the holon that is moving relative to the spin background, shifting the spins on the energetically unfavorable sublattice with respect to the staggered field. Before being substantially influenced by the potential $V(r)$, Eq. (4.9), it can travel as a free particle with velocity $v_h = 2t_h$, marked on Fig. 4.6 with a dashed line. However, its spread is eventually inhibited by $V(r)$. In the second stage (ii) the local spin perturbation, created by holon in the first stage, propagates into the system via magnons. The maximal velocity for the propagation of magnon fronts,

$$v_m = h + J - \sqrt{h(h + 2J)}, \quad (4.11)$$

can be established from the calculation of the time-evolution for a single overturned spin in the Néel ordered background, as determined in the following, and is marked on Fig. 4.6 by a solid line. A slight mismatch between the propagation of the first magnon front and the solid line is due to the fact, that as in 2D the kinetic energy of holon again saturates somewhat above the g.s. value so that the particle still has some remaining group velocity as well.

Drawing connections to the discussion on 'warmer' vicinity around the holon in 2D, this can be observed also in Fig. 4.6 via larger spin perturbation around holon $C_s(t, j \sim 1)$ with respect to the rest of the system, $C_s(t, j > 3)$.

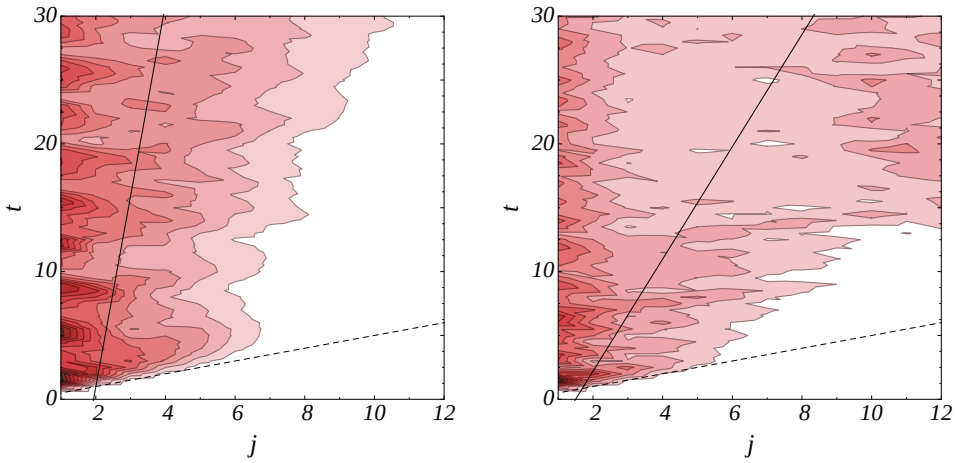

Figure 4.6: $C_s(t,j)$ for $h = 0.6$ and $J = 0.35$ (left) and $J = 0.75$ (right). Dashed line is obtained from the free holon propagation velocity v_h, $j = v_h t$, while the solid one from the maximal magnon velocity v_m, $j = r_0 + v_m t$.

Emission of local spin energy via magnons

Here we derive the maximal velocity at which a local spin perturbation is dispersed into the system via magnon waves and show that such scenario is indeed appropriate for our case. Let a be the sublattice of the chain (odd sites) where spins are preferentially *up*, while on the sublattice b (even sites) they are *down*. To treat excitations on such a chain we do the Holstein-Primakoff transformation

$$\begin{aligned} S^+_{aj} &= \sqrt{1 - a^\dagger_j a_j}\; a_j; \quad a_j = \frac{1}{\sqrt{N}} \sum_k c_k e^{ikj}, \\ S^+_{bj} &= b^\dagger_j \sqrt{1 - b^\dagger_j b_j}; \quad b_j = \frac{1}{\sqrt{N}} \sum_k d_k e^{ikj}, \end{aligned} \tag{4.12}$$

where $a^\dagger_j, b^\dagger_j$ are creation operators for local excitations on each sublattice, $c^\dagger_k, d^\dagger_k$ their Fourier transforms, and the N number of sites on each sublattice. Note that $k \in [-\pi/2, \pi/2]$. In terms of the $c^\dagger_k, d^\dagger_k$ Hamiltonian is not diagonal, therefore we do a transformation to operators α_k, β_k,

$$\alpha_k = u_k c_k - v_k d^\dagger_k, \quad \beta_k = u_k d_k - v_k c^\dagger_k \tag{4.13}$$

in terms of which it is [164]. Here u_k, v_k are real and satisfy [165]

$$\begin{pmatrix} 2u_k^2 \\ 2v_k^2 \end{pmatrix} = \pm 1 + \left(1 - \frac{J^2 \cos^2 k}{(J+h)^2}\right)^{-1/2}, \quad 2u_k v_k = -\left(1 - \frac{J^2 \cos^2 k}{(J+h)^2}\right)^{-1/2}. \tag{4.14}$$

Eigenmodes $|\phi_{\delta,k}\rangle; |\phi_{1,k}\rangle = \alpha^\dagger_k |\phi_0\rangle, |\phi_{2,k}\rangle = \beta^\dagger_k |\phi_0\rangle$, here written with the g.s. $|\phi_0\rangle$, have energy dispersion [164]

$$\omega_k^2 = (J+h)^2 - (J\cos k)^2, \tag{4.15}$$

which is gapped in contrast to 2D case. Suppose we make a local excitation on both lattices,

$$|\psi^i\rangle = \frac{1}{\sqrt{\mathcal{N}}}\,(a_1^\dagger + b_2^\dagger)|\phi_0\rangle$$
$$= \frac{1}{\sqrt{\mathcal{N}N}}\sum_k \left(e^{-ik}(\alpha_k^\dagger u_k + \beta_k v_k) + e^{-2ik}(\alpha_k v_k + \beta_k^\dagger u_k)\right)|\phi_0\rangle. \tag{4.16}$$

where $\mathcal{N}$ is an appropriate normalization. Since $|\phi_0\rangle$ is the g.s. β_k and α_k act trivially on it. The time-evolved wave function is then

$$|\psi^i(t)\rangle = \frac{1}{\sqrt{\mathcal{N}N}}\sum_k e^{-i\omega_k t}u_k(e^{-ik}\alpha_k^\dagger + e^{-2ik}\beta_k^\dagger)|\phi_0\rangle. \tag{4.17}$$

In order to follow the spread of initially local spin excitations, we should go back to the real space and use

$$\alpha_k^\dagger|\phi_0\rangle = \frac{1}{\sqrt{N}}\sum_j (e^{ikj}u_k a_j^\dagger - e^{-ikj}v_k b_j)|\phi_0\rangle,$$
$$\beta_k^\dagger|\phi_0\rangle = \frac{1}{\sqrt{N}}\sum_j (e^{ikj}u_k b_j^\dagger - e^{-ikj}v_k a_j)|\phi_0\rangle. \tag{4.18}$$

If we neglect $a_j|\phi_0\rangle, b_j|\phi_0\rangle$ then

$$|\psi^i(t)\rangle = \frac{1}{\sqrt{\mathcal{N}}N}\sum_{k,j} e^{-i\omega_k t+ikj}u_k^2(e^{-ik}a_j^\dagger + e^{-2ik}b_j^\dagger)|\phi_0\rangle \tag{4.19}$$

The maximal velocity of magnons

$$v_m = \left.\frac{\partial\omega_k}{\partial k}\right|_{k=k_0} = h + J - \sqrt{h(h+2J)} \tag{4.20}$$

is also the velocity with which travels the front of spin excitations in the upper solution.

If we turn more spins with amplitudes $A_d(B_d)$ on several sites d within the sublattice $a(b)$, then the propagation of such distortion is approximately

$$|\psi^i(t)\rangle = \frac{1}{\sqrt{\mathcal{N}'}N}\sum_{k,d,j} e^{-i\omega_k t+ik(j-d)}u_k^2(A_d\ a_j^\dagger + B_d\ b_j^\dagger)|\phi_0\rangle. \tag{4.21}$$

To demonstrate the appropriateness of the latter expression for our case of the excited holon, we compare the correlation $C_s(t+t_i, j_0)$, Eq. (4.10), with

$$C_m(t, j_0) = \begin{cases} \left|N^{-1}\sum_{k,d} e^{-i\omega_k t+ik(j_0-d)}u_k^2 A_d\right|^2 & \text{if } j_0 \text{ odd,} \\ \left|N^{-1}\sum_{k,d} e^{-i\omega_k t+ik(j_0-d)}u_k^2 B_d\right|^2 & \text{if } j_0 \text{ even,} \end{cases}$$

where only summation over the initial distortion within $|d| < j_0$ is taken into account through $B_d(A_d)$. Namely, coefficients A_d, B_d for Eq. (4.21) are obtained numerically from $C_s(t_i, j)$ at time $t_i \approx 5$ (when the initial spreading of holon is over) as $A_d = |C_s(t_i, d)|^{1/2}$ for even d and $B_d = |C_s(t_i, d)|^{1/2}$ for odd d. In this way the phase that

relates excitations at different sites in $C_s(t_i, j)$ is neglected, however, Fig. 4.7 still demonstrates that the actual numerical spread of the local spin excitation follows the simple argumentation made above. It turns out that comparison is better between $C_s(t + t_i, j_0)$ and $2C_m(t, j_0)$, which might be related to the fact that local spin perturbation created by holon has only half of the chain unperturbed and is therefore spreading into it with doubled amplitude.

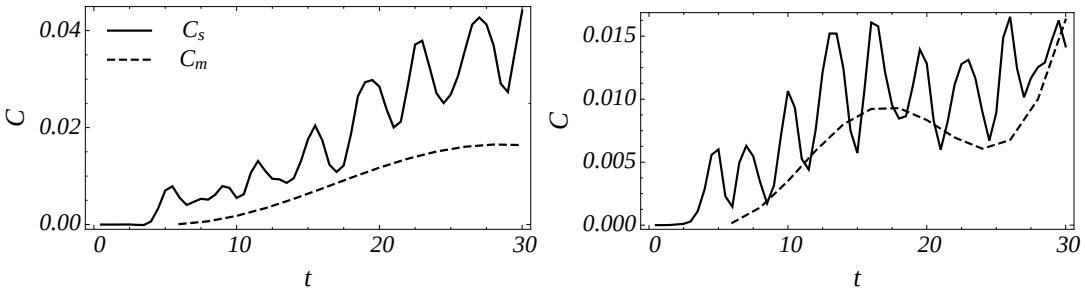

Figure 4.7: Comparison of correlations $C_s(t + t_i, j_0)$ with $2C_m(t, j_0)$ at site $j_0 = 10$ for $h = 0.6$ and $J = 0.55, 0.85$, respectively.

Adding phonon bath

Switching on the electron-phonon coupling by including to the Hamiltonian (4.8) the term

$$H_{ep} = g \sum_i n_i^h (a_i^\dagger + a_i) + \omega_0 \sum_i a_i^\dagger a_i, \tag{4.22}$$

adds an additional degree of freedom coupled to the holon.

The most discernible effect of a nonzero g is the shortening of the polaron formation, which is now of a combined spin-lattice type. As shown on Fig. 4.8 this is clearly observed in shortening of the time within which the kinetic energy of the excited holon saturates, and happens progressively with increasing $\lambda = g^2/2t_h\omega_0$. Presented results are obtained with the EDLFS method.

Even more interesting observation is that at short times, depending on the coupling strength λ, holon preferentially emits its energy to the more efficient bath, which is at small λ the spin one while at large λ the phonon one. However, on the longer timescale two baths equilibrate between each other as seen e.g. in the decrease of ΔE_{phon} and increase of ΔE_{spin} at largest $\lambda = 0.4$, Fig. 4.8 (f). Here $\Delta E_{phon}(t)$ and $\Delta E_{spin}(t)$ are the amount of the energy transmitted to the phonon and the spin degree of freedom by the time t. While there is no direct coupling between the spin and the lattice sector, such redistribution can only take place via coupling to the charge. It is thus not surprising that we obtain a much longer timescale for this energy exchange process, with a very rough estimate $t_{ex} \sim 50$. A better understanding and characterization of the equilibration process is yet to be pursued.

Moreover, also the discrepancy between the g.s. and the stationary state kinetic energy, $\Delta\tilde{E}_{kin}$ gets reduced by increasing λ as shown in the inset of Fig. 4.8 (b). This can be interpreted in two (intertwined) ways: (i) an additional bosonic degree of freedom make it easier for the holon to relax, since constraints due to momentum

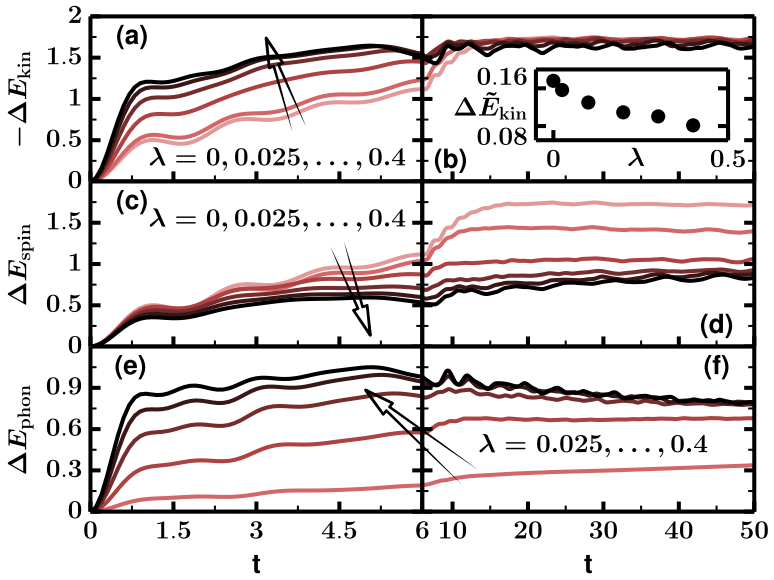

Figure 4.8: Time-dependence of the change of kinetic energy of a holon ΔE_{kin} (relative to the initial value), total spin energy ΔE_{spin}, phonon energy ΔE_{phon} for different values of $\lambda = g^2/2\omega_0 t_0 = 0.0, 0.025, 0.1, 0.2, 0.3, 0.4$, and $J = 0.3$, $h = 0.7J$, $\omega_0 = 1.0$. Inset in (b) represents $\Delta\tilde{E}_{kin} = \langle\psi(t)|H_{kin}|\psi(t)\rangle - \langle\psi_G|H_{kin}|\psi_G\rangle$ where $|\psi_G\rangle$ is the respective g.s. wave function of the quenched Hamiltonians (with $t_h = 1$). Open slanted arrows indicate ordering of the data according to increasing values of λ.

and energy conservation and the presence of a gap in spin excitations Eq. (4.15) are relaxed, (ii) holon can cool down buy coupling to phonons and therefore has a lower kinetic energy due to the lower local temperature. Both scenarios remain to be further examined.

Chapter 5

Charge recombination in photo-doped Mott insulators

The lifetime of a double occupancy excited within a Mott insulator has attracted attention in several contexts, from optical lattices with cold atoms to strongly correlated materials. In optical lattices double occupancies can be created by a sinusoidal modulation of the lattice depth with a frequency close to U, while in correlated material they are created by applying a short laser (pump) pulse of a frequency larger than the Mott-Hubbard (MH) gap. What makes the decay of the double occupancy slow, compared to the intrinsic scale of the dynamics set by the hopping parameter $\hbar/t$, is the large energy that has to be instantaneously transmitted to some other (typically bosonic) degrees of freedom. As revealed by ours [34, 35, 40] and other [64, 65, 87] studies the complexity of the process results in a decay rate that is approximately exponentially suppressed by the number $n = \Delta/\epsilon_0$ of excitations to which the energy is transfered,

$$\Gamma \sim \Gamma_0 \exp(-\alpha\Delta/\epsilon_0). \tag{5.1}$$

Here Δ is the MH gap and ϵ_0 the typical energy of relevant (bosonic) excitations that are emitted in the recombination process. Therefore it is essential to recognize the most efficient decay channel. However, it is not only ϵ_0 but also the actual coupling of the charge with the selected degree of freedom (which might be dimension dependent) that effects the result.

In this Chapter we focus on the lifetime of double occupancies created with a short pump pulse applied to a correlated material that in equilibrium behaves as a Mott insulator. Each creation of a doubly occupied site (doublon) is accompanied by the creation of a non-occupied site (holon). Of course this is only a simplified description for materials that are actually charge transfer insulators, which should be characterized by a multi-orbital model. At low densities holons and doublons bear some resemblance to the holes and electron quasiparticles in semiconductors: (a) they are oppositely charged relative to the reference insulator, (b) they are well mobile with an effective band dispersion within the lower and the upper Hubbard band, respectively, and (c) they can form a bound excitonic-like state, i.e. a holon-doublon (HD) exciton. On the other hand, unlike in a pure semiconductor a single HD pair (neglecting the coupling to phonon degrees of freedom) is not an eigenstate and has an intrinsic recombination rate Γ.

In experiments using optical spectroscopy the HD density is indirectly observed

through deviations in the reflectivity $R(\omega)$ from its equilibrium value. Simply speaking, the deviation in $R(\omega)$ at any ω is proportional to the density of holons and doublons, therefore the time dependence of its amplitude reflects the time dependence of the charge density. Slightly more convincing, by using Kramers-Kronig relations optical conductivity can be obtained, in which the presence of charges (at least in effectively two-dimensional materials with spin correlations) is reflected in in-gap peaks that can even be compared with peaks at the chemical doping [14]. As determined from the amplitude decay of e.g. in-gap peaks, holon-doublon (HD) pairs are recombining on the ps timescale. As reported in more detail in Sec. 1.2.1 this has been observed in different types of system, ranging from two-dimensional (2D) cuprates [13, 14], one-dimensional (1D) cuprates [38], Ni-chains [23, 24], to organic molecular compounds [20, 21]. Common to all materials is that the recombination process is slower than $\hbar/t$ but still much faster than in semiconducting materials [166] and carbon nanotubes [42, 43, 44].

The central goal of this Chapter is to introduce two mechanisms of the recombination for effectively 2D and 1D systems that can qualitatively explain observed recombination times in 2D cuprates (La_2CuO_4, Nd_2CuO_4) [13, 14] and 1D organic salts (ET-F_2TCNQ) [21]. As relevant for the low charge density n_{HD} (created by the pump excitation with a low photon density) we assume that at shorter times holon and doublon bind into an exciton, which is then taken as the initial state for the process of the recombination. We support this assumption with a model-based calculation and by experimental observation that decay of the charge density is exponential in time with decay rate independent of the (initial) charge density. If the recombination of HD pair would depend on the probability for holon and doublon to meet, then

$$-\frac{dn_{HD}}{dt} \propto n_{HD}^{\gamma}, \quad \gamma = 2, 3, \tag{5.2}$$

which clearly does not lead to an exponential decay. $\gamma = 2$ is applicable to cases where energy is transmitted to some bosonic excitations, while $\gamma = 3$ is for the case of Auger type of the recombination where energy is transferred to the kinetic energy of another (remaining) holon or doublon.

Each of mechanisms is based on a dominant decay channel that depends on the specifics of the system, e.g. dimensionality, energy of phononic excitations, etc. We suggest and confirm the appropriateness of each decay channel by deriving the minimal model and calculating the recombination rate using Fermi golden rule (FGR) approximation.

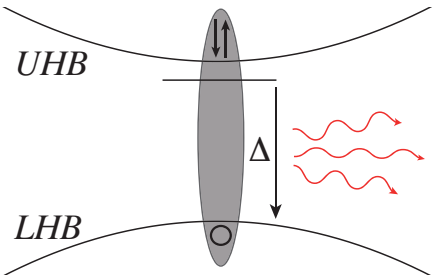

(i) We propose that in 2D systems with at least short-range spin ordering HD pair recombines by emission of *several dispersive spin excitations*. It turns out that

the spin dressing (assisting the HD binding and as a consequence) involved in the HD exciton crucially boosts the decay.

(ii) In 1D system, on the other hand, due to charge-spin separation [167, 168] similar dressing with spins is not present, resulting in a decay that would be too slow as compared to experiments. Especially in organic salts, consisting of complex molecules with rich internal structure and consequently energetic intra-molecular vibrations, *coupling of the charge to phonons* seems important. Partially eliminating the spin degree of freedom in order to reduce the complexity of the problem, we treat the recombination in nearly spin polarized sector and couple the holon and doublon to phonons. At a sensible strength of coupling the experimental recombination rate is reproduced.

(iii) However, the latter mechanism cannot explain experiments on 1D cuprates [38] where energy of phonons is much smaller. As suggested also by previous studies [169], in this case the exchange constant J might be phonon modulated, yielding $J(x)$. Such phonon-spin coupling might eventually assist a HD spin dressing, enhancing the decay. Test of such scenario remains to be performed.

(iv) In case of pump excitations with higher photon density and/or when HD exciton does not exist other types of the decay might become dominant. If the bandwidth of e.g. the upper Hubbard band is larger than the MH gap, then recombination is a much simpler process consisting of a single scattering of HD pair with another holon or doublon (Auger type). However, it is highly dependent on the charge density and should be dominant only at larger charge densities. Experiments partly supporting such reasoning are reported in [170].

The problem of the doublon decay has been addressed before in connection with ultracold bosons [67] and fermions [64, 65] in optical lattices using the diagrammatic approach. In the latter case charge densities are quite high so that the dominant mechanism relies on energy transfer to the kinetic energy of other particles. However, since the bandwidth of the upper Hubbard band is smaller than the gap, the decay of a doublon is still a complex many-scattering process, as revealed in an exponential dependence of the decay rate on U/t, where U is the Coulomb on-site repulsion and t the hopping parameter, setting the energy scale of initial and final excitations. Similar dependence that suggests the same recombination mechanism has been obtained also in excited half-filled Hubbard model via the time-dependent single-site dynamical mean-field theory (DMFT) [28, 66]. Due to rather strong excitation (simulating the pump pulse) system starts at rather high effective temperatures T with a high density of HD pairs, similar to the experimental situation with cold atoms. Furthermore, by construction the single-site DMFT method does not incorporate non-local spin fluctuations and therefore cannot comment on the recombination into spin excitations. This could be improved by implementing a cluster of size of a HD exciton. The recombination of a HD pair into spin excitations at low and high temperatures has been addressed within the nth order perturbation theory [87]. However, possible correlations between the holon and the doublon, i.e. the HD binding (an essential ingredient of our work) were neglected, since the prime interest was actually the decay of unpaired fermions in the attractive Hubbard model. A similar process of the exciton recombination has been theoretically addressed in

carbon nanotubes [41, 171], where the importance of initial conditions has been examined as well, concluding that the multi-phonon emission can be efficient in the case of localized excitons, however, it becomes subdominant in doped nanotubes.

This Chapter is organized as follows. In Sec. 5.1 we obtain an analytical expression for the recombination rate of an exciton wave function coupled to some general bosons, based on a toy exciton-boson model. In Sec. 5.2 we work on the theory for recombination in 2D systems: In Sec. 5.2.1 we present the derivation of the effective model from a single-band Hubbard model via the canonical transformation. An analogous procedure is applied in Sec. 5.2.2 to the three-band charge-transfer model as directly relevant for undoped cuprates. Based on the existence of the bound HD exciton within the 2D effective model on a square lattice we concentrate in Sec. 5.2.3 on the calculation of the recombination rate Γ within the FGR approximation and compare it with results obtained with the direct time evolution and in 5.2.4 with experimental result. In Sec. 5.3 we move to 1D systems and in Sec. 5.3.2 obtain the recombination rate within a nearly polarized system, adding comments on the non-polarized system in Sec. 5.3.3, and finally compare the result with experiments in Sec. 5.3.4.

Content of this Chapter is reported in Refs. [34, 35, 40].

5.1 Toy model for charge recombination

We tackle the problem of the charge recombination by first solving it within a toy model, tailored for mechanisms that we try to convey as plausible and using assumptions that will be for each concrete example confirmed in the following sections. The beauty of such an approach is that the recombination rate for a HD pair can be found analytically and is of a very general form, exhibiting the exponential suppression with the number of excitations to which the energy is transmitted. The recombination rate is calculated:

a) assuming a bound state of holon and doublon (MH exciton) as the initial state,

b) coupling this exciton to bosons as described below,

c) using the FGR to establish the transition rate between the initial exciton to the final state with bosonic excitations (that receive the energy of exciton).

Our toy (exciton-boson) model consists of

$$\begin{aligned} H &= H_e + H_{eb} + H_b + H_{rc} \\ &= E_e e^\dagger e + e^\dagger e \sum_q \lambda_q (a_q^\dagger + a_{-q}) + \sum_q \omega_q a_q^\dagger a_q + g_{rc}(e + e^\dagger). \end{aligned} \tag{5.3}$$

where $e^\dagger$ is a creation operator for the exciton with energy E_e and $a_q^\dagger$ a creation operator for boson with momentum q and energy ω_q. The exciton-boson coupling is mediated by the term H_{eb}, while H_{rc} represents the simplest form of the exciton recombination/creation and will be taken as a perturbation with respect to the dynamics that conserves the exciton. Latter assumption is justified by the experimental observation that recombination is a very slow process. A similar model has been used to address the charge recombination in carbon nanotubes via the multi-phonon emission [41, 171], and is here generalized to dispersive bosons. Dispersive

nature of bosons is conceptually crucial since only in such case recombination is a non-reversible process.

The toy model Eq. (5.3) basically describes the two-level system coupled to bosons, and was used when discussing related question of radiationless transitions in large molecules [172], quantum dissipation [173], and in numerous other problems. It is well analyzed and solvable in several limits, in particular if H_{rc} is treated as a perturbation.

First of all we would like to get rid of the coupling between exciton and bosons on the level of the unperturbative part of the Hamiltonian. Therefore we do the standard Lang-Firsov transformation $\tilde{H} = e^{-S} H e^{S}$, which eliminates H_{eb} with

$$S = -e^\dagger e \sum_q \alpha_q (a_q^\dagger - a_{-q}), \tag{5.4}$$

where $\alpha_q = \lambda_q/\omega_q$ and yields the transformed Hamiltonian (see App. C.1)

$$\begin{aligned} \tilde{H} &= \tilde{H}_0 + \tilde{H}_{rc}, \\ \tilde{H}_0 &= (E_e - \epsilon_{eb}) e^\dagger e + \sum_q \omega_q a_q^\dagger a_q, \\ \tilde{H}_{rc} &= g_{rc} \exp\left[- \sum_q \alpha_q (a_q^\dagger - a_{-q}) \right] e + \text{H.c.}. \end{aligned} \tag{5.5}$$

The exciton-boson binding energy $\epsilon_{eb} = \sum_q |\lambda_q|^2/\omega_q$ that lowers the exciton's energy implicitly indicates its bosonic dressing. However, it is assumed to be modest, i.e. $\epsilon_{eb} \ll E_e$.

As the initial wave function we take the dressed exciton $|\psi_0^e\rangle = e^\dagger |0\rangle$ with energy $E_0^e = E_e - \epsilon_{eb}$, which is the ground state of $\tilde{H}_0$ in the sector with an exciton. In a real experiment this state would be supposedly reached after a short-time relaxation of the HD pair, created by a pump pulse. Due to the charge-boson coupling the pair must necessarily get dressed with them. However, such exciton state is not an eigenstate when recombination term $\tilde{H}_{rc}$ is taken into account. Its recombination rate Γ is established using the FGR,

$$\Gamma = 2\pi \sum_{\mathbf{m}} |\langle \psi_{\mathbf{m}}^0 | H_{rc} | \psi_0^e \rangle|^2 \; \delta(E_0^e - E_{\mathbf{m}}^0), \tag{5.6}$$

where $|\psi_{\mathbf{m}}^0\rangle$ is a state with m bosons (and no exciton) and with the common momentum and the energy $E_{\mathbf{m}}^0$ that have to equal the momentum and the energy of the initial excitonic state. We will rather use an integral form

$$\begin{aligned} \Gamma(\omega = E_0^e) &= 2\pi \langle \psi_0^e | \tilde{H}_{rc} \sum_{\mathbf{m}} |\psi_{\mathbf{m}}^0\rangle\langle\psi_{\mathbf{m}}^0| \; \delta\big(\omega - (\tilde{H}_0 - E_{\tilde{0}})\big) \; \tilde{H}_{rc} | \psi_0^e \rangle \\ &= 2Re \; \langle \psi_0^e | \tilde{H}_{rc} \int_0^\infty dt e^{i\omega t - i(\tilde{H}_0 - E_{\tilde{0}})t} \; \tilde{H}_{rc} | \psi_0^e \rangle \end{aligned} \tag{5.7}$$

that has to be evaluated at $\omega = E_0^e = E_e - \epsilon_{eb}$ in order to be equivalent to the expression (5.6). Such ω is actually the difference in the g.s. energy of $\tilde{H}_0$ in the sector with and without the exciton, which will in the following section correspond to the MH gap Δ. In addition, we used that $\sum_{\mathbf{m}} |\psi_{\mathbf{m}}^0\rangle\langle\psi_{\mathbf{m}}^0|$ is a full set of wave

functions in the subspace without the exciton. Taking into account well known relations for coherent states (for derivation see App. C.1)

$$\langle\psi_0^e|\tilde{H}_{rc}e^{-i(\tilde{H}_0-E_{\tilde{0}})t}\ \tilde{H}_{rc}|\psi_0^e\rangle = g_{rc}^2\exp\Big(\sum_q|\alpha_q|^2(e^{-i\omega_q t}-1)\Big), \tag{5.8}$$

we finally get

$$\Gamma(\omega) = 2g_{rc}^2\ Re\int_0^\infty dt\exp\Big(i\omega t+\sum_q|\alpha_q|^2(e^{-i\omega_q t}-1)\Big). \tag{5.9}$$

Saddle point approximation

While Eq. (5.9) can be evaluated numerically for arbitrary parameters, i.e. the coupling strength g_{rc} and dispersions λ_q, ω_q, it is instructive to get result in a form that reveals the relevant quantities entering Γ. For this purpose we first simplify the general dispersions λ_q, ω_q by assuming that the boson coupling function $g(\omega)$ has mean energy ω_0 and a σ spread around that value, fixing the form

$$g(\omega) = \sum_q|\alpha_q|^2\ \delta(\omega-\omega_q) = \frac{\xi}{\sqrt{2\pi}\sigma}\ e^{-(\omega-\omega_0)^2/2\sigma^2} \tag{5.10}$$

with a Gaussian function centered at $\omega=\omega_0$. The dimensionless prefactor $\xi = \sum_q|\alpha_q|^2$ takes into account the strength of the coupling. Such approximation is well justified for bosons with weak dispersion, e.g. the optical phonons, however it should be reasonable also for the 2D magnons with $\omega_0\approx J$. Nevertheless, the dispersion $\sigma>0$ is essential for a smooth variation of Γ vs ω, and conceptually crucial for the final dispersion of bosons into the system.

The advantage of the form Eq. (5.10) is that the integral Eq. (5.9) can be analytically evaluated by the saddle point approximation [174], i.e.

$$\int_{-\infty}^{\infty}\exp\big(f(t)\big)dt \approx \exp\big(f(t_0)\big)\sqrt{\frac{2\pi}{-f''(t_0)}},\quad f'(t)|_{t_0}=0. \tag{5.11}$$

The function $f(t)$ and its saddle point t_0, correct up to $\mathcal{O}(\sigma^4/\omega_0^4)$, are in our case

$$\begin{aligned}
&f(t) = i\omega t+\xi\ \exp\left(-i\omega_0 t-\frac{\sigma^2t^2}{2}\right),\\
&f'(t)|_{t_0}=0\quad\rightarrow\quad\ln\left(\frac{\omega}{\xi(\omega_0-i\sigma^2t_0)}\right) = -i\omega_0t_0-\frac{\sigma^2t_0^2}{2}\\
&t_0\approx\frac{i}{\omega_0+\tilde{\sigma}}\ln\left(\frac{\omega}{\xi(\omega_0+2\tilde{\sigma})}\right),\quad\tilde{\sigma}=\frac{\sigma^2}{2\omega_0}\ln\frac{\omega}{\xi\omega_0}.
\end{aligned} \tag{5.12}$$

A drawback of the Gaussian coupling is that t_0 cannot be find exactly, like for Lorentzian $g(\omega)$. However, in order to establish comparison between approaches (as in Fig. 5.1) in case of the Lorentzian coupling, tails at $\omega\gg\omega_0$ are difficult to treat within the numerical integration in Eq. (5.9). For the cases when $\sigma\ll\omega_0$, we use

the Gaussian form, Eq. (5.10), and expand within $\mathcal{O}(\sigma^4/\omega_0^4)$ the relevant quantities that enter (5.11),

$$f(t_0) \approx -\omega t_{0i} + \frac{\omega}{\omega_0 + \sigma^2 t_{0i}} \approx -\frac{\omega}{\omega_0}\left(\ln\frac{\omega}{e\xi\omega_0} - \frac{\sigma^2}{2\omega_0^2}\ln^2\frac{\omega}{\xi\omega_0}\right) \tag{5.13}$$
$$f''(t_0) \approx -\omega\left((\omega_0 + \sigma^2 t_{0i}) + \frac{\sigma^2}{(\omega_0 + \sigma^2 t_{0i})}\right) \approx -\omega\omega_0\left(1 + \frac{\sigma^2}{\omega_0^2}\ln\frac{e\omega}{\xi\omega_0}\right),$$

where $t_{0i} = \text{Im } t_0$. Because in Mott insulators the energy transmitted to bosons equals the MH gap, we use notation $\omega = \Delta$ already here. If we neglect also the contributions of order σ^2/ω_0^2 then Γ has especially compact form

$$\Gamma \approx g_{rc}^2 e^{-\xi}\sqrt{\frac{2\pi}{\Delta\omega_0}}\ \exp\left[-\frac{\Delta}{\omega_0}\ln\left(\frac{\Delta}{e\ \xi\omega_0}\right)\right]. \tag{5.14}$$

It transparently shows that recombination rate is exponentially suppressed by the number of bosonic excitations created Δ/ω_0, while the strength of the exciton-boson coupling ξ enters only through the logarithmic correction. Still, depending on its strength it can assist a faster decay.

To test the applicability of Eq. (5.11) for our case we compare in Fig. 5.1: a) the numerical evaluation of Γ from Eq. (5.9), b) the saddle point result for numerically (exactly) established saddle, c) the saddle point result for approximate saddle Eq. (5.12), and d) compact form of Eq. (5.14) with $\sigma = 0$.

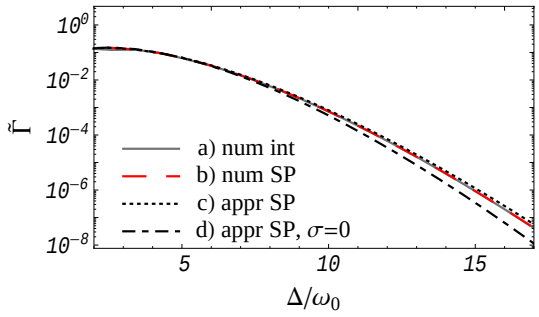

Figure 5.1: Comparison of the result for $\tilde{\Gamma} = \Gamma/g_{rc}^2$, if calculated with a) the numerical evaluation of Γ from Eq. (5.9), b) the saddle point result for numerically (exactly) established saddle, c) the saddle point result for approximate saddle Eq. (5.12), and d) compact form of Eq. (5.14). Parameters $\omega_0 = 5, \xi = 3, \sigma = \omega_0/4$ are used so that numerical integration a) is well defined.

Expression (5.14) will be compared with numerical results on 2D recombination, where role of bosons will be played by spin excitations and recycled again for the 1D recombination, where appropriate bosons will be phonons.

5.2 Recombination in 2D correlated systems

In this Section we address the recombination process in 2D systems, as relevant for effectively 2D cuprates. First we derive the minimal model needed to explain

the recombination of a HD pair via an emission of spin excitations. We derived it from the prototypical single-band Hubbard model, but also from a more realistic multi-band charge transfer model. We establish the existence of MH exciton in such a model and assume it as the initial condition for the recombination. Its decay rate is then established using FGR. Numerical results are compared to the analytical expression for the recombination rate obtained from the toy model in the previous Section and to the experimental results on La_2CuO_4 and Nd_2CuO_4 [13, 14].

5.2.1 Single-band Hubbard model

We start with the prototype model for studies of the Mott insulator - the single-band Hubbard model,

$$H = -t \sum_{\langle ij \rangle s} (c^\dagger_{js} c_{is} + \text{H.c.}) + U \sum_i n_{i\uparrow} n_{i\downarrow}, \tag{5.15}$$

where sum runs over nearest-neighbor (n.n.) pairs of sites $\langle ij \rangle$ on a 2D square lattice. We are interested in the half-filled case, $\bar{n} = 1$, with a low density of holons $\bar{n}_h \ll 1$ and doublons $\bar{n}_d \ll 1$. The Hubbard model, Eq. (5.15), contains the recombination term with coupling t as the simple n.n. hopping between neighboring holon and doublon. However, if such a process does not conserve the energy it is virtual and observed only as an oscillation in the charge density. To eliminate virtual processes already on the level of the recombination operator we perform the usual canonical transformation of the Hubbard model [6, 175, 176] that in the lowest order decouples sectors with different number of HD pairs, however still relates them perturbatively. Based on the observation that recombination is a slow process it should be only a perturbation on top of the dynamics that conserved the number of charges. Indeed, as shown later on, the transformed Hamiltonian in addition to the standard t-J model [162] contains also terms causing recombination that were usually neglected in the studies of doped systems. Such an effective model on one hand serves us to find the initial HD bound state - by neglecting the recombination, and then yields its decay - by taking it into account.

Hence, we rederive here the effective model employing Hubbard operators X_i^{pq}, elaborated in Ref. [177]. If we define the holon state as $|H\rangle = |0\rangle$ and the doublon state as $|D\rangle = c^\dagger_{i\uparrow} c^\dagger_{i\downarrow} |0\rangle$ operators are expressed as

$$\begin{aligned} &X_i^{sH} = c^\dagger_{is}(1 - n_{i\bar{s}}),\ X_i^{Ds} = -s c^\dagger_{i\bar{s}} n_{is},\ X_i^{DH} = s c^\dagger_{is} c^\dagger_{i\bar{s}}, \\ &X_i^{s\bar{s}} = c^\dagger_{is} c_{i\bar{s}},\ X_i^{ss} = n_{is}(1 - n_{i\bar{s}}), \\ &X_i^{HH} = (1 - n_{i\downarrow})(1 - n_{i\uparrow}),\ X_i^{DD} = n_{i\downarrow} n_{i\uparrow}, \end{aligned} \tag{5.16}$$

where $s = \pm 1$ stands for the up/down electron spin. Upper indices pq in X_i^{pq} encode the initial (q) and final (p) state after the application of the operator. During the calculation their commutation relations

$$[X_f^{p_1 q_1}, X_g^{p_2, q_2}]_\pm = \delta_{fg} \left(\delta_{q_1 p_2} X_f^{p_1, q_2} \pm \delta_{p_1, q_2} X_f^{p_2, q_1} \right) \tag{5.17}$$

will be repeatedly used, with $\pm$ for fermionic (half-integer) and bosonic (integer change of spin) operators, respectively. In terms of Hubbard operators the starting

Hubbard model Eq. (5.15) can be re-expressed as

$$\begin{aligned} H &= H_U + H_t + H_{trc} \\ &= U\sum_i X_i^{DD} - t\sum_{ij,s}\left(X_i^{sH}X_j^{Hs} + X_i^{D\bar{s}}X_j^{\bar{s}D}\right) - t\sum_{ij,s} s\left(X_i^{sH}X_j^{\bar{s}D} + X_i^{D\bar{s}}X_j^{Hs}\right), \end{aligned} \tag{5.18}$$

where i, j are n.n., while H_U, H_t, H_{trc} are the on-site-repulsion, the HD-hopping and the HD-recombination/creation terms, respectively.

Canonical transformation

The canonical transformation is performed in the standard way [6, 175]

$$\tilde{H} = e^S H e^{-S} = H + [S, H] + \frac{1}{2}[S, [S, H]] + \dots \tag{5.19}$$

so that H_{trc} is transformed out, consequently fixing S with the condition $H_{trc} + [S, H_U] = 0$ (for derivation see App. C.2.1) to

$$S = \frac{t}{U}\sum_{ij,s} s\left(X_i^{sH}X_j^{\bar{s}D} - X_i^{D\bar{s}}X_j^{Hs}\right), \tag{5.20}$$

and the transformed Hamiltonian up to second order in t to

$$\tilde{H} = H_U + H_t + [S, H_t] + \frac{1}{2}[S, H_{trc}]. \tag{5.21}$$

Using X-operator commutation relations Eq.(5.17) we obtain several terms,

$$\tilde{H} = H_{tJ} + H_{rc} + H_c \tag{5.22}$$

where H_{tJ} conserves the HD number

$$H_{tJ} = -t\sum_{ij,s} X_i^{sH}X_j^{Hs} - t\sum_{ijs} X_i^{D\bar{s}}X_j^{\bar{s}D} + U\sum_i X_i^{DD} + \frac{t^2}{U}\sum_{ij,s}(X_i^{s\bar{s}}X_j^{\bar{s}s} - X_i^{ss}X_j^{\bar{s}\bar{s}}), \tag{5.23}$$

and H_{rc} is the essential term describing the HD recombination/creation

$$H_{rc} = \frac{t^2}{U}\sum_{(ijk),s} s[X_k^{sH}(X_i^{ss} - X_i^{\bar{s}\bar{s}})X_j^{\bar{s}D} + 2X_k^{\bar{s}H}X_i^{s\bar{s}}X_j^{\bar{s}D} + \text{H.c.}], \tag{5.24}$$

where j, k are n.n. sites to site i, and $j \neq k$. Further terms $H_c = H_4 + H_5 + H_6$ with parameters of order t^2/U are

$$\begin{aligned} H_4 &= \frac{t^2}{U}\sum_{(ijk),s} s[(X_j^{sH}X_k^{\bar{s}H} - X_j^{D\bar{s}}X_k^{Ds})X_i^{HD} + X_k^{sH}X_j^{\bar{s}D}(X_i^{HH} - X_i^{DD}) + \text{H.c.}], \\ H_5 &= \frac{t^2}{U}\sum_{(ijk),s}(-X_j^{sH}X_i^{DD}X_k^{Hs} + X_j^{D\bar{s}}X_i^{HH}X_k^{\bar{s}D} - X_j^{sH}X_i^{HD}X_k^{Ds} + X_j^{Hs}X_i^{DH}X_k^{sD} \\ &\qquad - X_j^{sH}X_k^{Hs}X_i^{\bar{s}\bar{s}} + + X_j^{sH}X_k^{H\bar{s}}X_i^{\bar{s}s} + X_j^{D\bar{s}}X_k^{\bar{s}D}X_i^{ss} - X_j^{Ds}X_k^{\bar{s}D}X_i^{s\bar{s}}), \\ H_6 &= \frac{t^2}{U}\sum_{ij} 2(X_i^{DD}X_j^{HH} + X_i^{DH}X_j^{HD}). \end{aligned} \tag{5.25}$$

Within the order t^2/U the coupling between sectors with different number of HD-pairs is present in terms H_{rc}, Eq. (5.24), and H_4, Eq. (5.25). Term H_4 could be relevant for recombination only at higher HD densities, since it is active only when three charged particles are n.n. to each other (as noted by right upper indices being e.g. HHD or HDD) and is negligible at $\bar{n}_d, \bar{n}_h \ll 1$. Therefore it should not play a key role in the recombination at low density of holons and doublons discussed here, and will be neglected further on. However, it could be necessary for the description of the short-time behavior in experiments where strong excitations produce an abundance of initially unbounded HD pairs. The terms H_5 and H_6 correspond to the two-site hopping of holon or doublon and could be used to correct the initial exciton wave functions within the order t^2/U. However, they will be neglected in comparison to the effect of the leading hopping term, contained in H_{tJ}, Eq. (5.23).

Effective model

The effective Hamiltonian that we consider further on contains terms Eqs. (5.23, 5.24). With the introduction of holon and doublon creation and annihilation operators

$$\begin{aligned} h_{is} &= c^\dagger_{is}(1 - n_{i\bar{s}}) = X^{sH}_i, \\ d_{is} &= c_{i\bar{s}} n_{is} = -s\ X^{sD}_i, \end{aligned} \tag{5.26}$$

it can be written in a more compact and transparently spin-invariant way (for transcription see App. C.2.2)

$$H = H_{tJ} + H_{rc}$$

$$H_{tJ} = t \sum_{\langle ij\rangle, s} (h^\dagger_{is} h_{js} - d^\dagger_{is} d_{js} + \text{H.c.}) + U \sum_i n_{di} + J \sum_{\langle ij\rangle} \left(\mathbf{S}_i \cdot \mathbf{S}_j - \frac{1}{4}\delta_{1,n_i n_j} \right) \tag{5.27}$$

$$H_{rc} = t_{rc} \sum_{(ijk), ss'} \left(h_{ks} d_{js'} \boldsymbol{\sigma}_{s\bar{s}'} \cdot \mathbf{S}_i + \text{H.c.} \right), \quad t_{rc} = \frac{J}{2}, \tag{5.28}$$

where $n_{di} = (1/2)\sum_s d^\dagger_{is} d_{is}$ and $\boldsymbol{\sigma} = \{\sigma^x, \sigma^y, \sigma^z\}$ is a vector of Pauli matrices. In the above notation $\sigma^a_{s,s'}$ correspond to $(\frac{3-s}{2}, \frac{3-s'}{2})$ component of the σ^a matrix. Again (ijk) signifies that j, k are the n.n. sites to site i, and $j \neq k$. From the derivation we obtain that the recombination term, Eq. (5.28), has the coupling parameter $t_{rc} = 2t^2/U = J/2$.

5.2.2 Charge-transfer Hubbard model

It is well known that on a microscopic level undoped and doped cuprates cannot be fully described within the single-band Hubbard model, since they are undoped or doped Mott insulators of the charge-transfer type, where more orbitals have to be included in the starting microscopic model. Therefore it is sensible to verify whether the recombination coupling t_{rc} obtained from the canonical transformation of the single-band Hubbard model is qualitatively correct approximation for the description of 2D cuprates. We take the accepted multi-band tight-binding model for electrons on the 2D CuO_2 layers, including $3d_{x^2-y^2}$ orbitals on Cu atoms and $2p_x/2p_y$ on O atoms [5, 178, 179, 180, 181, 182]. In contrast to numerous theoretical

studies and models of hole doped systems, both type of charge carriers, positive an negative, have to be treated on the same level of approximation [183, 184, 185, 186] in the present case of excited Mott insulator with holons and doublons.

Multi-band model

In the following states are as usual (but in contrast to the previous section) defined relative to the filled 3d orbitals on copper and 2p orbitals on oxygen [179]. Including the n.n. Cu-O and O-O hopping, and the Coulomb repulsion on/between Cu and O orbitals, the three-band p-d model is written as

$$H = \sum_{is} \epsilon_i n_{is} + \sum_{\langle ij \rangle s} t_{ij} (c^\dagger_{is} c_{js} + \text{H.c.}) + \sum_i U_i n_{i\uparrow} n_{i\downarrow} + \sum_{\langle ij \rangle} V_{ij} n_i n_j. \tag{5.29}$$

Here c_i (with corresponding n_i) stands for the annihilation of holes on different orbitals, therefore equals either $c_i \equiv \bar{d}_i$ for d orbitals with energy ϵ_d on copper at site i or $c_i \equiv p_{xi}(p_{yi})$ for p orbitals with energy ϵ_p on oxygen with displacement $x(y)$ relative to the n.n. copper at site i. We use notation $\bar{d}$ to avoid further confusion with

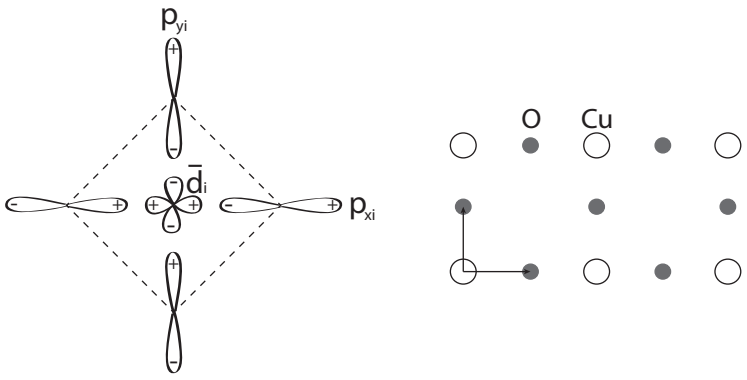

Figure 5.2: Left: sign of hopping parameter t_{ij} between n.n. Cu-O and O-O orbitals. Right: position of O and Cu orbital on a 2D lattice.

doublon operators. Hopping parameters equal $|t_{ij}| = t_{pd}, t_{pp}$ for hopping between n.n. Cu-O and O-O orbitals, respectively, with sign dependent on the phases of facing orbitals as sketched in Fig. 5.2. Parameters $U_i = U_d, U_p$ take into account the on-site Coulomb repulsion on Cu and O orbitals, respectively, while $V_{ij} = V_{pd}$ accounts for the repulsion between neighboring Cu-O orbitals. Introduced parameters have been extensively discussed in the literature. For numerical estimates further on we use the concrete values $\epsilon_p - \epsilon_d = 2.7, t_{pd} = 1, t_{pp} = 0.5, U_d = 7, U_p = 3, V_{pd} = 1$, all in units of $t_{pd} \approx 1.3eV$, as used by others [182, 184].

In the analysis we retain only the symmetrized oxygen orbital $(1/2)(|p_x\rangle - |p_y\rangle - |p_{-x}\rangle + |p_{-y}\rangle)$ that hybridizes with the $d_{x^2-y^2}$ orbitals [187] (leading to a two-band model [5, 179, 181]), and neglect the superposition $(1/2)(|p_x\rangle + |p_y\rangle - |p_{-x}\rangle - |p_{-y}\rangle)$. Furthermore, we introduce their combinations - orthonormal Wannier orbitals [5], in framework of which the Hamiltonian can be separated into two parts: the local Hamiltonian H_0 describing the noninteracting cells, and the inter-cell coupling term H_{cc}. Latter locality should be taken with some reservation, since it actually means that it involves one cell, containing a Cu orbital and a Wannier O orbital, however,

the Wannier orbital is still actually not an entirely local object. Local part of the Hamiltonian has the form of a sum $H_0 = \sum_i \mathcal{H}_{0i}$ of local intra-cell terms

$$\begin{aligned}\mathcal{H}_{0i} = \Delta_0 \sum_s n^p_{is} - \bar{t}_{pd} \sum_\sigma (\bar{d}^\dagger_{is} p_{is} + \text{H.c.}) \\ + U_d \; n^{\bar{d}}_{i\uparrow} n^{\bar{d}}_{i\downarrow} + \bar{U}_p \; n^p_{i\uparrow} n^p_{i\downarrow} + \bar{V}_{pd} \sum_{ss'} n^{\bar{d}}_{is} n^p_{is'},\end{aligned} \tag{5.30}$$

where $p^\dagger_i$ creates hole in the O Wannier orbital. Within the Wannier-orbital transformation parameters equal $\Delta_0 = \epsilon_p - \epsilon_d - 1.45\ t_{pp}$, $\bar{t}_{pd} = 1.92\ t_{pd}, \bar{U}_p = 0.21\ U_p, \bar{V}_{pd} = 0.92\ V_{pd}$, as taken from Ref. [184]. In the inter-cell part H_{cc} we retain only the dominant Cu-O and the O-O hopping,

$$H_{cc} = 2t_{pd}\mu_{10} \sum_{ijs} (\bar{d}^\dagger_{is} p_{js} + p^\dagger_{is} \bar{d}_{js}) + 2t_{pp}\nu_{10} \sum_{ijs} p^\dagger_{is} p_{js}, \tag{5.31}$$

with coefficients $\mu_{10} = 0.14, \nu_{10} = 0.27$ for n.n. i and j sites, as taken from [184, 185].

Local charge and spin states

To discuss the recombination between holons and doublons we first have to identify states that represent them. The actual form and the energy of relevant states is given in App. C.2.3, while here we outline how to get them. Such procedure has been used before with the purpose of describing doped materials, so that now just the necessary pieces should be combined.

Using the hole picture, doublon is represented by the filled Cu orbital, hence being the vacuum state $|D\rangle = |0\rangle$. On the other hand, holon is the generalized Zhang-Rice singlet [5, 184] $|H\rangle = H^\dagger|0\rangle$, obtained as the g.s. of the local Hamiltonian $\mathcal{H}_0$ in the singlet spin sector spanned by the states

$$\frac{1}{\sqrt{2}}(\bar{d}^\dagger_\uparrow p^\dagger_\downarrow - \bar{d}^\dagger_\downarrow p^\dagger_\uparrow)|0\rangle,\ \bar{d}^\dagger_\uparrow \bar{d}^\dagger_\downarrow |0\rangle,\ p^\dagger_\uparrow p^\dagger_\downarrow |0\rangle, \tag{5.32}$$

and has energy E_H. To describe the situation after the recombination we need also the single-hole state $|g_s\rangle$ (having correspondence to the spin background states in the single-band model), which is calculated as the g.s. of $\mathcal{H}_0$ within the doublet sector spanned by

$$\bar{d}^\dagger_s |0\rangle,\ p^\dagger_s |0\rangle \tag{5.33}$$

and has energy E_g. Besides the latter, we consider also the triplet states

$$\begin{aligned}|T_0\rangle &= \frac{1}{\sqrt{2}}(\bar{d}^\dagger_\uparrow p^\dagger_\downarrow + \bar{d}^\dagger_\downarrow p^\dagger_\uparrow)|0\rangle, \\ |T_{-1}\rangle &= \bar{d}^\dagger_\downarrow p^\dagger_\downarrow |0\rangle,\ |T_1\rangle = \bar{d}^\dagger_\uparrow p^\dagger_\uparrow |0\rangle\end{aligned} \tag{5.34}$$

with energy E_T. These are higher in energy, yet they contribute to an additional recombination channel as compared to the single-band model. Other states, i.e. excited states within each total spin sector, which can also be obtained with the diagonalization of H_0, will be neglected in our further analysis. Having higher energies they might be needed for the proper description of the early dynamics after the pump excitation, when highly excited states might be created. However, after

the initial relaxation, we assume that system can be represented by the lowest lying states (which still represent also the excitations across the charge-transfer gap).

Although states $|H\rangle, |D\rangle, |g_s\rangle$ are a combinations of Wannier orbitals each of them is attributed to a single cell. Moreover, the hybridization between copper and oxygen orbitals, intrinsically present in them (as a consequence of basis vectors or diagonalization procedure), turns out essential when addressing the inter-cell hopping matrix elements of H_{cc}, Eq. (5.31), as discussed in App. C.2.4. Still, they obviously bridge the single- and the multi-band consideration by having analogies in the single-band picture.

Reduced Hamiltonian

We can now proceed by writing the effective Hamiltonian in analogy with the single-band one by using the relevant states introduced in the previous subsection. It is convenient to write the Hamiltonian with X operators, analogously to those in the single-band model, Eq. (5.16),

$$\begin{aligned}
&\bar{X}_i^{sD} = g_{is}^\dagger (1-n_i^{\bar{d}})(1-n_i^p), \\
&\bar{X}_i^{sH} = g_{is}^\dagger H_i,\ \bar{X}_i^{sT_{s'}} = g_{is}^\dagger T_{is'}, \\
&\bar{X}_i^{ss} = g_{is}^\dagger g_{is},\ \bar{X}_i^{s\bar{s}} = g_{is}^\dagger g_{i\bar{s}}, \\
&g_s^\dagger = \cos\theta\ (1-n_{\bar{s}}^d)(1-n^p)\bar{d}_s^\dagger + \sin\theta\ (1-n_{\bar{s}}^p)(1-n^d)p_s^\dagger
\end{aligned} \tag{5.35}$$

where $g_{is}^\dagger, H_i^\dagger, T_{is}^\dagger$ create the doublet g.s., the holon (generalized Zhang-Rice singlet) and the triplet state, respectively. It still holds that $\bar{X}_i^{AB} = (\bar{X}_i^{BA})^\dagger$. Again $s = \pm 1$ associated with g_{is} stands for the hole spin, whereas in T_{is} it can have values $s = \pm 1, 0$ according to definitions in Eqs. (5.34). To insure X_i^{As} is nonzero only when applied to the doublet g.s., its creation operator is written out explicitly, using parametrization elaborated in App. C.2.3. In terms of such X operators we can present the Hamiltonian as the sum $H = H_t + H_{trc} + H_{dg}$, representing the effective HD hopping (containing possible creation of triplet states), their recombination and the diagonal part, respectively,

$$\begin{aligned}
H_t = &\sum_{ij,s=\pm 1} \left(t^h \bar{X}_i^{Hs} \bar{X}_j^{sH} + t^d \bar{X}_i^{sD} \bar{X}_j^{Ds} \right) \\
&+ \sum_{ij,s=\pm 1} \left(-s\ t^{T_0} \bar{X}_i^{sH} \bar{X}_j^{T_0 s} + s\ t^{T_1} \bar{X}_i^{\bar{s}H} \bar{X}_j^{T_s s} + \text{H.c.} \right)
\end{aligned} \tag{5.36}$$

$$H_{trc} = \sum_{ij,s=\pm 1} \left(-s\ t^r \bar{X}_i^{\bar{s}H} \bar{X}_j^{sD} + t^{r_0} \bar{X}_i^{\bar{s}T_0} \bar{X}_j^{sD} + t^{r_1} \bar{X}_i^{sT_s} \bar{X}_j^{sD} + \text{H.c.} \right) \tag{5.37}$$

$$H_{dg} = \sum_i \left(\epsilon_H \bar{X}_i^{HH} + \epsilon_D \bar{X}_i^{DD} + \epsilon_T \sum_{s=\pm 1,0} \bar{X}_i^{T_s T_s} \right), \tag{5.38}$$

where i, j are n.n.. Values $\epsilon_H = E_H - E_g$, $\epsilon_D = -E_g$, $\epsilon_T = E_T - E_g$ are the single-cell energies of holon, doublon and triplet relative to the doublet g.s., respectively. Dependence of the introduced couplings $t^c, c = h, d, T_0, T_1, r, r_0, r_1$ and energies $\epsilon_H, \epsilon_D, \epsilon_T$ on the parameters of the original Hamiltonian Eqs. (5.30,5.31) is presented in the App. C.2.4.

Effective Hamiltonian

Similarly to the treatment of the single-band Hubbard model within the $U \gg t$ limit in Sec. 5.2.1 we transform out the recombination/creation term H_{trc} with a canonical transformation $e^S H e^{-S}$. Operator S is determined by the condition $[S, H_{dg}] + H_{trc} = 0$. After the transformation (for details see App. C.2.5) the HD recombination/creation term H_{rc},

$$H_{rc} = -\sum_{(ijk),s} s[\bar{X}_k^{sH}(r^h \bar{X}_i^{ss} - r^d \bar{X}_i^{\bar{s}\bar{s}})\bar{X}_j^{\bar{s}D} + r^{hd}\bar{X}_k^{\bar{s}H}\bar{X}_i^{s\bar{s}}\bar{X}_j^{\bar{s}D} + \text{H.c.}], \tag{5.39}$$

again acts between the next n.n. cells, however, now one has to distinguish between channels leading to different configurations of spins in the doublets of final state, since their amplitudes r^i are different,

$$r^h = \left(\frac{t^h t^r}{\epsilon_H + \epsilon_D} + \frac{t^{T_0} t^{r0}}{\epsilon_T + \epsilon_D}\right), \quad r^d = \left(\frac{t^d t^r}{\epsilon_H + \epsilon_D} - \frac{t^{T_1} t^{r1}}{\epsilon_T + \epsilon_D}\right), \tag{5.40}$$
$$r^{hd} = \left(\frac{t^d t^r + t^h t^r}{\epsilon_H + \epsilon_D} - \frac{t^{T_0} t^{r0}}{\epsilon_T + \epsilon_D}\right).$$

Not only different amplitudes of holon and doublon hopping parameters, but also new processes of the recombination via intermediate triplet states (second term in each r^i) alter the result. To obtain the latter, hopping terms involving the singlet-to-triplet transition and the doublon-triplet recombination were included in H_t and H_{trc} in the first place. Although they exhibit a richer physics of the multi-band model, one should be aware that recombination via triplet state causes only smaller corrections in the coupling strengths, since $\epsilon_H \ll \epsilon_T$. However, the pure form of Eq. (5.39) is very similar to its single-band analogue Eq. (5.24) with an additional overall minus that is a consequence of the transition from the electron to the hole picture.

If we calculate all three relevant recombination couplings $2r^d, r^{hd}, 2r^h$ at realistic parameters we confirm that they are not far away from $t_{rc} = J/2$, the value obtained from the single-band model. Their dependence on Δ_0 is plotted in Fig. 5.3. Rescalations are made for clearer comparison with $J/2$. Using the same procedure

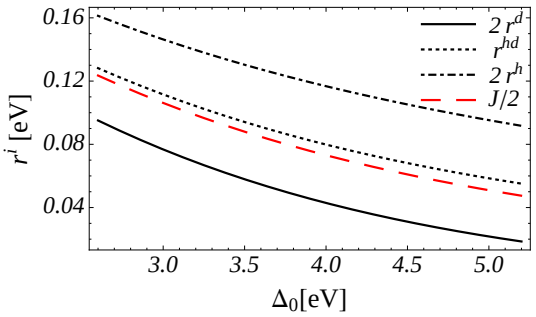

Figure 5.3: Comparison of coupling parameters $r^i = 2r^d, r^{hd}, 2r^h$ for different recombination channels with the (rescaled) exchange coupling $J/2$ as a function of the charge-transfer gap Δ_0. For other parameters standard values are used.

via intra-cell diagonalization, the exchange coupling plotted is expressed as

$$J = 4\left(\frac{(t^r)^2}{\epsilon_H + \epsilon_D} - \frac{(t^{r_0})^2}{\epsilon_T + \epsilon_D}\right). \tag{5.41}$$

To exhibit the spin invariance of H_{rc} we define (as in the single-band model) $\tilde{d}_{is} = -s\bar{X}_i^{sD}, \tilde{h}_{is} = \bar{X}_i^{sH}$ in term of which H_{rc} obtains a form similar to Eq. (5.28),

$$H_{rc} = -\sum_{(ijk)ss'}\left[\tilde{h}_{is}\tilde{d}_{ks'}\left(r^{hd}\boldsymbol{\sigma}_{s\bar{s}'}\cdot\mathbf{S}_j + \bar{r}^{hd}\mathbb{1}_{s\bar{s}'}\right) + \text{H.c.}\right], \tag{5.42}$$

where we used $\bar{r}^{hd} = (r^h - r^d)/2$ and $t^{T_1}t^{r1} = 2t^{T_0}t^{r0}$, see App. C.2.4.

5.2.3 Exciton recombination rate

In previous Secs. it has been shown that both the single-band Hubbard model as well as the three-band model for cuprates reduce at low HD density to the same effective model with the only difference being strengths of the recombination/creation terms in H_{rc}. Therefore we are confident to model the recombination process with the effective model derived from the single-band Hubbard model.

Holon-doublon exciton

In order to explain the experimentally observed independence of the decay rate Γ on the pump fluence (photon excitation density), i.e. also the exponential decay of the HD density, we first have to determine the existence of the bound HD pair. This is based on the argumentation that if pairs were not bound, the recombination process would depend on the probability to encounter the oppositely charged particle,

$$-\frac{dn}{dt} \propto n^\gamma, \quad \gamma = 2, 3, \tag{5.43}$$

evidently leading to a non-exponential decay. Here we used $n = n_{HD} \sim n_d \sim n_h$. One should be aware that in the case of very strong excitation, when already the thermal charge density n_{th} is high, decay might look like exponential since only the deviation $\tilde{n}$ around the thermal value is observed,

$$-\frac{d\tilde{n}}{dt} \propto (n_{th} + \tilde{n})^\gamma \approx n_{th} + \gamma\tilde{n} \tag{5.44}$$

However, this is not the case we are addressing. The present problem of HD binding has analogies with binding of holes in doped cuprates, also studied within the t-J model [162, 188]. The origin of the binding is in both cases the same, since it is a consequence of minimizing the perturbation of the spin background. However, indistinguishable two holes $N_h = 2$ form a d-type bound state, whereas the distinguishable doublon and holon form a s-type (A_1 symmetry) bound state, as confirmed numerically independent of our study [33]. Since the latter state has even symmetry it is not accessible by optical transition from the insulator AFM state. On the other hand, the lowest optically active p-type state with binding energy $\epsilon_b \gtrsim 0$ within our calculation does not seem to be a bound one. The relaxation from the odd state created with the pump pulse to the even exciton is beyond the scope of this thesis,

still, we believe that the change of the symmetry must be assisted by the emission of phonons or magnons with proper momentum. It would be fair to establish the timescale for binding and the fraction of excited HD pairs that end up in the exciton state by simulating the process, or at least by using the FGR approximation. However, this is intimately related to the proper description of excitation process, i.e., what state is really created with the pump pulse, how to model the pump pulse beyond the Peierls substitution, etc. Nevertheless, binding is expected to be much faster then recombination (within few tens of fs) because the reduction of the energy of HD pair can be progressive (similarly to the processes described in the previous Chapter).

Knowing that at low charge density the coupling between sectors with different number of HD pairs is weak, we first neglect the recombination/creation term H_{rc} that causes transitions between sectors and extract the initial HD state $|\psi_0^{hd}\rangle$ from the spectrum of eigenstates of H_{tJ}, Eq. (5.27), as the g.s. in the sector with one HD pair. Calculating it in the single HD pair sector for system of limited size we neglect possible interaction between different pairs, justified for the cases of low charge density.

Binding properties of the HD state $|\psi_0^{hd}\rangle$ are obtained via exact diagonalization of H_{tJ} using the Lanczos technique on the square lattices with $N \leq 26$ sites and periodic boundary conditions. The HD binding energy ϵ_b is obtained by comparing the energy of the HD pair E_0^{hd} (relative to the AFM g.s. E_0^0) with the energy of a (free) single holon or doublon, E_0^h, E_0^d (again relative to the energy of AFM g.s.),

$$\epsilon_b = (E_0^{hd} - E_0^0) - (E_0^d - E_0^0) - (E_0^d - E_0^0) = E_0^{hd} - E_0^h - E_0^d + E_0^0. \tag{5.45}$$

In the regime of interest for cuprates ($J/t = 0.3 - 0.4$) the lowest (s-type) state shows appreciable binding $\epsilon_b/t \sim -0.4$, quite robust towards the finite size effects, as presented in Fig. 5.4. It should be pointed out that the inclusion of the longer-range Coulomb repulsion would even enhances $|\epsilon_b|$, but is not expected to be the driving or the dominant effect in the 2D square lattice, unlike in 1D where it is crucial to establish the exciton. For simplicity we study only the effect of the n.n. repulsion, which in the reduced Eq. (5.27) leads to additional n.n. HD attraction, i.e.

$$\Delta H_{tj} = -V \sum_{\langle ij \rangle} (n_{hi} n_{dj} + n_{di} n_{hj}) \tag{5.46}$$

Its effect on binding is presented in Fig. 5.4, while its effect on recombination is commented in the next subsection. As an additional proof of the HD binding we calculate also the exciton density correlations

$$D_j = \langle \psi_0^{hd} | n_{hj} n_{d0} | \psi_0^{hd} \rangle \tag{5.47}$$

(for the purpose of presentation the position of the doublon is chosen as the origin). D_j obtained on $N = 26$ for $J = 0.4$ are presented in Fig. 5.4, where correlation strength is visualized by the size and intensity of the dot at the position of the holon relative to the doublon at the origin. D_j shows consistence with the binding since HD pair is with the largest probability on a distance $d_0 = \sqrt{2}$, as is also the case for the d-wave hole binding within the 2D t-J model [162, 188].

An alternative insight into the HD exciton is obtained also through its optical

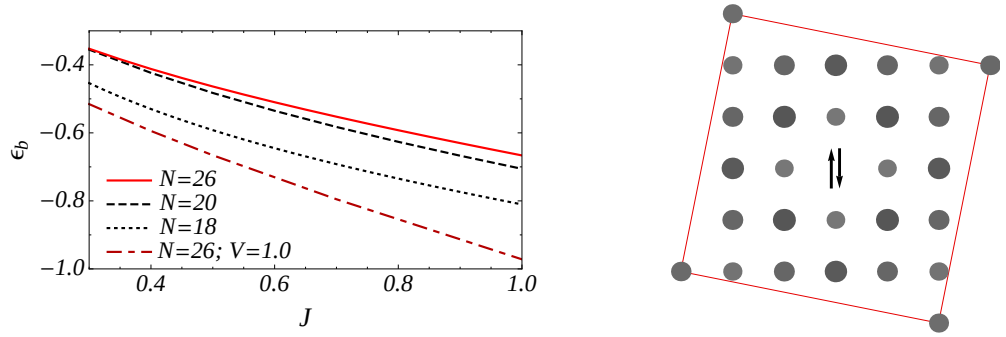

Figure 5.4: Left: HD pair binding energy ϵ_b vs. J. The plotted results are for the s-type g.s. for $N = 18, 20, 26$ lattices with $V = 0$ as well as the for $V = 1$ on a $N = 26$ lattice. Right: Holon-doublon density correlation D_j.

conductivity, here calculated as if the state was stationary [148],

$$\sigma_{reg}(\omega) = \frac{\pi}{2\omega} \sum_m |\langle \psi_m^{hd}|j|\psi_0^{hd}\rangle|^2 \delta(\omega - E_m^{hd} + E_0^{hd}) \tag{5.48}$$

i.e. neglecting its decay. As presented in left Fig. 5.5, within its regular part $\sigma_{reg}(\omega)$, a peak corresponding to the transition into the lowest p-type state and the so called mid-infra red (MIR) peak(s) (corresponding to the creation of string spin excitations due to the motion of holon and doublon in the AFM background) are clearly observed. Although the former peak is especially pronounced in our study, only the later structure is actually observed also in experiments [14], possibly because the peak due to the transition into p-type state is right on the edge of the experimental low-frequency resolution. Right Fig. 5.5 presents the experimental data obtained in pump-probe experiments on Nd_2CuO_4, showing the difference in absorption spectra to the equilibrium one at different delay times after the initial pump pulse. To simulate the holon-doublon asymmetry, present in cuprates that are

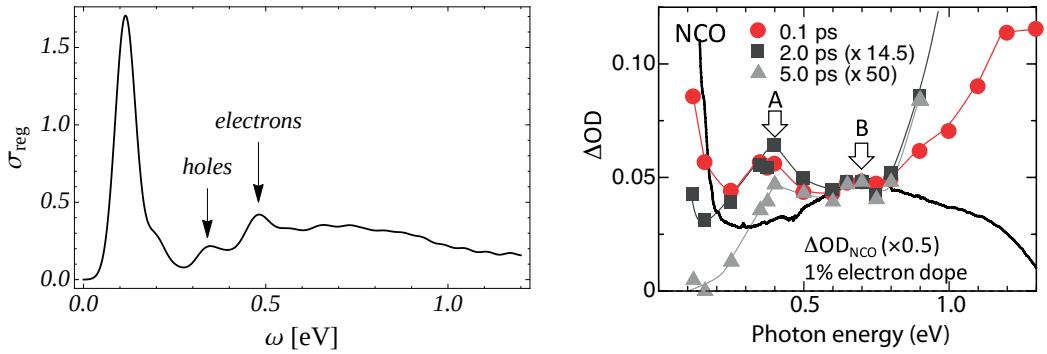

Figure 5.5: Left: $\sigma_{reg}(\omega)$, Eq. (5.48) calculated on $N = 26$ sites with diagonal hopping $t' = -0.3t$ and $J = 0.4$. For comparison with experiment $t = 0.35eV$ is used. Right: (taken from Ref. [14]) the difference in absorption spectra (relative to the equilibrium value) at different delays of the probe pulse obtained on Nd_2CuO_4.

actually not Mott but charge transfer insulators (see previous Sec.), we include into

theoretical calculation an additional effective diagonal hopping term with a typical strength $t' = -0.3t$ [186]. It splits the MIR peak into two; one coming from free holon(s) and the other from doublon(s) (or holes and electrons in the language of the chemical-doping), as shown in Fig. 5.5. The experimental data shows a similar double-peak structure whose origin has also been assigned to holons (peak A) and doublons (peak B), as confirmed by the comparison with absorption on hole- or electron-doped samples [14]. For the purpose of comparison between the theoretical calculation and the experimental data on Nd_2CuO_4 the hopping parameter of a standard value $t = 0.35eV$ is used to set the absolute energy scale of our theoretical result. Approximate qualitative agreement suggests that what is being probed in experiments really is a MH exciton.

Recombination rate via Fermi golden rule

The HD exciton $|\psi_0^{hd}\rangle$ is not an eigenstate of the effective model when perturbation H_{rc}, Eq. (5.28), is included. A standard approach to evaluate the decay rate into a continuum of states is the FGR,

$$\Gamma = 2\pi \sum_m |\langle \psi_m^0 | H_{rc} | \psi_0^{hd} \rangle|^2 \ \delta(E_m^0 - E_0^{hd}), \tag{5.49}$$

where the matrix elements are highly nontrivial since they represent the overlap of the modified exciton wave function $H_{rc}|\psi_0^{hd}\rangle$ on highly spin-excited (multi-magnon) states $|\psi_m^0\rangle$ with energy E_m^0 within the undoped AFM spin system. Note that if we neglect the creation part of H_{rc} then $H_{rc}|\psi_0^{hd}\rangle$ is essentially a projection onto the components with HD pair on next n.n. sites, with pair being recombined by H_{rc} operator, so that finally it is only in the spin sector. For the numerical consideration it is crucial that Eq. (5.49) can be represented as a resolvent $\Gamma = -2\mathrm{Im}C(\omega = \Delta)$, where $\Delta = E_0^{hd} - E_0^0$ is the excitation gap (between the bound HD-pair state and the AFM g.s.), and

$$C(\omega) = \langle \psi_0^{hd} | H_{rc} \frac{1}{\omega^+ + E_0^0 - H_J} H_{rc} | \psi_0^{hd} \rangle, \tag{5.50}$$

with $\omega^+ = \omega + i\epsilon$. In the evaluation only the exchange part H_J of the H_{tJ}, Eq. (5.27), is relevant. To prove this we use the standard relation

$$\big(\omega^+ + E_0^0 - H_J\big)^{-1} = -i\pi\delta\big(\omega + E_0^0 - H_J\big) + P\big((\omega + E_0^0 - H_J)^{-1}\big), \tag{5.51}$$

where P is the principal value. Since H_{rc} and H_J are hermitian, only the first component contributes to the ImC.

$$\begin{aligned} -ImC(\omega) &= \pi \langle \psi_0^{hd} | H_{rc} \ \delta(\omega + E_0^0 - H_J) \ H_{rc} | \psi_0^{hd} \rangle \\ &= \pi \langle \psi_0^{hd} | H_{rc} \ \sum_m |\psi_m^0\rangle\langle\psi_m^0| \ \delta(\omega + E_0^0 - H_J) H_{rc} | \psi_0^{hd} \rangle \\ &= \pi \sum_m |\langle \psi_m^0 | H_{rc} | \psi_0^{hd} \rangle|^2 \delta(\omega + E_0^0 - E_m^0) \end{aligned} \tag{5.52}$$

As explained in Ref. [74] function $C(\omega)$ can be easily calculated using Lanczos procedure. Starting with

$$|\tilde{\phi}_0\rangle = \frac{1}{\alpha} H_{rc} |\psi_0^{hd}\rangle, \quad \alpha = \sqrt{\langle \psi_0^{hd} | H_{rc}^\dagger \ H_{rc} | \psi_0^{hd} \rangle} \tag{5.53}$$

as the first Lanczos vector, after $\tilde{M}$ steps one generates Lanczos space $\tilde{L}_m = \{|\tilde{\phi}_j\rangle\}, j \in [0, \tilde{M}]$. In this space the matrix for H_J within Lanczos basis is tridiagonal with $\tilde{a}_j$ matrix elements on the diagonal and $\tilde{b}_j$ elements off-diagonal. It has approximate eigenvectors $|\tilde{\psi}_j^0\rangle$ and eigenenergies $\tilde{E}_j^0$. One way to evaluate $C(\omega)$ is as a resolvent of the $H_{\tilde{M}}$ matrix, expressed in the so called continued-fraction form

$$C(\omega) = \cfrac{\alpha^2}{\omega^+ + E_0^0 - \tilde{a}_0 - \cfrac{\tilde{b}_1^2}{\omega^+ + E_0^0 - \tilde{a}_1 - \cfrac{\tilde{b}_2^2}{\omega^+ + E_0^0 - \tilde{a}_2 - \ldots}}} \tag{5.54}$$

Smoothing can be included through $\omega^+ = \omega + i\epsilon$. In this way one simulates the continuous limit within the finite-size system. However, such damping has the drawback that it artificially prolongs the tail of $C(\omega)$ at large ω values.

However, this problem can be overcome with a different type of broadening. $C(\omega)$ can be presented also as a sum of $\tilde{M}$ poles at energies $\omega = \tilde{E}_j^0 - E_0^0$ with corresponding weights w_j,

$$w_j = |\langle\tilde{\psi}_j^0|H_{rc}|\psi_0^{hd}\rangle|^2 = \alpha^2|\langle\tilde{\psi}_j^0|\tilde{\phi}_0\rangle|^2 = \alpha^2\tilde{v}_{j0}^2, \tag{5.55}$$

where relation between approximate eigenfunctions and Lanczos vectors $|\tilde{\psi}_j^0\rangle = \sum_{i=0}^{M} v_{ji}|\tilde{\phi}_i\rangle$ has been used. At the end we need only coefficients of the excited states at the first Lanczos state. Peak at each j can be now broaden with a Gaussian functions $g(x) = (w_j/\sqrt{2\pi\epsilon^2})\exp\left(-(x-\tilde{E}_j^0)^2/(2\epsilon^2)\right)$ with σ given e.g. with the average energy differences between two adjacent states. The more Lanczos step we make, smaller it is. For such widening tails vanish exponentially and do not accumulate uncontrollably.

Within the Lanczos procedure Eq. (5.50) can be evaluated on 2D square lattice with up to $N = 26$ sites [34, 35]. The convergence of results with the system size is presented in Fig. 5.6, where Γ is evaluated for fixed $J = 0.4$ and different lattices with $N = 20, 24, 26$ ($N = 24 = 4 \times 6$ sites is a rectangular lattice) sites. Taking Δ as a variable corresponds to assuming U in Eq. (5.27) to be an independent parameter, which could deviate from the relation $U = 4t^2/J$ obtained within the $U \gg t$ limit. We note from Fig. 5.6 that even small $\epsilon = 0.07$ is enough to obtain continuous $\Gamma(\Delta)$ for the largest system $N = 26$. Clearly, the system size N should be big enough to capture the initial exciton wave function and to accommodate enough multi-magnon excitations in order to get reliable results in the relevant tails $\Gamma \ll 1$.

In Fig. 5.6 the dependence $\Gamma(\Delta)$ for different $J = 0.3, 0.4, 0.6$ is presented. It suggests that the decay rate Γ has an approximately exponential dependence on the number of spin excitations $n \sim \Delta/J$ created,

$$\Gamma \sim \Gamma_0 \exp(-\alpha\Delta/J), \tag{5.56}$$

with effective α in the range $0.3 < \alpha < 0.7$ (for chosen $0.3 \leq J \leq 0.6$), in agreement with the main message from the exciton-boson toy model result, Eq. (5.14). Observed α dependence signals that there is still some additional subtle J dependence, which could be related to the logarithmic correction in the expression (5.14) from the toy model, as shown below. In contrast to the HD binding in Fig. 5.4, the effect of $V > 0$ on the dependence $\Gamma(\Delta)$ is for modest $0 < V < 2$ hardly visible (related to

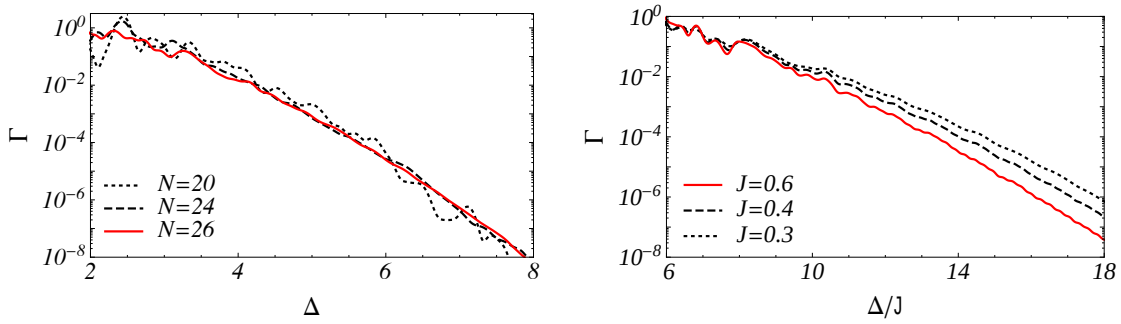

Figure 5.6: Left: exciton recombination rate Γ vs. gap Δ for $J = 0.4$ and different planar systems with $N = 20, 24, 26$ sites. Right: exciton recombination rate Γ vs. Δ/J for different $J = 0.3, 0.4, 0.6$ as calculated for $N = 26$ sites. Results are smoothed with $\epsilon = 0.07$.

the nearly constant next n.n. probability within the HD pair). It should be however stresses that $V > 0$ reduces Δ due to change of the HD binding, and so results in slightly enhanced Γ.

Comparison with exciton-boson toy model

Let us apply the compact expression for the recombination rate obtained from the exciton-boson model (Eq. (5.14)),

$$\Gamma \approx g_{rc}^2 e^{-\xi} \sqrt{\frac{2\pi}{\Delta\omega_0}} \exp\left[-\frac{\Delta}{\omega_0} \ln\left(\frac{\Delta}{e\,\xi\omega_0}\right)\right], \tag{5.57}$$

to the above results. We set $\omega_0 = J$ as the typical spin-excitation energy and fit Eq. (5.57) to the numerically obtained dependence $\Gamma(\Delta)$ for various J, with the dimensionless coupling ξ and prefactor g_{rc} as the fitting parameters. As shown in Fig. 5.7, formula Eq. (5.57) captures the dependence $\Gamma(\Delta)$ for ξ that is mildly dependent on J, as also presented in Fig. 5.7.

This result has a fundamental importance since it signifies that the recombination of the HD bound pair via multi-magnon emission can be described in a much broader frame - as a decay via many bosons. Besides the exponential form the most important message from Fig. 5.7 is that the effective exciton-boson coupling is very strong $\xi \sim 3$. The dependence of ξ on J resembles $|\epsilon_b|/J$, where ϵ_b is the numerically established binding energy of the HD pair, but with a substantially bigger prefactor. Latter relation is deduced from Eq. (5.10) if we associate the HD pair binding energy with the exciton-boson binding energy, which might be oversimplified. In any case one should take the absolute value of ξ with some reservations since it is correlated with the choice of ω_0. We use $\omega_0 = J$, since J sets the scale of magnon excitations, although in reality there is a range of magnon dispersions around it, and taking a larger value would reduce ξ. The prefactor dependence $g_{rc} \sim J$ is in qualitative agreement with the original model Eq. (5.28).

Dressing of the exciton with spins

The essential ingredient for the substantial decay turns out to be the dressing of the HD pair with spin excitations. It is known already from numerous numerical [162]

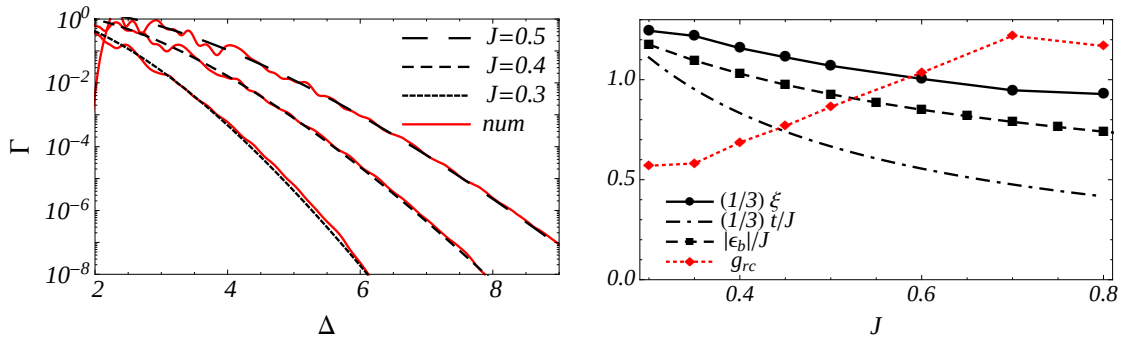

Figure 5.7: Left: fit of Eq. (5.57) with ξ, g_{rc} as the fitting parameters to the numerical result (num) for $\Gamma(\Delta)$ obtained on 2D system (as described in previous section) for $J = 0.3, 0.4, 0.5$. Right: values of the fitting parameters ξ (boson coupling) and g_{rc} (recombination prefactor) as a function of J. For comparison $|\epsilon_b|/J, t/J$ are plotted as well. Prefactor $1/3$ was used with ξ and t/J to unify the scales.

and analytical [189] studies of the single hole $N_h = 1$ within the t-J model that a holon (or doublon) strongly perturbs the AFM background in the strong correlation regime $J < t$. This is the case even more for two (bound) holes $N_h = 2$ [162] and for the present example of a bound HD pair, $N_h = N_d = 1$. This is revealed by deviations in the bond energy of the exciton state relative to the AFM g.s. (in units of AFM $\langle \mathbf{S}_i \cdot \mathbf{S}_{i+1} \rangle_{AFM}$),

$$\delta\langle \mathbf{S}_i \cdot \mathbf{S}_j \rangle = \frac{\langle \mathbf{S}_i \cdot \mathbf{S}_j \rangle_{HD} - \langle \mathbf{S}_i \cdot \mathbf{S}_j \rangle_{AFM}}{\langle \mathbf{S}_i \cdot \mathbf{S}_{i+1} \rangle_{AFM}}. \tag{5.58}$$

Calculated for $J = 0.4$ and for the most probable HD configuration with the pair distance $d_0 = \sqrt{2}$, they are presented in Fig. 5.8. In the process of the recombination this local spin perturbation can be even enhanced, and finally has to disperse into the whole system.

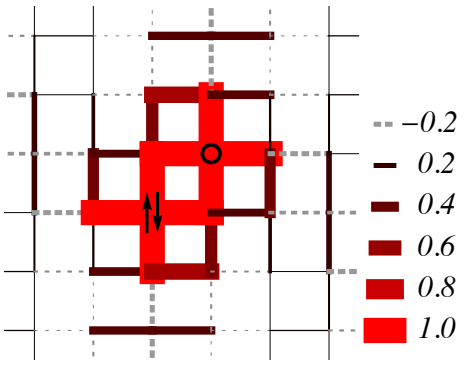

Figure 5.8: Deviations $\delta\langle \mathbf{S}_i \cdot \mathbf{S}_j \rangle$ of bond energies for the HD exciton state relative to the AFM g.s as calculated for the most probable pair configuration and $J = 0.4$.

A viewpoint

An attempt to relate different aspects; $\Gamma(\Delta, J)$ dependence, toy-model result, and the spin dressing, is to motivate the dependence of the recombination rate on Δ and J via the construction of a sufficient spin dressing of cca. n spin flips as a n-th order perturbation process, as suggested by previous similar considerations [64, 65, 87]. In the simplified reasoning, we could inject e.g. a holon into non-perturbed spin background so that with each hopping (parametrized by t) it would perturb the spin background due to shifts of the previously AFM ordered system. Roughly speaking, each hopping lifts the background energy for J, so that the matrix element for n spin flips is

$$M = \frac{t}{J} \cdot \frac{t}{2J} \cdots \frac{t}{nJ} = \frac{1}{n!} \left(\frac{t}{J}\right)^n . \tag{5.59}$$

Using Stirling's approximation $n! \sim \sqrt{2\pi n}(n/e)^n$, recombination rate gets the form

$$\Gamma \propto M^2 \propto \left(\frac{et}{nJ}\right)^{2n} \propto \exp\left[-\alpha_0 \frac{\Delta}{J} \ln \frac{\Delta}{et}\right] \tag{5.60}$$

with $\alpha_0 = 2$. However, when fitting Eq. (5.60) to the numerical data, $\alpha_0 \approx 0.8$ with a modest J dependence is obtained. In Ref. [87] an additional structure of constant α_0 was treated with a self-avoiding path reasoning, taking care not to destroy some of already created excitations, though not for the bound HD pair.

Both expressions, from the perturbation theory and the toy-model contain the main message of the exponential suppression with the number of excitations created, and differ only in the logarithmic correction. Taking $\xi = t/J$ would for $\alpha_0 = 1$ actually unite both relations. As shown in Fig. 5.7, ξ has a milder J dependence yet similar strength as t/J.

To give a definite comment on which approach, the perturbation expansion or the exciton-boson model, gives a better description could be pointless since they must be essentially intertwined: hopping of charges coupled to bosons causes dressing. Still, consideration of the exciton coupled to bosons seems natural and the interpretation of fitting parameters rather clear. On the other hand, the precise form of α_0 might not be trivial and one should be aware that here the perturbation procedure has been used with a non-perturbative (hopping) operator without taking into account the energy of the excitation carefully and neglecting the correlation between holon and doublon.

Recombination rate via direct time evolution

In order to validate the approximation using the FGR, Eq. (5.49), we perform also a direct time evolution of the same initial excitonic state $|\psi_0^{hd}\rangle$ under the whole Hamiltonian $H = H_{tJ} + H_{rc}$, however, we restrict the Hilbert space only to the sectors with zero and one HD pair. As defined in Sec. 5.2.1 H_{tJ} term, Eq. (5.27), is a generalized t-J model, preserving the number of HD pairs, whereas H_{rc}, Eq. (5.28), recombines/creates a HD pair. In Fig. 5.9 we present the time evolution of the doublon (also the HD pair) occupation number,

$$n_d(\tau) = \frac{1}{2}\langle\psi(\tau)| \sum_{is} d_{is}^\dagger d_{is} |\psi(\tau)\rangle. \tag{5.61}$$

The evolution of $|\psi(\tau)\rangle$ is obtained by solving the time-dependent Schrödinger equation using the Lanczos method [74, 158]. In Fig. 5.9 we present and compare results for $J = 0.4$ and different effective gaps $\Delta = 4.8, 5.2, 6.0$, as calculated for the system with $N = 26$ sites. Effective gap is defined using $|\psi_{gs}\rangle$ (g.s. of H within our restricted Hilbert space) as

$$\Delta = \langle\psi_0^{hd}|H|\psi_0^{hd}\rangle - \langle\psi_{gs}|H|\psi_{gs}\rangle, \tag{5.62}$$

since it turns out to be a function of the coupling strength t_{rc} due to adiabatic change of the eigenspectra of H caused by H_{rc}. By adiabatic we mean that even though the whole energy of each eigenstate is shifted (especially due to the weak mixing of spin and charge sector), when projected onto the spin sector the fraction of spin excitations (characterized by the potential energy) within it is preserved. Eventually, it is the amount of spin excitations that should label the states receiving the energy of the HD pair. The recipient (eigenstate) must have the energy of the exciton $\langle\psi_0^{hd}|H|\psi_0^{hd}\rangle$, and the potential energy of spin excitations within it to a good approximation equals Eq. (5.62).

Rapid oscillations seen in Fig. 5.9 emerge due to fast switching of H_{rc} and finite-size effects, however, they get evidently reduced with bigger N. For clarity averaging over $\delta\tau = 3$ is used. From Fig. 5.9 we can confirm that after an initial

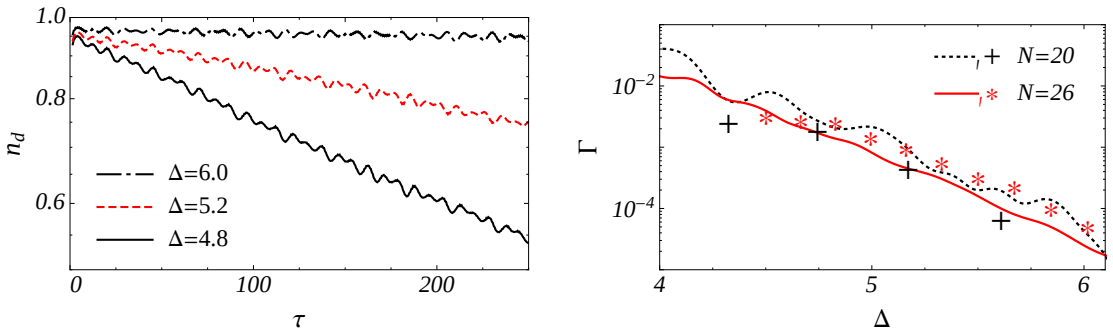

Figure 5.9: Left: doublon (and also HD pair) occupation number n_d (in logarithmic scale) as a function of time τ, calculated for different gaps $\Delta = 4.8, 5.2, 6.0$ and parameter $J = 0.4$ for system of size $N = 26$. Right: comparison of the exciton recombination rate Γ vs gap Δ as calculated using the FGR (lines) and time evolution (dots) for $J = 0.4$ and systems of size $N = 20, 26$.

transient an exponential decay is established. When simulating recombination on a finite system one should be aware that the finite-size level distance $\delta\omega$ limits the long-time evolution to $\tau \approx 2\pi/\delta\omega$, when the recurrence of HD pair appears, and is for system with $N = 26$ sites of order $\delta\omega \approx 10^{-1}$. This numerically confirms the importance of the continuum of states (implicitly assumed in the FGR) for a complete decay. Using the fit $\log n_d(\tau) = -\Gamma\tau + \log n_{d0}$, one can compare the result obtained for Γ with the one calculated with the FGR. Fig. 5.9 shows this comparison for $J = 0.4$ and system sizes $N = 20, 26$. Lines correspond to the result from the FGR, while dots are obtained from fits to $\log n_d(\tau)$ in the span of interesting Δ. We obtain a quite good agreement between the two methods, as shown in Fig. 5.9. Both methods confirm the exponential dependence Eq. (5.56). Somewhat smaller

Γ obtained with time evolution on $N = 20$ lattice could be attributed to the decay into the discrete multi-magnon spectra, which is sparser at smaller lattices.

5.2.4 Comparison with experiments and discussion

When discussing the application of the theory to cuprates most parameters are well established. The t-J model has been used by many authors for the quantitative comparison of experimental results for various properties. In this sense typically used parameters are $t \approx 0.35$ eV and $J/t \approx 0.4$, slightly varying within the cuprates. Since the MH gap (or more directly the optical gap) Δ_{ct} is also determined by optical absorption, the only undetermined parameter is the prefactor t_{rc}, Eq. (5.28), which we fix to the theoretically obtained $t_{rc} = J/2$. It should be noted that to get Δ relevant for the s-type bound state, as defined in Sec. 5.2.3, energy difference to the p-type unbound but optically active state has to be subtracted, $\Delta = \Delta_{ct} - |\epsilon_b|$. The theory developed above is in particular applicable to undoped 2D cuprates. Within this family experiments have been performed on Nd_2CuO_4 and La_2CuO_4 [13, 14]. The characteristic microscopic unit time in these systems is given by the elementary process of intercell hopping, i.e. $\tau_0 = \hbar/t \sim 2$ fs.

Nd_2CuO_4: Standard values quoted for this material are [14]: the optical gap $\Delta_0 = 1.6$ eV and $J = 0.155$ eV, so that $\Delta = 4.1\ t$ and from Eq. (5.49) $\Gamma \sim 2.2 \cdot 10^{-2}/\tau_0$. Finally this leads to $\tau = \Gamma^{-1} \sim 0.09$ ps, which is fairly close to the experimentally measured $\tau \sim 0.2$ ps [14].

La_2CuO_4: Analogous values for this compound are: optical gap $\Delta_{ct} = 2$ eV and $J = 0.133$ eV, so that $\Delta = 5.3\ t$ and $\Gamma \sim 1.3 \cdot 10^{-4}/\tau_0$, yielding $\tau \sim 15$ ps. For this material detailed analysis was not performed, yet it is reported to have considerably longer relaxation [14], consistent with our result. From our theory the difference is quite evident, appearing due to smaller J and larger Δ_{ct} in the case of LCO.

5.3 Charge recombination in 1D Mott insulators

In spite of similarities with 2D Mott insulators, in quasi-1D Mott insulators the scenario involving coupling to spin degrees of freedom cannot be effective, neither for the MH exciton formation nor for the multi-boson emission, due to the phenomenon of the charge-spin separation [167, 168]. In short, in 1D hopping of charge only shifts the spin background and therefore cannot frustrate it more than on cca. one bond. In the following we show that in systems containing phonons with large frequencies, e.g. due to the intra-molecular vibrations, the multi-phonon emission can be a viable recombination mechanism. Such mechanism is applicable to effectively 1D organic materials where energetic vibrations of their complex units, having also strong electron-phonon coupling, indeed exist [26, 190]. Again, we discuss recombination only for the cases when the initial state is a 1D MH exciton, which can be stable in the case of the longer range Coulomb repulsion [37]. Since the photo-excited exciton is of the odd symmetry we show that its decay into even g.s. becomes allowed only due to the electron-phonon coupling. As a test of scenario we analyze and explain the data on ET-F_2TCNQ where the pressure dependence of the recombination rate was measured [21].

5.3.1 Model containing charge-phonon interaction

As the starting model for the charge recombination we consider the 1D extended Hubbard model, where in addition to the local Hubbard repulsion U, the nearest-neighbor Coulomb repulsion $V > 0$ is included as well, since it is crucial to stabilize the exciton state in 1D [37]. Assuming half-filling, i.e. $\bar{n} = 1$, the charge excited states are again holons (empty sites) and doublons (doubly occupied sites) with creation operators $h^\dagger_{i,s} = c_{i,s}(1 - n_{i,\bar{s}})$ and $d^\dagger_{i,s} = c^\dagger_{i,\bar{s}} n_{i,s}$, respectively, defined already in the previous Section. With such operators one can rewrite the kinetic term of the Hamiltonian H_t (taking into account the corresponding shifts in the spin background), the recombination term H_{rc} (noting that after the recombination of the HD pair two spin configurations are possible), and interaction term H_U,

$$H_t = t \sum_{i,s} (h^\dagger_{i+1,s} h_{i,s} - d^\dagger_{i+1,s} d_{i,s} + \text{H.c.}), \tag{5.63}$$

$$H_{rc} = -t \sum_{i,s} (h_{i,\bar{s}} d_{i+1,s} + h_{i+1,\bar{s}} d_{i,s} + \text{H.c.}), \tag{5.64}$$

$$H_U = U \sum_i n^d_i (1 - n^h_i) - V \sum_i (n^d_i n^h_{i+1} + n^h_i n^d_{i+1}), \tag{5.65}$$

where $n^h_i = (1/2) \sum_s h^\dagger_{i,s} h_{i,s}$, $n^d_i = (1/2) \sum_s d^\dagger_{i,s} d_{i,s}$ are HD density operators, respectively. The coupling to phonons is taken via a local electron density potential

term

$$H_{ep} = \sum_{ij} \lambda_{ij}(a_j^\dagger + a_j)\tilde{n}_i = \frac{1}{\sqrt{L}} \sum_{ijq} e^{-iqj}\lambda_{ij}(a_q^\dagger + a_{-q})\tilde{n}_i = \sum_{iq} \lambda_q^i (a_q^\dagger + a_{-q})\tilde{n}_i,$$

$$\lambda_q^i = \frac{1}{\sqrt{L}} \sum_j e^{-iqj}\lambda_{ij} = e^{-iqi}\lambda_q, \quad \lambda_q = \frac{1}{\sqrt{L}} \sum_j \lambda_{ij} e^{iq(i-j)}, \tag{5.66}$$

$$H_{ph} = \sum_q \omega_q a_q^\dagger a_q, \quad \tilde{n}_i = n_i^d - n_i^h, \tag{5.67}$$

where $\tilde{n}_i$ takes into account the opposite effect of the holon and the doublon on displacements of other units. Obviously, the coupling λ_q^i is site dependent and related to the Fourier transform of λ_{ij}.

5.3.2 Recombination in a spin-polarized system

We approach the problem of the charge recombination by first calculating the recombination rate in (nearly) spin-polarized system, i.e., with all but one spin turned up, which yields a clean analytical result. Similar to the process of the dielectric breakdown, Sec. 2, at least one turned spin suffices to study the (opposite process of) recombination of a single HD pair. We claim later on that the recombination rate in the non-polarized system is not substantially different.

For the nearly polarized system and $\lambda_q = 0$ there are at most three states below the continuum of unbound HD states: the g.s. $|\Phi_0\rangle$ with exponentially suppressed density of HD pairs, and two excitons, $|\Phi_1\rangle$ with odd and $|\Phi_2\rangle$ with even parity, which exist if $V > 2t$ and $V > 4t$, respectively [37]. Since the odd exciton $|\Phi_1\rangle$ has (besides the proper symmetry also) a lower energy, we assuming that the photo-excited system relaxes into it on the short timescale after the pump pulse. We introduce the single HD-pair basis $|\psi_q^l\rangle$,

$$|\psi_q^l\rangle = \frac{1}{\sqrt{L}} \sum_j e^{iqj} |\varphi_{j,j+l}\rangle, \tag{5.68}$$

$$|\varphi_{jm}\rangle = \begin{cases} (-1)^j d_{m,\uparrow}^\dagger h_{j,\uparrow}^\dagger |\tilde{0}\rangle & \text{for } j \neq m, \\ (-1)^j c_{j,\downarrow}^\dagger c_{j,\uparrow} |\tilde{0}\rangle & \text{for } j = m, \end{cases}$$

with the reference vacuum $|\tilde{0}\rangle = \prod_j c_{j,\uparrow}^\dagger |0\rangle$ (within which operators are ordered according to the ascending index j), Then the relevant $|\Phi_0\rangle, |\Phi_1\rangle$ can be expressed exactly. While $|\Phi_0\rangle \sim |\psi_{q=0}^0\rangle$, the odd exciton $|\Phi_1\rangle$ is given by

$$|\Phi_1\rangle = \sum_{l>0} \beta_l \big(|\psi_{q=0}^l\rangle - |\psi_{q=0}^{-l}\rangle\big), \ \beta_l = \beta_0 e^{-\kappa_1 l} \tag{5.69}$$

where $\kappa_1 = \ln(V/2t)$. We note that both the g.s. and the odd exciton state have minimal energies at $q = 0$ with $E_0 \approx -8t^2/(U-V)$, $E_1 = U - V - 4t^2/V$, respectively.

It is evident from Eqs. (5.64, 5.69) that without the electron-phonon coupling the HD exciton $|\Phi_1\rangle$ has the opposite symmetry to the g.s. $|\Phi_0\rangle$ and cannot decay into it, although this is observed in experiments. Coupling to phonons actually causes that system relaxes into a dressed exciton state and allows such a recombination.

To treat the effect of phonons we use a similar approach as in Sec. 5.1 via the Lang-Firsov transformation $\tilde{H} = e^{-S} H e^{S}$, choosing S of the form

$$S = \sum_{i,q} \alpha_q^i (a_q^\dagger - a_{-q}) \tilde{n}_i = \sum_i p_i \tilde{n}_i, \tag{5.70}$$

and applying it to the full H, Eqs. (5.63-5.66), in order to eliminate the term linear in λ_q^i, i.e. $H_{ep} - [S, H_{ph}] = 0$. This sets $\alpha_q^i = -\lambda_q^i/\omega_q$. The electron-phonon coupling now enters only via the dressed hopping $\tilde{H}_t$ and the recombination $\tilde{H}_{rc}$ term,

$$\tilde{H}_t = -t \sum_{i,s} \big(d_{i+1,s}^\dagger d_{i,s} \; e^{\tilde{p}_{i,i+1}} - h_{i+1,s}^\dagger h_{i,s} \; e^{-\tilde{p}_{i,i+1}} + \text{H.c.} \big), \tag{5.71}$$

$$\tilde{H}_{rc} = -t \sum_{i,s} (h_{i,\bar{s}} d_{i+1,s} \; e^{-\tilde{p}_{i,i+1}} + h_{i+1,\bar{s}} d_{i,s} \; e^{\tilde{p}_{i,i+1}} + \text{H.c.}), \tag{5.72}$$

$$\tilde{H}_U = H_U - \sum_{ii'} \epsilon_{ii'} \tilde{n}_i \tilde{n}_{i'}, \tag{5.73}$$

$$\tilde{p}_{i,i+1} = p_i - p_{i+1}, \quad \epsilon_{ii'} = 2 \sum_q \frac{\lambda_q^i \lambda_{-q}^{i'}}{\omega_q}, \quad \tilde{H}_0 = \tilde{H}_t + \tilde{H}_U. \tag{5.74}$$

The upper dressing of hopping is obtained from relations like

$$e^{-S} d_{i+1,s}^\dagger d_{i,s} e^{S} = d_{i+1,s}^\dagger d_{i,s} \; e^{(-p_{i+1}+p_i)}, \tag{5.75}$$

and equivalently for the other cases.

As in the problem of the exciton decay in 2D we separate the Hamiltonian into parts that conserve the number of HD pairs, $\tilde{H}_0 = \tilde{H}_t + \tilde{H}_U, H_{ph}$, and the perturbation $\tilde{H}_{rc}$ that does not, and establish the recombination rate using the FGR approximation. Using $\tilde{H}_{rc}$ as a perturbation, we shall neglect the effect of exchange, $J \to 0$, since it is obtained perturbatively through $\tilde{H}_{rc}$. Even though the coupling constant t in $\tilde{H}_{rc}$ is not small, usage of the FGR is justified by the smallness of the transition matrix element. Again, we write the FGR in an integral form and use some of the results from the exciton-boson toy model, Sec. 5.1,

$$\Gamma(\omega) = 2\pi \sum_{\mathbf{m},q_0} |\langle \tilde{\Phi}_{0,q_0}^{\mathbf{m}} | \tilde{H}_{rc} | \tilde{\Phi}_1 \rangle|^2 \delta\big(\omega - (E_{0,q_0}^{\mathbf{m}} - E_0)\big) \tag{5.76}$$

$$= 2\pi \langle \tilde{\Phi}_1 | \tilde{H}_{rc} \sum_{\mathbf{m},q_0} |\tilde{\Phi}_{0,q_0}^{\mathbf{m}}\rangle\langle \tilde{\Phi}_{0,q_0}^{\mathbf{m}}| \; \delta\big(\omega - (\tilde{H}_0 + H_{ph} - E_0)\big) \; \tilde{H}_{rc} | \tilde{\Phi}_1 \rangle$$

$$= 2Re \; \langle \tilde{\Phi}_1 | \tilde{H}_{rc} \int_0^\infty d\tau e^{i\omega\tau - i(\tilde{H}_0 + H_{ph} - E_0)\tau} \; \tilde{H}_{rc} | \tilde{\Phi}_1 \rangle \tag{5.77}$$

where $|\tilde{\Phi}_{0,q_0}^{\mathbf{m}}\rangle = |\Phi_{0,q_0}\rangle |\mathbf{m}_{ph}\rangle$ is the HD-pair g.s. with charge momentum q_0 ($|\Phi_{0,q_0}\rangle \sim |\psi_{q_0}^0\rangle$ according to Eq. (5.68)), and additional phonon excitations $|\mathbf{m}_{ph}\rangle$ that in the process of the recombination absorb the energy of the charge exciton. The energy of such state is $E_{0,q_0}^{\mathbf{m}}$. The recombination rate has to be evaluated at the MH gap Δ, $\omega = \Delta$. To obtain Eq. (5.77) we used the fact that $\sum_{\mathbf{m},q_0} |\tilde{\Phi}_{0,q_0}^{\mathbf{m}}\rangle\langle \tilde{\Phi}_{0,q_0}^{\mathbf{m}}|$ is the full set in the subspace without HD pair and at the same time neglected also the creation part of $\tilde{H}_{rc}$.

In principle $|\tilde{\Phi}_1\rangle$ is the eigenstate of the transformed Hamiltonian without the recombination term, $\tilde{H}_0 + H_{ph}$, however, we shall neglect the additional dressing

with phonons due to the phonon operators in the kinetic term, taking $\tilde{H}_t \approx H_t$. Still, one should not forget that due to the canonical transformation we now work in a rotated basis, so that $|\tilde{\Phi}_1\rangle$ does contain some phonon dressing even within this approximation, as evident from the shift of its energy, Eq. (5.73)).

We proceed with the calculation of the recombination rate from Eq. (5.77). First we apply the recombination operator to the exciton wave function

$$\begin{aligned}\tilde{H}_{rc}|\tilde{\Phi}_1\rangle &= -\frac{t\beta_1}{\sqrt{L}}\sum_j \big(- e^{\tilde{p}_{j-1,j}}(|\varphi_{j,j}\rangle + |\varphi_{j-1,j-1}\rangle) + e^{-\tilde{p}_{j,j+1}}(|\varphi_{j,j}\rangle + |\varphi_{j+1,j+1}\rangle)\big)|0_{ph}\rangle \\ &= \frac{t\beta_1}{\sqrt{L}}\sum_j |\varphi_{j,j}\rangle\big(e^{\tilde{p}_{j-1,j}} + e^{\tilde{p}_{j,j+1}} - e^{-\tilde{p}_{j,j+1}} - e^{-\tilde{p}_{j-1,j}}\big)|0_{ph}\rangle \\ &= \frac{t\beta_1}{\sqrt{L}}\sum_j |\varphi_{j,j}\rangle(A_{j,j+1} + A_{j-1,j})|0_{ph}\rangle, \quad A_{j,j+1} = e^{\tilde{p}_{j,j+1}} - e^{-\tilde{p}_{j,j+1}}. \end{aligned} \tag{5.78}$$

Using projection

$$|\varphi_{j,j}\rangle = \sum_{q_0} |\Psi^0_{q_0}\rangle\langle\Psi^0_{q_0}|\varphi_{j,j}\rangle = \frac{1}{L}\sum_{q_0,j'} e^{iq_0(j'-j)}\ |\varphi_{j',j'}\rangle, \tag{5.79}$$

the time evolution yields

$$\begin{aligned} e^{-i(\tilde{H}_0+H_{ph}-E_0)\tau}\tilde{H}_{rc}|\tilde{\Phi}_1\rangle &= \frac{t\beta_1}{\sqrt{L}}\sum_j e^{-i(\tilde{H}_0-E_0)\tau}|\varphi_{j,j}\rangle\ e^{-iH_{ph}\tau}(A_{j,j+1} + A_{j-1,j})|0_{ph}\rangle \\ &= \frac{t\beta_1}{L^{3/2}}\sum_{q_0,j',j} e^{-i\omega_{q_0}\tau}e^{iq_0(j'-j)}|\varphi_{j',j'}\rangle e^{-iH_{ph}\tau}(A_{j,j+1} + A_{j-1,j})|0_{ph}\rangle, \\ &= \frac{t\beta_1}{\sqrt{L}}\sum_j |\varphi_{j,j}\rangle\ e^{-iH_{ph}\tau}(A_{j,j+1} + A_{j-1,j})|0_{ph}\rangle, \end{aligned} \tag{5.80}$$

where the magnon dispersion was neglected, $\omega_{q_0} \approx 0$, due to our choice of perturbation hierarchy, setting $J \to 0$. The expression for the decay rate $\Gamma(\omega)$, Eq. (5.77), is then

$$\begin{aligned}\Gamma(\omega) &= 2Re\ \frac{t^2|\beta_1|^2}{L}\int_0^\infty d\tau e^{i\omega\tau}\sum_{i,j}\langle\varphi_{i,i}|\varphi_{j,j}\rangle\ \times \\ &\qquad \times \langle 0_{ph}|(A^\dagger_{i,i+1} + A^\dagger_{i-1,i})\ e^{-iH_{ph}\tau}(A_{j,j+1} + A_{j-1,j})|0_{ph}\rangle \end{aligned} \tag{5.81}$$

$$= 2Re\ t^2|\beta_1|^2\int_0^\infty d\tau e^{i\omega\tau}\ (2\gamma^{ph}_0(\tau) + \gamma^{ph}_1(\tau) + \gamma^{ph}_{-1}(\tau)), \tag{5.82}$$

where we used the space-translational invariance and

$$\begin{aligned}\gamma^{ph}_d(\tau) &= \langle 0_{ph}|A^\dagger_{0,1}\ e^{-iH_{ph}\tau}A_{d,d+1}|0_{ph}\rangle = 4e^{-\sum_q|\tilde{\alpha}_q|^2}\sinh\zeta_d(\tau), \\ |\tilde{\alpha}_q|^2 &= \frac{2|\lambda_q|^2}{\omega_q^2}(1-\cos q), \\ \zeta_d(\tau) &= \sum_q |\tilde{\alpha}_q|^2 e^{-idq}e^{-i\omega_q\tau}. \end{aligned} \tag{5.83}$$

Upper relations are obtained using the fact that $A_{j,j+1}$ creates a sum of coherent states (see App. C.3.1). In the case of the nearly polarized system there are only

$d = 0, \pm 1$ contributions, since HD pair in the bra and ket wave function of the matrix element (5.77) can be for at most $|d| = 1$ apart, otherwise there is not overlap between spin configurations after the recombination. In the non-polarized case there can be also additional contributions (as explained later), therefore the expression γ_d^{ph} has been written for a general d. However, it is clear that for λ_q, ω_q with a mild dispersion, the $d = 0$ term is dominant anyway.

The decay rate for the nearly polarized case can be written as

$$\Gamma(\omega) = 16Re\ t^2|\beta_1|^2 e^{-\zeta_0(0)} \int_0^\infty d\tau e^{i\omega\tau} \Big[\sinh \zeta_0(\tau) + \sinh \zeta_1(\tau) \Big], \tag{5.84}$$

where we used $\zeta_d(\tau) = \zeta_{-d}(\tau)$. The time-integration in Eq. (5.84) can be performed numerically for any kind of dispersions λ_q, ω_q, however, assuming that exciton is coupled to the optical phonons further simplification are justified. We shall assume a constant coupling $\lambda_q = \lambda/\sqrt{L}$ and a phonon dispersion $\omega_q = \omega_0 + \delta\omega \cos(q)$ with a spread $\delta\omega$ around its mean value. As seen later on, the crucial message of the final result should not depend on this particular choice.

(a) The coupling strength can be approximated by

$$\sum_q |\tilde{\alpha}_q|^2 = \zeta_0(0) \approx 2\xi, \quad \xi \equiv \frac{\lambda^2}{\omega_0^2}. \tag{5.85}$$

(b) After the integration over q function $\zeta_d(\tau)$ can be compactly expressed as

$$\zeta_d(\tau) \approx 2\xi\ e^{-i\omega_0\tau}(-i)^d \Big[J_d(\delta\omega\tau) + \frac{i}{2}\big(J_{d+1}(\delta\omega\tau) - J_{d-1}(\delta\omega\tau) \big) \Big] \tag{5.86}$$

where $J_d(x)$ is the Bessel function.

(c) In order to smear out the sharp edge of the dispersion ω_q and the consequent singularity in the density of states, we shall suppose that we have a set of phonons with dispersions ω_q, but with the mean value distributed around ω_0 with a width σ, leading to an additional smoothening of the integral over τ. Furthermore, we shall approximate sinh in the integrand with exp; based on the Fourier transformation of exp and sinh, latter contains only resonances around odd multiples of ω_0, resulting in a $(1/2)$ prefactor in the limit of large ω where resonances merge, $\mathcal{S}_d(\omega) \approx \mathcal{E}_d(\omega)$,

$$\mathcal{S}_d(\omega) = \int_0^\infty d\tau e^{i\omega\tau} \sinh\big(e^{-\sigma^2\tau^2/2} \zeta_d(\tau) \big) \tag{5.87}$$

$$\mathcal{E}_d(\omega) = \frac{1}{2} \int_0^\infty d\tau e^{i\omega\tau} \exp\big(e^{-\sigma^2\tau^2/2} \zeta_d(\tau) \big). \tag{5.88}$$

At least for $d = 0$ the integral (5.88) can be established by its saddle point again. Furthermore, as demonstrated in Fig. 5.10, its dependence on ω/ω_0 can be captured also by the compact form obtained from the saddle point approximation for the the Gaussian coupling, as in Sec. 5.1, Eq. (5.14),

$$\mathcal{G}_p(\omega) = \frac{1}{2}\sqrt{\frac{2\pi}{\Delta\omega_0}}\ \exp\left[-\frac{\Delta}{\omega_0} \ln\left(\frac{\Delta}{e\ p\xi\omega_0} \right) \right], \tag{5.89}$$

as long as $\sigma \ll \omega_0$, since within it the effect of spread σ is neglected in order $\mathcal{O}(\sigma^2/\omega_0^2)$. As relevant for the first term in Eq. (5.84), we plot in left Fig. 5.10 the comparison between the direct numerical integration of Eq. (5.87) ($\mathcal{S}_0$) and Eq. (5.88) ($\mathcal{E}_0$) for $d = 0$, and the compact expression G_2 for the Gaussian coupling with $p = 2$. Such choice of p is a consequence of the strength of effective coupling, Eq. (5.86), parameterized by ξ. As relevant for the second term in Eq. (5.84), we plot in right Fig. 5.10 numerical integration of Eq. (5.87) ($\mathcal{S}_1$) for $d = 1$ and G_1 for $p = 1$. Now we use $p = 1$ since the dominant contribution from Eq. (5.86) comes from J_{d-1} with a prefactor 1/2. One should note that $\mathcal{S}_1$ is negative, therefore it has to be compared with $-G_1$.

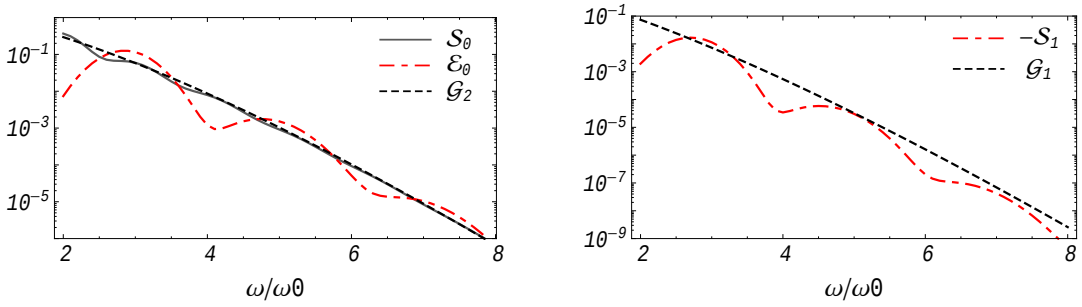

Figure 5.10: Comparison of different (approximate) evaluations $\mathcal{S}_d, \mathcal{E}_d, \mathcal{G}_p$ of terms appearing in Eq. (5.84) for parameters $\omega_0 = 1, \delta\omega = 0.1\omega_0, \sigma = 0.2\omega_0, \xi = 0.3$.

In the recombination process the energy transmitted to phonons equals the MH gap Δ. As confirmed with Fig. 5.10 we are confident to approximate the expression (5.84) with a compact form, following from the saddle point for the Gaussian coupling,

$$\Gamma(\Delta) \approx 4t^2|\beta_1|^2 e^{-2\xi}\sqrt{\frac{2\pi}{\Delta\omega_0}}\Big\{\exp\Big[-\frac{\Delta}{\omega_0}\ln\Big(\frac{\Delta}{2e\xi\omega_0}\Big)\Big] - \exp\Big[-\frac{\Delta}{\omega_0}\ln\Big(\frac{\Delta}{e\xi\omega_0}\Big)\Big]\Big\}, \tag{5.90}$$

We claim that the latter expression is appropriate also for other specific forms of λ_q, ω_q with a mild q dependence. This form will be used for the comparison with experiments [21]. Among the two terms, first (and positive one) is dominant.

5.3.3 Recombination in non-polarized system

Of course experiments are not performed at nearly polarized spin background. However, they are performed at room temperature and possibly additionally heat the system by performing pump excitations above the gap, therefore it might be sensible to assume that spin background has no ordering. For the sake of simplicity, we may assume that we start with a (classical) random spin configuration. The pump pulse then creates a HD pair at some sites. By hopping, and consequently shifting the spin background, holon and doublon form a (translationally invariant) exciton. However, in the $J \to 0$ approximation, this exciton is uniquely given by the spin background. Even if we start with a quantum superposition of spin backgrounds, each of them will host a unique exciton again, so that the state after a short-time

relaxation can be seen as a superposition of different excitons with a negligible overlap, since already the different spin configurations in the starting superposition have an overlap that is negligible (or precisely zero for orthogonal configurations). The only difference to the recombination in the nearly polarized case is that within the matrix element in Eq. (5.77) HD pairs (in bra- and ket-wave function), originating from different shifts of the same spin background, can recombine on different sites and will contribute to the decay rate as long as there is an overlap between both shifted spin configurations. Probability for the overlap between HD pairs shifted for d is given by P_d, while an additional suppression of contributions with $d > 0$ comes also from the phononic part of the matrix element, γ_d^{ph}, Eq. (5.83). The general decay rate therefore has the form

$$\Gamma(\omega) = 2Re\ t^2|\tilde{\beta}_1|^2 \sum_d P_d \int_0^\infty d\tau e^{i\omega\tau}\gamma_d^{ph}(\tau). \tag{5.91}$$

Weight P_d is related to the probability for the existence of a section within the spin background with Néel AFM order on d successive sites, since only then the two components of the (recombined) exciton have a complete overlap. For any spin background $P_0 = 2, P_{\pm 1} = 1$. For $|d| > 1$ it equals $P_d = 2^{-d+1}$ for a classical random background, while for a quantum state it would be given by an appropriate correlation function, which is for a disordered background expected to decay exponentially with distance. $|\tilde{\beta}_1|$ takes into account possible modification of the exciton wave function.

In addition to that, as shown in Fig. 5.11 the integral (5.87) is for each $|d| > 0$ more than an order smaller than for $|d| - 1$, therefore the only non-negligible contributions again come from $d = 0, \pm 1$, fully contained already in the calculation within the nearly polarized system. Another reasonable observation, made from

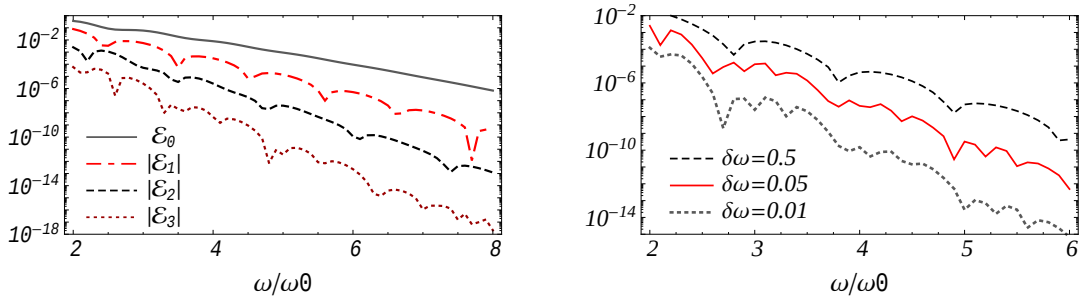

Figure 5.11: Comparison of integrals $|\mathcal{E}_d|$, Eq. (5.88), for different d (left) and different $\delta\omega$ (right), calculated at fixed parameters $\omega_0 = 1, \delta\omega = 0.1\omega_0, \sigma = 0.2\omega_0, \xi = 0.3$ (for left Fig.) and $d = 2, \omega_0 = 1, \sigma = 0.1\omega_0, \xi = 0.3$ (for right Fig.).

numerical evaluation of $|\mathcal{E}_d|$, right Fig. 5.11, is that for $|d| > 1$ it gets substantially reduced by choosing smaller $\delta\omega$, which confirms the intuition that the off-diagonal phonon matrix element can be non-zero only for dispersive phonons.

5.3.4 Comparison with experiment

Finally we compare the recombination time $\tau_r = \Gamma^{-1}$ obtained from Eq. (5.90) with experimentally measured one [21], where its pressure dependence was pursued.

All quantities but the strength of the charge-phonon coupling ξ are experimentally set, with t, V being specified functions of pressure. It seems reasonable to assume that the measured hopping parameter actually corresponds to the dressed hopping $\tilde{t} = te^{-\xi}$, while the interaction terms are renormalized according to Eq. (5.73). Then $\tilde{U} = 0.84eV$, while $\tilde{t}$ and $\tilde{V}$ range approximately linearly within intervals $\tilde{t} \in [0.04, 0.06]eV$ and $\tilde{V} \in [0.12, 0.16]eV$, [21]. The relevant phonon frequencies should be in the window $\omega_0 \in [0.22, 0.25]eV$ [26], therefore we take $\omega_0 = 0.23$. The MH gap can be expressed as

$$\Delta \approx \tilde{U} - \tilde{V} - \frac{4\tilde{t}^2}{\tilde{V}} + \frac{8\tilde{t}^2}{\tilde{U} - \tilde{V}}. \tag{5.92}$$

Left Fig. 5.12 shows τ_r as a function of pressure p for three different values $\xi = 0.25, 0.27, 0.3$, suggesting that $\xi = 0.27$ best captures the experimentally measured recombination times [21], displayed in the right Fig. 5.12. Parameter ξ being small

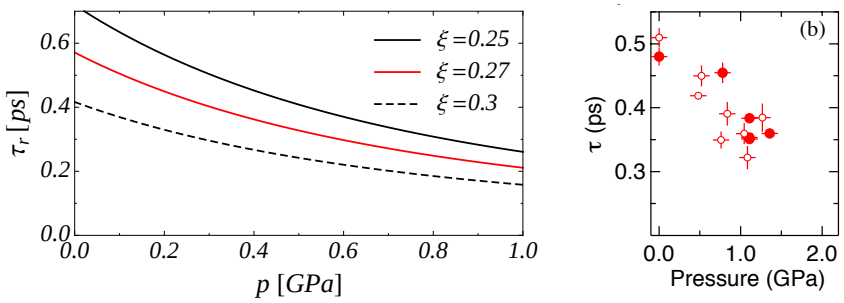

Figure 5.12: Left: recombination time τ_r as a function of the pressure p calculated from Eq. (5.90) using the experimental parameters written in the text. Right: experimentally measured dependence of the recombination rate on the pressure, taken from [21].

at partially justifies our calculation within exciton, whose additional dressing due to phonon phases in $\tilde{H}_t$, Eq. (5.71), has been neglected.

From $(1/L)\sum_q |\lambda_q|^2/\omega_q^2 \approx \lambda^2/\omega_0^2 \approx \xi$ we can estimate $\lambda \approx \omega_0\sqrt{\xi} = 0.12eV$, which was measured and calculated for a similar organic material, finding $\lambda \in [0.05eV, 0.1eV]$ [190]. Such comparison confirms that the electron-phonon coupling needed to reproduce the experimental results is indeed realistic and not weak, emerging mostly from the coupling to intra-molecular vibrations. Still, it is essential that it is not as strong as to induce the self trapping and the small-polaron formation. We note that the usual dimensionless parameter $\tilde{\lambda} = \lambda^2/2\omega_0 t$, which is relevant for the self-trapping of the holon (and the doublon) due to the polaron formation is for $\xi = 0.27$ in the interval $\tilde{\lambda} \approx \xi\omega_0/2\tilde{t}e^{\xi} \in [0.4, 0.6]$, i.e. below the threshold for self-trapping, which depends also on the ratio ω_0/t and is for $\omega_0/t \approx 4$ (as in our case) $\tilde{\lambda}_c \approx 4$ [191]. This result a posteriori justifies our calculation with mobile holon and doublon.

Chapter 6

Conclusions

In this Chapter we revisit the main points of comprehension, gathered on the round tour of this thesis, including excitation and relaxation of Mott insulators. With a special interest in the behavior of excitations above the Mott-Hubbard gap, corresponding to effectively charged particles, majority of studies was formulated in the language of holons and doublons that in the single-band Hubbard picture represent those charges as the non- and doubly-occupied sites. Following a natural, chronological way; we first summarize on the topic that addressed the rate at which holon-doublon pairs are created due to the presence of a strong constant electric field, while in the second part of the thesis we focused on the opposite process - the relaxation and eventual recombination of holons and doublons, when created with a strong pulsed field, as is the case in pump-probe experiments.

The only topic within this thesis not formulated in terms of holons and doublons is the problem where we treated a chain of spinless interacting fermions, possibly in the Mott insulating regime, coupled to the environment at the chain ends and exposed to an additional external field as well.

Correlated systems in strong fields

We treated the effect of a strong electric field on two different interacting 1D fermionic systems: spin-1/2 system at different magnetizations and spinless chain coupled to the environment also through an incoherent sink and source dissipation at the boundaries. Each system has its own features that leave consequence on the manifestation of the electric field in it, however, there is also some overlap.

Dielectric breakdown of Mott insulator: We considered a system of spin-1/2 fermions within the Hubbard model with a goal to determine the rate at which the system is exited over the Mott-Hubbard gap, if initially in its insulating ground state, but then exposed to an external electric field. This is tightly related to the production of effectively charged particles, doublons and holons. A particular innovation of our approach was to treat the system in different magnetization sectors, starting from the nearly spin-polarized one - with a single over-turned spin, down to the non-polarized system - where the global ground state for the case without the external magnetic field actually is. The experimental realization of polarized systems could be obtained with an additional magnetic field, while the theoretical motivation for such an approach is the apparent simplification of the problem, yielding even analytical results at the extreme nearly polarized system.

An advantage of the nearly polarized system is that several physically important

features get simplified and consequentially more clear. A prominent example is the nature of Mott insulator, which can be in this sector undisputedly explained via binding of the holon-doublon pair. In such state the dominant configuration has no double occupancy (which can formally be presented with holon and doublon being on the same site), while configuration with holon and doublon separated for $l > 0$ are exponentially suppressed as described with the localization parameter κ, determined by the interaction U. Exciting (and destroying the insulating nature of) such state then literally corresponds to the unbinding process. Even when magnetization is reduced and more spins are overturned, different holon-doublon pairs tend to be maximally separated and therefore influence each other only through the exponential tails, inducing collective effects seen e.g. in a slight reduction of the Mott-Hubbard gap Δ.

In the case of the dielectric breakdown it is the electric field that causes unbinding of the holon-doublon pair. In a simplified, yet intuitive picture latter process can be viewed as a tunneling over distance of at least the holon-doublon pair localization length $1/\kappa$. There is a threshold field for that process, which is in this simplified tunneling picture related to the effective potential slope, and approximately satisfies $F_{th}/\kappa \sim \Delta$.

For more precise characterization of this threshold field F_{th} we first performed a numerical time evolution in the nearly polarized system that confirmed the decay of the insulating ground state with a rate of the form $\Gamma \propto \exp(-\pi F/F_{th})$. As observed in numerical results, the ground state is excited into a continuum of states. A crucial observation was that excited states can be approximated with states of the free holon-doublon pair with dispersion $\epsilon_k(\phi) = U - 4t\cos(\phi - k)$, k being the relative momentum of both particles and $\phi = F\tau$ the time-dependent flux. Within this and some other more technical approximation the threshold field was found analytically and scales with Mott-Hubbard gap as $F_{th} \propto \Delta^{3/2}$, unlike in the Landau-Zener case with $F_{th} \propto \Delta^2$. Below some critical U, above which the free holon-doublon states are not a good approximation any more, numerical results confirm the analytical expression.

When reducing the magnetization the central question is whether excitation rate is simply proportional to the number of turned spins, since this would confirm the independent behavior of different pairs, following the same mechanism as in the nearly polarized system. It proves to be true down to 1/4 of overturned spins, while for larger fractions the threshold field is reduced and no longer strictly follows $F_{th} \propto \Delta^{3/2}$, possibly due to more collective nature of overlapping neighboring holon-doublon pairs. On a conceptual level, the result from nearly polarized case is important since it is the only to give a physical insight into the process, which is extendable towards smaller polarization, giving at least qualitatively appropriate threshold field.

We should note that the concept of the holon-doublon binding can serve as a characterization of the (equilibrium) metal-to-insulator transition due to interaction U as well. Especially in higher dimensional systems, $d \geq 3$, there exist a critical U_c below which there is no binding even for a single holon-doublon pair. For $d = 1, 2$ binding and as a consequence the Mott-Hubbard gap shows only crossover-like behavior as a function of U, being exponentially small for small interactions U.

Boundary driven XXZ chain: The effect of a strong electric field was treated on another example; 1D chain of spinless fermions with nearest neighbor interaction,

which can be mapped to a spin chain in a magnetic field using the Jordan-Wigner transformation. Technically, we treated an inhomogeneous XXZ spin 1/2 chain dissipated with incoherent source/sink baths at chain ends and developed a systematic asymptotic expansion of the spin current in the limit of a strong transverse magnetic field gradient. It turned out that regardless of the sign of the magnetic field gradient, the source and the sink always impose the direction of the spin current. Moreover, strong field actually leads to the Stark localization of excitations, e.g. observed in the one-magnon spectra, causing the bulk of the system to behave as a 'Stark' insulator and preventing possibly high currents even due to the incoherent driving. For that reason the current is exponentially suppressed with the system size n as $J \propto g^{-n}$, where g is the field gradient. However, due to interactions, it matters whether external field and bias drive the system in the same or in the opposite way, resulting in $J(g) \neq J(-g)$. Defining rectification coefficient $R = (J(g)-J(-g))/(J(g)+J(-g))$, there are two mechanisms for enhancing current rectification: (i) $R \to 1$ in thermodynamic limit $n \to \infty$, at fixed large gradient g as a result of our asymptotic current formula; (ii) for resonant field (gradient) values where our asymptotic analysis fails, the current is of higher order in $1/g$ for one direction of the field than in the other. This clearly yields rectification coefficient $R \to 1$ even at fixed finite size n. The physical interpretation of unusually large current at resonant fields is that they appear when (on the level of the Hamiltonian that governs the coherent part of the dynamics) the insulating state with step-like magnetization profile is degenerate with some less insulating one.

Notably, asymptotic formula can be generalized also to other situations with a bulk insulator; e.g. due to the large anisotropy parameter or a strong random transverse magnetic field (related to the topic of the many-body localization), where in the latter case we have no control over the resonant values.

Overlap: Because one model has spin-1/2 and the other spinless fermions we cannot expect to observe the same physics when adding the external electric field. Namely, the focus of the former study was to determine the rate at which double occupancy is produced in a fixed magnetization sector, while in the latter system (where the insulating regime is in principle present at half filling and sufficient nearest neighbor interaction) number of effective holons/doublons (two subsequent empty/occupied sites) cannot be restricted. Moreover, by opening the system we cannot even guarantee a strict half-filling. However, the effect of the Stark localization is actually common to both, since it localizes also the proper holon-doublon pair on a distance $l_s = 8/F$. Therefore one should be aware that contribution to the current in such system is actually local, due to the production of charges, which conduct only over a limited area set by the Stark localization. It was not particularly investigated how collective effects at lower magnetizations relax this constraint. On the other hand, our asymptotic formula for the spinless model is valid in the regime when this localization is non-negligible and it effects the global current.

Charge (pre-)thermalization in pump-probe experiments

When proposing the theory for the pump-probe experiments on Mott insulators we first addressed the short-time dynamics of holons and doublons created with an initial strong pump pulse with energy larger than the Mott-Hubbard gap. We assumed that at very short times charged particles behave as independent, therefore we treated the relaxation of a single one, e.g. a holon. We simulated the initial

state by injecting the holon into the ordered spin background, which is only a sensible approximation that should be further tested with a more proper study of the excitation process.

First we coupled the charge to spin degrees of freedom using the t-J model. We observed a very fast relaxation (within few fs) of the initial excited state towards a stationary one, whose features were compared to the ground state spin polaron and to what is thermally expected, based on the amount of energy that has been introduced into the system.

Mechanism: An insight into different stages of the fast relaxation has been obtained by a toy 1D model, combining the t-J model with a staggered field h which mimics the spin ordering absent in 1D, but present in 2D. Especially through the holon-spin correlation it has been revealed that the mechanism of the relaxation consists of two stages: the initially localized holon first perturbs the spin ordering in its vicinity and in such a way reduces its kinetic energy, as has been seen and explained before by generation of string (spin-excited) states [160]. In the second stage local spin perturbation is dispersed into the whole system via magnons. The appropriateness of such scenario has been confirmed by observing in the correlations the Lieb-Robinson velocity of each stage; in the first stage holon moves relative to the background as a free particle with velocity $v_h \approx 2$, while in the second stage the local spin excitation is spread into the system with maximal magnon velocity $v_m = h + J - \sqrt{h(h+2J)}$.

If charge is coupled also to (dispersionless) phonons then the stationary state is a spin-lattice polaron. It turns out that at short times holon preferentially emits energy to the more efficient bath, which is in case of a small charge-phonon coupling the spins and in case of a large coupling the phonons. However, on a longer timescale both bosonic baths equilibrate between each other, even though they are coupled only through the charge. A better understanding and precise timescale of this equilibration is yet to be obtained.

Nonequilibrium optical conductivity: To get another insight into the dynamics, especially close to experimentally relevant quantities, the linear optical conductivity was generalized to nonequilibrium situations for tight binding models. Related to pump-probe experiments, within it the probe pulse is taken as a perturbation in the linear order, while effect of the pump pulse is accounted for through the initial wave function, or more appropriately through the time-dependent zeroth order of the density matrix. The most apparent difference to the equilibrium optical conductivity is that system does not have the time-translational invariance so that $\sigma(t', t)$, relating the response in current at time t' to the field applied at time t really is a function of two times, not just of their difference. In order to obtain an equivalent to (equilibrium) $\sigma(\omega)$, which is in principle more informative, since it points out e.g. possible absorptions in the system, we can Fourier transform $\sigma(t', t)$ over one time, which we choose to be the later t' in order to preserve the information about when the probe pulse is applied and to insure causality (i.e. not transform over times prior to the pump pulse). Within such formulation quantities like optical sum rule and Drude weight are well defined and time-dependent as well.

We used this formalism to calculate the response of an excited holon in 2D t-J model mentioned above. For an initially localized holon that approximately describes the state right after the creation of charged particle from an insulating system, optical response shows build-up of the mid-infrared (in-gap) and the Drude

peak from the initially featureless $\sigma(\omega, t \sim 0)$. Both, the mid-infrared and the Drude peak turned out to be surprisingly close to what is observed in the ground state spin polaron response, again suggesting that the relaxation is some kind of spin polaron formation. However, the energy that has been introduced into the finite system under consideration should lead to a more thermal response, smearing out latter peaks.

Time-dependent temperature: With a wish to characterize the stationary state better and possibly find reasons for its pre-thermal nature we used the fluctuation-dissipation relation, which for a thermal state relates two-time correlations with the linear response function (for any observables) via $\tanh(\beta\omega/2)$, where $T = 1/\beta$ is the temperature of the system. Pretending that at any time t our system behaves as thermal, we computed current-current correlations and checked if the fluctuation-dissipation relation is obeyed at some (a priori) unknown β. It turned out that after a very short transient with undefined β, the extracted temperature later on is exponentially decreasing toward a stationary value. Being obtained from the current-current correlations it can only be interpreted as the local temperature of the spin polaron. Its stationary value turns out to be higher then what is canonically expected from the total energy, however it is consistent with the temperature that would be extracted from the kinetic energy of the steady-state, supposing this is also the thermal value.

This example shows that fluctuation-dissipation relation can be used as an interesting, possibly even local probe of the temperature. Namely, by applying it to different observables we have a handle on which part of the system is being examined

Unfortunately, even this analysis did not reveal the reasons for the pronounced mid-infrared and Drude peak in the optical response of the excited holon. Actually the high local temperature, obtained from the fluctuation-dissipation relation, would suggest they should be smeared out. This and the actual cause for the prethermalization remain to be further examined, possibly also by adding the charge-phonon coupling.

Charge recombination in pump-probe experiments

As the central topic of this thesis we tackled the problem of the charge recombination, a crucial and nearly final stage in pump-probe experiments, which is in the correlated materials typically observed in ps range. This process is especially theoretically challenging due to the large energy of charges (doublons) that must be instantaneously transmitted to other degrees of freedom, e.g. spins, phonons or other fermions, having a lower energy scale. We addressed only the cases with low density of charges created by a pump pulse, when the scattering among charged particles is improbable. It turned out that independent of the specifics of mechanisms for doublon decay, recombination rate is exponentially suppressed by the number of (bosonic) excitations created in the process. As the initial state for the recombination we always assumed a bound pair of a holon and a doublon, which is proven to exist experimentally as well as by our model-based calculations. Since the dimension of the system proved to play an important role we separately treated 2D and 1D systems, as relevant for experiment on cuprates (Nd_2CuO_4 and La_2CuO_4) [13, 14] and organic salts (ET–F_2TCNQ) [21], with effectively 2D and 1D nature, respectively. We proposed that in 2D systems with pronounced charge-spin coupling the holon-doublon pair can recombine via emission of several spin excitations, while in

1D, where charge and spin degrees of freedom are in principle decoupled, the energy can be transmitted to phonons. The latter scenario can reproduce ps recombination if phonons have high frequency ω_0, which is the case for organic salts with energetic intra-molecular vibrations, and is therefore somewhat specific for such materials and could not be applied e.g. to 1D cuprates [18], where lattice phonons are known to have much smaller typical frequencies. Due to the exponential suppression of the decay rate with the number of created bosons, this should be reflected in much longer recombination times. A possible explanation might be that through phonon-spin coupling [169] charge and spin are not decoupled (as it is in principle the case for 1D systems), so that recombination process can involve emission of spin and phonon excitations. Similar reasoning might be applied also to Ca_2CO_3 [38], with an additional complications that in this case holon and doublon pairs are not bound into an exciton [19]. These remain to be more extensively studied theoretically, as well as experimentally.

In the following we separately revisit the main points and issues:

Role of dimension: The crucial distinction between strongly correlated systems of different dimension seems to be the charge-spin coupling. It is inherently present in the 2D and also higher dimensional system, as modeled within the Hubbard model with $U \gg t$ or the t-J model with $J < t$, where mobile photo-excited or doped charges crucially perturb and frustrate the spin background. On the other and, the physics in 1D correlated system can be quite different due to the phenomenon of the charge-spin separation. It is established that e.g. within the 1D t-J model the charge-spin coupling is quite ineffective and the motion of holons/doublons nearly free for $J \ll t$, since hopping of charges only shifts the spin background and cannot frustrate it on more than a single bond. Therefore other mechanisms have to be invoked to deal with the photoexcited 1D Mott insulators, both for the exciton formation as well as for the holon-doublon recombination.

Effective models: The aim of our theoretical consideration of the problem was to establish the mechanisms based on a minimal sufficient model. As mentioned in the previous paragraph it depends on the dimensionality of the system.

2D systems could be in principle described by the prototypical Hubbard model, but we rather canonically transformed it, leading to a generalized t-J model, consisting of a kinetic term for holons and doublons, a Heisenberg-like interacting between spin and a recombination/creation term as a perturbation. A clear advantage of such model is that by separating sectors with different number of holon-doublon pairs in the lowest order, as suggested by experimentally measured timescales of recombination, a) it assists to extract the excitonic state of a bound holon-doublon pair from the otherwise complex spectra of the Hubbard model, b) takes into account that this state is not an eigenstate (and should therefore decay) in a transparent way - via the creation/recombination term, which serves as a perturbation causing the decay. Since undoped cuprates, being of primary interest of the whole discussion, are actually Mott insulators of the charge-transfer type we derived a similar minimal model also from a more realistic multi-band tight binding model including relevant Cu and O orbitals. Contrary to the previous studies of doped cuprates, hole- and electron-like excitations in this case have to be addressed on equal footing. As observed in older studies the hole-electron (holon-doublon) symmetry is broken in such model, seen e.g. in different strength of effective hopping parameters for holon and doublon, but also in distinguishable recombination channels (with

respect to the final spin configuration). However, the effective model describing recombination, even when derived from a multi-band charge-transfer model, has a similar form with quantitatively comparable strength of operators causing the decay of holon-doublon pairs as its single-band analogue. Only the internal structure of recombination/creation operators is somewhat richer - allowing new intermediate states. From this we conclude that minimal model derived from the single-band Hubbard is sufficiently good, with a conceptual modification of the Mott-Hubbard gap being interpreted as the charge-transfer gap. As shown a posteriori the main physics of the recombination is actually captured already with a toy exciton-boson model, where the boson role is played by spin excitations. For it the recombination rate can be calculated analytically, revealing the dependence on the Mott-Hubbard gap, the boson energy and the strength of the coupling between them.

In 1D systems we coupled the charge to phonon degrees of freedom through a general local electron density potential, which takes into account that holon and doublon have an opposite effect on the displacement of units, and where phonons are in general not necessarily of the Holstein type. Due to the charge-spin decoupling and since for materials considered the phonon modes are very energetic, $J \ll \omega_0$, we assumed that spin degrees of freedom are less important, setting $J \to 0$, and first treating the problem in the spin sector with nearly maximal magnetization, i.e. with one overturned spin. To establish the holon-doublon exciton in 1D system, the nearest neighbor Coulomb repulsion that yields an effective attraction between holon and doublon has to be added to the Hamiltonian. First neglecting the coupling to phonons, exciton can be easily found in the spectra (for the nearly spin-polarized system even analytically). Since we anyway took $J \to 0$ and because the on-site number of phonons is unlimited, we do not make any transformation of the initial Hamiltonian in order to make the recombination term a two-step process, as was the case in 2D. Even though the recombination/creation operator does not have a form of perturbation (with a weak coupling strength), usage of Fermi golden rule can be eventually justified by the smallness of matrix element for the transition from holon-doublon exciton into phonons. After adding the coupling to phonons, we did make a standard Lang-Firsov transformation of the Hamiltonian in order to transform out the explicit coupling between charge and phonons, which effectively dresses the kinetic and recombination term of the Hamiltonian, but also the exciton wave function as must be the case also in experiments after a short-time relaxation of charges. Still, such dressing is more convenient for an analytical approach and also insures the non-zero matrix element for the transition from the exciton with odd parity to the even ground state, which would not be allowed without coupling to phonons. Sensible argumentation showed that the recombination in non-polarized case does not differ much from the nearly polarized one.

Existence of exciton: Our calculation of the recombination rate relies on the assumption that after being created, on a timescale shorter than the recombination one, holon and doublon form a bound state, which is in 2D systems of even (s-type) and in 1D of odd symmetry. Optically non-active even excitons and their energy difference to the active odd ones can be experimentally established via nonlinear optical, typically third-oder susceptibility [19, 36]. Besides that, an indirect evidence for the formation of such excitons in the pump-probe experiments is the fluence (pump intensity) independent recombination rate with an exponential decay of the charge density. If pairs were not bound, recombination process would depend on

the probability to encounter the oppositely charged particle, evidently leading to a non-exponential decay.

In 2D systems the holon-doublon pair binds in order to minimize the distortion of the ordered spin background in its vicinity, therefore the exciton should cease to exist in experimental conditions when the order is melted, e.g. when pumping the insulator with high fluence or well above the gap.

Validity of Fermi golden rule: To establish the recombination rate from the Fermi golden rule is an approximation, however it is technically useful and conceptually reasonable since the recombination of charged particles is a slow process as compared to the scale $\hbar/t$ of the time-dependent simulations. For the recombination in 2D system we tested how important are the higher order terms that were neglected by performing the time-dependent evolution of the initial excitonic state under Hamiltonian containing the recombination/creation term as well. We observed again an exponential decay of the holon-doublon pair occupation number. One should beware that such calculation has its limitations too: (a) the discreteness of the spectra sets upper bound for the propagation due to the recurrence of the holon-doublon pair, (b) virtual processes cause short time oscillations that destabilize the pair yet do not lead to true recombination, (c) the presence of perturbation alters the whole spectra, shifting the energies and leading to the reconsideration of the definition of the gap, (d) we restricted the Hilbert space to the subspace of one and zero holon-doublon pairs. Still, the recombination rates obtained with both methods are comparable, and in the larger system with $N = 26$ sites, where finite system artifacts are less pronounced, show slightly faster recombination in time-dependent calculation, as one would expect from the inclusion of additional processes.

The origin of the fast recombination: It is experimentally clear that the recombination in correlated systems happens much faster that in semiconductors, where timescales are within ms. Therefore it should be understood, where the difference comes from.

According to our comprehension, the main reason for a fast recombination in 2D cuprates primarily lies in the strong coupling between charged particles (holons and doublons) and the spin background, in addition to obviously larger scale of spin excitations J then the typical phonon energies ω_0. In spite of strong correlations, photoexcited (as well as chemically doped) holes and doublons are quite mobile in cuprates, with only modestly enhanced effective mass. For this reason they can perturb the ordering of spin background, as revealed in deviations of spin correlations in holon-doublon exciton relative to the AFM ground state. In the process of recombination this dressing with spin excitations can be even further enlarged due to possible additional spin flips caused by recombination/creation term of Hamiltonian. Of the course probability for dressing with $n \sim \Delta/J \gg 1$ spin flips is low, but this is precisely the reason that makes the process of recombination slow. Pure feasibility of creation of such large number of spin excitations itself has been shown experimentally by the phonon assisted multi-magnon light absorption [192, 193].

The story of the 1D recombination in organic salts resembles the scenario proposed for (non-correlated) carbon nanotubes [41, 171] in a greater deal. The distinct role of correlations is played in the holon-doublon exciton formation process, while fast recombination seems to be a consequence of high phonon frequencies ω_0, typical for organic salts with a complex structure of unit cell, yielding energetic

intra-molecular vibrational modes that were taken into account in our scenario. Of course those local vibrations have to couple to lattice phonons in order to disperse the energy into the whole system in a non-reversible way. On the level of our calculation a combined effect has been used; we took ω_0 corresponding to intra-molecular vibrations, however, gave it some dispersion that might realistically actually come from the coupling to lattice vibrations. The inherent nature of strongly correlated systems might play a greater role in recombination scenario for 1D cuprates with smaller phonon frequencies, where so far only the Ca_2CO_3 chains have been extensively examined [38]. A scenario with phonon-assisted coupling between charge and spin remains to be built and tested for systems of the latter kind.

Short-range vs. long-range order in 2D systems: It should be pointed out that the existence of the AFM long-range order and standard magnon excitations is not a necessary precondition for our analysis. The relevant excitations that receive the energy of holon-doublon pair are general multiple spin excitations or paramagnons, present also in the paramagnetic phase. All those excitations should have is dispersive nature in order to distribute the local spin perturbation. On the other hand, short-range spin correlations are necessary to provide the dressing of the holon-doublon pair with spin excitations, and ensure the existence of the exciton. After all, our calculations are done in a small system, which is big enough to accommodate the dressing of the holon-doublon pair, however does not display long-range order in the strict sense. The role of the latter is consequently not present in the result for recombination rate Γ. Another study [87] of the decay of a unbound uncorrelated holon and doublon in completely spin disordered background revealed very slow recombination, proving the necessity of at least short-range correlated spin-background.

Higher photoexcited charge densities: Mechanisms for the recombination that we proposed should be relevant for systems with low density of photoexcited carriers that in such conditions presumably form holon-doublon excitons. In experiments using pump pulses with high fluence, creating high density of photoexcited charge carriers, other mechanism might become dominant, e.g. so called Auger processes where energy of holon-doublon pair is transmitted to other charged carriers created within the pump. When sufficient density of charges is provided, dominance of such processes originates in easier instantaneous energy transmission - simply raising kinetic energy of the remaining charge (as long as the Mott-Hubbard gap is smaller then the Hubbard band width). Clear experimental indication for such processes should be non-exponential decay of the particle density, as long as what is observed is not only deviation around the thermal density of charges. Moreover, related kinetic-assisted recombination mechanism, possibly consisting of several scattering processes (that finally lead to the exponential decay), are dominant in experiments on fermionic cold atoms [64, 65] and in DMFT studies [28, 66].

Generality of the result: As the very last remark we should stress again that regardless of the specific case, the recombination rate calculated in ours and other studies [64, 65, 66, 87] always proved to be (super-)exponentially suppressed with the number of excitations to whom the energy of the holon-doublon pair has been transmitted. As every theoretician I am attracted by universalities, and observing the latter one was a satisfying windfall of my thesis.

Chapter 7

List of publications

Z. Lenarčič and P. Prelovšek, "Dielectric Breakdown in Spin-Polarized Mott Insulator", Phys. Rev. Lett. **108**, 196401 (2012)

Z. Lenarčič and P. Prelovšek, "Ultrafast charge recombination in photoexcited Mott-Hubbard insulator", Phys. Rev. Lett. **111**, 016401 (2013)

Z. Lenarčič, D. Golež, J. Bonča and P. Prelovšek, "Optical response of highly excited particles in a strongly correlated system", Phys. Rev. B **89**, 125123 (2014)

J. Kogoj, Z. Lenarčič, D. Golež, M. Mierzejewski, P. Prelovšek and J. Bonča, "Multistage dynamics of the spin-lattice polaron formation", Phys. Rev. B **90**, 125104 (2014)

Z. Lenarčič and P. Prelovšek, "Charge recombination in undoped cuprates", Phys. Rev. B **90**, 235139 (2014)

Z. Lenarčič and T. Prosen, "Exact asymptotics of the current in boundary-driven dissipative quantum chains in large external fields", Phys. Rev. E **91**, 030103(R) (2015)

P. Prelovšek, J. Kokalj, Z. Lenarčič, and R. H. McKenzie, "Holon-Doublon Binding as the Mechanism for the Mott transition", arXiv:1505.01498 (2015)

Z. Lenarčič, M. Eckstein and P. Prelovšek, "Exciton Recombination in One - Dimensional Organic Mott insulators", to be submitted.

Bibliography

[1] J. H. de Boer and E. J. W. Verwey, "Semi-conductors with partially and with completely filled 3d-lattice bands", Proceedings of the Physical Society **49**, 59 (1937).

[2] N. F. Mott and R. Peierls, "Discussion of the paper by de Boer and Verwey", Proceedings of the Physical Society **49**, 72 (1937).

[3] N. F. Mott, "The basis of the electron theory of metals, with special reference to the transition metals", Proceedings of the Physical Society. Section A **62**, 416 (1949).

[4] J. Hubbard, "Electron correlations in narrow energy bands", Proceedings of the Royal Society of London. Series A. Mathematical and Physical Sciences **276**, 238 (1963).

[5] F. C. Zhang and T. M. Rice, "Effective Hamiltonian for the superconducting Cu oxides", Phys. Rev. B **37**, 3759 (1988).

[6] K. A. Chao, J. Spałek and A. M. Oleś, "Kinetic exchange interaction in a narrow S-band", J. Phys. C **10**, L271 (1977).

[7] E. H. Lieb and F. Y. Wu, "Absence of Mott Transition in an Exact Solution of the Short-Range, One-Band Model in One Dimension", Phys. Rev. Lett. **20**, 1445 (1968).

[8] I. Bloch, J. Dalibard and W. Zwerger, "Many-body physics with ultracold gases", Rev. Mod. Phys. **80**, 885 (2008).

[9] T. Langen, R. Geiger and J. Schmiedmayer, "Ultracold Atoms Out of Equilibrium", Annual Review of Condensed Matter Physics **6**, 201 (2015).

[10] L. Perfetti, P. A. Loukakos, M. Lisowski, U. Bovensiepen, H. Eisaki and M. Wolf, "Ultrafast Electron Relaxation in Superconducting $Bi_2Sr_2CaCu_2O_{8+\delta}$ by Time-Resolved Photoelectron Spectroscopy", Phys. Rev. Lett. **99**, 197001 (2007).

[11] R. Cortes, L. Rettig, Y. Yoshida, H. Eisaki, M. Wolf and U. Bovensiepen, "Momentum-Resolved Ultrafast Electron Dynamics in Superconducting $Bi_2Sr_2CaCu_2O_{8+\delta}$", Phys. Rev. Lett. **107**, 097002 (2011).

[12] K. Matsuda, I. Hirabayashi, K. Kawamoto, T. Nabatame, T. Tokizaki and A. Nakamura, "Femtosecond spectroscopic studies of the ultrafast relaxation process in the charge-transfer state of insulating cuprates", Phys. Rev. B **50**, 4097 (1994).

[13] H. Okamoto, T. Miyagoe, K. Kobayashi, H. Uemura, H. Nishioka, H. Matsuzaki, A. Sawa and Y. Tokura, "Ultrafast charge dynamics in photoexcited Nd2CuO4 and La2CuO4 cuprate compounds investigated by femtosecond absorption spectroscopy", Phys. Rev. B **82**, 060513 (2010).

[14] H. Okamoto, T. Miyagoe, K. Kobayashi, H. Uemura, H. Nishioka, H. Matsuzaki, A. Sawa and Y. Tokura, "Photoinduced transition from Mott insulator to metal in the undoped cuprates Nd2CuO4 and La2CuO4", Phys. Rev. B **83**, 125102 (2011).

[15] C. Giannetti, F. Cilento, S. Dal Conte, G. Coslovich, G. Ferrini, H. Molegraaf, M. Raichle, R. Liang, H. Eisaki, M. Greven *et al.*, "Revealing the high-energy electronic excitations underlying the onset of high-temperature superconductivity in cuprates", Nature communications **2**, 353 (2011).

[16] D. Fausti, R. Tobey, N. Dean, S. Kaiser, A. Dienst, M. Hoffmann, S. Pyon, T. Takayama, H. Takagi and A. Cavalleri, "Light-induced superconductivity in a stripe-ordered cuprate", science **331**, 189 (2011).

[17] L. Stojchevska, P. Kusar, T. Mertelj, V. V. Kabanov, Y. Toda, X. Yao and D. Mihailovic, "Mechanisms of nonthermal destruction of the superconducting state and melting of the charge-density-wave state by femtosecond laser pulses", Phys. Rev. B **84**, 180507 (2011).

[18] T. Ogasawara, M. Ashida, N. Motoyama, H. Eisaki, S. Uchida, Y. Tokura, H. Ghosh, A. Shukla, S. Mazumdar and M. Kuwata-Gonokami, "Ultrafast Optical Nonlinearity in the Quasi-One-Dimensional Mott Insulator Sr_2CuO_3", Phys. Rev. Lett. **85**, 2204 (2000).

[19] M. Ono, K. Miura, A. Maeda, H. Matsuzaki, H. Kishida, Y. Taguchi, Y. Tokura, M. Yamashita and H. Okamoto, "Linear and nonlinear optical properties of one-dimensional Mott insulators consisting of Ni-halogen chain and CuO-chain compounds", Phys. Rev. B **70**, 085101 (2004).

[20] H. Uemura, H. Matsuzaki, Y. Takahashi, T. Hasegawa and H. Okamoto, "Ultrafast Charge Dynamics in One-Dimensional Organic Mott Insulators", Journal of the Physical Society of Japan **77**, 113714 (2008).

[21] M. Mitrano, G. Cotugno, S. Clark, R. Singla, S. Kaiser, J. Stähler, R. Beyer, M. Dressel, L. Baldassarre, D. Nicoletti, A. Perucchi, T. Hasegawa, H. Okamoto, D. Jaksch and A. Cavalleri, "Pressure-Dependent Relaxation in the Photoexcited Mott Insulator ET˘F_2TCNQ: Influence of Hopping and Correlations on Quasiparticle Recombination Rates", Phys. Rev. Lett. **112**, 117801 (2014).

[22] I. Vaskivskyi, I. Mihailovic, S. Brazovskii, J. Gospodaric, T. Mertelj, D. Svetin, P. Sutar and D. Mihailovic, "Fast non-thermal switching between macroscopic charge-ordered quantum states induced by charge injection", arXiv:1409.3794 (2014).

[23] S. Iwai, M. Ono, A. Maeda, H. Matsuzaki, H. Kishida, H. Okamoto and Y. Tokura, "Ultrafast Optical Switching to a Metallic State by Photoinduced Mott Transition in a Halogen-Bridged Nickel-Chain Compound", Phys. Rev. Lett. **91**, 057401 (2003).

[24] T. Miyagoe, S. Tao, A. Maeda, H. Matsuzaki, H. Ohtsu, M. Hasegawa, S. Takaishi, M. Yamashita and H. Okamoto, "Ultrafast Optical Responses in a One-Dimensional Mott Insulator of a Br-Bridged Ni Compound", Journal of the Physical Society of Japan **77**, 023711 (2008).

[25] S. Wall, D. Brida, , S. R. Clark, H. P. Ehrke, D. Jaksch, A. Ardavan, S. Bonora, H. Uemura, Y. Takahashi, T. Hasegawa, H. Okamoto, G. Cerullo and A. Cavalleri, "Quantum interference between charge excitation paths in a solid-state Mott insulator", Nat. Phys. **7**, 114 (2011).

[26] S. Kaiser, S. R. Clark, D. Nicoletti, G. Cotugno, R. I. Tobey, N. Dean, S. Lupi, H. Okamoto, T. Hasegawa, D. Jaksch and A. Cavalleri, "Optical Properties of a Vibrationally Modulated Solid State Mott Insulator", Sci. Rep. **4**, 3823 (2014).

[27] T. Oka, "Nonlinear doublon production in a Mott insulator: Landau-Dykhne method applied to an integrable model", Phys. Rev. B **86**, 075148 (2012).

[28] M. Eckstein and P. Werner, "Photoinduced States in a Mott Insulator", Phys. Rev. Lett. **110**, 126401 (2013).

[29] W. Shen, T. P. Devereaux and J. K. Freericks, "Beyond Planck-Einstein quanta: Amplitude-driven quantum excitation", Phys. Rev. B **90**, 195104 (2014).

[30] R. Peierls, Z. Phys. **80**, 763 (1933).

[31] D. Golež, J. Bonča, M. Mierzejewski and L. Vidmar, "Mechanism of ultrafast relaxation of a photo-carrier in antiferromagnetic spin background", Phys. Rev. B **89**, 165118 (2014).

[32] S. Dal Conte, L. Vidmar, D. Golez, M. Mierzejewski, G. Soavi, S. Peli, F. Banfi, G. Ferrini, R. Comin, B. M. Ludbrook, L. Chauviere, N. D. Zhigadlo, H. Eisaki, M. Greven, S. Lupi, A. Damascelli, D. Brida, M. Capone, J. Bonca, G. Cerullo and C. Giannetti, "Snapshots of the retarded interaction of charge carriers with ultrafast fluctuations in cuprates", .

[33] T. Tohyama, "Symmetry of Photoexcited States and Large-Shift Raman Scattering in Two-Dimensional Mott Insulators", J. Phys. Soc. Jpn **75**, 034713 (2006).

[34] Z. Lenarčič and P. Prelovšek, "Ultrafast Charge Recombination in a Photoexcited Mott-Hubbard Insulator", Phys. Rev. Lett. **111**, 016401 (2013).

[35] Z. Lenarčič and P. Prelovšek, "Charge recombination in undoped cuprates", Phys. Rev. B **90**, 235136 (2014).

[36] A. Maeda, M. Ono, H. Kishida, T. Manako, A. Sawa, M. Kawasaki, Y. Tokura and H. Okamoto, "Third-order nonlinear susceptibility spectra of CuO chain compounds investigated by the Z-scan method", Phys. Rev. B **70**, 125117 (2004).

[37] F. H. L. Essler, F. Gebhard and E. Jeckelmann, "Excitons in one-dimensional Mott insulators", Phys. Rev. B **64**, 125119 (2001).

[38] H. Matsuzaki, H. Nishioka, H. Uemura, A. Sawa, S. Sota, T. Tohyama and H. Okamoto, "Ultrafast charge and lattice dynamics in one-dimensional Mott insulator of CuO-chain compound Ca_2CuO_3 investigated by femtosecond absorption spectroscopy", Phys. Rev. B **91**, 081114 (2015).

[39] M. Beyer, "Photo-doping phenomena in the high-temperature superconductor $La_{2-x}Sr_xCuO_4$", dissertation at Universität Konstanz (2011).

[40] Z. Lenarčič, M. Eckstein and P. Prelovšek, "Exciton Recombination in One - Dimensional Organic Mott Insulators", to be submitted.

[41] V. Perebeinos and P. Avouris, "Phonon and Electronic Nonradiative Decay Mechanisms of Excitons in Carbon Nanotubes", Phys. Rev. Lett. **101**, 057401 (2008).

[42] G. N. Ostojic, S. Zaric, J. Kono, M. S. Strano, V. C. Moore, R. H. Hauge and R. E. Smalley, "Interband Recombination Dynamics in Resonantly Excited Single-Walled Carbon Nanotubes", Phys. Rev. Lett. **92**, 117402 (2004).

[43] F. Wang, G. Dukovic, L. E. Brus and T. F. Heinz, "Time-Resolved Fluorescence of Carbon Nanotubes and Its Implication for Radiative Lifetimes", Phys. Rev. Lett. **92**, 177401 (2004).

[44] L. Huang, H. N. Pedrosa and T. D. Krauss, "Ultrafast Ground-State Recovery of Single-Walled Carbon Nanotubes", Phys. Rev. Lett. **93**, 017403 (2004).

[45] Y. Taguchi, T. Matsumoto and Y. Tokura, "Dielectric breakdown of one-dimensional Mott insulators Sr_2CuO_3 and $SrCuO_2$", Phys. Rev. B **62**, 7015 (2000).

[46] T.-L. Wu, L. Whittaker, S. Banerjee and G. Sambandamurthy, "Temperature and voltage driven tunable metal-insulator transition in individual $W_xV_{1-x}O_2$ nanowires", Phys. Rev. B **83**, 073101 (2011).

[47] V. Guiot, L. Cario, E. Janod, B. Corraze, V. T. Phuoc, M. Rozenberg, P. Stoliar, T. Cren and D. Roditchev, "Avalanche breakdown in GaTa4Se8- xTex narrow-gap Mott insulators", Nature communications **4**, 1722 (2013).

[48] C. Vaju, L. Cario, B. Corraze, E. Janod, V. Dubost, T. Cren, D. Roditchev, D. Braithwaite and O. Chauvet, "Electric-Pulse-driven Electronic Phase Separation, Insulator–Metal Transition, and Possible Superconductivity in a Mott Insulator", Advanced Materials **20**, 2760 (2008).

[49] V. Dubost, T. Cren, C. Vaju, L. Cario, B. Corraze, E. Janod, F. Debontridder and D. Roditchev, "Electric-Field-Assisted Nanostructuring of a Mott Insulator", Advanced Functional Materials **19**, 2800 (2009).

[50] L. Cario, C. Vaju, B. Corraze, V. Guiot and E. Janod, "Electric-Field-Induced Resistive Switching in a Family of Mott Insulators: Towards a New Class of RRAM Memories", Advanced Materials **22**, 5193 (2010).

[51] E. Souchier, L. Cario, B. Corraze, P. Moreau, P. Mazoyer, C. Estournès, R. Retoux, E. Janod and M.-P. Besland, "First evidence of resistive switching in polycrystalline GaV4S8 thin layers", physica status solidi (RRL)-Rapid Research Letters **5**, 53 (2011).

[52] J. L. Hudgins, G. S. Simin, E. Santi and M. A. Khan, "An assessment of wide bandgap semiconductors for power devices", Power Electronics, IEEE Transactions on **18**, 907 (2003).

[53] F. Sawano, I. Terasaki, H. Mori, T. Mori, M. Watanabe, N. Ikeda, Y. Nogami and Y. Noda, "An organic thyristor", Nature **437**, 522 (2005).

[54] B. Mayer, C. Schmidt, A. Grupp, J. Bühler, J. Oelmann, R. Marvel, R. Haglund Jr, T. Oka, D. Brida, A. Leitenstorfer *et al.*, "Tunneling Breakdown of a Strongly Correlated Insulating State in VO _2 Induced by Intense Multi-Terahertz Excitation", arXiv:1505.01273 (2015).

[55] C. Chin, R. Grimm, P. Julienne and E. Tiesinga, "Feshbach resonances in ultracold gases", Rev. Mod. Phys. **82**, 1225 (2010).

[56] M. Greiner, O. Mandel, T. W. Hänsch and I. Bloch, "Collapse and revival of the matter wave field of a Bose–Einstein condensate", Nature **419**, 51 (2002).

[57] E. Haller, R. Hart, M. J. Mark, J. G. Danzl, L. Reichsöllner and H.-C. Nägerl, "Inducing Transport in a Dissipation-Free Lattice with Super Bloch Oscillations", Phys. Rev. Lett. **104**, 200403 (2010).

[58] T. Schumm, S. Hofferberth, L. M. Andersson, S. Wildermuth, S. Groth, I. Bar-Joseph, J. Schmiedmayer and P. Krüger, "Matter-wave interferometry in a double well on an atom chip", Nature Physics **1**, 57 (2005).

[59] A. Widera, S. Trotzky, P. Cheinet, S. Fölling, F. Gerbier, I. Bloch, V. Gritsev, M. D. Lukin and E. Demler, "Quantum Spin Dynamics of Mode-Squeezed Luttinger Liquids in Two-Component Atomic Gases", Phys. Rev. Lett. **100**, 140401 (2008).

[60] A. de Paz, A. Sharma, A. Chotia, E. Maréchal, J. H. Huckans, P. Pedri, L. Santos, O. Gorceix, L. Vernac and B. Laburthe-Tolra, "Nonequilibrium Quantum Magnetism in a Dipolar Lattice Gas", Phys. Rev. Lett. **111**, 185305 (2013).

[61] R. Jördens, N. Strohmaier, K. Günter, H. Moritz and T. Esslinger, "A Mott insulator of fermionic atoms in an optical lattice", Nature **455**, 204 (2008).

[62] J. P. Ronzheimer, M. Schreiber, S. Braun, S. S. Hodgman, S. Langer, I. P. McCulloch, F. Heidrich-Meisner, I. Bloch and U. Schneider, "Expansion Dynamics of Interacting Bosons in Homogeneous Lattices in One and Two Dimensions", Phys. Rev. Lett. **110**, 205301 (2013).

[63] T. Langen, S. Erne, R. Geiger, B. Rauer, T. Schweigler, M. Kuhnert, W. Rohringer, I. E. Mazets, T. Gasenzer and J. Schmiedmayer, "Experimental Observation of a Generalized Gibbs Ensemble", arXiv:1411.7185 (2014).

[64] R. Sensarma, D. Pekker, E. Altman, E. Demler, N. Strohmaier, D. Greif, R. Jördens, L. Tarruell, H. Moritz and T. Esslinger, "Lifetime of double occupancies in the Fermi-Hubbard model", Phys. Rev. B **82**, 224302 (2010).

[65] N. Strohmaier, D. Greif, R. Jördens, L. Tarruell, H. Moritz, T. Esslinger, R. Sensarma, D. Pekker, E. Altman and E. Demler, "Observation of Elastic Doublon Decay in the Fermi-Hubbard Model", Phys. Rev. Lett. **104**, 080401 (2010).

[66] M. Eckstein and P. Werner, "Thermalization of a pump-excited Mott insulator", Phys. Rev. B **84**, 035122 (2011).

[67] A. L. Chudnovskiy, D. M. Gangardt and A. Kamenev, "Doublon Relaxation in the Bose-Hubbard Model", Phys. Rev. Lett. **108**, 085302 (2012).

[68] T. Langen, M. Gring, M. Kuhnert, B. Rauer, R. Geiger, D. A. Smith, I. E. Mazets and J. Schmiedmayer, "Prethermalization in one-dimensional Bose gases: Description by a stochastic Ornstein-Uhlenbeck process", The European Physical Journal Special Topics **217**, 43 (2013).

[69] T. Langen, R. Geiger, M. Kuhnert, B. Rauer and J. Schmiedmayer, "Local emergence of thermal correlations in an isolated quantum many-body system", Nature Physics **9**, 640 (2013).

[70] R. Geiger, T. Langen, I. Mazets and J. Schmiedmayer, "Local relaxation and light-cone-like propagation of correlations in a trapped one-dimensional Bose gas", New Journal of Physics **16**, 053034 (2014).

[71] J. Kogoj, Z. Lenarčič, D. Golež, M. Mierzejewski, P. Prelovšek and J. Bonča, "Multistage dynamics of the spin-lattice polaron formation", Phys. Rev. B **90**, 125104 (2014).

[72] H. Aoki, N. Tsuji, M. Eckstein, M. Kollar, T. Oka and P. Werner, "Nonequilibrium dynamical mean-field theory and its applications", Rev. Mod. Phys. **86**, 779 (2014).

[73] U. Schollwöck, "The density-matrix renormalization group in the age of matrix product states", Annals of Physics **326**, 96 (2011).

[74] A. Avella and F. Mancini, *Strongly Correlated Systems - Numerical Methods* (Springer, Berlin, 2013) pp. 1–29.

[75] T. Oka, R. Arita and H. Aoki, "Breakdown of a Mott Insulator: A Nonadiabatic Tunneling Mechanism", Phys. Rev. Lett. **91**, 066406 (2003).

[76] T. Oka, N. Konno, R. Arita and H. Aoki, "Breakdown of an Electric-Field Driven System: A Mapping to a Quantum Walk", Phys. Rev. Lett. **94**, 100602 (2005).

[77] T. Oka and H. Aoki, "Ground-State Decay Rate for the Zener Breakdown in Band and Mott Insulators", Phys. Rev. Lett. **95**, 137601 (2005).

[78] T. Oka and H. Aoki, "Dielectric breakdown in a Mott insulator: Many-body Schwinger-Landau-Zener mechanism studied with a generalized Bethe ansatz", Phys. Rev. B **81**, 033103 (2010).

[79] Z. Lenarčič and P. Prelovšek, "Dielectric Breakdown in Spin-Polarized Mott Insulator", Phys. Rev. Lett. **108**, 196401 (2012).

[80] C. Zener, "Non-adiabatic crossing of energy levels", *Proceedings of the Royal Society of London A: Mathematical, Physical and Engineering Sciences*, **137**, 696 (1932).

[81] L. D. Landau, "Collected papers of LD Landau", (1965).

[82] M. Eckstein, T. Oka and P. Werner, "Dielectric Breakdown of Mott Insulators in Dynamical Mean-Field Theory", Phys. Rev. Lett. **105**, 146404 (2010).

[83] F. Heidrich-Meisner, I. González, K. A. Al-Hassanieh, A. E. Feiguin, M. J. Rozenberg and E. Dagotto, "Nonequilibrium electronic transport in a one-dimensional Mott insulator", Phys. Rev. B **82**, 205110 (2010).

[84] G. Mazza, A. Amaricci, M. Capone and M. Fabrizio, "Electronic transport and dynamics in correlated heterostructures", arXiv:1412.6415 (2014).

[85] T. Oka and H. Aoki, "Nonequilibrium quantum breakdown in a strongly correlated electron system", in *Quantum and Semi-classical Percolation and Breakdown in Disordered Solids* (Springer, 2009) pp. 1–35.

[86] C. Aron, "Dielectric breakdown of a Mott insulator", Phys. Rev. B **86**, 085127 (2012).

[87] R. Sensarma, D. Pekker, A. M. Rey, M. D. Lukin and E. Demler, "Relaxation of Fermionic Excitations in a Strongly Attractive Fermi Gas in an Optical Lattice", Phys. Rev. Lett. **107**, 145303 (2011).

[88] A. Polkovnikov, K. Sengupta, A. Silva and M. Vengalattore, "Nonequilibrium dynamics of closed interacting quantum systems", Rev. Mod. Phys. **83**, 863 (2011).

[89] J. Lux, J. Müller, A. Mitra and A. Rosch, "Hydrodynamic long-time tails after a quantum quench", Phys. Rev. A **89**, 053608 (2014).

[90] M. Srednicki, "Chaos and quantum thermalization", Phys. Rev. E **50**, 888 (1994).

[91] M. Rigol, V. Dunjko and M. Olshanii, "Thermalization and its mechanism for generic isolated quantum systems", Nature **452**, 854 (2008).

[92] M. Mierzejewski, P. Prelovšek and T. c. v. Prosen, "Identifying Local and Quasilocal Conserved Quantities in Integrable Systems", Phys. Rev. Lett. **114**, 140601 (2015).

[93] M. Rigol, V. Dunjko, V. Yurovsky and M. Olshanii, "Relaxation in a Completely Integrable Many-Body Quantum System: An *Ab Initio* Study of the Dynamics of the Highly Excited States of 1D Lattice Hard-Core Bosons", Phys. Rev. Lett. **98**, 050405 (2007).

[94] P. Calabrese and J. Cardy, "Time Dependence of Correlation Functions Following a Quantum Quench", Phys. Rev. Lett. **96**, 136801 (2006).

[95] B. Wouters, J. De Nardis, M. Brockmann, D. Fioretto, M. Rigol and J.-S. Caux, "Quenching the Anisotropic Heisenberg Chain: Exact Solution and Generalized Gibbs Ensemble Predictions", Phys. Rev. Lett. **113**, 117202 (2014).

[96] M. Mierzejewski, P. Prelovšek and T. c. v. Prosen, "Breakdown of the Generalized Gibbs Ensemble for Current-Generating Quenches", Phys. Rev. Lett. **113**, 020602 (2014).

[97] M. Mierzejewski and P. Prelovšek, "Nonlinear Current Response of an Isolated System of Interacting Fermions", Phys. Rev. Lett. **105**, 186405 (2010).

[98] F. H. L. Essler, S. Kehrein, S. R. Manmana and N. J. Robinson, "Quench dynamics in a model with tuneable integrability breaking", Phys. Rev. B **89**, 165104 (2014).

[99] V. Oganesyan and D. A. Huse, "Localization of interacting fermions at high temperature", Phys. Rev. B **75**, 155111 (2007).

[100] J. Z. Imbrie, "On many-body localization for quantum spin chains", arXiv:1403.7837 (2014).

[101] R. Vosk and E. Altman, "Many-Body Localization in One Dimension as a Dynamical Renormalization Group Fixed Point", Phys. Rev. Lett. **110**, 067204 (2013).

[102] E. Altman and R. Vosk, "Universal Dynamics and Renormalization in Many-Body-Localized Systems", Annual Review of Condensed Matter Physics **6**, 383 (2015), http://dx.doi.org/10.1146/annurev-conmatphys-031214-014701 .

[103] J. Berges, S. Borsányi and C. Wetterich, "Prethermalization", Phys. Rev. Lett. **93**, 142002 (2004).

[104] M. Gring, M. Kuhnert, T. Langen, T. Kitagawa, B. Rauer, M. Schreitl, I. Mazets, D. A. Smith, E. Demler and J. Schmiedmayer, "Relaxation and prethermalization in an isolated quantum system", Science **337**, 1318 (2012).

[105] M. Marcuzzi, J. Marino, A. Gambassi and A. Silva, "Prethermalization in a Nonintegrable Quantum Spin Chain after a Quench", Phys. Rev. Lett. **111**, 197203 (2013).

[106] T. Grover and M. P. Fisher, "Quantum disentangled liquids", Journal of Statistical Mechanics: Theory and Experiment **2014**, P10010 (2014).

[107] K. Agarwal, S. Gopalakrishnan, M. Knap, M. Müller and E. Demler, "Anomalous diffusion and Griffiths effects near the many-body localization transition", arXiv:1408.3413 (2014).

[108] M. Moeckel and S. Kehrein, "Interaction Quench in the Hubbard Model", Phys. Rev. Lett. **100**, 175702 (2008).

[109] M. Eckstein, M. Kollar and P. Werner, "Thermalization after an Interaction Quench in the Hubbard Model", Phys. Rev. Lett. **103**, 056403 (2009).

[110] N. Tsuji, M. Eckstein and P. Werner, "Nonthermal Antiferromagnetic Order and Nonequilibrium Criticality in the Hubbard Model", Phys. Rev. Lett. **110**, 136404 (2013).

[111] P. Smacchia, M. Knap, E. Demler and A. Silva, "Exploring dynamical phase transitions and prethermalization with quantum noise of excitations", arXiv:1409.1883 (2014).

[112] J. Berges, A. Rothkopf and J. Schmidt, "Nonthermal Fixed Points: Effective Weak Coupling for Strongly Correlated Systems Far from Equilibrium", Phys. Rev. Lett. **101**, 041603 (2008).

[113] D. Bernard and B. Doyon, "Energy flow in non-equilibrium conformal field theory", Journal of Physics A: Mathematical and Theoretical **45**, 362001 (2012).

[114] V. Jakšić and C.-A. Pillet, "Non-Equilibrium Steady States of Finite¶Quantum Systems Coupled to Thermal Reservoirs", Communications in Mathematical Physics **226**, 131 (2002).

[115] H. Wichterich, M. J. Henrich, H.-P. Breuer, J. Gemmer and M. Michel, "Modeling heat transport through completely positive maps", Phys. Rev. E **76**, 031115 (2007).

[116] F. Petruccione and H.-P. Breuer, *The theory of open quantum systems* (Oxford Univ. Press, 2002).

[117] T. Prosen, New J. Phys. **10**, 040326 (2008).

[118] T. Prosen, "Nonequilibrium Steady State and a Strict Bound on Ballistic Transport", Phys. Rev. Lett. **106**, 217206 (2011).

[119] E. Ilievski and T. Prosen, "Exact steady state manifold of a boundary driven spin-1 Lai–Sutherland chain", Nuclear Physics B **882**, 485 (2014).

[120] T. Prosen, "Exact Nonequilibrium Steady State of an Open Hubbard Chain", Phys. Rev. Lett. **112**, 030603 (2014).

[121] L. Faddeev, "Algebraic aspects of the Bethe ansatz", International Journal of Modern Physics A **10**, 1845 (1995).

[122] L. Faddeev, "How Algebraic Bethe Ansatz works for integrable model", arXiv:9605187 (1996).

[123] T. Prosen, "Matrix product solutions of boundary driven quantum chains", arXiv:1504.00783 (2015).

[124] Z. Lenarčič and T. Prosen, "Exact asymptotics of the current in boundary-driven dissipative quantum chains in large external fields", Phys. Rev. E **91**, 030103 (2015).

[125] M. Schreiber, S. S. Hodgman, P. Bordia, H. P. Lüschen, M. H. Fischer, R. Vosk, E. Altman, U. Schneider and I. Bloch, "Observation of many-body localization of interacting fermions in a quasi-random optical lattice", arXiv:1501.05661 (2015).

[126] A. Öttl, S. Ritter, M. Köhl and T. Esslinger, "Correlations and Counting Statistics of an Atom Laser", Phys. Rev. Lett. **95**, 090404 (2005).

[127] M. Mierzejewski, L. Vidmar, J. Bonča and P. Prelovšek, "Nonequilibrium Quantum Dynamics of a Charge Carrier Doped into a Mott Insulator", Phys. Rev. Lett. **106**, 196401 (2011).

[128] L. Vidmar, J. Bonča, T. Tohyama and S. Maekawa, "Quantum Dynamics of a Driven Correlated System Coupled to Phonons", Phys. Rev. Lett. **107**, 246404 (2011).

[129] L. Vidmar, J. Bonča, M. Mierzejewski, P. Prelovšek and S. A. Trugman, "Nonequilibrium dynamics of the Holstein polaron driven by an external electric field", Phys. Rev. B **83**, 134301 (2011).

[130] D. Golež, J. Bonča and L. Vidmar, "Dissociation of a Hubbard-Holstein bipolaron driven away from equilibrium by a constant electric field", Phys. Rev. B **85**, 144304 (2012).

[131] A. Amaricci, C. Weber, M. Capone and G. Kotliar, "Approach to a stationary state in a driven Hubbard model coupled to a thermostat", Phys. Rev. B **86**, 085110 (2012).

[132] M. Eckstein and P. Werner, "Nonequilibrium dynamical mean-field simulation of inhomogeneous systems", Phys. Rev. B **88**, 075135 (2013).

[133] A. Avella and F. Mancini, *Strongly Correlated Systems* (Springer, 2012).

[134] A. Ovchinnikov, "Quantum Dynamics of a Driven Correlated System Coupled to Phonons", Zh. Eksp. Teor. Fiz **57**, 2137 (1969).

[135] P. Prelovšek, J. Kokalj, Z. Lenarčič and R. H. McKenzie, "Holon-Doublon Binding as the Mechanism for the Mott transition", arXiv:1505.01498 (2015).

[136] G. Lindblad, "On the generators of quantum dynamical semigroups", Communications in Mathematical Physics **48**, 119 (1976).

[137] V. Gorini, A. Kossakowski and E. C. G. Sudarshan, "Completely positive dynamical semigroups of N-level systems", Journal of Mathematical Physics **17**, 821 (1976).

[138] D. Karevski and T. Platini, "Quantum Nonequilibrium Steady States Induced by Repeated Interactions", Phys. Rev. Lett. **102**, 207207 (2009).

[139] G. Benenti, G. Casati, T. Prosen, D. Rossini and M. Žnidarič, "Charge and spin transport in strongly correlated one-dimensional quantum systems driven far from equilibrium", Phys. Rev. B **80**, 035110 (2009).

[140] G. T. Landi, E. Novais, M. J. de Oliveira and D. Karevski, "Flux rectification in the quantum XXZ chain", Phys. Rev. E **90**, 042142 (2014).

[141] G. D. Mahan, *Many-particle physics* (Springer Science & Business Media, 2000).

[142] A. Shimizu and T. Yuge, "Sum rules and asymptotic behaviors for optical conductivity of nonequilibrium many-electron systems", Journal of the Physical Society of Japan **80** (2011).

[143] M. Eckstein and M. Kollar, "Theory of time-resolved optical spectroscopy on correlated electron systems", Phys. Rev. B **78**, 205119 (2008).

[144] J. K. Freericks, H. R. Krishnamurthy and T. Pruschke, "Theoretical Description of Time-Resolved Photoemission Spectroscopy: Application to Pump-Probe Experiments", Phys. Rev. Lett. **102**, 136401 (2009).

[145] D. Rossini, R. Fazio, V. Giovannetti and A. Silva, "Quantum quenches, linear response and superfluidity out of equilibrium", EPL (Europhysics Letters) **107**, 30002 (2014).

[146] B. Moritz, A. F. Kemper, M. Sentef, T. P. Devereaux and J. K. Freericks, "Electron-Mediated Relaxation Following Ultrafast Pumping of Strongly Correlated Materials: Model Evidence of a Correlation-Tuned Crossover between Thermal and Nonthermal States", Phys. Rev. Lett. **111**, 077401 (2013).

[147] Z. Lenarčıč, D. Golež, J. Bonča and P. Prelovšek, "Optical response of highly excited particles in a strongly correlated system", Phys. Rev. B **89**, 125123 (2014).

[148] J. Jaklič and P. Prelovšek, "Finite-temperature properties of doped antiferromagnets", Advances in Physics **49**, 1 (2000).

[149] H. Castella, X. Zotos and P. Prelovšek, "Integrability and Ideal Conductance at Finite Temperatures", Phys. Rev. Lett. **74**, 972 (1995).

[150] S. Dal Conte, C. Giannetti, G. Coslovich, F. Cilento, D. Bossini, T. Abebaw, F. Banfi, G. Ferrini, H. Eisaki, M. Greven *et al.*, "Disentangling the electronic and phononic glue in a high-Tc superconductor", Science **335**, 1600 (2012).

[151] F. Novelli, G. De Filippis, V. Cataudella, M. Esposito, I. V. Kausel, F. Cilento, E. Sindici, A. Amaricci, C. Giannetti, D. Prabhakaran *et al.*, "Witnessing the formation and relaxation of massive quasi-particles in a strongly correlated electron system", Nat. Commun. **5** (2014).

[152] E. H. Lieb and D. W. Robinson, "The finite group velocity of quantum spin systems", Communications in Mathematical Physics **28**, 251 (1972).

[153] M. Eckstein and P. Werner, "Ultra-fast photo-carrier relaxation in Mott insulators with short-range spin correlations", arXiv:1410.3956 (2014).

[154] M. Eckstein and P. Werner, "Ultrafast Separation of Photodoped Carriers in Mott Antiferromagnets", Phys. Rev. Lett. **113**, 076405 (2014).

[155] K. Balzer, F. A. Wolf, I. P. McCulloch, P. Werner and M. Eckstein, "Nonthermal melting of Neel order in the Hubbard model", arXiv:1504.02461 (2015).

[156] A. Bauer, F. Dorfner and F. Heidrich-Meisner, "Temporal decay of Neel order in the one-dimensional Fermi-Hubbard model", arXiv:1503.02010 (2015).

[157] D. Golež, J. Bonča, L. Vidmar and S. A. Trugman, "Relaxation Dynamics of the Holstein Polaron", Phys. Rev. Lett. **109**, 236402 (2012).

[158] T. J. Park and J. C. Light, "Unitary quantum time evolution by iterative Lanczos reduction", J. Chem. Phys. **85**, 5870 (1986).

[159] J. Bonča, S. Maekawa and T. Tohyama, "Numerical approach to the low-doping regime of the t-J model", Phys. Rev. B **76**, 035121 (2007).

[160] D. Golež, J. Bonča, M. Mierzejewski and L. Vidmar, "Mechanism of ultrafast relaxation of a photo-carrier in antiferromagnetic spin background", Phys. Rev. B **89**, 165118 (2014).

[161] N. Tsuji, T. Oka and H. Aoki, "Nonequilibrium Steady State of Photoexcited Correlated Electrons in the Presence of Dissipation", Phys. Rev. Lett. **103**, 047403 (2009).

[162] E. Dagotto, "Correlated electrons in high-temperature superconductors", Rev. Mod. Phys. **66**, 763 (1994).

[163] L. Foini, L. F. Cugliandolo and A. Gambassi, "Dynamic correlations, fluctuation-dissipation relations, and effective temperatures after a quantum quench of the transverse field Ising chain", Journal of Statistical Mechanics: Theory and Experiment **2012**, P09011 (2012).

[164] C. Kittel and C. Y. Fong, *Quantum theory of solids*, Vol. 33 (Wiley New York, 1963).

[165] F. Schwabl, R. Hilton and A. Lahee, *Advanced quantum mechanics* (Springer Science & Business Media, 2005).

[166] P. Yu and M. Cardon, *Fundamentals of semiconductors: physics and materials properties* (Springer, Berlin, 1996).

[167] M. Ogata and H. Shiba, "Bethe-ansatz wave function, momentum distribution, and spin correlation in the one-dimensional strongly correlated Hubbard model", Phys. Rev. B **41**, 2326 (1990).

[168] H. Matsueda, S. Sota, T. Tohyama and S. Maekawa, "Relaxation Dynamics of Photocarriers in One-Dimensional Mott Insulators Coupled to Phonons", Journal of the Physical Society of Japan **81**, 013701 (2012).

[169] J. Lorenzana and R. Eder, "Dynamics of the one-dimensional Heisenberg model and optical absorption of spinons in cuprate antiferromagnetic chains", Phys. Rev. B **55**, R3358 (1997).

[170] M. Beyer, *Photo-Doping Phenomena in the High-Temperature Superconductor* $La_{2-x}Sr_xCu)_4$ (dissertation at Universität Konstanz, 2011).

[171] P. Avouris, J. Chen, M. Freitag, V. Perebeinos and J. C. Tsang, "Carbon nanotube optoelectronics", Phys. Status Solidi B **243**, 3197 (2006).

[172] R. Englman and J. Jortner, "The energy gap law for radiationless transitions in large molecules", Molecular Physics **18**, 145 (1970).

[173] A. J. Leggett, S. Chakravarty, A. T. Dorsey, M. P. A. Fisher, A. Garg and W. Zwerger, "Dynamics of the dissipative two-state system", Rev. Mod. Phys. **59**, 1 (1987).

[174] P. M. Morse and H. Feshbach, *Methods of theoretical physics*, International Series in Pure and Applied Physics, New York: McGraw-Hill, 1953 **1** (1953).

[175] K. A. Chao, J. Spałek and A. M. Oleś, "Canonical perturbation expansion of the Hubbard model", Phys. Rev. B **18**, 3453 (1978).

[176] A. H. MacDonald, S. M. Girvin and D. Yoshioka, "t/U expansion for the Hubbard model", Phys. Rev. B **37**, 9753 (1988).

[177] S. G. Ovchinnikov and V. Valkov, *Hubbard operators in the theory of strongly correlated electrons* (World Scientific, 2004).

[178] V. J. Emery, "Theory of high-T_c superconductivity in oxides", Phys. Rev. Lett. **58**, 2794 (1987).

[179] J. Zaanen and A. M. Oleś, "Canonical perturbation theory and the two-band model for high-T_c superconductors", Phys. Rev. B **37**, 9423 (1988).

[180] V. I. Belinicher and A. L. Chernyshev, "Consistent low-energy reduction of the three-band model for copper oxides with O-O hopping to the effective t - J model", Phys. Rev. B **49**, 9746 (1994).

[181] A. Ramšak and P. Prelovšek, "Comparison of effective models for CuO2 layers in oxide superconductors", Phys. Rev. B **40**, 2239 (1989).

[182] E. Müller-Hartmann and A. Reischl, "Derivation of effective spin models from a three band model for CuO -planes", Eur. Phys. J. B **28**, 173 (2002).

[183] V. I. Belinicher, A. L. Chernyshev and L. V. Popovich, "Range of the t - J model parameters for CuO_2 planes: Experimental data constraints", Phys. Rev. B **50**, 13768 (1994).

[184] L. F. Feiner, J. H. Jefferson and R. Raimondi, "Effective single-band models for the high-T_c cuprates. I. Coulomb interactions", Phys. Rev. B **53**, 8751 (1996).

[185] R. Raimondi, J. H. Jefferson and L. F. Feiner, "Effective single-band models for the high-T_c cuprates. II. Role of apical oxygen", Phys. Rev. B **53**, 8774 (1996).

[186] T. Tohyama, "Asymmetry of the electronic states in hole- and electron-doped cuprates: Exact diagonalization study of the t-t′-t″-J model", Phys. Rev. B **70**, 174517 (2004).

[187] S. Maekawa, T. Tohyama, S. E. Barnes, S. Ishihara, W. Koschibae and G. Khaliullin, *Physics of transition metal oxides*, Vol. 144 (Springer, 2004).

[188] A. L. Chernyshev, P. W. Leung and R. J. Gooding, "Comprehensive numerical and analytical study of two holes doped into the two-dimensional $t-J$ model", Phys. Rev. B **58**, 13594 (1998).

[189] G. Martinez and P. Horsch, "Spin polarons in the t-J model", Phys. Rev. B **44**, 317 (1991).

[190] A. Girlando, "Charge Sensitive Vibrations and Electron-Molecular Vibration Coupling in Bis(ethylenedithio)-tetrathiafulvalene (BEDT-TTF)", The Journal of Physical Chemistry C **115**, 19371 (2011).

[191] E. Jeckelmann and S. R. White, "Density-matrix renormalization-group study of the polaron problem in the Holstein model", Phys. Rev. B **57**, 6376 (1998).

[192] J. D. Perkins, J. M. Graybeal, M. A. Kastner, R. J. Birgeneau, J. P. Falck and M. Greven, "Mid-infrared optical absorption in undoped lamellar copper oxides", Phys. Rev. Lett. **71**, 1621 (1993).

[193] J. Lorenzana, J. Eroles and S. Sorella, "Does the Heisenberg Model Describe the Multimagnon Spin Dynamics in Antiferromagnetic CuO Layers?", Phys. Rev. Lett. **83**, 5122 (1999).

Appendix A

Mott insulator in strong constant external fields

A.1 Ground state wave function and energy for 1D nearly polarized system

For the g.s. wave function $|\varphi_0\rangle = \sum_j d_j^0 |\Psi_q^j\rangle$, the ansatz $d_j^0 = N_0 e^{-\kappa|j|} e^{iq''j}$ is taken, where κ, q'' are established from

$$H|\Psi_q^l\rangle = -e^{-i\phi}(1+e^{-iq})|\Psi_q^{l-1}\rangle - e^{i\phi}(1+e^{iq})|\Psi_q^{l+1}\rangle + U(1-\delta_{l,0})|\Psi_q^l\rangle, \tag{A.1}$$

yielding relations between coefficients d_j^0 when applied to the $|\varphi_0\rangle$,

$$(E_0 - U(1-\delta_{j,0}))d_j^0 + e^{-i\phi}(1+e^{-iq})d_{j+1}^0 + e^{i\phi}(1+e^{iq})d_{j-1}^0 = 0. \tag{A.2}$$

$q'' = \phi + q/2$ is fixed by demanding E_0 to be real, while for κ we obtain

$$e^{-\kappa} = \frac{-U + \sqrt{U^2 + 16\cos(\frac{q}{2})^2}}{4\cos(\frac{q}{2})} \;\rightarrow\; \cosh\kappa = \frac{\sqrt{U^2 + 16\cos(\frac{q}{2})^2}}{4\cos(\frac{q}{2})}. \tag{A.3}$$

Ground state energy E_0, Eq. (2.6), is obtained by integrating over momentum the eigenvalue equation (2.4),

$$\begin{aligned} -\frac{1}{U} &= \frac{1}{2\pi}\int_{-\pi}^{\pi} \frac{dq''}{E_0 - U + 4\cos(\frac{q}{2})\cos(q'' - \phi - \frac{q}{2}))} \\ &= -\frac{1}{\sqrt{(E_0-U)^2 - 16\cos^2(\frac{q}{2})}}, \\ E_0 &= U - \sqrt{U^2 + 16\cos^2\left(\frac{q}{2}\right)} \end{aligned} \tag{A.4}$$

which has minimum at $q = 0$.

A.2 Saddle point approximation

With the method of the steepest descent [174] integrals of the following form can be approximated with the saddle point of their integrand as

$$\int_C dt e^{f(t)} \approx e^{f(t_0)} \sqrt{\frac{2\pi}{-f''(t_0)}}, \tag{A.5}$$

where $f'(t_0) = 0$ and contour C must be such, that the integrand goes to zero at its ends. For the integral in our case,

$$I = \int_{-\pi}^{\pi} d\xi \exp\left(\frac{i}{F}\int_{-\pi}^{\xi} d\xi' \omega_\pi(\xi')\right), \quad \omega_\pi(\xi) \approx \Delta + 2\xi^2 \tag{A.6}$$

we extend the integration interval to $\xi \to \pm\infty$, where integrand is actually a rapidly oscillating function. Such behavior is typically appropriate for treatment for saddle point approximation. First we have to establish the saddle point t_0 of $f(t) = (i/F)\int_0^t \omega_\pi(x)dx$,

$$f'(t_0) = \Delta + 2t_0 = 0 \to t_0 = i\sqrt{\Delta/2}, \quad f''(t_0) = 4t_0 = -\frac{\sqrt{8\Delta}}{F}. \tag{A.7}$$

The saddle point approximation to the integral then actually agrees with the Eq. (2.15),

$$I = \sqrt{\frac{2\pi F}{\sqrt{8\Delta}}} \exp\left(\frac{i}{F}\int_0^{i\sqrt{\frac{\Delta}{2}}} \omega_\pi(x)dx\right) = \sqrt{\frac{\pi F}{\sqrt{2\Delta}}} \exp\left(-\frac{\Delta^{3/2}\sqrt{2}}{3F}\right). \tag{A.8}$$

Moreover, an appropriate contour of the integration, not important for the final expression, could be in principle found as well.

A.3 Ground state wave function for general dimension

The form of the g.s. wave function in general dimension d can be approximately obtained from the solution of the Schroedinger equation in the continuous limit (for the kinetic term) $\triangle\psi = |E_0|\psi$, $\psi = K_{(d-2)/2}(\sqrt{|E_0|}r)/r^{(d-2)/2}$. Using large r limit for the modified Bessel function $K_{(d-2)/2}$, we obtain the ansatz

$$d^0_{\mathbf{R}_j} = \begin{cases} B\ e^{-\kappa|\mathbf{R}_j| + i\mathbf{k}\cdot\mathbf{R}_j}\ |\mathbf{R}_j|^{-(d-1)/2} & \text{for } \mathbf{R}_j \neq 0, \\ A & \text{for } \mathbf{R}_j = 0. \end{cases}$$

A phase k and the localization κ are established from the eigenvalue equation

$$(E_0 - U(1-\delta_{\mathbf{R}_j,0}))d_{\mathbf{R}_j} + \sum_m \left[e^{i\mathbf{e}_m\cdot\mathbf{A}}(1 - e^{-i\mathbf{e}_m\cdot\mathbf{q}})d_{\mathbf{R}_j+\mathbf{e}_m} + e^{-i\mathbf{e}_m\cdot\mathbf{A}}(1 - e^{i\mathbf{e}_m\cdot\mathbf{q}})d_{\mathbf{R}_j-\mathbf{e}_m}\right] = 0. \tag{A.9}$$

Away from the $\mathbf{R}_j = 0$,

$$-(E_0 - U) = \sum_{p=\pm1}\sum_m \left(e^{ip\mathbf{e}_m\cdot(\mathbf{k}+\mathbf{A})}(1 - e^{-ip\mathbf{e}_m\cdot\mathbf{q}})\ e^{-p\kappa(|\mathbf{R}_j+\mathbf{e}_m| - |\mathbf{R}_j|)}\ \frac{|\mathbf{R}_j|^{(d-1)/2}}{|\mathbf{R}_j + p\mathbf{e}_m|^{(d-1)/2}}\right. \tag{A.10}$$

The g.s. has lowest energy at total momentum $\mathbf{q} = \{\pi, \pi, \dots\}$, while by demanding E_0 to be real we set $\mathbf{k} = -\mathbf{A}$. From the large $|\mathbf{R}_j|$ limit where

$$|\mathbf{R}_j \pm \mathbf{e}_m| - |\mathbf{R}_j| \approx \frac{\pm\mathbf{R}_j\cdot\mathbf{e}_m}{|\mathbf{R}_j|}, \quad \frac{|\mathbf{R}_j \pm \mathbf{e}_m|^{(d-1)/2}}{|\mathbf{R}_j|^{(d-1)/2}} \approx 1 \pm \frac{(d-1)}{2}\frac{\mathbf{R}_j\cdot\mathbf{e}_m}{|\mathbf{R}_j|^2}, \tag{A.11}$$

Eq. (A.10) is simplified significantly

$$\begin{aligned} |E_0| + U &\approx 4 \sum_m \left[\cosh\left(\frac{\kappa \mathbf{R}_j \cdot \mathbf{e}_m}{|\mathbf{R}_j|} \right) + \sinh\left(\frac{\kappa \mathbf{R}_j \cdot \mathbf{e}_m}{|\mathbf{R}_j|} \right) \frac{(d-1)}{2} \frac{\mathbf{R}_j \cdot \mathbf{e}_m}{|\mathbf{R}_j|^2} \right] \\ &\approx 4d + 2\kappa^2 + \mathcal{O}(|\mathbf{R}_j|^{-1}) \end{aligned} \tag{A.12}$$

and yields relation $2\kappa^2 \approx \Delta$. Coefficients A and B are related through the eigenvalue equation as well,

$$-|E_0|A + 4de^{-\kappa}B = 0. \tag{A.13}$$

Appendix B

Nonequilibrium optical linear response

B.1 Time-dependent linear response

Based on an ansatz

Let us show that

$$\rho_1(t') = -i \int_t^{t'} dt'' f(t'') U(t', t'') \; [F, \rho_0(t'')] \; U(t'', t') \tag{B.1}$$

satisfies the relation (3.2). We assumed that the perturbation was turned on at time t. To calculate the time derivative of $\rho_1(t')$, we first need the derivative of the zero-th order time propagation operator

$$U(t', t) = \begin{cases} \hat{T}[\exp(-i \int_t^{t'} H_0(t'')dt'')] & t' \geq t, \\ \hat{\tilde{T}}[\exp(i \int_{t'}^{t} H_0(t'')dt'')] & t' < t. \end{cases}$$

(where $\hat{T}$ is operator of the time ordering and $\hat{\tilde{T}}$ of the anti-time ordering), which are

$$\frac{\partial}{\partial t'} U(t', t) = -iH_0(t')U(t', t), \quad t' \geq t, \tag{B.2}$$

$$\frac{\partial}{\partial t} U(t', t) = iU(t', t)H_0(t), \qquad t' < t. \tag{B.3}$$

Finally we use this in

$$\begin{aligned} i\frac{\partial}{\partial t'}\rho_1(t') &= f(t')[F, \rho_0(t')] + \int_t^{t'} dt'' f(t'') \Big(- iH_0(t') \; U(t', t'') \; [F, \rho_0(t'')] \; U(t'', t') \\ &\qquad + U(t', t'') \; [F, \rho_0(t'')] \; U(t'', t') \; iH_0(t') \Big) \\ &= f(t')[F, \rho_0(t')] + [H_0(t'), \rho_1(t')] \end{aligned} \tag{B.4}$$

and obtain Eq. (3.2) from the main text.

Having $\rho_1(t')$ it is easy to calculate the effect of the perturbation on the expectation of observables, e.g. B, at time $t' > t$ if the perturbation was turned on at time t,

$$\begin{aligned}\delta\langle B\rangle_{t'} &= Tr\big[\rho_1(t')B\big] = -i\int_t^{t'} dt'' f(t'')\; Tr\big[U(t',t'')[F,\rho_0(t'')]U(t'',t')B\big] \\ &= -i\int_t^{t'} dt'' f(t'')\; Tr\big[U(t',t)U(t,t'')\; F\; U(t'',t)\rho_0(t)\; U(t,t')B \\ &\qquad\qquad -U(t',t)\rho_0(t)U(t,t'')\; F\; U(t'',t)U(t,t')B\big] \\ &= -i\int_t^{t'} dt'' f(t'')\; Tr\big[\rho_0(t)\; [B^I(t'),F^I(t'')]\big], \end{aligned} \tag{B.5}$$

where $B^I(t') = U(t,t')BU(t',t)$ is the interaction representation of B.

Based on the propagation of the initial pure state

If system is initially in a pure state $|\psi(0)\rangle$, its time evolution can serve to establish $\rho_1(t)$ as well. Let us determine the first order corrections due to $\tilde{F}(t) = f(t)F$ to the full time propagation operator

$$\begin{aligned}&\hat{T}\exp\big(-i\int_t^{t'}(H_0(t'')+\tilde{F}(t''))dt''\big) \qquad\qquad (B.6)\\ &= \hat{T}\Big[\exp\big(-i\int_t^{t'}H_0(t'')dt''\big)\exp\big(-i\int_t^{t'}\tilde{F}(t'')dt''\big)\exp\big(-\frac{1}{2}[\int_t^{t'}H_0(t'')dt'',\int_t^{t'}\tilde{F}(t'')dt'']\big)\Big] \\ &\approx \hat{T}\Big\{\exp\big(-i\int_t^{t'}H_0(t'')dt''\big)\Big(1-i\int_t^{t'}\tilde{F}(t'')dt''\Big)\Big(1-\frac{1}{2}[\int_t^{t'}H_0(t'')dt'',\int_t^{t'}\tilde{F}(t'')dt'']\Big)\Big\}.\end{aligned}$$

One of terms linear in $\tilde{F}$ can be rewritten as

$$\begin{aligned}&-i\hat{T}\Big(U(t',t)\int_t^{t'}\tilde{F}(t'')dt''\Big) = -i\hat{T}\Big(U(t',t)\sum_n\tilde{F}(t+n\Delta t)\Delta t\Big) \qquad (B.7)\\ &= -i\sum_n U(t',t+n\Delta t)\;\tilde{F}(t+n\Delta t)\;U(t+n\Delta t,t)\;\Delta t \\ &= -i\int_t^{t'}U(t',t'')\tilde{F}(t'')U(t'',t)\;dt'',\end{aligned}$$

while the other two (from the commutator) cancel out due to the time ordering. Therefore the first order correction to the propagator operator is

$$U_1(t',t) = U(t',t) - i\int_t^{t'}dt''\;\Big(U(t',t'')\tilde{F}(t'')U(t'',t)\Big) \tag{B.8}$$

The linear response of the operator B to the perturbation applied at t is then calculated from $|\psi_1(t')\rangle = U_1(t',t)|\psi_0(t)\rangle$, where $|\psi_0(t)\rangle = U(t,0)|\psi(0)\rangle$. Eq. (B.1) for $\rho_1(t')$ can be now obtained from the part of $|\psi_1(t')\rangle\langle\psi_1(t')| - |\psi_0(t')\rangle\langle\psi_0(t')|$ linear in $\tilde{F}$,

$$\begin{aligned}\rho_1(t') &= i\int_t^{t'}dt''\Big(U(t',t)\rho_0(t)U(t,t'')\tilde{F}(t'')U(t'',t') - U(t',t'')\tilde{F}(t'')U(t'',t)\rho_0(t)U(t,t')\Big) \\ &= -i\int_t^{t'}dt''U(t',t'')\;[\tilde{F}(t''),\rho_0(t'')]\;U(t'',t'). \end{aligned} \tag{B.9}$$

B.2 Time-dependent Drude component

To calculated the Drude component from the time average

$$\frac{1}{2e^2 t_m}\int_0^{t_m} ds\ \sigma(t+s,t) = \frac{1}{2Vt_m}\int_0^{t_m} ds\Big[\langle\tau\rangle_{t+s} - \int_t^{t+s} dt''\chi(t+s,t'')\Big], \quad \text{(B.10)}$$

where $t_m \to \infty$, we first write the differential conductivity in Lehmann representation, i.e. in terms of eigenvectors of H_0, so that $|\psi(t)\rangle = \sum_m a_m e^{-i\epsilon_m t}|\phi_m\rangle$. Especially the paramagnetic part

$$\sigma^p(t',t) = -\frac{e^2}{V}\int_t^{t'} dt''\chi(t',t'') = \frac{e^2}{V}\int_t^{t'} dt''\ 2Im\ \langle\psi(t')|jU(t',t'')j|\psi(t'')\rangle \quad \text{(B.11)}$$

has to be treated carefully,

$$\begin{aligned}
\sigma^p(t',t) =& -\frac{ie^2}{V}\int_t^{t'} dt''\sum_{m,n}\Big(a_m^* a_n\langle\phi_m|je^{-iH_0(t'-t'')}j|\phi_n\rangle e^{i\epsilon_m t'-i\epsilon_n t''} - \text{H.c.}\Big)\\
=& -\frac{ie^2}{V}\int_t^{t'} dt''\sum_{m,n,l}\Big(a_m^* a_n\ j_{ml}j_{ln}\ e^{-i\epsilon_l(t'-t'')}e^{i\epsilon_m t'-i\epsilon_n t''} - \text{H.c.}\Big)\\
=& -\frac{e^2}{V}\sum_{m,n,l\neq m,n}\Big(a_m^* a_n\ \frac{j_{ml}j_{ln}}{\omega_{ln}}\ \alpha - a_m a_n^*\ \frac{j_{nl}j_{lm}}{\omega_{nl}}\ \alpha^*\Big) \quad \text{(B.12)}\\
&-\frac{ie^2}{V}\sum_{m,n}\Big(a_m^* a_n\ j_{mn}j_{nn}\ e^{i\omega_{mn}t'}(t'-t) - a_m a_n^*\ j_{nn}j_{nm}\ e^{-i\omega_{mn}t'}(t'-t)\Big), \quad \text{(B.13)}
\end{aligned}$$

where $\omega_{mn} = \epsilon_m - \epsilon_n$ and $\alpha = e^{i\omega_{ml}t'}\left(e^{i\omega_{ln}t'} - e^{i\omega_{ln}t}\right)$. Following from Eq. (B.10), the Drude component has several contributions:
(a) from the diamagnetic part

$$\begin{aligned}
\int_0^\infty ds\sum_{m,n} a_m^* a_n e^{i\omega_{mn}(t+s)}\tau_{mn} &= \pi\sum_{m,n} a_m^* a_n e^{i\omega_{mn}t}\delta(\omega_{mn})\tau_{mn}\\
&= \pi\sum_n |a_n|^2\tau_{nn} \quad \text{(B.14)}
\end{aligned}$$

(b) from the part (B.12) of the paramagnetic term

$$\begin{aligned}
&-\int_0^\infty ds\sum_{m,n,l\neq n}\Big[a_m^* a_n\frac{j_{ml}j_{ln}}{\omega_{ln}}(e^{i\omega_{mn}s} - e^{i\omega_{ml}s})e^{i\omega_{mn}t} + \text{H.c.}\Big]\\
&= -\pi\sum_{m,n,l\neq n}\Big[a_m^* a_n\frac{j_{ml}j_{ln}}{\omega_{ln}}e^{i\omega_{mn}t}(\delta(\omega_{mn}) - \delta(\omega_{ml})) + \text{H.c.}\Big]\\
&= \pi\sum_{m,n\neq m}\Big[-2|a_m|^2\frac{|j_{mn}|^2}{\omega_{nm}} + a_m^* a_n\ \frac{j_{mn}(j_{mm}-j_{nn})}{\omega_{mn}}\ e^{i\omega_{mn}t}\Big] \quad \text{(B.15)}
\end{aligned}$$

(c) from the part (B.13) of the paramagnetic term

$$i\int_0^\infty ds\ s\sum_{mn}(a_m^* a_n j_{mn} j_{nn} e^{i\omega_{mn}(t+s)} - a_m a_n^* j_{nn} j_{nm} e^{-i\omega_{mn}(t+s)}) \tag{B.16}$$

$$= i\int_0^\infty ds\ s\ \sum_{mn} a_m^* a_n j_{mn} e^{i\omega_{mn}(t+s)}(j_{nn} - j_{mm})$$

$$= \pi\sum_{mn} a_m^* a_n j_{mn} e^{i\omega_{mn}t}(j_{nn} - j_{mm})\frac{\partial\delta(\omega_{mn})}{\partial\omega_{mn}} = 0 \tag{B.17}$$

since for $m = n$ already the integrand in Eq. (B.16) is zero.

Appendix C

Charge recombination in photo-doped cuprates

C.1 The exciton-boson toy model

Lang-Firsov transformation of Hamiltonian

Operator S that defines the canonical transformation is set by the condition that H_{eb} is eliminated in the first order, $H_{eb} - [S, H_e + H_b] = 0$, which fixes the parameter α_q in $S = -e^\dagger e \sum_q \alpha_q (a_q^\dagger - a_{-q})$,

$$[S, H_e + H_b] = -e^\dagger e \sum_{q,p} \alpha_q \omega_p [(a_q^\dagger - a_{-q}), a_p^\dagger a_p] = -e^\dagger e \sum_{q,p} \alpha_q \omega_p (-a_p^\dagger \delta_{q,p} - a_p \delta_{-q,p})$$
$$= H_{eb}, \quad \text{if } \alpha_q = \frac{\lambda_q}{\omega_q}. \tag{C.1}$$

Then the transformed Hamiltonian $\tilde{H}$ is obtained from

$$[S, H_{eb}] = -\sum_{q,p} \alpha_q \lambda_p [(a_p^\dagger - a_{-p}), (a_q^\dagger + a_{-q})] e^\dagger e$$
$$= -\sum_{q,p} \alpha_q \lambda_p (-\delta_{-p,q} - \delta_{-q,p}) e^\dagger e$$
$$= 2 \sum_q \alpha_q \lambda_q e^\dagger e,$$
$$[S, [S, H_e + H_b]] = [S, H_{eb}], \tag{C.2}$$
$$\tag{C.3}$$

and equals

$$\tilde{H} = H_e + H_b - \frac{1}{2}[S, H_{eb}] + \tilde{H}_{rc}$$
$$= \Big(E_{hd} - \sum_q \frac{\lambda_q^2}{\omega_q}\Big) e^\dagger e + \sum_q \omega_q a_q^\dagger a_q + g_{rc}(\tilde{e}^\dagger + \tilde{e}). \tag{C.4}$$

The dressing of the recombination/creation operator due to Lang-Firsov transformation is obtained from the expansion to all orders

$$\tilde{e} = e - [S, e] + \frac{1}{2}[S, [S, e]] + \dots \tag{C.5}$$

Using $[e^\dagger e, e] = -e$, then

$$
\begin{aligned}
[S, e] &= \Big[-\sum_q \alpha_q (a_q^\dagger - a_{-q}) e^\dagger e, e \Big] = \sum_q \alpha_q (a_q^\dagger - a_{-q})\ e, \\
[S, [S, e]] &= \Big[-\sum_q \alpha_q (a_q^\dagger - a_{-q}) e^\dagger e, \sum_p \alpha_p (a_p^\dagger - a_{-p}) e \Big] \\
&= \Big(\sum_q \alpha_q (a_q^\dagger - a_{-q}) \Big)^2 e, \\
[S,\ \ldots [S, e]] &= \Big(\sum_q \alpha_q (a_q^\dagger - a_{-q}) \Big)^n e,
\end{aligned}
\tag{C.6}
$$

so that finally

$$
\tilde{e} = \exp\Big(-\sum_q \alpha_q (a_q^\dagger - a_{-q}) \Big)\ e. \tag{C.7}
$$

Matrix element

Here we derive the matrix element that enters the expression for the FGR in the integral form, Eq. (5.7). Its evaluation heavily relies on the fact that $\tilde{H}_{rc}|\psi_0^e\rangle$ creates a coherent state. If we explicitly write

$$
\begin{aligned}
g_{rc}^{-1} e^{-i(\tilde{H}_0 - E_{\tilde{0}})t} \tilde{H}_{rc} |\psi_0^e\rangle &= e^{-i(\tilde{H}_0 - E_{\tilde{0}})t} \prod_q e^{-(\alpha_q a_q^\dagger - \alpha_{-q} a_q)} |0, 0\rangle \\
&= e^{-i(\tilde{H}_0 - E_{\tilde{0}})t} \prod_q e^{\frac{|\alpha_q|^2}{2}\ [a_q^\dagger, a_q]}\ e^{-\alpha_q a_q^\dagger} |0, 0\rangle \\
&= e^{-i(\tilde{H}_0 - E_{\tilde{0}})t} e^{-\sum_q |\alpha_q|^2/2}\ \prod_q \sum_{n_q} \frac{(-\alpha_q)^{n_q}}{\sqrt{n_q!}}\ |0, n_q\rangle \\
&= e^{-\sum_q |\alpha_q|^2/2}\ \prod_q \sum_{n_q} \frac{(-\alpha_q)^{n_q} e^{-i n_q \epsilon_q t}}{\sqrt{n_q!}}\ |0, n_q\rangle \\
&= e^{-\sum_q |\alpha_q|^2/2}\ \prod_q \sum_{n_q} \frac{(-\alpha_q(t))^{n_q}}{\sqrt{n_q!}}\ |0, n_q\rangle
\end{aligned}
\tag{C.8}
$$

where we defined $\alpha_q(t) \equiv \alpha_q e^{-i\epsilon_q t}$ via a single phonon mode energy ϵ_q. Notation $|m, n_q\rangle$ stands for the state with m excitons and n phonon modes with wave vector q. In the scalar product $\langle \psi_0^e | \tilde{H}_{rc}\ e^{-i(\tilde{H}_0 - E_{\tilde{0}})t}\ \tilde{H}_{rc} | \psi_0^e \rangle$ only the terms with the same q give nonzero contribution

$$
\begin{aligned}
\langle \psi_0^e | \tilde{H}_{rc}\ e^{-i(\tilde{H}_0 - E_{\tilde{0}})t}\ \tilde{H}_{rc} | \psi_0^e \rangle &= g_{rc}^2\ e^{-\sum_q \alpha_q^2}\ \prod_q \sum_{n_q} \frac{(\alpha_q(t) \alpha_q^*)^{n_q}}{n_q!} \\
&= g_{rc}^2\ \exp\Big(\sum_q \alpha_q^2 (e^{-i\omega_q t} - 1) \Big)
\end{aligned}
\tag{C.9}
$$

C.2 Recombination in 2D systems with spin correlations

C.2.1 Canonical transformation of single band Hubbard model

We parametrize the S for canonical transformation S by

$$S = \xi \sum_{ijs} s \left(X_i^{sH} X_j^{\bar{s}2} - X_i^{2\bar{s}} X_j^{Hs} \right). \tag{C.10}$$

With it we would like to transform out the charge recombination in the lowest order of t, therefore $H_{trc} + [S, H_U] = 0$ should be satisfied. Then

$$\begin{aligned}
[S, H_U] &= \xi U \sum_{ijk,s} s[X_i^{sH} X_j^{\bar{s}2} - X_i^{D\bar{s}} X_j^{Hs}, X_k^{DD}] \\
&= \xi U \sum_{ijk,s} s \left(X_i^{sH} [X_j^{\bar{s}D}, X_k^{DD}] - [X_i^{D\bar{s}} X_k^{DD}] X_j^{Hs} \right) \\
&= \xi U \sum_{ijk,s} s \left(\delta_{jk} X_i^{sH} X_j^{\bar{s}D} + \delta_{ik} X_i^{D\bar{s}} X_j^{Hs} \right) \\
&= -\frac{\xi U}{t} H_{trc} \quad \rightarrow \quad \xi = \frac{t}{U}.
\end{aligned} \tag{C.11}$$

To obtain the transformed Hamiltonian up to t^2/U we have to evaluate $[S, H_t]$ and $[S, H_{trc}]$, which is a tedious task.

Evaluating $[S, H_t]$

$$-\frac{U}{t^2}[S, H_t] = \sum_{ijs,km\sigma} s[X_i^{sH} X_j^{\bar{s}D} - X_i^{2\bar{s}} X_j^{Hs}, X_i^{\sigma H} X_j^{H\sigma} + X_i^{D\bar{\sigma}} X_j^{\bar{\sigma}D}] \tag{C.12}$$

where i, j and k, m are nearest neighbor sites. If we evaluate each term separately 1.i]

$$\begin{aligned}
&\sum_{ijs,km\sigma} s[X_i^{sH} X_j^{\bar{s}D}, X_k^{\sigma H} X_m^{H\sigma}] \\
&= -\sum_{ijs,km\sigma} s\big(X_i^{sH} \left(X_k^{\sigma H} \{X_m^{H\sigma}, X_j^{\bar{s}D}\} - \{X_k^{\sigma H}, X_j^{\bar{s}D}\} X_m^{H\sigma} \right) \\
&\qquad + \left(X_k^{\sigma H} \{X_m^{H\sigma}, X_i^{sH}\} - \{X_k^{\sigma H}, X_i^{sH}\} X_m^{H\sigma} \right) X_j^{\bar{s}D} \big) \\
&= -\sum_{ijs,km\sigma} s \left(X_i^{sH} X_k^{\sigma H} \delta_{mj} \delta_{\sigma\bar{s}} X_j^{HD} + X_k^{\sigma H} \delta_{mi} \delta_{\sigma s} X_i^{HH} X_j^{\bar{s}D} + X_m^{\sigma H} \delta_{mi} X_i^{s\sigma} X_j^{\bar{s}D} \right) \\
&= -\sum_{kij,s} s(X_j^{sH} X_k^{\bar{s}H} X_i^{HD} + X_k^{sH} X_i^{HH} X_j^{\bar{s}D} + \sum_{\sigma} X_k^{\sigma H} X_i^{s\sigma} X_j^{\bar{s}D})
\end{aligned} \tag{C.13}$$

1.ii]

$$
\begin{aligned}
&\sum_{ijs,km\sigma} s[X_i^{sH}X_j^{\bar{s}D}, X_k^{D\bar{\sigma}}X_m^{\bar{\sigma}D}] \\
&= -\sum_{ijs,km\sigma} s\big(X_i^{sH}\left(X_k^{D\bar{\sigma}}\{X_m^{\bar{\sigma}D}, X_j^{\bar{s}D}\} - \{X_k^{D\bar{\sigma}}, X_j^{\bar{s}D}\}X_m^{\bar{\sigma}D}\right) \\
&\qquad + \left(X_k^{D\bar{\sigma}}\{X_m^{\bar{\sigma}D}, X_i^{sH}\} - \{X_k^{D\bar{\sigma}}, X_i^{sH}\}X_m^{\bar{\sigma}D}\right)X_j^{\bar{s}D}\big) \\
&= -\sum_{ijs,km\sigma} s\left(-X_i^{sH}X_k^{DD}\delta_{kj}\delta_{\bar{\sigma}\bar{s}}X_m^{\bar{\sigma}D} - X_i^{DH}\delta_{ki}\delta_{\bar{\sigma}s}X_m^{\bar{\sigma}D}X_j^{\bar{s}D} - X_i^{sH}\delta_{kj}X_j^{\bar{s}\bar{\sigma}}X_m^{\bar{\sigma}D}\right) \\
&= \sum_{kij,s} s(X_j^{sH}X_i^{DD}X_k^{\bar{s}D} + X_i^{DH}X_k^{sD}X_j^{\bar{s}D} + \sum_{\sigma} X_j^{sH}X_i^{\bar{s}\bar{\sigma}}X_k^{\bar{\sigma}D})
\end{aligned}
\tag{C.14}
$$

1.iii]

$$
\begin{aligned}
&-\sum_{ijs,km\sigma} s[X_i^{D\bar{s}}X_j^{Hs}, X_k^{\sigma H}X_m^{H\sigma}] \\
&= \sum_{ijs,km\sigma} s\big(X_i^{D\bar{s}}\left(X_k^{\sigma H}\{X_m^{H\sigma}, X_j^{Hs}\} - \{X_k^{\sigma H}, X_j^{Hs}\}X_m^{H\sigma}\right) \\
&\qquad + \left(X_k^{\sigma H}\{X_m^{H\sigma}, X_i^{D\bar{s}}\} - \{X_k^{\sigma H}, X_i^{D\bar{s}}\}X_m^{H\sigma}\right)X_j^{Hs}\big) \\
&= \sum_{ijs,km\sigma} s\left(-X_i^{D\bar{s}}X_j^{HH}\delta_{kj}\delta_{\sigma s}X_m^{H\sigma} - X_i^{DH}\delta_{ki}\delta_{\sigma\bar{s}}X_m^{H\sigma}X_j^{Hs} - X_i^{D\bar{s}}\delta_{kj}X_j^{\sigma s}X_m^{H\sigma}\right) \\
&= -\sum_{kij,s} s(X_j^{D\bar{s}}X_i^{HH}X_k^{Hs} + X_i^{DH}X_k^{H\bar{s}}X_j^{Hs} + \sum_{\sigma} X_j^{D\bar{s}}X_i^{\sigma s}X_k^{H\sigma})
\end{aligned}
\tag{C.15}
$$

1.iv]

$$
\begin{aligned}
&-\sum_{ijs,km\sigma} s[X_i^{D\bar{s}}X_j^{Hs}, X_k^{D\bar{\sigma}}X_m^{\bar{\sigma}D}] \\
&= \sum_{ijs,km\sigma} s\big(X_i^{D\bar{s}}\left(X_k^{D\bar{\sigma}}\{X_m^{\bar{\sigma}D}, X_j^{Hs}\} - \{X_k^{D\bar{\sigma}}, X_j^{Hs}\}X_m^{\bar{\sigma}D}\right) \\
&\qquad + \left(X_k^{D\bar{\sigma}}\{X_m^{\bar{\sigma}D}, X_i^{D\bar{s}}\} - \{X_k^{D\bar{\sigma}}, X_i^{D\bar{s}}\}X_m^{\bar{\sigma}D}\right)X_j^{Hs}\big) \\
&= \sum_{ijs,km\sigma} s\left(X_i^{D\bar{s}}X_k^{D\bar{\sigma}}\delta_{mj}\delta_{\bar{\sigma}s}X_j^{HD} + X_k^{D\bar{\sigma}}\delta_{mi}(\delta_{\bar{\sigma}\bar{s}}X_i^{DD} + X_i^{\bar{\sigma}\bar{s}})X_j^{Hs}\right) \\
&= \sum_{kij,s} s(X_j^{D\bar{s}}X_k^{Ds}X_i^{HD} + X_k^{D\bar{s}}X_i^{DD}X_j^{Hs} + \sum_{\sigma} X_k^{D\bar{\sigma}}X_i^{\bar{\sigma}\bar{s}}X_j^{Hs})
\end{aligned}
\tag{C.16}
$$

where in all cases i is n.n. of k and j.

Evaluating $[S, H_{trc}]$

$$
-\frac{U}{t^2}[S, H_{trc}] = \sum_{ijs,km\sigma} s\sigma[X_i^{sH}X_j^{\bar{s}D} - X_i^{D\bar{s}}X_j^{Hs}, X_i^{\sigma H}X_j^{\bar{\sigma}D} + X_i^{D\bar{\sigma}}X_j^{H\sigma}] \tag{C.17}
$$

2.i]

$$\begin{aligned}
&\sum_{ijs,km\sigma} s\sigma[X_i^{sH}X_j^{\bar{s}D}, X_k^{\sigma H}X_m^{\bar{\sigma}D}] \\
&= -\sum_{ijs,km\sigma} s\sigma\big(X_i^{sH}\left(X_k^{\sigma H}\{X_m^{\bar{\sigma}D}, X_j^{\bar{s}D}\} - \{X_k^{\sigma H}, X_j^{\bar{s}D}\}X_m^{\bar{\sigma}D}\right) \\
&\qquad + \left(X_k^{\sigma H}\{X_m^{\bar{\sigma}D}, X_i^{sH}\} - \{X_k^{\sigma H}, X_i^{sH}\}X_m^{\bar{\sigma}D}\right)X_j^{\bar{s}D}\big) \\
&= 0
\end{aligned} \tag{C.18}$$

2.ii]

$$\begin{aligned}
&\sum_{ijs,km\sigma} s\sigma[X_i^{sH}X_j^{\bar{s}D}, X_k^{D\bar{\sigma}}X_m^{H\sigma}] \\
&= -\sum_{ijs,km\sigma} s\sigma\big(X_i^{sH}\left(X_k^{D\bar{\sigma}}\{X_m^{H\sigma}, X_j^{\bar{s}D}\} - \{X_k^{D\bar{\sigma}}, X_j^{\bar{s}D}\}X_m^{H\sigma}\right) \\
&\qquad + \left(X_k^{D\bar{\sigma}}\{X_m^{H\sigma}, X_i^{sH}\} - \{X_k^{D\bar{\sigma}}, X_i^{sH}\}X_m^{H\sigma}\right)X_j^{\bar{s}D}\big) \\
&= -\sum_{ijs,km\sigma} s\sigma(X_i^{sH}X_k^{D\bar{\sigma}}\delta_{mj}\delta_{\sigma\bar{s}}X_j^{HD} - X_i^{sH}\delta_{kj}(\delta_{\bar{\sigma}\bar{s}}X_j^{DD} \\
&\qquad + X_j^{\bar{s}\bar{\sigma}})X_m^{H\sigma} + X_k^{D\bar{\sigma}}\delta_{mi}(\delta_{\sigma s}X_i^{HH} + X_i^{s\sigma})X_j^{\bar{\sigma}D} - \delta_{ki}\delta_{\bar{\sigma}s}X_i^{DH}X_m^{H\sigma}X_j^{\bar{s}D}) \\
&= \sum_{kij,s}(X_j^{sH}X_k^{Ds}X_i^{HD} + X_j^{sH}X_i^{DD}X_k^{Hs} - X_k^{D\bar{s}}X_i^{HH}X_j^{\bar{s}D} - X_i^{DH}X_k^{H\bar{s}}X_j^{\bar{s}D}) \\
&+ \sum_{kij,s\sigma} s\sigma(X_j^{sH}X_i^{\bar{s}\bar{\sigma}}X_k^{H\sigma} - X_k^{D\bar{\sigma}}X_i^{s\sigma}X_j^{\bar{s}D})
\end{aligned} \tag{C.19}$$

2.iii]

$$\begin{aligned}
&-\sum_{ijs,km\sigma} s\sigma[X_i^{D\bar{s}}X_j^{Hs}, X_k^{\sigma H}X_m^{\bar{\sigma}D}] \\
&= \sum_{ijs,km\sigma} s\sigma\big(X_i^{D\bar{s}}\left(X_k^{\sigma H}\{X_m^{\bar{\sigma}D}, X_j^{Hs}\} - \{X_k^{\sigma H}, X_j^{Hs}\}X_m^{\bar{\sigma}D}\right) \\
&\qquad + \left(X_k^{\sigma H}\{X_m^{\bar{\sigma}D}, X_i^{D\bar{s}}\} - \{X_k^{\sigma H}, X_i^{D\bar{s}}\}X_m^{\bar{\sigma}D}\right)X_j^{Hs}\big) \\
&= \sum_{ijs,km\sigma} s\sigma(X_i^{D\bar{s}}X_k^{\sigma H}\delta_{mj}\delta_{\bar{\sigma}s}X_j^{HD} - X_i^{D\bar{s}}\delta_{kj}(\delta_{\sigma s}X_j^{HH} \\
&\qquad + X_j^{\sigma s})X_m^{\bar{\sigma}D} + X_k^{\sigma H}\delta_{mi}(\delta_{\bar{\sigma}\bar{s}}X_i^{DD} + X_i^{\bar{\sigma}\bar{s}})X_j^{Hs} - \delta_{ki}\delta_{\sigma\bar{s}}X_i^{DH}X_m^{\bar{\sigma}D}X_j^{Hs}) \\
&= \sum_{kij,s}(-X_j^{D\bar{s}}X_k^{\bar{s}H}X_i^{HD} - X_j^{D\bar{s}}X_i^{HH}X_k^{\bar{s}D} + X_k^{sH}X_i^{DD}X_j^{Hs} + X_i^{DH}X_k^{sD}X_j^{Hs}) \\
&+ \sum_{kij,s\sigma} s\sigma(-X_j^{D\bar{s}}X_i^{\sigma s}X_k^{\bar{\sigma}D} + X_k^{\sigma H}X_i^{\bar{\sigma}\bar{s}}X_j^{Hs})
\end{aligned} \tag{C.20}$$

2.iv]

$$
\begin{aligned}
&- \sum_{ijs,km\sigma} s\sigma[X_i^{D\bar{s}}X_j^{Hs}, X_k^{D\bar{\sigma}}X_m^{H\sigma}] \\
&= \sum_{ijs,km\sigma} s\sigma\big(X_i^{D\bar{s}}\left(X_k^{D\bar{\sigma}}\{X_m^{H\sigma}, X_j^{Hs}\} - \{X_k^{D\bar{\sigma}}, X_j^{Hs}\}X_m^{H\sigma}\right) \\
&\qquad + \left(X_k^{D\bar{\sigma}}\{X_m^{H\sigma}, X_i^{D\bar{s}}\} - \{X_k^{D\bar{\sigma}}, X_i^{D\bar{s}}\}X_m^{H\sigma}\right)X_j^{Hs}\big) \\
&= 0
\end{aligned} \tag{C.21}
$$

The Heisenberg part of the Hamiltonian is hidden in some of the terms with $j = k$. Note also that bosonic and fermionic operators for different sites commute between each other. For example:

$$
\sum_{ijk,s} X_j^{sH}X_i^{\bar{s}\bar{s}}X_k^{Hs} = \sum_{ijs} X_j^{ss}X_i^{\bar{s}\bar{s}} + \sum_{i,j\neq k,k,s} X_j^{sH}X_i^{\bar{s}\bar{s}}X_k^{Hs}
$$

C.2.2 Recombination term expressed with doublon and holon creation operators

The usual presentation of the Heisenberg term can be recognized using

$$
\sum_s X_i^{s\bar{s}}X_j^{\bar{s}s} = (S_i^-S_j^+ + S_i^+S_j^-) = 2(\boldsymbol{S}_i \cdot \boldsymbol{S}_j - S_i^zS_j^z) \tag{C.22}
$$

$$
\sum_s X_i^{ss}X_j^{\bar{s}\bar{s}} = \frac{1}{2}(n_in_j - 4S_i^zS_j^z)\delta_{1,n_in_j} \tag{C.23}
$$

where δ_{1,n_in_j} explicitly states that latter operator is nontrivial only on sites without doublon or holon. To transcript the recombination term (Eq. (5.24) in the main text),

$$
H_{rc} = \frac{t^2}{U}\sum_{(ijk),s} s[X_k^{sH}(X_i^{ss} - X_i^{\bar{s}\bar{s}})X_j^{\bar{s}D} + 2X_k^{\bar{s}H}X_i^{s\bar{s}}X_j^{\bar{s}D} + \text{H.c.}], \tag{C.24}
$$

in the language of holon and doublon creating operators $h_{is} = c_{is}^\dagger(1 - n_{i\bar{s}}) = X_i^{sH}, d_{is} = c_{i\bar{s}}n_{is} = -s\ X_i^{sD}$, we separately consider first two terms in Eq. (C.24),

$$
\begin{aligned}
&\sum_{ijk,s}\left(X_j^{sH}sX_j^{ss}X_k^{\bar{s}D} + X_j^{sH}\bar{s}X_j^{\bar{s}\bar{s}}X_k^{\bar{s}D}\right) = \sum_{ijk,s}\left(h_{js}d_{k\bar{s}}(-\bar{s})sX_j^{ss} + h_{js}d_{k\bar{s}}(-\bar{s})\bar{s}X_j^{\bar{s}\bar{s}}\right) \\
&= \sum_{ijk,s} h_{js}d_{k\bar{s}}\left(X_j^{ss} - X_j^{\bar{s}\bar{s}}\right) = \sum_{ijk}\left(h_{j\uparrow}d_{k\downarrow}(\delta_{S_i^z,\uparrow} - \delta_{S_i^z,\downarrow}) + h_{j\downarrow}d_{k\uparrow}(\delta_{S_i^z,\downarrow} - \delta_{S_i^z,\uparrow})\right) \\
&= 2\sum_{ijk}\left(h_{j\uparrow}d_{k\downarrow} - h_{j\downarrow}d_{k\uparrow}\right)S_i^z
\end{aligned} \tag{C.25}
$$

and the third term in Eq. (C.24),

$$
\begin{aligned}
\sum_{ijk,s} 2sX_j^{\bar{s}H}X_{s\bar{s}}X_k^{\bar{s}D} &= 2\sum_{ijk,s} sh_{j\bar{s}}X_i^{s\bar{s}}(-\bar{s})d_{i\bar{s}} = 2\sum_{ijk,s} h_{j\bar{s}}X_i^{s\bar{s}}d_{i\bar{s}} \\
&= 2\sum_{ijk}\left(h_{j\uparrow}d_{k\uparrow}S_i^- + h_{j\downarrow}d_{k\downarrow}S_i^\dagger\right).
\end{aligned} \tag{C.26}
$$

Now we can explicitly check via

s	s'	$h_{is}d_{ks'}\boldsymbol{\sigma}_{s\bar{s}'}\cdot\mathbf{S}$
$\uparrow$	$\downarrow$	$\sigma^3_{11}S^z_j = S^z_j$
$\downarrow$	$\uparrow$	$\sigma^3_{22}S^z_j = -S^z_j$
$\uparrow$	$\uparrow$	$(\sigma^1_{12}S^x_j + \sigma^2_{12}S^y_j) = (S^x_j - iS^y_j) = S^-_j$
$\downarrow$	$\downarrow$	$(\sigma^1_{21}S^x_j + \sigma^2_{21}S^y_j) = (S^x_j + iS^y_j) = S^+_j$

that the compact form of the recombination operator,

$$H_{rc} = \frac{J}{2}\sum_{(ijk),ss'}\left(h_{ks}d_{js'}\boldsymbol{\sigma}_{s\bar{s}'}\cdot\mathbf{S}_i + \text{H.c.}\right), \tag{C.27}$$

Eq. (5.28) in the main text, is indeed appropriate.

C.2.3 Intra-site diagonalization for charge-transfer Hubbard model

Recombination/creation operator H_{rc}, Eq. (5.42), derived from the original three-band Hamiltonian, Eq. (5.29), could have been obtained from higher order perturbative hopping processes, in a similar manner as the exchange coupling in Ref. [182]. Instead, our derivation of H_{rc} is based on the introduction of states associated with a single cell, where each cell contains a Cu orbital and a Wannier O orbital. Those states represent holon and doublon as well as neutral states and are calculated as the eigenstates of the single-cell Hamiltonian H_{0i}, Eq. (5.30). Coupling between cells is then established by the relevant matrix elements for states on adjacent cells, nontrivial due to hybridization between Cu and O orbitals in the single-cell states. The coupling strengths are set by the Hamiltonian (5.31) with the Wannier-orbital transformation inherently present in the hopping parameters. As originally proposed by [184], the intra-cell diagonalization that gives us the single-cell states has to be performed within each total spin sector. In the doublet basis, Eq. (5.33), we diagonalize the Hamiltonian

$$h^{1/2} = \begin{pmatrix} 0 & -\bar{t}_{pd} \\ -\bar{t}_{pd} & \Delta_0 \end{pmatrix} \tag{C.28}$$

yielding the g.s. $|g_\sigma\rangle$ that represents the charge-neutral (in the language of the single-band Hubbard model spin-like) state with the energy E_g

$$|g_s\rangle = \cos\theta|\bar{d}_s\rangle + \sin\theta|p_s\rangle, \tag{C.29}$$

$$E_g = \frac{\Delta_0}{2}\left(1 - \sqrt{1+\tan^2(2\theta)}\right), \tag{C.30}$$

where

$$\tan 2\theta = 2\bar{t}_{pd}/\Delta_0. \tag{C.31}$$

Within the singlet subspace, Eq. (5.32), holon is represented by the generalized Zhang-Rice singlet, which in addition to the dominant Zhang-Rice component $(1/\sqrt{2})(\bar{d}^\dagger_\uparrow p^\dagger_\downarrow - \bar{d}^\dagger_\downarrow p^\dagger_\uparrow)|0\rangle$ contains also some fraction of $\bar{d}^\dagger_\downarrow \bar{d}^\dagger_\uparrow|0\rangle, p^\dagger_\downarrow p^\dagger_\uparrow|0\rangle$ states. The fraction of each basis state is obtained by numerical diagonalization of the 3×3 local Hamiltonian. Since $U_d \approx \bar{U}_p + 2\Delta_0$ it turns out satisfactory to use basis

$$\{|S_0\rangle = \frac{1}{\sqrt{2}}(\bar{d}^\dagger_\uparrow p^\dagger_\downarrow - \bar{d}^\dagger_\downarrow p^\dagger_\uparrow)|0\rangle, \quad |S_1\rangle = \frac{1}{\sqrt{2}}(\bar{d}^\dagger_\uparrow \bar{d}^\dagger_\downarrow + p^\dagger_\uparrow p^\dagger_\downarrow)|0\rangle\}, \tag{C.32}$$

in which local Hamiltonian is

$$h^0 = \begin{pmatrix} \Delta_0 + \bar{V}_{pd} & -2\bar{t}_{pd} \\ -2\bar{t}_{pd} & \frac{1}{2}(U_d + \bar{U}_p) + \Delta_0. \end{pmatrix}, \tag{C.33}$$

yielding explicit expression for the holon state $|H\rangle$ and its energy

$$|H\rangle = \cos\phi\ |S_0\rangle + \sin\phi\ |S_1\rangle, \tag{C.34}$$

$$E_H = \Delta_0 + \bar{V}_{dp} + \frac{U_d + \bar{U}_p - 2\bar{V}_{pd}}{4}\left(1 - \sqrt{1+\tan^2(2\phi)}\right),$$

where

$$\tan 2\phi = 8\bar{t}_{pd}/(U_d + \bar{U}_p - 2\bar{V}_{pd}). \tag{C.35}$$

In order to check how much such approximation effects the recombination couplings Eq. (5.40) for different channels, we compared those values if $|H\rangle$ and E_H are calculated accurately by numerical diagonalization of 3×3 Hamiltonian, or within the latter approximation. The difference in coupling strengths $\delta r = r_{num} - r_{appr}$ is not substantial, as shown in Fig. C.1.

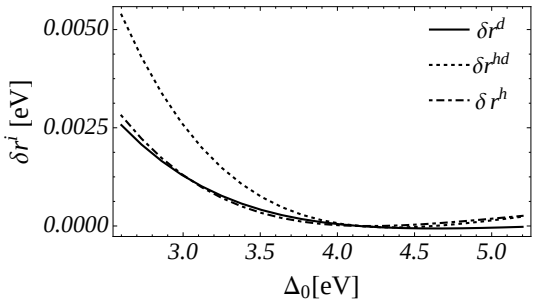

Figure C.1: The error in recombination coupling parameters, $\delta r = r_{num} - r_{appr}$, originating in approximate calculation Eq. (C.34) of the holon state $|H\rangle$ and its energy E_H as a function of Δ_0. For other parameters standard values are used.

The triplet states $|T_s\rangle$ within each cell are decoupled and have energy $E_T = \Delta_0 + \bar{V}_{pd}$.

C.2.4 Effective hopping parameters for charge-transfer Hubbard model

Hopping parameters that are introduced in the reduced single-band-like Hamiltonian, Eqs. (5.36,5.37), are obtained by evaluation of matrix elements for the inter-cell Hamiltonian H_{cc}, Eq. (5.31), between the states $|H\rangle, |D\rangle, |T_s\rangle, |g_s\rangle$, Eqs. (C.34, 5.34, C.29), on adjacent sites. For example, parameter t^h associated with hopping of holon is calculated from the matrix element for inter-site H_{cc} between states with holon and doublet g.s. at interchanged positions, $\langle H_i, g_{js}|H_{cc}|g_{is}, H_j\rangle$. Parametrized by θ, ϕ (Eqs. (C.31,C.35)), and $\tilde{\tau} = 2t_{pd}\mu_{01}, \tau' = 2t_{pp}\nu_{01}$ they are presented in the Table C.1.

These effective hopping parameters are together with the relative energies $\epsilon_H = E_H - E_g$, $\epsilon_D = -E_g$, $\epsilon_T = E_T - E_g$ the essential ingredient of recombination coupling strengths, as explicitly written in Eqs. (5.40).

Holon hopping	$t^h = t^h_d + t^h_p$; $t^h_d = \tilde{\tau}(\sin 2\theta + \sin 2\phi)/2$, $t^h_p = \tau' \cos^2(\theta - \phi)/2$.
Doublon hopping	$t^d = t^d_d + t^d_p$; $t^d_d = \tilde{\tau} \sin 2\theta, \quad t^d_p = \tau' \sin^2 \theta$.
Triplet hopping	$t^{T_0} = t^{T_0}_d + t^{T_0}_p, \quad t^{T_1} = t^{T_1}_d + t^{T_1}_p$; $t^{T_0}_d = \tilde{\tau} \cos 2\theta \sin \phi/2$, $t^{T_1}_d = \tilde{\tau} \cos 2\theta \sin \phi/\sqrt{2}$. $t^{T_0}_p = \tau' \cos\theta \cos(\theta - \phi)/2$, $t^{T_1}_p = \tau' \cos\theta \cos(\theta - \phi)/\sqrt{2}$.
Holon-doublon recombination	$t^r = t^r_d + t^r_p$; $t^r_d = \tilde{\tau}(\cos\phi + \sin 2\theta \sin\phi)/\sqrt{2}$, $t^r_p = \tau' \cos(\theta - \phi) \sin\theta/\sqrt{2}$.
Triplet-doublon recombination	$t^{r_0} = t^{r_0}_d + t^{r_0}_p, \quad t^{r_1} = t^{r_1}_d + t^{r_1}_p$; $t^{r_0}_d = \tilde{\tau} \cos 2\theta/\sqrt{2}$, $t^{r_1}_d = \tilde{\tau} \cos 2\theta$, $t^{r_0}_p = \tau' \sin 2\theta/2\sqrt{2}$, $t^{r_1}_p = \tau' \sin 2\theta/2$.

Table C.1: Hopping parameters for reduced single-band-like Hamiltonian, Eqs. (5.36,5.37), parametrized by θ, ϕ and $\tilde{\tau} = 2t_{pd}\mu_{01}, \tau' = 2t_{pp}\nu_{01}$.

C.2.5 Recombination term in the charge-transfer model

Recombination term

The condition $[S, H_{dg}] + H_{trc} = 0$ fixes the operator S that generates the canonical transformation to

$$S = \sum_{ij,s=\pm 1} \Big(- s \, \frac{t^{r}}{\epsilon_H + \epsilon_D} \bar{X}_i^{\bar{s}H} \bar{X}_j^{sD} + \frac{t^{r_0}}{\epsilon_T + \epsilon_D} \bar{X}_i^{\bar{s}T_0} \bar{X}_j^{sD} + \frac{t^{r_1}}{\epsilon_T + \epsilon_D} \bar{X}_i^{sT_s} \bar{X}_j^{sD} - \text{H.c.} \Big). \tag{C.36}$$

In the transformed Hamiltonian $e^S H e^{-S}$ the recombination/creation term is again in the lowest order nontrivial for HD pairs on next n.n. cells and is contained in $[S, H_t]$. Rather than calculating the latter commutator, it is much easier and more transparent to look at its effect on one of the states, nontrivial under its application to it, e.g. $g_{js}^\dagger H_k |0\rangle = |D_i g_{js} H_k\rangle \equiv |D g_s H\rangle$, where we choose ordering $i < j < k$ and i, k cells n.n. to j cell. In the above notation we explicitly write just states at cells under consideration. In the same way we define also the triplet state $T_{is}|0\rangle = |T_{is}\rangle$. Then

$$\begin{aligned}
[S, H_t]|D g_s H\rangle &= S H_t |D g_s H\rangle \\
&= S \left(-t^h |D H g_s\rangle + t^d |g_s D H\rangle - s \; t^{T_0} |D T_0 g_s\rangle + s \; t^{T_1} |D T_s g_{\bar{s}}\right) \\
&= \sum_\sigma \Big(- \sigma \; \frac{t^h t^r}{\epsilon_H + \epsilon_D} \; |g_{\bar{\sigma}} g_\sigma g_s\rangle + \sigma \; \frac{t^d t^r}{\epsilon_H + \epsilon_D} \; |g_s g_{\bar{\sigma}} g_\sigma\rangle \\
&\qquad - s \; \frac{t^{T_0} t^{r_0}}{\epsilon_T + \epsilon_D} \; |g_{\bar{\sigma}} g_\sigma g_s\rangle + s \; \frac{t^{T_1} t^{r_1}}{\epsilon_T + \epsilon_D} \; |g_s g_s g_{\bar{s}}\rangle \Big) \\
&= -s \left(\frac{t^d t^r}{\epsilon_H + \epsilon_D} - \frac{t^{T_1} t^{r1}}{\epsilon_T + \epsilon_D} \right) |g_s g_s g_{\bar{s}}\rangle \\
&\quad + s \left(\frac{t^d t^r + t^h t^r}{\epsilon_H + \epsilon_D} - \frac{t^{T_0} t^{r0}}{\epsilon_T + \epsilon_D} \right) |g_s g_{\bar{s}} g_s\rangle \\
&\quad - s \left(\frac{t^h t^r}{\epsilon_H + \epsilon_D} + \frac{t^{T_0} t^{r0}}{\epsilon_T + \epsilon_D} \right) |g_{\bar{s}} g_s g_s\rangle,
\end{aligned} \tag{C.37}$$

which explicitly shows that recombination channels leading to distinct final spin configurations have different strength of constants, used in the main text in Eqs. (5.39,5.40).

Exchange term

Equivalently, the exchange coupling J, used for comparison with recombination couplings in Fig. 5.3, is obtained from $[S, H_{trc}]$,

$$\begin{aligned}
S H_{trc} |g_{\bar{s}} g_s\rangle &= S \left(-s t^r (|HD\rangle + |DH\rangle) + t^{r_0} (|T_0 D\rangle - |D T_0\rangle) \right) \\
&= 2 \left(\frac{(s t^r)^2}{\epsilon_H + \epsilon_D} + \frac{t^{r_0}(-t^{r_0})}{\epsilon_T + \epsilon_D} \right) |g_s g_{\bar{s}}\rangle + 2 \left(- \frac{(s t^r)^2}{\epsilon_H + \epsilon_D} + \frac{t^{r_0}(-t^{r_0})}{\epsilon_T + \epsilon_D} \right) |g_{\bar{s}} g_s\rangle.
\end{aligned} \tag{C.38}$$

and $H_{trc} S |g_s g_{\bar{s}}\rangle = -S H_{trc} |g_s g_{\bar{s}}\rangle$. Therefore

$$\begin{aligned}
H'_J &= 2 \left(\frac{(t^r)^2}{\epsilon_H + \epsilon_D} - \frac{(t^{r_0})^2}{\epsilon_T + \epsilon_D} \right) \sum_{\langle i,j \rangle} (S_i^+ S_j^- + S_i^- S_j^+) \\
&= 4 \left(\frac{(t^r)^2}{\epsilon_H + \epsilon_D} - \frac{(t^{r_0})^2}{\epsilon_T + \epsilon_D} \right) \sum_{\langle i,j \rangle} (\mathbf{S}_i \cdot \mathbf{S}_j - S_i^z S_j^z),
\end{aligned} \tag{C.39}$$

yielding

$$J = 4\left(\frac{(t^r)^2}{\epsilon_H + \epsilon_D} - \frac{(t^{r_0})^2}{\epsilon_T + \epsilon_D}\right). \tag{C.40}$$

C.3 Charge recombination in 1D systems with phonons

C.3.1 Recombination in a spin-polarized system

Matrix element

The evaluation of the matrix element that enters the expression for FGR in the integral form (5.77) is very similar to the one performed for the toy model, App. C.1. Its phonon part $\langle 0_{ph}|A^\dagger_{0,1}\ e^{-iH_{ph}\tau}A_{d,d+1}|0_{ph}\rangle$ is somewhat more complicated, since $A_{j,j+1}|0_{ph}\rangle$ (where $A_{j,j+1} = e^{\tilde{p}_{j,j+1}} - e^{-\tilde{p}_{j,j+1}}$, Eqs. (5.74, 5.78)) creates a sum of coherent states. Similarly as for the toy model, Eq. (C.8), we expand

$$A_{j,j+1}|0_{ph}\rangle = e^{-\sum_q |\tilde{\alpha}_q|^2/2}\Big(\prod_q \sum_{n_q} \frac{(\tilde{\alpha}^j_q)^{n_q}}{\sqrt{n_q!}} - \prod_q \sum_{n_q} \frac{(-\tilde{\alpha}^j_q)^{n_q}}{\sqrt{n_q!}}\Big)|n_q\rangle, \tag{C.41}$$

where $|n_q\rangle$ is the wave function for n_q phonon modes and

$$\tilde{\alpha}^j_q \equiv \alpha^j_q - \alpha^{j+1}_q = -\frac{\lambda_q}{\omega_q}\ e^{-iqj}(1 - e^{-iq}), \tag{C.42}$$

$$|\tilde{\alpha}^j_q|^2 = \frac{2|\lambda_q|^2}{\omega_q^2}(1 - \cos q) \equiv |\tilde{\alpha}_q|^2, \quad \tilde{\alpha}^{j+d}_q\ (\tilde{\alpha}^j_q)^* = |\tilde{\alpha}_q|^2\ e^{-idq}. \tag{C.43}$$

For time propagation $e^{-iH_{ph}t}A_{j,j+1}|\tilde{\Phi}_1\rangle$ only substitution $\tilde{\alpha}^j_q \to \tilde{\alpha}^j_q(t) \equiv \tilde{\alpha}^j_q e^{-i\omega_q t}$ has to be made everywhere. The whole matrix element

$$\gamma^{ph}_d = \langle 0_{ph}|A_{j,j+1}\ e^{-iH_{ph}t}A_{j+d,j+d+1}|0_{ph}\rangle \tag{C.44}$$

is obtained similarly as in Eq. (C.9) from contributions with the same q, just that $\tilde{\alpha}^j_q$ in bra and ket wave function are in general different, possibly yielding an additional phase e^{-idq}, e.g.

$$\Big(\prod_q \sum_{n_q} \frac{(\tilde{\alpha}^j_q)^{n_q}}{\sqrt{n_q!}}|n_q\rangle\Big)^\dagger \Big(\prod_q \sum_{n_q} \frac{(\tilde{\alpha}^{j+d}_q(t))^{n_q}}{\sqrt{n_q!}}|n_q\rangle\Big) = \exp\Big(\sum_q |\tilde{\alpha}_q|^2 e^{-idq}e^{-i\omega_q t}\Big). \tag{C.45}$$

When we sum over all four terms in Eq. (C.44) of form (C.45), carefully taking into account $\pm$ prefactors, we obtain Eq. (5.83) from the main text.

Chapter 8

Razširjen povzetek

V tem poglavju zaobjamemo vse ključne ugotovitve, spoznane na krožni poti disertacije, vključujoč vzbujanje in relaksacijo Mottovega izolatorja. Posebna pozornost je posvečena vzbuditvam preko Mottove energijske vrzeli. Znotraj enopasovnega Hubbardovega modela lahko take eksitacije opišemo z efektivno pozitivnimi holoni in negativnimi dubloni, ki reprezentirajo nezasedena in dvojno zasedena mesta. Po kronološkem principu smo se naprej posvetili problemu kreacije nabojev, kot posledica konstantnega električnega polja, zato da bi določili hitrost, s katero so naboji ustvarjeni, potem pa smo obravnavamo obraten proces - relaksacijo in rekombinacijo holonov in dublonov, predvsem v povezavi s "pump-probe" eksperimenti.

Edina tema, ki ni bila formulirana z dubloni in holoni, je bil problem v katerem smo obravnavali interagirajočo brez-spinsko verigo fermionov, na konceh sklopljeno z okoljem in postavljeno v nehomogeno zunanje polje. Zanimal nas je predvsem preplet koherentnega in nekoherentnega vzbujanja, pri čemer je bila prisotnost Mottovega izolatorskega režima drugotnega pomena.

Interagirajoči sistemi v močnih poljih

Efekt močnega električnega polja smo obravnavali na primeru dveh interagirajočih 1D fermionskih sistemov: (a) s spinom 1/2 za primere različnih magnetizacij in (b) za brez-spinski sistem, sklopljen z okolico preko nehokerentnega izvora in ponora na robu verige. Vsak sistem ima svoje posebnosti, ki se zrcalijo tudi v različnem vplivu električnega polja, hkrati pa v ugotovitvah iz obeh študih obstajajo tudi stične točke.

Dielektrični preboj Mottovega izolatorja: V okviru Hubbardovega modela smo obravnavali pol-zapolnjen sistem spin 1/2 fermionov z namenom določiti stopnjo s katero je vzbujeno prvotno izolatorsko stanje, če ga postavimo v močno konstantno električno polje. Polje F je bilo v sistem s periodičnimi robnimi pogoji vpeljano preko Peierlsove substitucije, s časovno odvisnim magnetnim fluksom $\phi(\tau)$, $\dot{\phi}(\tau) = F$, ki prebada sistem,

$$H = -t \sum_{i,\sigma} (e^{i\phi} c^{\dagger}_{i+1,\sigma} c_{i\sigma} + \text{H.c}) + U \sum_{i} n_{i\uparrow} n_{i\downarrow}.$$

Proces vzbujanja se da opisati s produkcijo holonov in dublonov. Novost našega pristopa je bila v tem, da smo sistem obravnavali pri različnih magnetizacijah: od ekstremne situacije z enih samim obrnjenim spinom, do nepolariziranega, kjer se nahaja globalno osnovno stanje (brez prisotnosti magnetnega polja). Eksperimentalno je polarizirane sisteme možno realizirati z zunanjim magnetnim poljem, medtem

ko je teoretično tak pristop zanimiv, ker občutno poenostavi problem, tako, da je obravnava v primeru skoraj polariziranega sistema točna, lahko celo analitična.

Poenostavitev problema v skoraj polariziranem okolju z enim samim obrnjenim spinom je očitna, če se sprašujemo, kako interpretirati naravo Mottovega izolatorja. V tem primeru lahko obstaja kvečjemu en par holona in doublona. V izolatorskem osnovnem stanju ima dominantno težo stanje z enojno zasedenostjo na vseh mestih, medtem ko so konfiguracije s holonom in dublonom na razdalji j eksponentno zavrte in imajo težo

$$d_j^0 \propto e^{-\kappa|j|}, \quad \cosh\kappa = \sqrt{1+(U/4t)^2}.$$

Stanje lahko interpretiramo kot vezan par holona in dublona, z lokalizacijsko dolžino določeno z interakcijo U. Vzbujanje izolatorskega stanja zato res ustreza razvezavi para. Tudi za primere z več obrnjenimi spini in manjšo magnetizacijo se v osnovnem stanju različni pari prednostno postavijo na maksimalno razdaljo, zato je interakcija med njimi možna le skozi eksponentno šibke repe, kar se pozna na primer na rahlo zmanjšani Mottovi vrzeli.

V primeru dielektričnega preboja se razvezava para zgodi zaradi električnega polja. V preprosti, a intuitivni sliki lahko ta proces razumemo kot tuneliranje elektrona vsaj preko lokalizacijske razdalje para, zunanje električno polje pa je v tej sliki povezano z dodatnim linearnim potencialom. Njegova vrednost, potrebna za preboj, približno izpolnjuje $F_{th}/\kappa \sim \Delta$.

Za točnejše razumevanje prebojnega polja F_{th} smo najprej numerično izračunali časovno propagacijo znotraj skoraj polariziranega sistema, ki je pokazala, da osnovno stanje res razpada s stopnjo, ki kaže aktivacijsko obliko,

$$\Gamma \propto \exp\Big(-\frac{\pi F}{F_{th}}\Big).$$

Ker osnovno stanje sploh nima disperzije in ker so numerični rezultati nakazovali, da se prehod zgodi v višje vzbujena stanja, se zdi uporaba standardnega Landau-Zenerjevega izraza za prehod med dvema enodelčnima stanjema neupravičena. Tudi v skoraj polariziranem sistemu je analitično poznano samo osnovno stanje, ne pa tudi vzbujena. Za nadaljno analitično obravnano je bilo ključno opažanje, da lahko pas vzbujenih stanj približno opišemo s stanji prostega holona in dublona z relativnim momentom k in disperzijo $\epsilon_k(\phi)$,

$$d_j^k \propto e^{ikj}, \quad \epsilon_k(\phi) = U - 4t\cos(\phi - k),$$

kjer je disperzija funkcijo k in magnetnega pretoka $\phi = F\tau$. Znotraj tega in dodatnega, bolj tehničnega približka smo prišli do rezultata, da je mejno polje kot funkcija Mottove energijske vrzeli Δ

$$F_{th} \propto \Delta^{3/2},$$

in ne $F_{th} \propto \Delta^2$ kot pri standardnem Landau-Zenerjevem rezultatu. V okviru našega razumevanja je to predvsem posledica disperzije (približnih) vzbujenih stanj prostih holonov in dublonov. Pod določenim kritičnim U, nad katerim aproksimacija s prostimi dubloni in holoni ni več zadostna, numerični rezultati kažejo skladnost z analitičnimi.

Pri zmanjševanju magnetizacije je ključno vprašanje, ali stopnja, s katero razpada osnovno stanje, preprosto skalira s številom obrnjenih spinov. Tak rezultat bi potrdil, da se vsak vezan par razveže neodvisno. Numerična propagacija potrjujejo tak

scenarij do 1/4 obrnenjenih spinov, medtem ko je pri večjih deležih mejno polje rahlo zmanjšano, kar kaže na določen kolektivni efekt. Konceptualno je rezultat iz polariziranega sistema vseeno pomemben, saj je edini, ki lahko da preprost in točen vpogled v proces razpada.

Vredno je omeniti še, da lahko koncept vezave holona in dublona služi tudi pri karakterizaciji ravnovesnega prehoda med kovinsko in izolatorsko fazo kot funkcija interakcije U. Predvsem v $d \geq 3$ dimenzijah obstaja kritični U_c, pod katerim ni vezave, medtem ko pri $d = 1, 2$ vezava in posledično tudi Mottova energijska vrzel kot funkcija U kaže le postopni prehod (je eksponentno majhna pod določeno vrednostjo interakcije).

Neravnovesno stacionarno stanje odprte XXZ verige: Vpliv močnega zunanjena polja je bil obravnavan še na primeru 1D verige brez-spinskih fermionov z interakcijo med najbližjimi sosedi, ki se ga da z Jordan-Wignerjevo transformacijo preslikati na verigo spin 1/2 fermionov v okviru Heisenbergovega modela z dodatnim zunanjim magnetnim poljem, kar smo uporabili pri dejanskih izračunih. Veriga fermionov je bila na konceh sklopljena še z okoljem prek disipativnega izvira in ponora v okviru t.i. kvantne master enačbe, v kateri so disipacijski členi vključeni preko t.i. Lindbladovega disipacijskega člena $\hat{\mathcal{D}}$. Opis z Lindbladovo enačbo

$$\hat{\mathcal{L}}\rho = -i[H, \rho] + \hat{\mathcal{D}}\rho, \quad \hat{\mathcal{D}}\rho = \sum_k 2L_k\rho(t)L_k^\dagger - \{L_k^\dagger L_k, \rho(t)\}$$

narekuje neunitaren razvoj gostotne matrike ρ centralnega sistema. V primeru ekstremnega nehokerentnega vzbujanja imata Lindbladova operatorja znotraj $\hat{\mathcal{D}}$ formo $L_1 = \sqrt{\epsilon}\sigma_1^+, L_2 = \sqrt{\epsilon}\sigma_n^-$ (za sistem s prvim spinom na mestu 1 in zadnjim spinom na mestu n), Hamiltonian pa ima za obravnavan primer obliko

$$H = \sum_{j=1}^{n-1} \left(2\alpha(\sigma_j^+\sigma_{j+1}^- + \sigma_j^-\sigma_{j+1}^+) + \Delta\sigma_j^z\sigma_{j+1}^z\right) + \sum_{j=1}^{n} f_j\sigma_j^z.$$

Za primer močnega magnetnega polja (ali anizotropije v XXZ modelu) smo analitično izračunali izraz za spinski tok J,

$$J = \operatorname{tr}(J_j\rho_\infty)/\operatorname{tr}\rho_\infty, \quad J_j = 2i\alpha(\sigma_j^+\sigma_{j+1}^- - \sigma_j^-\sigma_{j+1}^+),$$

v neravnovesnem stacionarnem stanju ρ_∞, v katerem sistem pristane po začetni tranzitni dinamiki.

Izkaže se, da ne glede na predznak gradienta magnetnega polja, v primeru ekstremnega nekorentnega vzbujanja slednje vedno določa smer toka. Močno magnetno polje celo Starkovo lokalizira (npr. enomagnonske) eksitacije, kar povzroči izolatorski odziv sistema s tokom J, ki je exponentno zavrt z velikostjo sistema n. Asimptotska formula za tok v primeru velikih polj je

$$J = \frac{16\varepsilon}{g^n}\left(\frac{2\Delta}{g} - n\right)^{-2}\prod_{k=1}^{\frac{n}{2}-1}\left(\frac{2\Delta}{g} - k\right)^{-2},$$

kjer je g gradient magnetnega polja. Za primere z interakcijo $\Delta \neq 0$ je zunanje polje vseeno način kako v sistem vnesti asimetrijo, saj $J(g) \neq J(-g)$. Če definiramo rektifikacijski koeficient kot

$$R = \frac{J(g) - J(-g)}{J(g) + J(-g)},$$

potem obstajata dva mehanizma za $R \to 1$: (a) kot sledi iz asimptotske formule za tok se to zgodi v termodinamski limiti $n \to \infty$ in pri fiksnem gradientu g, poleg tega pa je (b) pri resonančnih gradientih, kjer naša asimptotska analiza odpove, tok pri enemu predznaku gradienta v resnici drugačnega reda v razvoju po $1/g$ kot pri drugemu. Resonančna polja, pri katerih je tok izrazito velik, se da razloziti s spektrom Hamiltonian, ki narekuje koherentni del dinamike. Pri teh vrednostih je namreč dominantno izolatorsko stanje z enkratno stopnico v magnetizaciji $|\uparrow \cdots \uparrow \downarrow \cdots \downarrow\rangle$ degenerirano z nekim drugim, manj izolatorskom stanje, ki je zato izraziteje prisotno v gostotni matriki, če ima le robne spine kompatibilne z disipativnim vzbujanjem.

Prekrivanje: Ker v enem primeru obravnavamo spin 1/2 v drugem pa brez-spinske fermione ne gre pričakovati, da bo električno polje povzročilo identičen vpliv. Fokus prve študije je bil določiti stopnjo, s katero pod vplivom električnega polja nastajajo parih holonov in dublonom pri določeni magnetizaciji, medtem ko v brez-spinskem sistemu maksimalno število holonov/dublonov (dveh zaporednih praznih/polnih mest) ne moremo omejiti. Še več, v odprtem sistemu ne moremo zagotoviti niti polovične zasedenosti. Kljub temu je efekt Starkove lokalizacije skupen obema študijama, saj lokalizira tudi dejanski par holona in dublona na razdalji $l_d = 8/F$. Zato se je dobro zavedati, da je prispevek k toku pri dielektričnem preboju predvsem posledica kreacije naboja, saj je kasneje le ta omejen s Starkovo lokalizacijo in ne more prispevati k toku na poljubnih razdaljah. Znotraj naše študije ni bilo posebej obravnavano, kako kolektivni efekti pri nižjih magnetizacijah sprostijo to omejitev. Na drugi strani pa je asimptotska formula za tok skozi odprt sistem veljavna prav v režimu, ko je Starkova lokalizacija nezanemarljiva.

Pre-termalizacija nabojev v pump-probe eksperimentih

Ko smo snovali teorijo za "pump-probe" eksperimente na Mottovih izolatorjih, smo se najprej posvetili kratkočasovni dinamiki holonov in dublonov, ki so ustvarjeni z začetnim "pump" pulzom, z energijo večjo od Mottove vrzeli. Privzeli smo, da se od začetka holoni in dubloni obnašajo kot neodvisni, zato lahko obravnavamo samo enega izmed njih, npr. en holon. Začetno stanje (takoj po vzbuditvi) smo simulariali z vstavitvijo holona v urejeno spinsko ozadje, kar je le smiselna poenostavitev, ki bi jo bilo potrebno točneje testirati s kvantnim opisom vzbuditvenega postopka.

Najprej smo holon sklopili s spinskimi prostostnimi stopnjami preko t-J modela,

$$H_0 = -t \sum_{\langle i,j\rangle,s} (\tilde{c}^\dagger_{i,s}\tilde{c}_{j,s} + \text{H.c.}) + J \sum_{\langle i,j\rangle} (\mathbf{S}_i \cdot \mathbf{S}_j - \frac{1}{4} n_i n_j),$$

kjer je $\tilde{c}_{i,s} = c_{i,s}(1 - n_{i,-s})$ fermionski operator projeciran na Hilbertov prostor brez dvojne zasedenosti. Opažena je bila hitra relaksacija (reda fs) začetnega stanja proti stacionarnemu stanju, katerega lastnosti smo primerjali z lastnostmi osnovnega stanja spinskega polarona in z termično pričakovanim stanjem (glede na energijo, ki smo jo vstavili v sistem).

Mehanizem: Jasnejši vpogled v hitro relaksacijo je bil pridobljen s poenostavljenim 1D modelom, ki kombinira t-J model z izmenjevalnim poljem h,

$$H = -t \sum_i (\tilde{c}^\dagger_{i,s}\tilde{c}_{i+1,s} + \text{H.c.}) + J \sum_i (\mathbf{S}_i \cdot \mathbf{S}_{i+1} - \frac{1}{4} n_i n_{i+1}) + h \sum_i (-1)^i S^z_i,$$

ki umetno zagotovi ureditev spinov v 1D in zato v resnici efektivno opišuje dogajanje v 2D, kjer je ureditev spinskega ozadja dejansko prisotna. Predvsem holon-spin korelacije pokažejo, da je relaksacija sestavljena iz dveh stopenj. (a) izvorno lokaliziran delec najprej poruši spinsko ureditev v svoji okolici in si na tak način zniža kinetično energijo. Skaliranje časa relaksacije v tem procesu je bilo razloženo že v predhodnih študijah z ustvarjanjem nizov spinskih eksitacij [160]. (b) v drugi stopnji pa se ustvarjena lokalna spinska vzbuditev razširi v celoten sistem, kar dobro opiše njena propagacije v bazi magnonskih stanj. Primernost takega opisa je bila potrjena z opazitvijo Lieb-Robinsonove hitrosti vsake stopnje: v (a) se holon glede na spinsko ozadnje giblje kot prost, s hitrostjo $v_h \approx 2$, v (b) pa je dominantno obnašanje lokalizirane spinske vzbuditve, ki se v sistem razširi z maksimalno magnonsko hitrostjo $v_m = h + J - \sqrt{h(h+2J)}$.

Če holon sklopimo tudi z (nedisperzivnimi) fononi, potem je stacionarno stanje polaron spinsko-fononske narave. Izkaže se, da v začetni fazi holon svojo energijo preda bozonski kopeli, ki je bolj efektivna: v primeru šibke sklopitve s fononi so to spini, v primeru močne sklopitve pa fononi. Ne glede na to, da sta obe kopeli sklopljeni le prek nabitega delca, je na dolgočasovni skali moč opaziti ekvilibracijo med kopelma. Točnejši opis tega procesa bi bilo potrebno še poiskati.

Neravnovesna optična prevodnost: Da bi pridobili dodaten vpogled v dinamiko, predvsem tak, ki je blizu eksperimentalno opazljivim količinam, smo optično prevodnost (računano znotraj modelov tesne vezi) generalizirali na neravnovesne situacije. V povezavi s "pump-probe" eksperimenti je "probe" pulz obravnavan kot šibka perturbacija (znotraj linearnega odziva), "pump" pulz pa je odgovoren za začetno eksitacijo, ki je efektivno vključena le preko začetne valovne funkcije oz. gostotne matrike. Ključna razlika v primerjavi z ravnovesno optično prevodnostjo je, da sistem ne poseduje časovne invariance, zato je $\sigma(t',t)$, ki je povezuje odziv toka ob času t' na polje, ki je bilo vključeno ob t,

$$\delta\langle \mathbf{j}_e\rangle_{t'} = V\int_t^{t'} d\tilde{t}\ \sigma(t',\tilde{t})\mathbf{E}(\tilde{t}), \quad \sigma(t',t) = \frac{e^2}{V}[\langle\tau\rangle_{t'} - \int_t^{t'} dt''\chi(t',t'')],$$
$$\tau = \sum_{i,j,s} t_{ij}(\mathbf{R}_j - \mathbf{R}_i)\otimes(\mathbf{R}_j - \mathbf{R}_i)c^\dagger_{js}c_{is}, \quad \chi(t',t'') = i\theta(t'-t")\langle[\mathbf{j}^I(t'),\mathbf{j}^I(t'')]\rangle_t,$$

res funkcija dveh časov in ne samo razlike med njima. V zgornji enačbi je V volumen sistema. Da dobimo ekvivalent k (ravnovesni) $\sigma(\omega)$, ki je v principu bolj informativna, saj nakaže npr. na možne absorpcije v sistemu, $\sigma(t',t)$ Fourierovo transformiramo prek enega časa. Izbrali smo si t',

$$\sigma(\omega,t) = \int_0^{t_m} ds\ \sigma(t+s,t)e^{i\omega s},$$

zato da ohranimo informacijo o tem, kdaj je bilo testno polje aplicirano in da ne kršimo kavzalnosti (s transformacijo čez čase pred "pump" pulzom). Znotraj take formulacije sta optično vsotno pravilo in Drudejeva utež dobro določena in časovno odvisna,

$$\int_{-\infty}^{\infty} d\omega\ \sigma'(\omega,t) = \frac{\pi e^2}{V}\langle\tau\rangle_t, \quad D(t) = \frac{1}{2Vt_m}\int_0^{t_m} ds[\langle\tau\rangle_{t+s} - \int_0^s ds'\chi(t+s,t+s')].$$

Formalizem smo uporabili na že omenjenem primeru vzbujenega (v začetku popolnoma lokaliziranega) holon, tokrat znotraj 2D t-J modela. Časovno odvisna

optična prevodnost pokaže, da se iz začetno precej neizrazitega odziva kaj hitro formulirata "mid-infra-red" in Drudejev vrh, ki sta presenetljivo podobna kot pri odzivu osnovnega stanja spinskega polarona. Rezultat je nenavaden (in bi lahko imel korenine predvsem v numeriki na majhnih sistemih), saj bi glede na energijo, ki jo dovedemo v sistem, pričakovali bolj termično obnašanje, pri katerem sta slednja vrhova veliko bolj razmazana.

Časovno odvisna temperatura: Da bi bolje označili stacionarno stanje in našli razloge za pre-termalno naravo tega stanja smo uporabili fluktuacijsko-disipacijski izrek, ki v eni izmed formulacij povezuje auto-korelacije s temperaturo. Z identično Fourierovo transformacijo kot pri optični prevodnosti smo ga razširili na neravnovesno stanje,

$$\frac{C^{AA}(\omega,t)-C^{AA}(-\omega,t)}{C^{AA}(\omega,t)+C^{AA}(-\omega,t)}=\tanh\Big(\frac{\beta(\omega,t)\omega}{2}\Big).$$

in temperaturi $T=1/\beta$ dopustili frekvenčno in časovno odvisnost. V kolikor $\beta(\omega,t)\approx\beta(t)$ potem lahko trdimo, da je temperatura vsaj lokalno (če je A lokalen operator) vzpostavljena tudi v stacionarnem ali celo prehodnem stanju. Na primeru vzbujenega holona smo zgornjo relacijo preverjali za operator toka $A=j$. Izkazalo se je, da je temperatura kaj kmalu precej dobro definirana in da pada eksponentno proti stacionarni vrednosti, ki je višja kot bi termično pričakovali. Ker smo uporabili operator toka, je izračunana temperatura seveda zgolj lokalna. V skladu s to trditvijo je tudi opažanje, da je stacionarna temperatura enaka, kot če jo določimo iz stacionarne vrednosti kinetične energije, ob predpostavki, da je to tudi termična vrednost.

Že ta primer nakazuje, da se fluktuacijsko-disipacijski izrek da uporabiti kot prostorsko-ločljiv termometer, saj imamo z izbiro operatorja A možnost testiranja različnih predelov sistema. Žal pa niti ta analiza ni obrazložila nenavadnega stacionarnega optičnega odziva holona. Glede na visoko lokalno temperaturo, pridobljeno iz fluktuacijsko-disipacijske relacije, bi pričakovali še večjo razmazanost vrhov. Razlog za pre-termalizacijo zato ostaja kot odprta možnost za prihodnje študije, mogoče z dodatno sklopitvijo s fononi.

Rekombinacija nabojev v "pump-probe" eksperimentih

Osrednja tema disertacije je bil problem rekombinacije nabojev, kot ključen in skorajda poslednji proces v "pump-probe" eksperimentih, na koreliranih sistemih opažen na ps skali. Teoretična razlaga takega procesa je poseben izziv zaradi velike energija para nabiti delcev (holona in dublona), ki mora biti hkrati predana drugim eksitacijam, npr. spinskim, fononskim ali drugim fermionom, z nižjo energijo. Obravnavali smo samo primere z nizko gostoto ustvarjenih nabitih delcev, ko je sipanje z ostalimi nabitimi delci malo verjetno. Glavna ugotovitev študije je bila, da je ne glede na detajle mehanizma rekombinacijska hitrost eksponentno zavrta s številom končnih eksitacij, ki jim je v procesu predana energija. Kot začetno stanje smo vedno predpostavili vezan par holona in dublona, ki je poleg ostalih [33] in naših teoretičnih afirmacij v obravnavanih materialih tudi eksperimentalno potrjen. Ker se je izkazalo, da dimenzija sistema ključno vpliva na primernost mehanizma, smo posamič obravnavali 2D in 1D sisteme, v relaciji z experimenti na efektivno 2D cupratih (Nd_2CuO_4 and La_2CuO_4) [13, 14] and efektivno 1D organskih soleh (ET–F_2TCNQ) [21]. Pokazali smo, da je v 2D sistemih z močno

sklopitvijo med nabojem in spinom rekombinacija lahko razložena z emisijo spinskih eksitacij, medtem ko so v 1D sistemih, kjer je slednja sklopitev šibka, za rekombinacijo lahko odgovorni fononi. Mehanizem, ki vključuje slednje lahko reproducira ps čase rekombinacij le, če je frekvenca fononov relativno visoka, kar drži v organskih soleh s kompleksno strukturo, ne pa tudi v 1D kupratih [18]. Ekstenzija spinsko posredovane rekombinacije na 1D je možna za sisteme, ki kažejo spinsko-fononsko sklopitev. Detajlna struktura takega mehanizma znotraj te disertacije ni bila obravnavana, lahko pa da je ključna za razlago nedavnih eksperimentov na Ca_2CO_3 [38], z dodatno komplikacijo, da se v teh materialih holon in dublon ne vežeta v eksiton [19].

V sledečem obiščemo ključne ugotovitve in probleme:

Vloga dimenzije sistema: Ključna razlika med koreliranimi sistemi v različnim dimenzijah se zdi sklopitev med nabojem in spini. Ta je inherentno prisotna v dvo- in višje-dimenzionalnih sistemih, kar se da zajeti s Hubbardovim modelom z $U \gg t$ ali t-J modelom z $J < t$, kjer gibljiv nabit delec lahko perturbira in frustrira spinsko ozadje. V 1D sistemih je ta sklopitev neefektivna, saj je gibanje holonov/dublonov skoraj prosto, saj s tem le zamikajo spinsko ozadje in ga frustrirajo kvečjemu na eni vezi. Zato je v 1D sistemih potrebno razviti drugačen mehanizem, tako za rekombinacijo, kot tudi formacijo eksitona.

Efektivni modeli: Naš namen je bil poiskati mehanizme rekombinacije na osnovi minimalnega modela. Kot že omenjeno je ta odvisen od dimenzije sistem.

2D sisteme bi v principu lahko obravnavali s Hubbardovi modelom,

$$H = -t \sum_{\langle ij \rangle s} (c^\dagger_{js} c_{is} + \text{H.c.}) + U \sum_i n_{i\uparrow} n_{i\downarrow},$$

vendar smo le tega raje kanonično transformirali v generaliziran t-J model, ki vsebuje kinetični člen za holone in dublone, Heisenbergovo interakcijo med spini in rekombinacijsko-kreacijski člen H_{rc} kot perturbacijo,

$$\begin{aligned}
H &= H_{tJ} + H_{rc} \\
H_{tJ} &= t \sum_{\langle ij \rangle, s} (h^\dagger_{is} h_{js} - d^\dagger_{is} d_{js} + \text{H.c.}) + U \sum_i n_{di} + J \sum_{\langle ij \rangle} \left(\mathbf{S}_i \cdot \mathbf{S}_j - \frac{1}{4} \delta_{1, n_i n_j} \right) \\
H_{rc} &= t_{rc} \sum_{(ijk), ss'} \left(h_{ks} d_{js'} \boldsymbol{\sigma}_{s\bar{s}'} \cdot \mathbf{S}_i + \text{H.c.} \right), \quad t_{rc} = \frac{J}{2}.
\end{aligned}$$

Prednosti takega modela, ki v najnižje redu separira sektorje z različnim številom parov, se sledeče: (a) z njim lažje izračunamo začetno eksitonsko stanje, in sicer tako, da na tej točki zanemarimo rekombinacijsko-kreacijski člen H_{rc} in poiščemo osnovno stanje znotraj Hilbertovega prostora z enim parom holona in dublona. (b) da eksitonsko stanje v resnici ni lastno je jasno, ko upoštevamo še H_{rc}, kot perturbacijo, ki povzroči razpad eksitona. Ker so nedopirani kuprati v resnici "charge-transfer" in ne Mottovi izolatorji smo podoben minimalen model izpeljali tudi iz več-orbitalnega modela, ki je vključeval relevantne Cu in O orbitale. V nasprotju s prejšnjimi študijami dopiranih kupratov, morajo biti v tem primeru holoni in dubloni vključeni enakopravno. Kot že opaženo je simetrija med holoni in dubloni v takem modelu kršena, kar se pozna npr. na različnih efektivnih prekrivalnih integralih in tudi na razločljivih rekombinacijskih kanalih (glede na končno spinsko konfiguracijo).

Pomembno je, da je končna oblika in tudi absolutne vrednosti parametrov obeh (multi- in eno-orbitalnih) efektivnih modelov rekombinacije podobna, le struktura rekombinacijskih členov multi-orbitalnega modela je nekoliko bogatejša, zaradi dodatnih možnih vmesnih stanj. S tem smo potrdili, da je efektivni model, izpeljan iz Hubbardovega modela primeren, če le uporabimo konceptualno modifikacijo, znotraj katere je Mottova vrzel za primerjavo z eksperimentom nadomeščena z eksperimentalno določeno vrednostjo "charge-transfer" vrzeli. Še več, pokazali smo tudi, da je ključna fizika rekombinacije zajeta že znotraj poenostavljenega eksiton-bozon modela,

$$H = \; E_e e^\dagger e + e^\dagger e \sum_q \lambda_q (a_q^\dagger + a_{-q}) + \sum_q \omega_q a_q^\dagger a_q + g_{rc}(e + e^\dagger),$$

kjer je $e^\dagger$ kreacijski operator eksitona, $a_q^\dagger$ pa bozona, pri čemer je bozonska vloga v tem primeru odigrana s spini. Za tak model se rekombinacijsko hitrost Γ da poiskati analitično,

$$\Gamma \approx g_{rc}^2 e^{-\xi} \sqrt{\frac{2\pi}{\Delta\omega_0}} \; \exp\left[-\frac{\Delta}{\omega_0} \ln\left(\frac{\Delta}{e\;\xi\omega_0}\right)\right].$$

Ta izraz eksplicitno razkrije odvisnost hitrosti od Mottove energijske vrzeli Δ, tipične energije bozonov ω_0 in močjo sklopitve med eksitonom in bozoni ξ.

V 1D sistemih smo nabite delce sklopili s fononi preko lokalne gostote naboja, in s tem upoštevali, da imata holon in dublon obraten vpliv na odmik osnovnih enot.

$$H_{ep} = \sum_{ij} \lambda_{ij}(a_j^\dagger + a_j)\tilde{n}_i, \quad \tilde{n}_i = n_i^d - n_i^h$$

Pri tem fononi niso nujno Holsteinovega tipa. Zaradi separacije naboja in spina in ker so v organskih soleh intra-molekularne vibracije zelo energične, $J \ll \omega_0$, smo privzeli, da so spinske prostostne stopnje manj pomembne, zato smo problem obravnavali v okviru spinsko skoraj polariziranega sistema, z enim samim obrnenjenim spinom. Za obstoj eksitona v 1D je potrebno upoštevati Coulombsko interakcijo med najbližjimi sosedi, ki se med sosednjim holonom in dublonom efektivno kaže kot privlak. Če najprej zanemarimo sklopitev s fononi, se eksitonsko stanje v spektru zlahka (v primeru skoraj polariziranega sistema celo analitično) najde. Ker je število fononov na enem mestu neomejeno in ker zanemarjamo spinske prostostne stopnje, tokrat ne naredimo kanonične transformacije Hamiltoniana, ki bi rekombinacijo dovolila šele v drugem redu, kot v 2D. Kljub temu, da rekombinacijski člen nima forme perturbacije (s šibko sklopitvijo), je uporaba Fermijevega zlatega pravila upravičena z majhnim matričnim elementom za tranzicijo iz eksitona v fononske eksitacije. Po tem, ko smo upoštevali sklopitev s fononi, smo na Hamiltonianu $H = H_t + H_{rc} + H_U + H_{ep} + H_{ph}$,

$$\begin{aligned}
H_t &= t \sum_{i,s} (h_{i+1,s}^\dagger h_{i,s} - d_{i+1,s}^\dagger d_{i,s} + \text{H.c.}),\\
H_{rc} &= -t \sum_{i,s} (h_{i,\bar{s}} d_{i+1,s} + h_{i+1,\bar{s}} d_{i,s} + \text{H.c.}),\\
H_U &= U \sum_i n_i^d (1 - n_i^h) - V \sum_i (n_i^d n_{i+1}^h + n_i^h n_{i+1}^d),\\
H_{ph} &= \sum_q \omega_q a_q^\dagger a_q,
\end{aligned}$$

naredili standardno Lang-Firsovo transformacijo, ki odtransformira eksplicitno sklopitev med nabojem in fononi H_{ep}, v zameno pa s fononskimi operatorji obleče kinetični in rekombinacijski člen, ter tudi eksitonsko stanje, ki (v okviru našega razumevanja) dejansko ustreza stanju v eksperimentih, po začetni hitri relaksaciji. Delo znotraj transformirane slike je primernejše za analitično analizo, hkrati pa eksplicitno pokaže, da je za neničelen matrični element med eksitonskim stanjem z liho parnostjo in osnovnim stanjem s sodo parnostjo, ključna sklopitev s fononi.

Obstoj eksitona: Pri računu rekombinacijske hitrosti predpostavljamo, da se na krajši časovni skali holon in dublon vežeta v eksiton, ki ima v 2D sodo (tipa s) in v 1D liho parnost. Eksperimentalna potrditev optično neaktivnih eksitonov s sodo parnostjo je možna preko nelinearne optične prevodnosti, ki je za obravnavane materiale potrdila njihov obstoj [19, 36]. Poleg tega je njihov obstoj pokazan tudi indirektno, v "pump-probe" eksperimentih, z eksponentnim razpadom gostote vzbujenega naboja in rekombinacijsko hitrostjo, ki je neodvisna od fluence (gostote fotonov) pulzov. Če holon in dublon pred rekombinacijo ne bi bila že vezana, bi bil rekombinacijski proces odvisen od verjetnosti, da se srečata,

$$-\frac{dn(\tau)}{d\tau} \propto n^{\gamma}, \quad \gamma = 2, 3,$$

kar pa ne vodi k eksponentnemu razpadu gostote nabojev.

V 2D je vezano stanje holona in dublona posledica minimizacije perturbacije spinsko urejenega ozadja. Zato bi v primerih, ko je zaradi eksperimentalnih pogojev urejenost spinskega ozadja uničena, npr. zaradi "pump" pulza z veliko fotonsko gostoto ali veliko energijo, moralo izginiti tudi eksitonsko stanje.

Veljavnost Fermijevega zlatega pravila: Čeprav je rekombinacijska hitrost s pomočjo Fermijevega zlatega pravila

$$\Gamma = 2\pi \sum_{m} |\langle \psi_m^0 | H_{rc} | \psi_0^{hd} \rangle|^2 \; \delta(E_m^0 - E_0^{hd})$$

določena le približno, je taka aproksimacija tehnično ugodna in konceptualno smiselna, saj je rekombinacija nabitih delcev mnogo počasnejši proces, kot pa je tipična skala $\hbar/t$ časovno odvisnih simulacij. Za rekombinacijo v 2D sistemih smo vpliv procesov, zanemarjenih znotraj Fermijevega zlatega pravila, ocenili s primerjavo z eksplicitno časovno propagacijo začetnega eksitonskega stanja pod vplivom celotnega Hamiltoniana, vključujoč rekombinacijsko-kreacijski člen. Spet je bilo opaženo eksponentno razpadanje nabitih delcev s stopnjo, ki je primerljiva z izračunom iz Fermijevega zlatega pravila. Potrebno se je zavedati, da ima tudi taka simulacija svoje omejitve: (a) zaradi diskretnosti spektra je po določenem času moč opaziti povratek nabitih delcev, kar določa zgornjo mejo za časovno propagacijo, (b) virtualni procesi, pri katerih energija ni ohranjena, povzročajo oscilacije v gostoti obstoječega naboja (in tako destabilizirajo eksitonsko stanje), hkrati pa ne vodijo k dejanski rekonbinaciji, (c) pod vplivom rekombinacijsko-kreacijskega člena se celoten spekter Hamiltoniana rahlo premakne, zato je energijo, ki je predana spinom, potrebno posebno pazljivo določiti, (d) pri numeričnem računu smo Hilbertov prostor omejili na stanja z nič ali enim parom holona in dublona. Ne glede na to sta rekombinacijski hitrosti Γ pridobljeni na oba načina primerljivi, predvsem na večjem sistemu z $N = 26$ mesti, kjer je Γ pridobljena iz časovne evolucije rahlo hitrejša, kot bi pričakovali.

Izvor hitre rekombinacije v koreliranih sistemih: Eksperimentalni rezultati kažejo, da je rekombinacija nabojev v koreliranih sistemih hitrejša kot v polprevodnikih, kjer se podobni procesi dogajajo na milisekundno skali. Zato je dobro razumeti odkod razlika.

Glede na naše razumevanje je glavni razlog za hitro rekombinacijo v 2D sistemih v močni sklopitvi med nabojem in spinsko okolico, ki ima hkrati tudi višjo energijsko skalo eksitacij J, v primerjavi s tipičnimi energijami fononov v polprevodnikih. Kljub močnim korelacijam so foto-eksitirani holoni in dubloni mobilni in zato lahko perturbirajo spinsko ozadje, kar se da preveriti z odstopanji v spinskih korelacijah v eksitonskem stanju glede na AFM osnovno stanje. V procesu rekombinacije je ta perturbacija spinskega ozadja lahko še povečana zaradi dodatnih možnih preobratov spinov v rekombinacijskem členu. Seveda je verjetnost za obdanost z $n \sim \Delta/J \gg 1$ preobrnjenimi spini majhna, a ravno to naredi rekombinacijski proces počasen (glede na mikroskopski dinamiko). Sama zmožnost oddaje takega velika števila magnonov je bila demonstrirana absorpcijo svetlobe zaradi multi-magnonskih eksitacij [192, 193].

Rekombinacija v 1D organskih soleh je v večji meri podobna rekombinaciji v (nekoreliranih) ogljikovih nanocevkah [41, 171]. Korelacije so potrebne za formacijo eksitona, medtem ko je hitra rekombinacija posledica visokih frekvenc udeleženih fononov, tipičnih za organske soli s kompleskno strukturo osnovne celice, znotraj katere so možne intra-molekularne vibracije z veliko energijo. Seveda morajo biti te vibracije sklopljene z mrežnimi fononi, ki lokalni presežek energije prenesejo v celoten sistem. V okviru našega računa smo oba aspekta upoštevali na efektivnem nivoju: za energijo fononov smo privzeli izmerjeno frekvenco intra-molekularnih nihanj, hkrati pa smo jim dodelili določeno disperzijo, ki bi efektivno lahko bila posledica sklopitve z mrežnimi fononi. Vplivi korelacij bi lahko bili večji v primeru 1D kupratov s tipično manjšimi frekvencami fononov, v okviru katerih je bil nedavno obravnavan Ca_2CO_3 [38]. Zdi se, da bi rekombinacijski mehanizem v slednjih materialih moral upoštevati fononsko posredovano sklopitev med nabitimi delci in spinskimi prostostnimi stopnjami.

Spinska ureditev kratkega oz. dolgega dosega: Omeniti gre, da obstoj spinske ureditve dolgega dosega ni predpogoj za našo analizo rekombinacije v 2D. Relevantne eksitacije, ki prevzamejo energijo para holon in dublona so splošne spinske eksitacije oz. paramagnoni, prisotni tudi v paramagnetni fazi. Ključno je, da imajo disperzivno naravo, tako da lahko v sistem distributirajo lokalno spinsko perturbacijo. Na drugi strani pa so korelacije kratkega dosega potrebne za to, da se holon in dublon obdata s spinskimi eksitaciji, proces ključen za obstoj eksitona in za razlago rekombinacije. Ker so naši numerični izračuni pridobljeni na končnih sistemih z $N \leq 26$ mesti, v njih niti ne moremo strogo govoriti o redu dolgega dosega. Ključno pa je, da je sistem dovolj velik, da lahko akomodira spinsko perturbacijo okrog eksitona. Kot je pokazala študija razpada nevezanega para holona in dublona v popolnoma neurejenem spinskem ozadju, je rekombinacijska hitrost v tem primeru zelo majhna [87].

Rekombinacija v sistemih z višjo gostoto vzbujenih nabojev: Mehanizmi rekombinacije, ki so bili obravnavani znotraj te disertacije ustrezajo pogojem, pri katerih je vzbujena majhna gostota nabitih delcev, ki po hitri relaksaciji tvorijo vezana eksitonska stanja. V eksperimentih z visoko fotonsko gostoto pulza, ki bi posledično ustvaril visoko gostoto nabitih delcev, bi lahko postali dominantni drugačni meha-

nizmi, npr. Auger procesi, pri katerih je energijo para holona in dublona predana tretjemu nabitemu delci, ki se mu ustrezno poveča kinetična energija. Tak proces je možen le, če je Mottova energijska vrzel manjša od širine zgodnjega Hubbardovega pasu. Jasna eksperimentalna indikacija takega procesa bi bil neeksponenten razpad gostote nabojev, če le ne opazujemo zgolj deviacij okrog termične vrednosti gostote. Podobni procesi, kjer je energija dublona predana s sipanjem z ostalimi fermioni, so dominantni v ekperimentih na fermionskih hladnih atomih [64, 65] in znotraj DMFT študij [28, 66], pri čemer so bili obravnavani procesi vseeno kompleksni zaradi pogoja, da je bila Mottova energijska vrzel večja od širine Hubbardovega pasu.

Splošnost rezultata: Nazadnje gre ponovno opozoriti na splošnost rezultata, ki je pokazal, da je rekombinacijska hitrost eksponentno zavrta s številom eksitacij, ki pri procesu prevzamejo energijo para holona in dublona, in to ne glede na detajlno formo mehanizma [34, 35, 40, 64, 65, 66, 87].